In vivo functional analysis of novel Congenital Heart Disease candidate genes using *Drosophila melanogaster* as a heart model

- *MYOM2, LRP2,* ribosomal protein genes -

Inaugural-Dissertation
to obtain the academic degree
Doctor rerum naturalium (Dr. rer. nat.)

submitted to the Department of Biology, Chemistry, Pharmacy
of Freie Universität Berlin

by

Tanja Nielsen

2021

This work was conducted between January 2017 and January 2019 in the laboratory of Prof. Silke Rickert-Sperling in the Department of *Cardiovascular Genetics* at Charité - Universitätsmedizin Berlin, Germany, and between February 2019 and December 2021 in Prof. Rolf Bodmer's laboratory in the Department of *Development, Aging and Regeneration* at Sanford Burnham Prebys Medical Discovery Institute in La Jolla, USA.

1st Reviewer: Prof. Rolf Bodmer

2nd Reviewer: Prof. Silke Rickert-Sperling

Date of defense: 22.03.2022

Statement of Originality

I hereby declare that I have written the present thesis independently, that I performed all the experiments unless specified in the text or the acknowledgment section in each chapter and that no help or resources other than described or referenced were used.

_____

Date, Signature

Table of contents

List of Figures

List of Tables

List of Abbreviations

Abbreviation	
APOB	apolipoprotein B
ATP	adenosine triphosphate
ATP1A3	ATPase Na+/K+ transporting subunit alpha 3
ASD	atrial septal defect
BMP	bone morphogenetic protein
bp	base pairs
bt	bent
CHD	congenital heart disease
CB	cardioblast
CM	cardiomyocyte
DD	diastolic diameter
Df ()	deficiency ()
DI	diastolic interval
diap1	death-associated inhibitor of apoptosis 1
DIOPT	DRSC Integrative Ortholog Prediction Tool
Doc	Dorsocross
DPP	decapentaplegic
EGFR	epidermal growth factor receptor
FGF	fibroblast growth factor
FHF	first heart field
FS	fractional shortening
fz	frizzled
FZD	frizzled
GATA4	GATA Binding Protein 4
GFP	green fluorescent protein
GOI	gene of interest
HCM	hypertrophic cardiomyopathy
hh	hedgehog
hiPSC-CM	human induced pluripotent stem cell
HLHS	hypoplastic left heart syndrome
HP	heart period
hpf	hours post fertilization
HWT	heart wall thickness

KD	knockdown
LA	left atrium
LRP2	LDL receptor related protein 2
LV	left ventricle
LVNC	left ventricular non-compaction
MAF	minor allele frequency
Mef2	myocyte enhancer factor 2
mgl	megalin
Mhc	myosin heavy chain
MnM	myomesin and myosin binding protein
MO	morpholino
MYBPC3	myosin binding protein C
MYH7	myosin heavy chain 7
MYOM2	myomesin-2
NKX2-5	NK2 Homeobox *5*
Nmr1	Neuromancer 1
OE	overexpression
OFT	outflow tract
PC	pericardial cell
PCGC	Pediatrics Cardiac Genetics Consortium
pnr	pannier
ptc	patched
PTCH 1	patched 1
pyd	polychaetoid
RA	right atrium
RING	rapid negative geotaxis
RNAi	RNA interference
RP	ribosomal protein
RT-qPCR	reverse transcription quantitative real-time polymerase chain reaction
RV	right ventricle
SD	systolic diameter
sd	scalloped
SF1	splicing factor 1
SHF	second heart field
SHH	Sonic Hedgehog

SI	systolic interval
sls	sallimus
smo	smoothened
SOHA	Semi-Automated Optical Heartbeat Analysis
svp	seven-up
TBX5	T-box 5
tdtK	tdTomato Klassen
tin	tinman
TJP1	tight junction protein ZO-1
TOF	Tetralogy of Fallot
TP53	tumor protein P53
TTN	titin
UAS	upstream activation sequence
wg	wingless
WGS	whole-genome sequencing
yki	yorkie
VLM	ventral longitudinal muscle
VSD	ventricular septal defect

Abstract

Congenital heart diseases (CHD) are the most common human birth defects, affecting approximately 0.8 % of all live births.[1] They comprise structural malformations of the heart occurring during development and functional disorders such as cardiomyopathies and arrhythmias. Often a treatment throughout life is required due to impaired cardiac functions through adult stages. The causal genetic underpinning of CHD, which are often complex and oligogenic, are still far from understood, and currently, only 25 % of all CHDs can be explained by gene mutations.[2] Therefore, there is a great unmet need to understand the genetic mechanisms leading to developmental defects, and likely the key to fight CHDs lies in understanding the exact molecular mechanisms underlying cardiac development and occurrence of disease. In this work I leverage CHD patient genomic data to identify novel potentially CHD-associated genes, gene networks and pathways, by taking advantage of *Drosophila melanogaster* as a heart model system.

In the first part of this thesis (conducted in the Rickert-Sperling lab) I concentrate on myomesin-2 (MYOM2), a functional component of the M-band of the sarcomeres. *MYOM2* was found mutated in patients with Tetralogy of Fallot (TOF) and hypertrophic cardiomyopathy (HCM), which did not carry mutations in any of the known disease genes.[3,4] Functional analysis in the *Drosophila* heart identified *CG14964* (which we named *MnM* for myomesin and myosin binding protein), a so far uncharacterized fly gene, as the likely ortholog for *MYOM2* and other myosin binding proteins. Moderate knockdown (KD) of *CG14964* in the fly heart led to dilation of the heart, while strong KD caused constrictions. Moreover, genetic interaction studies revealed synergism between *CG14964* and myosin heavy chain 6/7 (*MYH6/7)* fly ortholog *Mhc.* Overall, these data suggest a critical role for *MnM* in heart development and thus point towards a potential contribution of *MYOM2* variants to CHD manifestations, such as HCM and TOF (Chapter 1).

The second part of the thesis (conducted in the Bodmer lab) focusses on the genetic perturbations underlying hypoplastic left heart syndrome (HLHS), which represents the most lethal CHD and is most likely oligogenic in origin. In collaboration with the Mayo Clinic (MN, USA), whole-genome sequencing was performed in a cohort of HLHS proband-parent trios, which revealed enrichment of rare, predicted-damaging variants in LDL receptor-related protein 2 (*LRP2*).[5] Functional analysis in human iPSC-derived cardiomyocytes (hiPSC-CM), in *Drosophila* and zebrafish hearts with diminished *LRP2* function showed a requirement of the receptor for cardiomyocyte proliferation and differentiation.[5] In this manuscript and beyond, my contribution was to further study the consequence of systemic *LRP2* KD in the fly heart, which leads to cardiac dilation and constrictions. Furthermore, I show a genetic interaction between the multiligand receptor LRP2 and apolipoprotein B (ABOB) and

reveal connections with growth associated pathways SHH and Wnt/wg, suggesting that LRP2 potentially regulates cardiac proliferation and differentiation through modulation of these pathways (Chapter 3).

Segregation analysis in a familial case within the HLHS cohort from Mayo Clinic furthermore identified a rare promoter variant affecting ribosomal protein *RPS15A* that segregates with disease. In addition, enrichment analysis in 25 HLHS trios with poor clinical outcome revealed an over-representation of ribosomal protein (RP) gene variants. Functional testing in model systems, showed that KD of RPs reduced proliferation in generic human iPSC-CMs (Colas lab) and impaired cardiac differentiation in *Drosophila* (my work) resulting in a partial or 'no' heart phenotype in adult flies. Furthermore, I found that *RpS15Aa* KD leads to cardioblasts misspecifications during early cardiogenesis in the fly. Functional validation in zebrafish revealed that *rps15a* KD causes reduced cardiomyocyte numbers, diminished heart looping, and contractility, without affecting overall embryonic development (Ocorr lab). Strikingly, *RPS15A* KD-induced defects were significantly reversed by *p53* KD in hiPSC-CMs (Colas lab) or zebrafish (Ocorr lab), and by Hippo activation or *myc* KD in flies (my work). When testing for cardiac-specific RP functions, we found synergistic interactions between *RPS15A* and cardiac transcription factors, including *tinman/NKX2-5* and *Dorsocross/TBX5*, in both *Drosophila* and zebrafish (Ocorr lab and my work) suggesting similarly conserved synergistic interactions between RPs and cardiogenic genes in both zebrafish and fly hearts (Chapter 4).

Taken together, I conclude that *MYOM2, LRP2,* and RP genes play a critical role in cardiogenesis and could represent novel candidate genes (*MYOM2, LRP2*) or an emerging class of genetic effectors (RPs) in heart diseases, such as HCM, TOF, or HLHS. The discovery of disease-causing genes could help define new marker genes for early diagnostic and modeling of patient genotypes has a high potential to push the development of personalized patient care forward.

Zusammenfassung

Angeborene Herzfehler (im englischen Congenital Heart Diseases, kurz CHDs) sind die am häufigsten auftretenden Organfehlbildungen im Menschen und betreffen etwa 0,8 % aller Lebendgeburten. Dies umfasst strukturelle Fehlbildungen des Herzens, die während der embryonalen Entwicklung auftreten, sowie funktionelle Störungen wie Kardiomyopathien und Arrhythmien. Oft ist eine lebenslange Behandlung der Patienten aufgrund von Herzfunktionsstörungen im Erwachsenenalter erforderlich. Die genetischen Ursachen der angeborenen Herzfehler sind oft komplex und oligogen, und sind noch lange nicht verstanden. Derzeitig können nur etwa 25 % aller CHDs auf genetische Mutationen zurückgeführt werden. Daher besteht ein großer Bedarf, die genetischen Mechanismen zu verstehen, die zu Herzfehlbildungen führen, und der Schlüssel zur Bekämpfung von CHDs liegt höchstwahrscheinlich im Verständnis der molekularen Mechanismen, die der kardialen Entwicklung und dem Auftreten der Krankheiten zugrunde liegen. In dieser Studie nutze ich genomische Daten von CHD-Patienten in Verbindung mit dem Modellorganismus *Drosophila melanogaster*, um neue potenzielle CHD-assoziierte Gene, Gennetzwerke und Signalwege zu identifizieren.

Im ersten Teil dieser Arbeit (durchgeführt im Labor von Prof. Rickert-Sperling) konzentriere ich mich auf Myomesin-2 (*MYOM2*), einer funktionellen Komponente des M-Streifens des Sarkomers. Das Rickert-Sperling Labor hat Mutationen in *MYOM2* in Patienten mit Fallot-Tetralogie (kurz TOF) und mit hypertropher Kardiomyopathie (kurz HCM) gefunden, die keine Mutationen in einem der bereits bekannten Krankheitsgene trugen.[3,4] Wir identifizierten das bisher undefinierte Fliegen-Gen *CG14964*, welches wir myosin and myosin binding protein (kurz *MnM*) nannten, als wahrscheinliches Ortholog für *MYOM2* als auch für andere myosinbindende Proteine. Ein milder Knock-down (KD) von *CG14964* im Fliegenherzen führte zu einer Dilatation/Erweiterung des Herzens, während ein starker KD zu einer Verengung führte. Darüber hinaus zeigten genetische Interaktionsstudien einen Synergismus zwischen *CG14964* und *Mhc*, dem Fliegen-Ortholog von Myosin heavy chain 6/7 (*MYH6/7*). Insgesamt deuten diese Daten auf eine kritische Rolle von *MnM* in der Herzentwicklung hin und lassen vermuten, dass *MYOM2*-Mutationen zur Bildung von angeborenen Herzfehlern wie HCM oder TOF beitragen könnten (Kapitel 1).

Der zweite Teil meiner Doktorarbeit (durchgeführt im Bodmer Labor) konzentriert sich auf die genetischen Ursachen des hypoplastischen Linksherzsyndroms (kurz HLHS), dem schwersten aller angeborenen Herzfehler, welcher höchstwahrscheinlich oligogenen Ursprungs ist. In Zusammenarbeit mit der *Mayo Clinic* (MN, USA) wurden die Genome einer HLHS Patienten-Kohorte und der zugehörigen Eltern sequenziert (*whole genome sequencing*), und es wurde eine signifikante

Anreicherung seltener, vermutlich schädigender Genvarianten im LDL Receptor Related Protein 2 (*LRP2*) identifiziert.[5] Ein Knock-down von *LRP2* in Kardiomyozyten, die von humanen, induziert-pluripotenten Stammzellen differenziert wurden (hiPSC-CM), und Knock-downs in *Drosophila*- und Zebrafischherzen zeigten, dass der Rezeptor essentiell für die Proliferation und Differenzierung von Kardiomyozyten ist. Im Rahmen dieser Arbeit untersuche ich die Folgen eines systemischen Knock-downs von *LRP2* in der Fliege, der sowohl zu Herzerweiterungen als auch zu -verengungen führen kann. Darüber hinaus zeige ich eine genetische Interaktion zwischen dem Multi-Ligand-Rezeptor *LRP2* und Apolipoprotein B (*ABOB*) auf und weise Verbindungen mit den wachstumsassoziierten Signalwegen SHH und Wnt/wg nach. Dies deutet darauf hin, dass *LRP2* die Proliferations- und Differenzierungsvorgänge im Herzen möglicherweise durch Modulation dieser Signalwege reguliert (Kapitel 3).

In einer Familie innerhalb der HLHS-Kohorte der Mayo Clinic trat eine seltene Promotorvariante im ribosomalen Protein (RP) Gen *RPS15A* auf und Segragationsanalysen zeigten, dass diese Variante gemeinsam mit kardialer Erkrankung vererbt wurde. Des Weiteren wurde durch bioinformatische Analysen eine signifikante Anreicherung von Mutationen in RP Genen in einer Kohorte von 25 HLHS-Trios mit tödlichem Krankheitsverlauf identifiziert.

Funktionelle Genanalysen zeigten, dass ein KD von RPs die Proliferationskapazität in generischen hiPSC-CMs reduzierte (Colas Labor) und die kardiale Entwicklung in *Drosophila* beeinträchtigte, indem es zu einem partiellen oder kompletten Verlust der Herzstruktur in adulten Fliegen führte (meine Arbeit). Darüber hinaus verursachte ein *RpS15Aa* KD während der frühen Kardiogenese in der Fliege Fehlspezifikationen von Kardioblasten (meine Arbeit). Ein systemischer *rps15a* KD im Zebrafisch führte zu einer reduzierten Anzahl von Kardiomyozyten, und einer beeinträchtigten Herzschleifenbildung und Kontraktilität des Herzens, während die allgemeine Entwicklung des Embryos nicht beeinflusst wurde (Ocorr Labor). Bemerkenswerterweise wurden Defekte, die durch einen *RPS15A* KD induziert wurden, durch einen KD von *p53* in hiPSC-CMs (Colas Labor) und im Zebrafisch (Ocorr Labor) beziehungsweise durch Hippo-Signalweg-Aktivierung oder *myc* KD in Fliegen signifikant abgemildert (meine Arbeit). Des Weiteren konnten synergistische Interaktionen zwischen *RPS15A* und den kardialen Transkriptionsfaktoren *tinman/NKX2-5* und *Dorsocross/TBX5* in *Drosophila* und Zebrafischen nachgewiesen werden (Ocorr Labor und meine Arbeit), was auf ähnliche konservierte, synergistische Wechselwirkungen zwischen RPs und kardiogenen Genen in Zebrafisch- und Fliegenherzen hindeutet (Kapitel 4).

Zusammenfassend deuten die Ergebnisse auf eine wichtige Rolle von *MYOM2, LRP2* und *RP* Genen in der Kardiogenese hin, welche somit neue höchst relevante Kandidatengene für Herzerkrankungen wie HCM, TOF oder HLHS darstellen. Die Identifizierung krankheitsverursachender

Gene könnte helfen, neue Markergene für die Frühdiagnostik zu definieren, außerdem hat die Modellierung von patientenspezifischen Genotypen in der Fliege ein hohes Potenzial, die Entwicklung personalisierter Medizin voranzutreiben.

1. Introduction

1. 1 Genetics underlying Congenital heart diseases

Congenital heart diseases (CHDs) are the most common human birth defect, affecting approximately 0.8 % of all live births.[1] CHDs comprise a heterogenous collection of structural abnormalities of the heart as well as functional disorders such as cardiomyopathies and arrhythmias. Treatment is often required throughout life due to impaired cardiac function, e.g. cardiac arrhythmias or heart failure, even after surgery.

CHD is caused by abnormal cardiogenesis, which is a complex developmental process involving multiple interlinked and dose-depended pathways.[6] While 80-85 % of CHD cases are caused by unidentified or multifactorial causes, including genetic, epigenetic, and environmental causes[7–9], epidemiological studies revealed that 25 % of cases can currently be explained by genetic variations.[2] However, most CHD cases cannot be attributed to a single gene disorder and do not follow Mendelian inheritance ("missing heritability") suggesting an oligogenic origin of CHD and the interaction of multiple genetic and environmental factors is still considered as the primary etiology of unexplained CHD cases[7,8,10] A recent case study in humans nicely demonstrated that a combination of rare, inherited heterozygous mutations (among them cardiogenic transcription factor NK2 Homeobox 5 (*NKX2-5*)) can cause cardiac anomalies.[11] However, such familial cases are rare and consequently, despite evolving technologies, the identification of novel causal genes involved in CHD remains challenging.

One further layer of complexity is added to the genetics of CHD since the same genetic variants can produce a spectrum of different heart malformations and can be even present in controls[12–14] (i.e. *NKX2-5*).[15–17] This further substantiates the hypothesis that genetic risk factors or modifier alleles contribute to the manifestation of CHD. In this context, Akhirome et al. emphasize the importance of identifying genetic interactions to unravel the oligogenic basis of CHD and suggest system genetic approaches in model systems.[18]

Other studies propose a slightly different (but not opposing) concept for complex CHDs by showing that previously identified CHD risk factors functionally converge in protein networks.[19] This means that different CHD risk factors do not directly impact the same genes and molecules, but rather impact various different genes, which participate in the same discrete heart development network. This suggests a complex pattern of functional interactions between genomic variants and environmental factors that modulate critical biological networks/systems during heart development and where network perturbance can lead to disease. It was further proposed that this concept might explain the "missing heritability" in many CHDs.[19]

Since the first report on genetics in CHD in 1949[20], much research has been done to understand the heritability and genetic causes underlying CHD. Before 1940 more than 90 % of infants with complex CHDs died well before reaching adulthood. Notably, with advances in pediatric cardiology and cardiac surgery, >90 % of CHD patients survive to adulthood, therefore understanding the inheritance and genetics underlying CHD has become of increasing clinical importance.

In the early research around the 1990s, mainly familiar disease cases were studied using linkage analysis and candidate gene approaches. With these early technologies, many CHD-associated genes were identified including cardiac transcription factors *NKX2-5*[21], GATA Binding Protein 4 (*GATA4*)[22], T-box 5 (*TBX5*)[23], T-box 20 (*TBX20*)[24], and *NOTCH1* signaling.[25] However, most of these variants found were family-specific and could not explain the majority of CHD cases. For this reason, the focus of research shifted towards common variants utilizing genome-wide association studies (GWAS) with the hypothesis that multiple common variants in small effect size genes may act together in causing disease.[26] This led to the identification of a number of genomic regions, including CHD risk factors for Tetralogy of Fallot (TOF)[27] or atrial septal defects (ASDs)[28], but these associations still leave a large percentage of unexplained disease cases emphasizing the complexity of CHD. To identify more common genetic variants in CHD large cohorts with well-defined phenotypes are required, however, the phenotypical variability combined with the presence of genetic modifier genes makes it challenging. Nowadays, large-scale genomic initiatives including massive parallel sequencing (whole-exome sequencing or whole genome sequencing) are performed to cover both common and rare variants.

According to a statement from the American Heart Association in 2017, single-gene disorders are found in 3-5 % of cases, gross chromosomal anomalies/aneuploidy in 8-10 %, and pathogenic copy number variations (CNVs) in 3-25 % in patients with syndromic CHD and 3-10 % with isolated CHD (reviewed in Pierpont et al.[29]). To date, the largest genetic study on CHDs includes 2,871 CHD probands and provides evidence that 8 % of cases are based on *de novo* autosomal dominant variations and 2 % on inherited autosomal recessive variations.[30] There are some *de novo* mutations, CNV, and other genetic variants found to be not only associated with CHD but with multiple developmental disorders (commonly referred to as the genetic burden principle). Such cases are classified as syndromic CHD and comprise approximately 13 % of CHD cases.[31] One example is a linkage of the heart and brain based on data indicating shared genetic mechanisms contributing to both CHD and neurodevelopmental disabilities.[32] However, the following discussions concentrate on non-syndromic CHD, which is the main focus of this thesis.

In summary, the genetic heterogeneity of CHD diseases necessitates large-scale genomic and functional analysis of potential CHD-associated variants in model systems to understand the genetic architecture of CHD and the underlying regulatory mechanisms.

1.2 Human heart development

The heart is the first organ to develop and function during embryonic development. It begins to beat as soon as ca. 22 days after fertilization, emphasizing its critical function in distributing blood with nutrients and oxygen through the developing baby.[33] In the full-grown heart, oxygen-deprived blood from the body enters the heart at the right atrium (RA) and is pumped by the right ventricle (RV) towards the lungs. The oxygenated blood, in turn, enters the left atrium (LA) and is pumped by the left ventricle (LV) via the aorta into the rest of the body. The different components of the heart, including the sinus node and atrioventricular node, ensure an efficient contraction and relaxation of the different heart chambers.

The heart is largely derived by the mesoderm; however, some parts, such as the cushions of the outflow tract, have a contribution from the ectoderm-derived cardiac neural crest.[34] In specific, the heart is derived from two spatially and temporally overlapping cardiac progenitor populations, which arise from the most anterior lateral region of the splanchnic mesoderm forming the first and secondary heart fields (FHF, SHF).[35] Early in development, the FHF forms two crescent-like cardiogenic tubes (Figure 1), already expressing heart-specific genes such as *NKX2-5.*[36,37] Folding of the cardiac crescent towards the ventral midline results in the formation of the myocardial primitive heart tube (Day 20 post fertilization).[38] At this stage, the heart tube shows a specific gene expression pattern separating it into an anterior (ventricular) and posterior (atrial) region. Next, the heart undergoes a complicated looping process tightly regulated by genes essential for left-right programming (Day 24-35). During these processes, progenitor cells from the SHF are progressively added to the heart driving heart tube extension. The cardiac chambers grow out and form the looped heart tube in a process named ballooning[39] and eventually, septa and valves are formed to control blood flow in the developing heart. Descendants of the SHF are found in the right ventricle, both atria and the outflow tract (OFT), while descendants of the FHF give rise to the left ventricle and a portion of the left and right atrium as demonstrated in mouse cardiogenesis in Figure 1.[2,35]

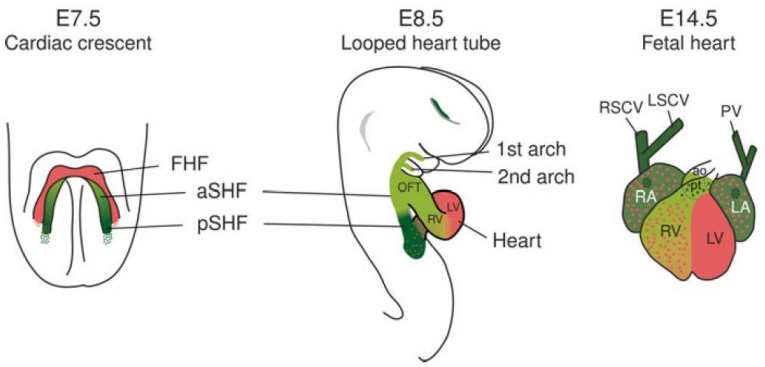

Figure 1: The developing mouse heart. Schematic of a developing mouse heart showing contribution of the first (FHF, red) and second heart field (SHF, aSHF = anterior SHF, pSHF = posterior SHF). In the mouse embryo, the early heart tube is formed around embryonic day (E) 8, equivalent to 3 weeks of human gestation. *Abbreviations: LA* left atrium, *RA* right atrium, *LV* left ventricle, *RV* right ventricle, *OFT* outflow tract, *ao* aorta, *pt* pulmonary trunk, *PV* pulmonary vein, *RSCV* right superior caval vein, *LSCV* left superior caval vein. Graphic from "Congenital heart Diseases: The Broken heart", S. Rickert Sperling, RG Kelly, DJ Driscoll.[2]

1.3 Tetralogy of Fallot and Hypertrophic Cardiomyopathy

Tetralogy of Fallot (TOF) is the most common cyanotic CHD, accounting for 4-8 % of congenital cardiac defects. It comprises four cardiac characteristics: (1) ventricular septal defect (VSD), (2) right ventricular outflow tract obstruction, (3) an overriding aorta, and (4) RV hypertrophy. As a consequence of the right-to-left shunt through the VSD and the decreased pulmonary blood flow, oxygen-poor blood is pumped from the heart to the rest of the body. Surgical cardiac repair is usually performed between 3 – 12 months of age and involves closure of the VSD and relief of the RV outflow tract obstruction. Although the surgery is often well tolerated during childhood, there is an ongoing risk of arrhythmia and late sudden death later in life and consequently, TOF patients need clinical treatment throughout life.[40]

The cause of TOF is elusive because of its multifactorial etiology, including genetic, epigenetic, and environmental risk factors. About 25 % of cases are associated with chromosomal abnormalities or syndromic disorders[41] and the risk of familial reoccurrence is about 3 %.[41] Genetic variants identified in isolated TOF cases include rare single-gene defects[42–44], copy number variations (CNVs)[45–47], or associations with common single nucleotide polymorphisms.[28] Because of the non-Mendelian patterns of inheritance, a polygenic genetic architecture has been hypothesized, where gene network disturbance results in a common phenotypic expression.[2,4,48] So far, only a few genes like transcription factor GATA4[49,50], NKX2-5[44,51], TBX5[43,52] and T-box 1 (TBX1)[51,53,54], Forkhead Box C2 (FOXC2)[54], or NOTCH ligand Jagged 1 (JAG1)[42,55] have been implicated in TOF. The Rickert-Sperling lab further identified several rare and private mutations in genes essential for apoptosis, cell growth, sarcomere assembly, neural crest, and secondary heart field that may contribute to the development of TOF.[4] In this study, mutations in sarcomeric genes such as Myosin Heavy Chain 7 (*MYH7*) and Myosin Binding Protein C (*MYBPC3*) (single TOF cases), as well as titin (*TTN*) and myomesin-2 (*MYOM2*) (multiple TOF

cases), have been identified.[4] Further evidence suggests that DNA methylation plays a role in TOF since methylation levels of *NKX2.5* and *HAND1* was found elevated in TOF patients.[56] These two genes were previously reported to be downregulated in TOF patients.[57]

In contrast to TOF, which is characterized by the four distinct features mentioned above, Hypertrophic Cardiomyopathy (HCM) mainly refers to defects of left-sided heart structures, such as the LV. HCM is a heterogeneous disease with variations in physiological manifestation and genetic underpinnings, which predominantly causes LV hypertrophy and outflow tract obstruction.[58,59] HCM can affect individuals of any age, but early onset of the disease is rather rare.

Cardiomyopathies in general are thought to be monogenic diseases, meaning that the mutation in one main driver gene causes the disease. However, the presence of mutations in two disease-causing genes is relatively frequent (3-5%) and is associated with more severe HCM phenotypes, including younger onset of disease or a higher risk of life-threatening arrhythmias.[2,60–63] In about 50-60 % of cases, a pathogenic gene mutation can be identified, which are mainly found in sarcomeric genes, such as *MYBPC3* or *MYH7*.[62,64–66] Despite alterations on the genomic level, alternative splicing events were reported in sarcomere genes, such as troponin T (*TNNT1* and *TNNT2*), troponin I (*TNNI1* and *TNNI3*) and *MYH7* in patients with ischemic cardiomyopathy[67] as well as TOF.[68] Although HCM and TOF exhibit different phenotypical manifestations, both diseases seem to be primarily based on genomic and transcriptomic alterations in sarcomeric genes.

The Rickert-Sperling lab identified several mutations in sarcomeric M-band protein MYOM2 in TOF and HCM patients[3,4], who do not exhibit mutations in the already known disease genes (for more details see result section, Chapter 1). As part of my thesis, I studied the role of *MYOM2* as a potential novel CHD candidate gene, using *Drosophila melanogaster* as a genetic model to evaluate its potential role in the heart.

1.3.1 Sarcomeric M-band protein myomesin-2

The M-band is located in the center of the sarcomere and arranges the thick filaments (myosin and associated proteins) into the A-bands (**Figure 2**). The elastic web of M-band filaments is suggested to stabilize the M-band and functions as the major absorber of mechanical stress sensor of force imbalances during muscle contraction (reviewed in Lange et al., 2020[69]). The members of the myomesin family, including myomesin, encoded by *MYOM1*[70], M-protein/myomesin-2, encoded by *MYOM2*[71], and myomesin-3, encoded by *MYOM3*[72] in humans, are believed to crosslink myosin and titin in the sarcomere[73], based on the observation that myomesin as well as myomesin-2 bind myosin and titin in biochemical assays.[73–75] All three myomesin proteins share a common protein structure with a unique head domain followed by twelve immunoglobulin and fibronectin type III domains.[72] Myomesin dimerizes in an antiparallel fashion through its C-terminal Ig domain, while its N-terminus

anchors it to myosin.[76,77] Similarly, Myomesin-3, but not myomesin-2, has a confirmed dimerization ability of the C-terminus.[72]

The expression pattern of the different myomesin proteins depends on muscle type and stage of development. While myomesin is constitutively expressed in all striated muscles, myomesin-2 tends to be found in muscle types that are exposed to higher forces (e.g. fast skeletal and cardiac muscle in mammals).[78,79] On the other hand, sarcomeres in slow fibers and the embryonic heart mainly harbor the myomesin splice variant EH-myomesin.[78] At later fetal stages (mouse embryonic day 14.5), myomesin-2 expression is switched on, and around birth, EH-myomesin gets downregulated while myomesin-2 gets upregulated.[80] Myomesin-3 is found mainly in intermediated speed fibers of skeletal muscles but is also detected in the human heart.[72,80]

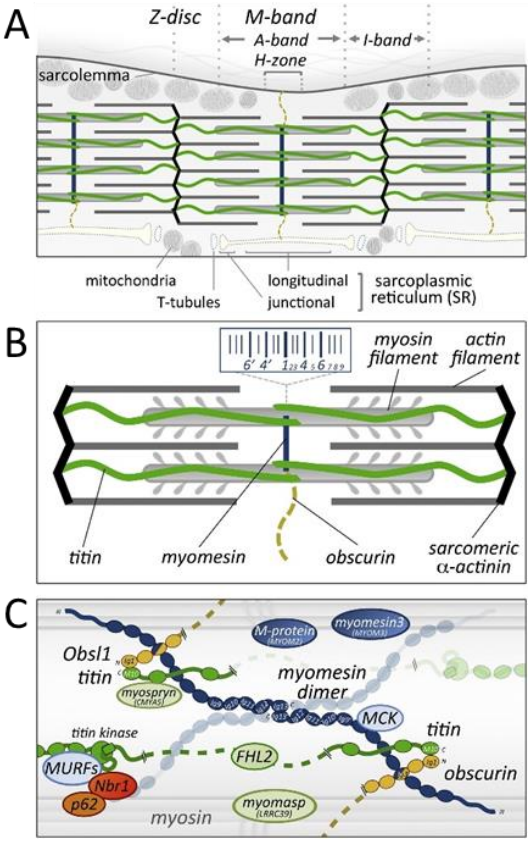

Figure 2: Schematic representation of the sarcomere. (A-B) Thick filaments (myosin and associated proteins) are depicted in grey and thin filaments (actin and associated proteins) in green; Z-discs are shown in black, the M-band in blue and obscurin in yellow. **(C)** Model of the molecular arrangement of the M-band. Only myomesin (not myomesin-2/-3) is depicted. Adapted from Lange et al. 2020.[69]

To date, all molecular evidence available suggests that myomesin-mediated crosslinking is crucial and abnormalities in the protein family are considered to be a cause for myopathies, such as Dilated Cardiomyopathy (DCM)[80,81], Hypertrophic Cardiomyopathy (HCM)[82,83], or myotonic dystrophy (DM1).[84] For example, re-expression of EH-myomesin in later stages was associated with DCM in mouse models and human patients as a consequence of alternative splicing - a common response in cardiomyopathy.[80,85] Furthermore, missense mutations in *MYOM1* caused decreased dimerization ability and thermal stability of its encoded protein, which was involved in HCM progression.[82] Knockdown of *MYOM1* by siRNA in neonatal rat cardiomyocytes led to a failure of M-band formation and disintegration of myofibrils, suggesting an important role of *MYOM1* for myofibril assembly and stabilization.[86] A recent study in human embryonic stem cells-derived cardiomyocytes further showed that knockout of *MYOM1* using CRISPR technology led to abnormal cell morphology, atrophic remodeling, and myocardial dysfunction; the latter is likely caused by impaired calcium homeostasis.[87]

However, to date, no knockout animal model or null mutant for any of the myomesin genes was reported, which is needed to comprehensively study the genotype-phenotype relationship. In an

indirect approach, the exons of titin which encode the binding site of titin and myomesin were deleted in the mouse heart, which led to the disintegration of myofibrils and cardiac atrophy.[88] This suggests that the proper linkage between titin and myomesin is essential for normal heart morphology and sarcomere integrity.

Overall, the role of the myomesin protein family in (cardio)myopathy is not well understood. The field needs clear functional genotype-phenotype studies using *in vivo* models to identify the underlying mechanism of how myomesin mutations or alternative splicing can lead to disease manifestation. The results of my studies on *MYOM2* are presented in Chapter I "Identification of myomesin-2 as a candidate gene in hypertrophic cardiomyopathy and Tetralogy of Fallot".

1.4 Hypoplastic Left Heart Syndrome

Hypoplastic left heart syndrome (HLHS) represents the most lethal congenital heart disease accounting for 2-3 % of all CHD cases.[89,90] It is characterized by a severely underdeveloped left ventricle, aorta and mitral valves, and aortic arch.[91] Babies born with HLHS are not able to efficiently pump oxygenated blood to the rest of the body and without intervention, the syndrome is universally fatal within the first week after birth. Patients have to undergo a 3-step highly invasive surgery: the Norwood procedure in the neonatal period, the Glenn procedure at 4-6 months of age, and the Fontan procedure at 3 years of age. During the different operations, the heart is stepwise remodeled into a two-chambered heart, with the right ventricle serving as the systemic ventricle.[92] However, these surgically reconstructed patients still need treatment throughout life, and many develop heart failure later in life for ill-understood reasons, which then requires heart transplantation as the only therapeutic solution.

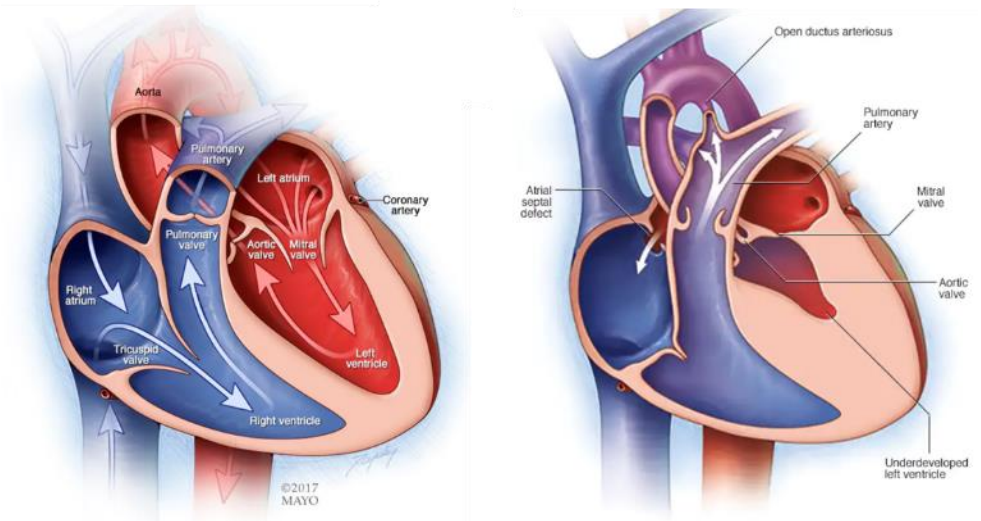

Figure 3: Hypoplastic Left Heart Syndrome. Morphology of the healthy heart (left) and an HLHS heart (right), showing underdevelopment (hypoplasia) of the left side of the heart — including the aorta, aortic valve, left ventricle, and mitral valve. Source: Mayo Clinic, www.mayoclinic.org/diseases-conditions/hypoplastic-left-heart-syndrome/symptoms-causes/syc-20350599.

While there is strong evidence for a genetic component based on its familial association with left-sided obstructive CHD[93,94], the disease mechanisms of HLHS are still poorly understood. Segregation analysis in HLHS families[94] and GWAS of larger cohorts[93] do not have sufficient power to identify HLHS-associated genes with small to moderate effect size and so far, only a few genes are implicated as contributors of HLHS, such as *NOTCH1*[95], ETS Proto-Oncogene 1 (*ETS1*)[96], *NKX2-5*[15], Myosin Heavy Chain 6 (*MYH6*)[97], and *GATA4*.[15,98] In addition, the phenotypic variability of HLHS, the largely sporadic occurrence (lack of inheritance) and the diversity of genetic loci, which were previously reported to be associated with the disease, suggest that HLHS is likely genetically heterogeneous and of oligogenic and multifactorial etiology, including genetic, epigenetic and environmental factors.[99,100]

The mechanisms underlying HLHS formation are not clear and there is controversy in the field regarding the HLHS pathogenic mechanisms. The most common theory assumes that the hypoplastic ventricle arises as a consequence of hemodynamic effects of restricted blood flow across the mitral valve during a critical step of ventricular growth and development during cardiogenesis ("no flow – no grow" theory).[91,100] However, recent studies propose additional primary defects in proliferation and differentiation of ventricular cardiomyocytes (CMs) as a root cause. In humans, Gaber et al. showed that LVs from patients with HLHS have cardiac damage associated with fewer CMs than in LVs from healthy subjects.[101] In a collaborative effort, the Bodmer lab (including my contribution) further provided evidence for CM-intrinsic proliferation defects in HLHS patient-derived iPSC-CMs.[5] Another recent study shows that hiPSC-CMs derived from HLHS patients with early right ventricle failure exhibit impaired contractility.[102]

In the *Ohia* HLHS mouse model, model-specific mutations in Sin3A Associated Protein 130 (*Sap130*) and Protocadherin Alpha 9 (*Pcdha9*) caused intrinsic CM proliferation and maturation defects underlying the left ventricle hypoplasia.[103] However, the penetrance of disease was only 26 %, suggesting additional genetic modifiers exist, which is in line with an oligogenic nature of the disease. Note, that although the majority of *Ohia* mutants displayed HLHS, some of the mutants presented double-outlet right ventricle which do not uniformly reflect human HLHS phenotypes.[100]

An overall unifying mechanism is missing of how the genetic heterogeneity of HLHS converges in common perturbations of sequential cellular processes involved in heart morphogenesis and how these contribute to disease manifestation. To identify and functionally evaluate genes potentially associated with CHD/HLHS, the Bodmer lab, in collaboration with the Colas lab, Ocorr lab, and the Mayo Clinic established an integrated analysis platform in multiple genetic model systems, which combines WGS patient sequencing coupled with systematic functional screening in patient-derived hiPSC-CMs, *Drosophila* and zebrafish *Danio rerio*.[5] As part of my Ph.D. thesis, I contributed to this

pipeline studying LDL Receptor Related Protein (*LRP2*) and ribosomal proteins as potential HLHS/CHD candidate genes in the fly heart model. The results of my studies are presented in Result Chapter III and IV of this work.

1.4.1 LDL Receptor Related Protein 2

LDL Receptor Related Protein 2 (LRP2), also called megalin, is a member of the LDL receptor family and functions as a multiligand receptor for e.g. fibroblast growth factor (FGF) 8[104] or bone morphogenic protein (BMP) 4.[105] LRP2 plays an important role in embryonic development and receptor dysfunction was shown to lead to severe malformation in humans and animal models, including overgrowth of the eye globe[106,107] as well as forebrain malformation or renal reabsorption defects.[108,109] In this context, LRP2 has been shown to act as an auxiliary receptor for sonic hedgehog (SHH) and promotes or inhibits signaling in a cellular- and context-depended manner. In the neuroepithelium, for example, LRP2 acts as a co-receptor to Patched1 to promote SHH signaling, which regulates patterning of the ventral midline of the forebrain.[110] In the eye, on the other hand, it functions as a clearance receptor for SHH, thus antagonizing growth promoting signals in the retina.[111]

LRP2 is expressed throughout development and adult stages and was also found expressed in mesothelial cells of the pericardial cavity and in the neural crest.[112,113] With the identification of a *de novo* mutation in *LRP2* in a large CHD patient cohort study (PCGC), *LRP2* was first implicated in CHD.[8] Additional evidence came from an EDU-induced mutagenesis study in mice, in which *Lrp2* mutants presented cardiac outflow tract (OFT) defects.[114] In another study, *Lrp2* null mutant mice were generated, which displayed a range of cardiac defects, including aortic arch anomalies, persistent truncus arteriosus, ventricular anomalies, ventricular septal defects, overriding of the tricuspid valve, and marked thinning of the ventricular myocardium, along with other developmental defects.[115]

All these data point towards a crucial role of LRP2 for cardiogenesis, however further studies are needed to reveal the underlying mechanisms and signaling pathways involved in *LRP2*-mediated cardiac defects. So far, LRP2 had not previously been linked to HLHS within curated bioinformatic networks. In this work, I used the fruit fly *Drosophila melanogaster* to characterize *LRP2* gene function in the fly heart and test for genetic interactions between *LRP2* and bioinformatical prioritized signaling pathways (more details in results, Chapter III) to identify the mechanism of action of *LRP2* during cardiogenesis.

1.4.2 Ribosomal proteins in heart disease

The eukaryotic ribosome consists of four ribosomal RNAs (rRNAs) and ~80 core ribosomal proteins (RPs) that catalyze protein synthesis.[116,117] The coordinated function of RPs is represented well in *Drosophila Minute* mutants, which harbor mutations in various RP genes and show a shared

phenotype characterized by developmental delay, reduced fertility, short thin bristles, and recessive lethality.[118,119] *Drosophila* has 88 genes encoding 79 different cytoplasmic ribosomal proteins (CRPs) and 75 nuclear-encoded mitochondrial ribosomal proteins (MRPs).[118] According to Marygold and colleagues, the 79 *Drosophila* CRPs correspond with all 79 human CRPs, while MRPs are more divergent between species.[118] Mutations in 66 out of 88 identified CRP genes caused classic *Minute* traits and have been attributed to alterations in translational processes. However, additional specific phenotypes, i.e. abnormally large wings, were observed in several RP mutant flies.[118]

RPs were assumed to be non-selective and ubiquitous regulators of translation, which includes the events during embryonic development. However, despite the manifestation of *Minute*-like features in vertebrates (delayed development, small body size, recessive lethality), recent studies suggest that, like in *Drosophila*, loss-of-function mutations in specific RPs lead to tissue and cell type-specific phenotypes.[120] For example, in mice, loss of RpL38 and RpL27 cause skeletal homeotic transformations[121] and cerebellar ataxia[122], respectively.

Importantly, an increasing number of variants in RP genes have been linked to CHD in humans; most notably in ~30% of patients with Diamond-Blackfan anemia (DBA)[123], which is a ribosomopathy characterized by hypo-proliferative, proapoptotic erythropoiesis. Moreover, the Bodmer lab (including my contribution) recently identified the RP gene *RpL13* as a novel potential candidate gene involved in CHD pathogenesis from a screen for *de novo* copy number variations (CNVs) in 167 patients with CHD.[124] Interestingly, KD of *RpL13* in embryonic cardiac progenitors in the fly leads to a failure of cardiac differentiation and remodeling in later cardiogenesis and results in a loss of the majority of the fly heart.[124] However, KD of *RpL13* at post-embryonic stages, during larval growth, has less of an impact on cardiac remodeling and establishment of adult heart function, suggesting an involvement of this RP gene in early programming for cardiac differentiation.[124] In addition, a previous study described cardiac dysfunction in flies haploinsufficient for a subset of *Minute*-associated RPs.[125]

It is still an open question as to why ribosomopathies, where one would expect to have global and in fact lethal effects on a developing organism, exhibit tissue-specific defects, like in the heart, as observed in DBA or *Minute* mutants. Casad and colleagues hypothesized that the heart phenotypes in *Drosophila* might occur due to sensitivity of heart size and function to a decrease in translational capacity or due to potential extra-ribosomal functions important for the integrity of the heart.[125] A recent study showed that RP haploinsufficiency in the developing mouse limb bud activates a common TP53 cascade, which led to tissue-specific changes of the translatome and which might confer the tissue-specific phenotypes often observed in ribosomopathies.[126]

Further investigation is needed to unravel the mechanisms and pathways regulating cardiac phenotypes following ribosomal protein loss and to substantiate a potential contribution of RP mutations in CHD manifestation, which I address further in Result Chapter IV.

1.5. *Drosophila melanogaster* as a genetic heart model

Similar to vertebrates, *Drosophila* owns an organ responsible for the circulation of hemolymph (the equivalent of blood in insects) through the body. The *Drosophila* heart, also known as the dorsal vessel, forms a tube, which although structure-wise very different from the four-chambered human heart, is comparable to the vertebrate heart at early stages.[127]

The genetic networks involved in cardiac development and function are well conserved between *Drosophila* and vertebrates[128,129] and over the years *Drosophila* became well-established as a genetic heart model organism. For instance, the homeobox transcription factor *tinman (tin)*, the first and essential cardiogenic regulator, was first identified in *Drosophila* and led to the discovery of the mammalian homologue *NKX2-5*.[130,131] Importantly, about 75 % of disease-causing genes are evolutionary conserved between humans and fly.[132] The fruit fly heart can be severely compromised without causing lethality, making it possible to manipulate and study critical factors of heart development since with its open tracheal system and open circulatory system, the heart is not required for oxygen supply to the rest of the body. Another major advantage is its lack of genetic redundancy, which is the existence of multiple genes that perform the same function, and which often occur due to gene duplications. Inactivation of one of these genes would have little effect by itself since the other genes compensate for its loss. Thus, the non-redundancy in *Drosophila* makes it easier to study and establish genotype-phenotype relationships as well as gene networks. Combined with its rapid generation time, this makes *Drosophila* highly suitable for high-throughput screening of disease-candidate genes.

Part of the power of *Drosophila* lies in its genetic tool kit, which allows performing multiple gene knockdowns simultaneously and which is more challenging and time-consuming in other model organisms such as the mouse. This opens the possibility of system genetic approaches to probe for genetic interactions between potential CHD genes (in a high-throughput manner), addressing one of the current needs in the field to unravel the oligogenic nature underlying most CHDs.

1.5.1 *Drosophila* Heart Formation

The *Drosophila* heart is built during early embryogenesis and consists of two single layer rows of cardioblasts opposing each other forming a luminal space (**Figure 4**). The embryonic heart is located between thoracic segment T3 and abdominal segment A7 and can be divided into the morphological distinctive thinner aorta (anterior) and the thicker heart proper (posterior). The heart is composed of two cell types: cardioblasts (CBs), which differentiate to contractile cardiomyocytes (CMs) and ostia cells (the future hemolymph inflow tracts), and of the non-myogenic pericardial cells (PCs), which are flanking the CBs on each side and function as nephrocyte-like-cells involved in ultrafiltration.[133] Each heart tube segment contains two rows of six CBs, from which two express *seven-up* (*svp*) (future ostia cells – inflow tracts) and the remaining four express *tinman* (future CMs – 'working myocardium') (**Figure 4**).[134] These processes are highly regulated during heart formation by a combinatorial network of signaling pathways and spatio-temporal expression of transcription factors, which specifies the cardiac progenitors. Both cell types (CBs and PCs) originate from the dorsal mesoderm.

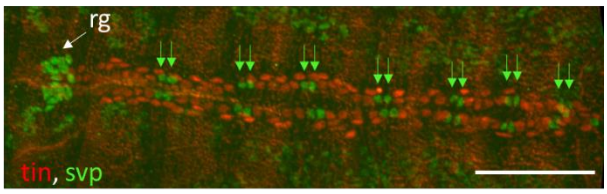

Figure 4: The embryonic fly heart. Stage 17 embryo heart stained for Tinman and Seven-up. rg = ring gland. Scale bar = 50 µm.

Very early in embryogenesis, the localization of the maternally contributed Dorsal protein activates bHLH transcription factor *twist* and zinc-finger transcription factor *snail*, which leads to the specification of the mesoderm domain.[135,136] At the beginning of gastrulation, the presumptive mesoderm then invaginates into the interior of the embryo and spreads dorsally to form a monolayer of cells close to the ectoderm (**Figure 5** A-C). The mesodermal spreading is regulated by FGF signaling, specifically FGF ligands pyramus and thisbe, which bind to the receptor Heartless.[137,138] The mesoderm receives inductive signals from the adjacent ectoderm (Wingless (wg/Wnt) and Decapentaplegic (Dpp/Bmp))[139], which in combination with mesoderm-endogenous transcription factors, coordinate the first subdivision of mesoderm into cardiac versus visceral mesodermal fate (reviewed in [133]). Those cells which migrated the most dorsally on either side of the embryo (in the trunk region) become specified as heart progenitors (**Figure 5** D) and undergo a number of cell specifications under the control of Notch signaling and its downstream effectors[139–142] and a highly coordinated genetic network of cardiac transcription factors including Tinman/NKX2-5, TBX and GATA family members (at stage 11-12). During this process, some cardiac progenitor cells divide symmetrically (progenitors of *tinman* CM lineage), while others undergo asymmetric cell division (progenitors of the *svp* or *eve* lineage), where cell fate decisions are depended on the absence or presence of Notch activity.[141] At this stage, the heart progenitors align to form two rows of bilaterally symmetric cells (100 µm apart)

and during dorsal closure the contralateral heart progenitors start to migrate towards each other at the dorsal midline to form the heart tube (starting from stage 13 of embryogenesis until stage 16) (**Figure 5** F-G). This migration process is analogous to the primitive heart tube formation in vertebrates before it undergoes complicated looping processes (**Figure 5** I).[143,144] At the end of embryogenesis, the heart starts beating.

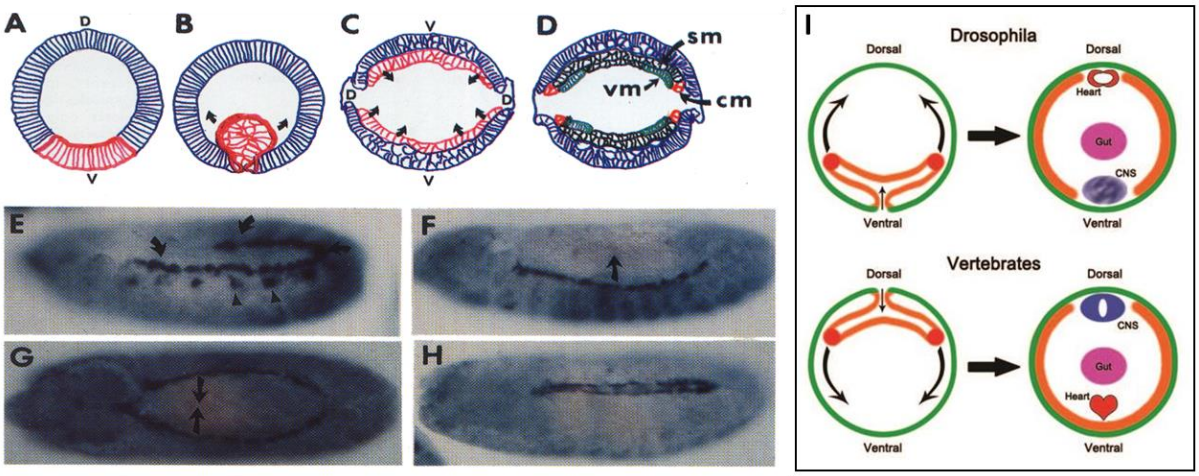

Figure 5: Gastrulation and heart formation in *Drosophila*. (A-D) Cross section through the embryo during gastrulation. Mesoderm is marked in red in A-C. **(A)** Blastoderm stage. **(B)** Early gastrula with mesoderm invaginated inside the embryo along the ventral midline. **(C)** Late gastrula with mesoderm flattened and spread dorsally (D = dorsal, V = ventral). **(D)** Embryo after subdivision of mesoderm into cardiac versus visceral mesodermal fate (sm = somatic mesoderm, vm = visceral mesoderm, cm = cardiac mesoderm). **(E-H)** Embryos in side-view (E, F) or dorsal view (G, H) labeled for Tinman (hybridization reaction with digoxigenin-labeled nucleotide probe). **(E)** Embryo around stage 11 with Tinman expression in heart precursor cells (arrows) and some remaining expression in vm (arrowheads). **(F)** Embryo around stage 12: Tinman expression exclusive in cardiac mesoderm on either side of the embryo. **(G)** Embryo stage 13-14: Contralateral heart progenitors migrate towards each other at the dorsal midline to form the heart tube. **(H)** Embryo at stage 16-17: Two rows of Tinman positive cells form the maturing heart. **(I)** Hearts of *Drosophila* and vertebrates originate from equivalent embryological positions, but the dorsal-ventral axis is reversed. In both organisms, the heart progenitors migrate towards each other to form the primitive heart tube. Images from Rolf Bodmer, 1995.[143]

The genetics and signaling cascades underlying cardiac specification are relatively well studied. As mentioned before, one of the first transcription factors identified to be essential for the cardiac specification is Tinman (NKX2-5 fly ortholog), which when mutated leads to a complete heart loss.[130] Initially, the expression of *tinman* is under control of *twist* and is broadly expressed in trunk mesoderm reflecting the *twist* distribution pattern.[131] However, after mesoderm invagination and during formation of the dorsal mesoderm, *tinman* comes under the control of a separate enhancer (*tin*D) and is directly responsive to Decapentaplegic (Dpp) and finally, at embryonic stage 10, *tinman* expression is restricted to CBs only.[145] Another critical cardiogenic factor is TBX transcription factor *Dorsocross* (*Doc*), which expression overlaps with the dorsally-restricted *tinman* expression in early stages. Together, both proteins[146] induce the expression of *GATA4* fly ortholog *pannier*[147], which itself is required for maintaining expression of *tinman* and *Dorsocross*. The combined co-expression of *tinman, Dorsocross,* and *pannier* leads to the activation of specific target genes, including *seven-up/COUP-TP, midline/TBX-20,* and myocyte enhancer factor 2 (*Mef2/MEF2)*, thereby promoting

progressive delineating and specification of heart progenitors. The regulatory network controlling early cardiogenesis and the downstream signaling cascades initiated by *tinman, Dorsocross,* and *pannier* has been described in great detail (for a detailed review see Bodmer and Frasch, 2010[132] or Reim and Frasch, 2005[146]). One important target of Tinman is the bHLH transcription factor *Hand* which is active from stage 12 of embryogenesis and throughout development in all CBs and PCs.[148,149] The *Hand* enhancer is often utilized for cardiac-specific expression of genes or RNA interference (RNAi) constructs.

During larval stages, the animal grows from 0.5 mm (embryo/1st instar larva) to ca. 3-4 mm (3rd instar larva). At the same time, the heart tube elongates and increases its heart lumen volume. These processes are exclusively mediated by cell growth but not cell proliferation, implying that the larval heart has the same number of CBs as the embryonic heart (104 cardiomyocytes).[150] During pupal stages, the heart tube undergoes metamorphosis and with this extensive morphological and functional changes. Most of the former heart proper of the heart histolyzes while the larval aorta widens and is remodeled into the future adult heart consisting of 84 cardiomyocytes. During this process, the steroid hormone ecdysone plays an important role, which regulates the expression of Hox gene Ultrabithorax (*Ubx*) and abdominal A (*abdA*).[151] New outflow tracts (ostia) develop from the *svp*-positive CBs and three new intracardiac valves are formed. In addition, a layer of ventral longitudinal muscles (VLMs) associated with the heart tube forms along its surface, originating through *org-1* dependent lineage reprogramming from a subset of syncytial alary muscles.[152–154] Finally, neuronal innervation of the heart occurs during pupal stages.[155] In contrast, the larval heart lacks innervation, suggesting that the cardiac impulses are solely of myogenic origin.[156]

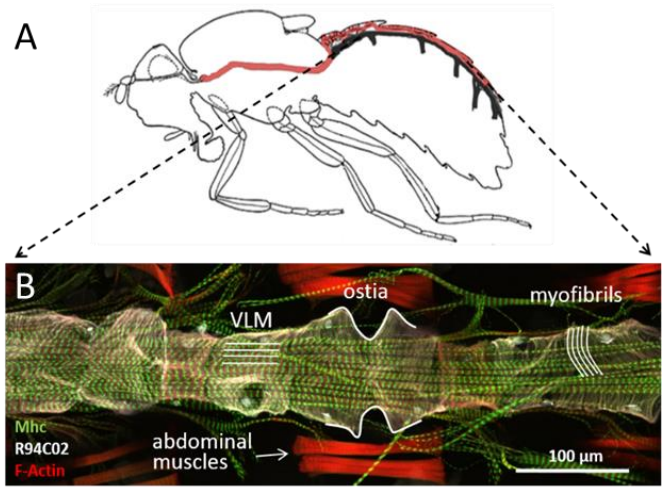

Figure 6: The adult fly heart. (A) Adult fly with dorsal vessel (indicated in red) and **(B)** a 3-week-old fly heart stained for Mhc (myosin heavy chain) and F-Actin. *R94C02* is a heart enhancer, from which tdTomato is specifically expressed in the heart (for more information see section 1.5.4 and 4.3.2). Structural features of the heart are highlighted in white. VLM = ventral longitudinal muscles

1.5.2 Conservation of heart development and function in *Drosophila*

Drosophila has emerged as a powerful model organism not only for heart diseases[157–160] but several human diseases including neurodegenerative diseases, diabetes or cancer. Since first proposed in 1995, a number of studies confirmed similar molecular and cellular mechanisms operating in *Drosophila* and vertebrate heart development.[143] For example, despite structural differences, both, the human and *Drosophila* heart, originate from a lateral plate mesoderm and initially form a heart tube near the midline.[143] In both, the most lateral part of the mesoderm becomes committed to cardiac fate (see also **Figure 5** I).[143] The genes and proteins mediating cardiac mesoderm specification and regulating positioning as well as shape changes of these differentiated cells were shown to be conserved with special focus on transcription factors like NK2, GATA, MEF2, T-box, LIM domain, and Hand proteins.[129,132,133,138,161–164] A recent review highlights the role of FGFR, EGFR, Wnt, BMP, Notch Hedgehog, Slit/Robo, and other signaling pathways in specific steps of *Drosophila* cardiogenesis – mesoderm migration, cardiac mesoderm establishment, differentiation, and cell specification and morphogenesis of the heart – and their cardiogenic conservation in vertebrates.[165]

Adult *Drosophila* cardiomyocytes exhibit circular myofibrils with a sarcomeric structure similar to mammalian cardiac cells, consisting of muscle-specific proteins, such as actin and myosin heavy chain, which ensure cardiac contraction.[152,166] Proteomic analysis revealed many similarities at the level of myofilament, structural as well as mitochondrial functions compared to the mouse heart proteome.[166] In line with this, dilated and restricted cardiomyopathies have been studied in the fly heart and are linked to mutations in human homologs (e.g. *MYH7*[167], δ-sarcoglycan[159], dystrophin[168]) with similar effects in the human heart.

As mentioned previously, in contrast to the *Drosophila* larval heart which is myogenic, the adult heart rate is additionally modulated by neuronal and hormonal input, similarly to vertebrates.[155] Furthermore, important regulators of excitation-contraction coupling, such as sarcoendoplasmic reticulum calcium ATPase (SERCA), troponin, ryanodine receptors, and ion channels, are expressed in the fly heart.[166] Mutations in several ion channels and transporters have been shown to modulate heart rate in the fly.[169,170] Studies involving pharmacological ion channel blockers indicate that cardiac action potential in *Drosophila* is mainly based on calcium and potassium[171] and it has been shown that, in contrast to humans, depolarization in *Drosophila* cardiomyocytes relies on calcium rather than sodium currents.[172] However, many components that underlie myocardial calcium transients have been shown to be evolutionarily conserved between *Drosophila* and mammals.[173] *Drosophila SERCA, CaP60A, f*or example, shows high similarity to human *SERCA*, which is responsible for removing calcium from the cytosol into the sarcoplasmic reticulum after cardiac contraction.[169] In both, humans and *Drosophila*, *SERCA* mutation was associated with cardiac dysfunction due to disruption of calcium

homeostasis.[169] Furthermore, potassium channels like the α-subunit for *KCNQ1* (Potassium Voltage-Gated Channel Subfamily Q Member 1) or Ether-a-go-go Related Gene (*hERG*), which are involved in myocardial repolarization in humans, exhibit similar functions in *Drosophila*.[170,174–176] Disruption of *KCNQ1* causes arrhythmias, due to prolonged duration of contraction phases –'long QT', both in humans and fly.[170] In contrast to *KCNQ1,* mutations in *seizure* (*hERG* fly ortholog) not only lead to electrical remodeling and arrhythmia but also cause structural remodeling of the *Drosophila* heart.[176] Interestingly, *hERG* and *KCNQ* do not play a role in action potential repolarization in adult mouse hearts.[177]

In summary, the translatability between humans and flies illustrates the utility of *Drosophila* as a model system to study heart development, structure, and function and highlights its potential to elucidate the genetic mechanisms underlying human heart development and disease.

1.5.3 Genetic Engineering in *Drosophila*

One option to study candidate genes in *Drosophila* is to use flies that harbor mutations in the gene of interest (GOI) or Deficiency lines (Df). Df lines have a deletion in a part of the genome including the GOI. One other commonly used method utilizes the Gal4/UAS-system (**Figure 7**), which allows control of the spatio-temporal expression of a GOI or an RNAi.[178] The ladder is a short RNA sequence, which directs enzyme complexes to degrade messenger RNA (mRNA) molecules complementary to the RNAi sequence itself. By reducing the amount of mRNA of a certain gene, translation is prevented, which results in decreased synthesis of the respective protein. The first part of this binary UAS/Gal4 system is the Gal4 protein, a transcription factor normally expressed in yeast, which is driven from a cell-specific promotor (i.e. *Hand*[4.2], which is active in the heart or *Mef2*, which is active in all muscle cells). The second construct is composed of a promotor sequence called the upstream activation sequence (UAS), which regulates the expression of a transgene of interest. Mating one Gal4 expressing fly line (driver line) with a UAS line (responder line), results in an F1 fly generation harboring both constructs so that the Gal4 binds to the UAS sequence and efficiently drives the expression of the transgene in a tissue of interest.

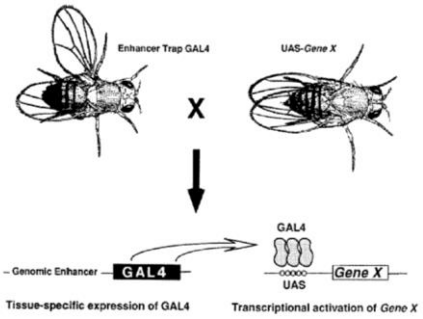

Figure 7: The Gal4-UAS system. This bipartite system allows inducible spatiotemporal expression of a gene of interest by crossing two transgenic lines, Gal4 (the driver) and UAS (the responder). From Brand and Perrimon (1993).[178]

1.5.4 Functional heart analysis in *Drosophila*

Various methods have been developed to perform functional heart analyses in *Drosophila*. In this work, we apply two different methods for analyzing the cardiac function of candidate genes in a high-throughput fashion. First, a semi-automated method, which allows assessment of the contractility and

rhythmicity parameters of the adult fly heart independent from nervous system input. Here, the adult fly is dissected in a semi-intact manner to expose the beating heart, filmed, and analyzed using the semi-automated optical heartbeat analysis (SOHA) method.[179,180] For the second method we use a fly line, which expresses tdTomato specifically in the cardiomyocytes using a specific novel heart enhancer *R94C02*. This reporter is named tdtK (tdTomato Klassen) and allows to record the beating heart of the intact fly *in vivo* by tracing fluorescence specifically expressed in the heart.[181] Based on edge tracing, the heart walls of the fly heart can automatically be detected and M-Modes are generated, which display contractility (systolic and diastolic diameters) and rhythmicity (heart rhythm or heart period) parameters of the fly heart (**Figure 8**).

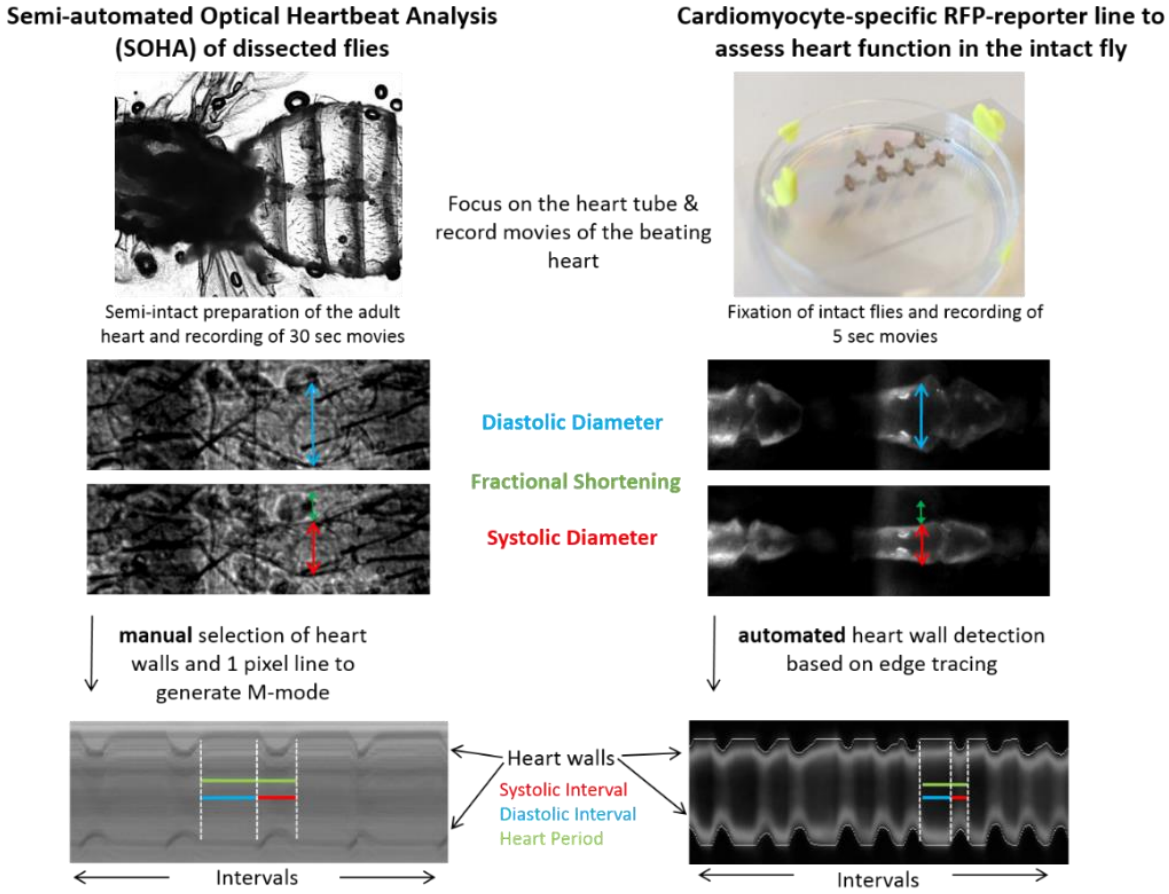

Figure 8: Functional heart analysis in *Drosophila*. Comparison of the Semi-automated Optical Heartbeat Analysis (SOHA) method (left) (Ocorr et al., 2009) and the fluorescence-based Klassen method (right) (Klassen et al., 2017). For the SOHA method, adult flies are dissected in a semi-intact manner in an artificial hemolymph solution and 30-second movies of the beating heart are taken. In the next step, the user has to manually define the heart walls and one-pixel line within the movie using the SOHA software. At this pixel position, two different algorithms detect the heart wall movement and an M-Mode is created, which gives insight into rhythmicity and contractility parameters of the fly heart. In the second method using flies expressing the heart specific tdtK reporter, the intact flies are immobilized on a glass slide with UV-sensitive glue. The flies are exposed to fluorescence light to record 5-second high frame rate movies of the fluorescent heart tube. Based on edge-tracing, the heart walls can automatically be tracked, and M-Modes are generated, using a custom *R*-script developed by Dr. Georg Vogler.

2. Aim of the study

The aim of the study is to better understand the genetic underpinnings and mechanisms underlying congenital heart diseases and to identify novel genes, their polygenic interactions (gene networks), mechanisms of action, and placement in interlinked pathways potentially involved in CHDs. Based on variants, that were prioritized from genomic datasets from patients with different CHDs, I use *Drosophila* as a heart model system to perform large scale *in vivo* functional analyses of genes and gene networks connected with *MYOM2, LRP2* and RP genes, to functionally and quantitatively assess their role as potential new CHD-associated genes in the heart and to translate these findings into a model for better understanding the disease-causing mechanisms underlying CHDs.

The discovery of novel disease-associated genes could help define novel markers for early diagnosis and ultimately could provide a path towards new therapeutic approaches to correct imbalances of cardiac gene networks in CHD patients. Especially, the modeling of clustered patient-derived mutation patterns in the fly has a high potential to push the development of patient-specific treatments forward, leading to a more tailored management of CHD.

3. Material

3.1 Key resource table

Table 1: Key resource table (fly stocks, zebrafish strains, antibodies, reagents).

Reagent type (species) or resource	Designation	Source or reference	Identifiers	Additional information
Genetic reagent (*D. melanogaster*)	$mgl^{MI14318}$	Bloomington *Drosophila* Stock Center (BDSC)	FBal0302551	BL-59689
Genetic reagent (*D. melanogaster*)	UAS-mgl RNAi	Vienna *Drosophila* Resource Center (VDRC)	FBst0456831	v27242
Genetic reagent (*D. melanogaster*)	$apolpp^{MB07263}$	Bloomington *Drosophila* Stock Center (BDSC)	FBal0221354	BL- 27749
Genetic reagent (*D. melanogaster*)	mgl^{168}	N. Dye	FBal0264251	
Genetic reagent (*D. melanogaster*)	mgl^{269}	N. Dye	FBal0264252	
Genetic reagent (*D. melanogaster*)	mgl^{406}	N. Dye	FBal0264254	
Genetic reagent (*D. melanogaster*)	mgl^{608}	N. Dye	FBal0264255	
Genetic reagent (*D. melanogaster*)	Df(2L)BSC291	Bloomington *Drosophila* Stock Center (BDSC)	FBab0045030	Df(wg), BL-23676
Genetic reagent (*D. melanogaster*)	UAS-fz 1 RNAi	Bloomington *Drosophila* Stock Center (BDSC)	FBal0257901	BL-34321
Genetic reagent (*D. melanogaster*)	UAS-fz 2 RNAi	Bloomington *Drosophila* Stock Center (BDSC)	FBal0242307	BL-27568
Genetic reagent (*D. melanogaster*)	UAS-ci RNAi	Bloomington *Drosophila* Stock Center (BDSC)	FBal0240324	BL-28984
Genetic reagent (*D. melanogaster*)	UAS-smo RNAi	Bloomington *Drosophila* Stock Center (BDSC)	FBal0220727	BL- 27037
Genetic reagent (*D. melanogaster*)	UAS-ptc	Bloomington *Drosophila* Stock Center (BDSC)	FBal0050312	BL-5817
Genetic reagent (*D. melanogaster*)	UAS-ptc	Bloomington *Drosophila* Stock Center (BDSC)	FBal0050312	BL-44614
Genetic reagent (*D. melanogaster*)	hh^{2}	Bloomington *Drosophila* Stock Center (BDSC)	FBal0005463	BL-3376
Genetic reagent (*D. melanogaster*)	hh^{Ac}	Bloomington *Drosophila* Stock Center (BDSC)	FBal0031481	BL-1749
Genetic reagent (*D. melanogaster*)	Mhc^{1}	NA	FBal0012242	O'Donnell and Bernstein, 1988
Genetic reagent (*D. melanogaster*)	Df(3L)BSC672	Bloomington *Drosophila* Stock Center (BDSC)	FBab0045738	Df(CG14964), BL-26524
Genetic reagent (*D. melanogaster*)	$CG14964^{CR01157\text{-}TG4.1}$	Bloomington *Drosophila* Stock Center (BDSC)	FBti0202699	BL-81199
Genetic reagent (*D. melanogaster*)	UAS-CG14964 RNAi GD	Vienna *Drosophila* Resource Center (VDRC)	FBst0465158	v43603
Genetic reagent (*D. melanogaster*)	UAS-CG14964 RNAi GD TRiP	Bloomington *Drosophila* Stock Center (BDSC)	FBal0322300	BL-65245
Genetic reagent (*D. melanogaster*)	w1118	Bloomington *Drosophila* Stock Center (BDSC)	FBal0018186	BL-3605
Genetic reagent (*D. melanogaster*)	GD control	Vienna *Drosophila* Resource Center (VDRC)	NA	v60000
Genetic reagent (*D. melanogaster*)	TRiP control	Bloomington *Drosophila* Stock Center (BDSC)	FBst0036303	BL-36303
Genetic reagent (*D. melanogaster*)	Mef2-Gal4	NA	FBtp0006434	Ranganayakulu et al., 1996
Genetic reagent (*D. melanogaster*)	$Hand^{4.2}$-Gal4	NA	PMID:16467358	Han and Olson, 2005

Genetic reagent (*D. melanogaster*)	tinD-Gal4, mid^{E19}GFP	mid^{E19}GFP (I. Reim)	NA	tinD-Gal4 (Jin et al., 2013)
Genetic reagent (*D. melanogaster*)	twist-Gal4, midE^{19}GFP	mid^{E19}GFP (I. Reim), twist-Gal4 (BDSC)	FBal0040491	Jin et al., 2013, BL-914
Genetic reagent (*D. melanogaster*)	sls^{31}	Frank Schnorrer	NA	NA
Genetic reagent (*D. melanogaster*)	sls^{1}	Bloomington *Drosophila* Stock Center (BDSC)	FBal0015717	BL-5078
Genetic reagent (*D. melanogaster*)	sls^{j1D7}	Bloomington *Drosophila* Stock Center (BDSC)	FBal0043793	BL-10017
Genetic reagent (*D. melanogaster*)	Df(4)ED6382 (bent)	KYOTO Stock Center	FBab0037606	150531
Genetic reagent (*D. melanogaster*)	UAS-Ras85D^{V12}	Bloomington *Drosophila* Stock Center (BDSC)	FBal0060587	BL-4847
Genetic reagent (*D. melanogaster*)	R94C02::tdTomato	Y. N. Jan	FBtp0137272	NA
Genetic reagent (*D. melanogaster*)	UAS-RpS15Aa^{RNAi}	Vienna Drosophila Resource Center (VDRC)	FBgn0010198	v19198
Genetic reagent (*D. melanogaster*)	Df(RpS15Aa)	Bloomington Drosophila Stock Center (BDSC)	FBab0047266	39614
Genetic reagent (*D. melanogaster*)	UAS-RpS15Aa	FlyORF	FBal0287447	F000765
Genetic reagent (*D. melanogaster*)	UAS-RPL26^{RNAi}	Vienna Drosophila Resource Center (VDRC)	FBgn0036825	v40402 v100280
Genetic reagent (*D. melanogaster*)	UAS-RPL36A^{RNAi}	Vienna Drosophila Resource Center (VDRC)	FBgn0031980	v108391
Genetic reagent (*D. melanogaster*)	UAS-RPS15^{RNAi}	Vienna Drosophila Resource Center (VDRC)	FBgn0034138	v35415 v104439
Genetic reagent (*D. melanogaster*)	UAS-RPL39^{RNAi}	Vienna Drosophila Resource Center (VDRC)	FBgn0023170	v23578 v108821
Genetic reagent (*D. melanogaster*)	UAS-RPL3^{RNAi}	Vienna Drosophila Resource Center (VDRC)	FBgn0020910	v109820
Genetic reagent (*D. melanogaster*)	UAS-RPL10^{RNAi}	Vienna Drosophila Resource Center (VDRC)	FBst0476362	v104504
Genetic reagent (*D. melanogaster*)	UAS-yorkie	D. Pan	NA	NA
Genetic reagent (*D. melanogaster*)	UAS-myc^{RNAi}	Bloomington Drosophila Stock Center (BDSC)	FBgn0262656	BL-25784
Genetic reagent (*D. melanogaster*)	UAS-myc^{RNAi}	Vienna Drosophila Resource Center (VDRC)	FBgn0262656	v106066
Genetic reagent (*D. melanogaster*)	UAS-myc	Bloomington Drosophila Stock Center (BDSC)	FBal0093088	BL-9674
Genetic reagent (*D. melanogaster*)	UAS-sd^{RNAi}	Vienna Drosophila Resource Center (VDRC)	FBgn0003345	v101497
Genetic reagent (*D. melanogaster*)	*Df(3L)DocA*	I. Reim	FBab0037663	NA
Genetic reagent (*D. melanogaster*)	tinEC40	NA	FBal0032861	NA
Genetic reagent (*D. melanogaster*)	tin^{346}	NA	FBal0035787	NA
Genetic reagent (*D. melanogaster*)	pnr^{VX6}	Bloomington Drosophila Stock Center (BDSC)	FBal0032468	BL-6334
Genetic reagent (*D. melanogaster*)	Df(pnr)	Bloomington Drosophila Stock Center (BDSC)	FBab0038315	BL-7982
Genetic reagent (*D. melanogaster*)	UAS-pyd^{RNAi}	Bloomington Drosophila Stock Center (BDSC)	FBal0240260	BL-28920
Genetic reagent (*D. melanogaster*)	UAS-pyd^{RNAi}	Bloomington Drosophila Stock Center (BDSC)	FBal0257163	BL-33386
Genetic reagent (*D. melanogaster*)	UAS-SF1^{RNAi}	Vienna Drosophila Resource Center (VDRC)	FBal0208441	v13425
Genetic reagent (*D. melanogaster*)	UAS-SF1^{RNAi}	Bloomington Drosophila Stock Center (BDSC)	FBal0240840	BL-28036

Genetic reagent (*D. melanogaster*)	UAS-atpalpha^{RNAi}	Bloomington Drosophila Stock Center (BDSC)	FBal0257087	BL-33646
Genetic reagent (*D. melanogaster*)	Mef2$^{25-34}$	Bloomington Drosophila Stock Center (BDSC)	FBal0156258	BL-9861
Genetic reagent (*D. melanogaster*)	UAS-CD4 tdTom	Bloomington Drosophila Stock Center (BDSC)	FBal0328169	BL-35837
Genetic reagent (*D. melanogaster*)	UAS-Xrp1^{RNAi}	Bloomington Drosophila Stock Center (BDSC)	FBal0263081	BL-34521
Genetic reagent (*D. melanogaster*)	UAS-Drice^{RNAi}	NA	NA	7788
Genetic reagent (*D. melanogaster*)	UAS-p35	Bloomington Drosophila Stock Center (BDSC)	FBal0062158	BL-5072
Genetic reagent (*D. melanogaster*)	Df (3L)H99	Bloomington Drosophila Stock Center (BDSC)	FBab0022359	BL-1576
Genetic reagent (*D. melanogaster*)	UAS-YAP$^{2-5}$/TM3 (M4)	NA	NA	this work
Genetic reagent (*D. melanogaster*)	p{UASykiS168A.V5}	Bloomington Drosophila Stock Center (BDSC)	FBal0239740	BL-28818
Genetic reagent (*D. melanogaster*)	p{UAS-ykiS111A,S168A,S250A.V5}	Bloomington Drosophila Stock Center (BDSC)	FBal0239743	BL-28817
Genetic reagent (*D. melanogaster*)	UAS-myb	Bloomington Drosophila Stock Center (BDSC)	FBal0244571	BL-32044
Genetic reagent (*D. melanogaster*)	UAS-myb	Bloomington Drosophila Stock Center (BDSC)	FBal0263375	BL-35053
Genetic reagent (*D. melanogaster*)	UAS-myb^{RNAi}	Bloomington Drosophila Stock Center (BDSC)	FBal0314140	BL-58482
Genetic reagent (*D. melanogaster*)	UAS-Stinger	Bloomington Drosophila Stock Center (BDSC)	FBal0157333	NA
Genetic reagent (*D. melanogaster*)	lifeAct-GFP/TM3 28788-1-M2-M- Ch3	this work	NA	NA
Genetic reagent (*D. melanogaster*)	lifeAct-GFP/TM3 28788-1-M4-M- Ch3	this work	NA	NA
Genetic reagent (*D. melanogaster*)	hid-EGFP.5'F-WT	Bloomington Drosophila Stock Center (BDSC)	FBal0243614	BL-50752
Genetic reagent (*D. melanogaster*)	w-; UAS-GFP::l(3)mbt/TM3,sb 0803	Lehmann lab	NA	l(3)mbt overexpression
Genetic reagent (*D. melanogaster*)	w-; UAS-RFP::l(3)mbt/CyO 0804	Lehmann lab	NA	l(3)mbt overexpression
Genetic reagent (*D. melanogaster*)	w-; UAS-RFP::l(3)mbt/TM3,sb 0805	Lehmann lab	NA	l(3)mbt overexpression
Genetic reagent (*D. melanogaster*)	UAS-l(3)mbt^{RNAi}	Vienna Drosophila Resource Center (VDRC)		v13994
Genetic reagent (*D. melanogaster*)	l(3)mbt$^{GM76-8\ FRT82B}$	Lehmann lab	NA	
Genetic reagent (*D. melanogaster*)	l(3)mbt^{E2-12}	Lehmann lab	NA	
Genetic reagent (*D. melanogaster*)	Df(3R)ED10961 (l(3)mbt)	Bloomington Drosophila Stock Center (BDSC)	FBab0044496	BL-150207
Genetic reagent (*D. melanogaster*)	Gp210 MIMIC Intronic	Bloomington Drosophila Stock Center (BDSC)	FBal0247051	BL-
Genetic reagent (*D. melanogaster*)	Gp210 MIMIC Exonic	Bloomington Drosophila Stock Center (BDSC)	FBal0242820	BL-30644
Genetic reagent (*D. melanogaster*)	Gp210^{EY21031} (Gp210 mut)	Bloomington Drosophila Stock Center (BDSC)	FBal0192606	BL-22445
Genetic reagent (*D. melanogaster*)	Df(2R)BSC697 (Gp210)	Bloomington Drosophila Stock Center (BDSC)	FBab0045762	BL-26549
Genetic reagent (*D. melanogaster*)	UAS-CG6051^{RNAi}	Vienna Drosophila Resource Center (VDRC)	FBal0204933	v25500

Genetic reagent (*D. melanogaster*)	UAS-CG6051^{RNAi}	Vienna Drosophila Resource Center (VDRC)	FBal0204933	v25503
Genetic reagent (*D. melanogaster*)	UAS-Dlg1^{RNAi}	Vienna Drosophila Resource Center (VDRC)	FBal0209360	v41134
Genetic reagent (*D. melanogaster*)	UAS-Dlg1^{RNAi}	Vienna Drosophila Resource Center (VDRC)	FBal0209360	v41136
Genetic reagent (*D. melanogaster*)	UAS-Dlg1^{RNAi}	Bloomington Drosophila Stock Center (BDSC)	FBal0257061	BL-33620
Genetic reagent (*D. melanogaster*)	lid^{10424}	Bloomington Drosophila Stock Center (BDSC)	FBal0008148	BL-12367
Genetic reagent (*D. melanogaster*)	lid^{C386}	Bloomington Drosophila Stock Center (BDSC)	FBal0288094	BL-43364
strain, strain background (*Danio rerio*)	Oregon AB wild-type			A commonly used wildtype strain
strain, strain background (*Danio rerio*)	Tg(myl7:EGFP)^{twu277}	Tsai Lab, National Taiwan University	PMID:12950077	A transgenic line of zebrafish labeled with heart-specific EGFP fluorescence.
strain, strain background (*Danio rerio*)	Tg(myl7:H2A-Cherry)^{sd12}	Yelon Lab, University of California, San Diego	PMID:24075907	A transgenic line of zebrafish specifically expressing mCherry in cardiomyocyte nuclei
antibody	donkey polyclonal anti-mouse Alexa Fluor 568	Invitrogen	A10037	1:1000
antibody	donkey polyclonal anti-chicken AlexaFluor 488	Jackson ImmunoResearch	703-545-155	1:200
antibody	donkey polyclonal anti-rabbit AlexaFluor 568	Invitrogen	A10042	1:200
antibody	mouse anti- sex-lethal protein	DSHB	M114	1:10
antibody	mouse anti-alpha-spectrin	DSHB	3A9	1:50
antibody	mouse anti-Mhc (Drosophila)	DSHB	3E8-3D3	1:50
other	Alexa Fluor 647 phalloidin	Invitrogen	A22287	1:500
other	Alexa Fluor 594 phalloidin	Invitrogen	A12381	1:500
antibody	anti-mouse-Alexa Fluor 488	Jackson Labs	115-545-003	1:250
antibody	goat anti-rabbit 594	Jackson Labs		1:250
antibody	goat anti-rabbit 647	Jackson Labs		1:250
antibody	goat anti-guinea pig 647	Jackson Labs		1:250
antibody	goat anti-guinea pig FITC	Jackson Labs		1:250
antibody	rabbit anti-Distroglycan	H. Ruohola-Baker		1:1000
antibody	guinea pig anti-Neuromancer 1	J. Skeath		1:2000
antibody	mouse monoclonal anti-Seven-up	DSHB	5B11	1:50
antibody	rabbit anti-Tinman	I. Reim		1:1500 (adults), 1:1000 (adults)
antibody	mouse monoclonal anti-smoothened	DSHB	20C6	1:20

3.2 Primer

Table 2: Primer sequences for Drosophila.

Primer name (for/rev)	Gene/Application	Primer sequence forward 5' -3'	Primer sequence reverse 5' -3'
TN35/TN36	CG14964	GTCGCCCCAAGAAGAATGTCC	CAGCAAAGCAACGAAACTGGT
TN73/TN74	CG14964	ATGGACTGATTGTTGAGGCG	TCACCCAATCGATTCCAAGC
TN58/TN59	Diap1	GATGCGATCTAATGCTTCGGC	AAATGCTTTTTCTGCGGCGT
TN12/TN17	Rp49	AAACGCGGTTCTGCATGAG	GCCACCAGTCGGATCGATAT
Plac4/Plac1	5' end P-element	ACTGTGCGTTAGGTCCTGTTCATT GTT	CACCCAAGGCTCTGCTCCCACAAT
Pyr4/Pyr1	3' end P-element	CAATCATATCGCTGTCTCACTCA	CCTTAGCATGTCCGTGGGGTTTG AAT
Sp1/iPCR rev	iPCR validation/ sequencing primer	ACACAACCTTTCCTCTCAACAA	CGCCTTCTGATGACACGTT
pattB tinC-LifeActScarlet FWD/ pattB tinC LifeActScarlet REV	Gibson assembly	CAGTCTTTGCGTCTGTTTCCGAGC GCCGGAGTATAAATAG	GTCAGACGGCGCGGAAAAGTGG ATCCGCTAGCATAACTTC
pMK3_R94C02_F1/ pMK3_R94C02_ R2	Gibson assembly	TTTCACTGGAACTAGGCTAGACTT TTCCGCGCCGTCTGAC	ATTTATACTCCGGCGCTCGAGGA AACAGACGCAAAGACTGA
JaJa PCR colony F1/ JaJa PCR colony R1	Colony PCR	CGACGAATGCCTGTTGTT	GGCATTCCACCACTGCTC

4. Methods

4.1 Study subjects

Written informed consent was obtained from all patients in the HCM cohort and the local institutional review board of the Charité – Universitätsmedizin Berlin approved the study. The study protocol conforms to the ethical guidelines of the 1975 Declaration of Helsinki. The cohort was characterized on the basis of medical history, physical examination, 12-lead electrocardiogram, and two-dimensional and M-mode echocardiography. Disease-causing mutations in known HCM genes in all 66 unrelated HCM patients of German origin were excluded using screening methods as previously described by the Rickert-Sperling lab and others[182–187] and *MYOM2* screening was performed using Sanger sequencing (for more details see Auxerre-Plantié et al. 2020).[3] The cohort of 13 clinically well-defined isolated TOF patients was previously described in Grunert et al., 2014.[4]

Written informed consent was obtained for the families in the HLHS cohort (including 75H and 5H), under a research protocol approved by the Mayo Clinic Institutional Review Board. Cardiac anatomy was assessed by echocardiography. Candidate genes were identified and prioritized by Whole-genome sequencing of genomic DNA followed by bioinformatical analyses (see also Theis et al., 2020[5]).

4.2 Fly husbandry

All fly stocks were maintained at 25 °C on standard fly food medium. All fly stocks used are listed in the key resource table (section 3.1). In optimal conditions, genetic crosses were set up using 10 female virgins and 5 male flies, for example, Hand$^{4.2}$-Gal4/CyO; tdtK/TM3 (10 virgins) x GDcon (5 males). Note, that flies are diploid and the genotype of the two copies (homologs) is separated by a slash mark "/". If no slash mark is used, the fly is homozygous for that specific allele (i.e GDcon). Different alleles on the same chromosome are separated by a comma and genotypes of different chromosomes are separated by a semicolon.

4.3 Functional heart analysis in *Drosophila*

Heart function of 1-week or 3-week-old adult female flies (n=20) was assessed with two different methods: the semi-automated optical heartbeat analysis (SOHA) method on semi-intact fly preparations and the *in vivo* fluorescent heart reporter-based method (Klassen method).

4.3.1 Semi-automated optical heartbeat analysis

Semi-automated optical heartbeat analysis (SOHA) was performed as previously described.[179,188] Artificial hemolymph (AHL) was prepared according to **Table 3**. Note, that sucrose and trehalose were added on the day of the experiment. The AHL was brought to room temperate and oxygenated for at least 30 min with compressed air.

The adult flies were anesthetized with FlyNap (*Carolina*®) and 10 flies were transferred into a 10 x 35 mm petri dish coated with a thin layer of vaseline and positioned ventral side facing up. Oxygenated AHL was added to cover the flies and flies were dissected as followed: First, the head, ventral nerve cord, and legs are removed with a single cut using a curved pair of spring scissors. Next, the posterior tip of the abdomen is removed and two lateral cuts along both edges of the abdomen were made and the ventral abdominal cuticle together with gut and other abdominal organs are removed using forceps. The beating heart tube is still attached to the dorsal cuticle and the surrounding fat bodies are carefully removed by liposuction using small glass capillaries without touching the heart. This preparation should equilibrate for about 20 min with oxygenation. Before the recording of heart movies, the AHL solution was replaced with fresh AHL.

Heart movies (30 s length at 140 frames/sec) were recorded of the 3rd abdominal segment using a Zeiss A1 Axioscope (10X magnification, Berlin set up) or an Olympus BX63 microscope (10X magnification, San Diego set up) with a Hamamatsu C11440 ORCA-flash 4.0 OLT digital camera and the HCImageLive software (*Hamamatsu*). Movie analysis was carried out using SOHA software (Oaktree Technologies, www.sohasoftware.com).[189] Furthermore, an R script developed by Dr. Georg Vogler with the support of Dr. Marcel Grunert was used, which calculates additional heart parameters, like stroke volume, cardiac output, or MAD index. All heart parameters are listed in **Table 4**.

Table 3: Artificial hemolymph

Ingredients	Final concentration	
NaCl	108 mM	saline solution (stored at 4 °C)
KCl	5 mM	
$CaCl_2$*$2H_2O$	2 mM	
$MgCl_2$*$6H_2O$	8 mM	
Hepes (pH 7.1)	15 mM	
NaH_2PO_4*H_2O	1 mM	
NaHCO3	4 mM	
Sucrose	10 mM	added fresh the day of the experiment
Trehalose	5 mM	

4.3.2 *In vivo* heartbeat analysis

For *in vivo* functional heart analysis (Klassen method) intact adult flies were anesthetized using FlyNap (*Carolina*®). Little drops of Norland optical glue (*Thorlabs*) were placed on a 22 x 50 mm glass coverslip and one fly was placed on each drop dorsal side facing down (n=20). Wings were positioned to each side of the fly body. For this method flies were used, which carry the tdtK fluorescent heart reporter (see also Introduction section 1.5.4). The glue was cured by exposure to UV light for 60 s. The coverslips were placed upside down on 10 x 35 mm petri dishes and secured by putty so that the

dorsal side of the flies are facing upwards. Exposing the flies to fluorescent lights, 5 s high-frame-rate movies (280 frames/s) of the beating hearts were recorded through the fly cuticle using a Zeiss A1 Axioscope (20X magnification, Berlin set up) an Olympus BX63 microscope (20X magnification, San Diego set up) with a Hamamatsu C11440 ORCA-flash 4.0 OLT digital camera and the HCImage Live software (*Hamamatsu*). Movie processing and analysis were fully automated using an *R* script developed by Dr. Vogler.

Table 4: Heart parameter

Heart Parameter [unit]	Acquisition	Definition
Heart period (HP) [s]		time needed to complete one full contraction (systole) and one relaxation (diastole), measured as time between ends of two consecutive diastolic intervals
Heart rate (HR) [1/s]	= 1/HP	number of contractions per second
Diastolic Interval (DI) [s]		time needed to complete one relaxation (diastole)
Systolic Interval (SI) [s]	= HP-DI	time needed to complete one contraction (systole)
Arrhythmia Index (AI)	= standard deviation (HP)/ median(HP)*100	estimates the rhythmicity of the heartbeat
Median Absolute Deviation (MAD)	= median ($\lvert DI_i$ – median (DI)$\rvert$	measures the variability of the diastolic intervals; defined as median of the absolute deviations from the data's median
nMAD	=MAD (DI)/mean (HP)	median absolute deviation of the DI normalized over the mean HP
Diastolic Diameter (DD) [µm]		diameter of the heart tube when fully relaxed
Systolic Diameter (SD) [µm]		diameter of the heart tube when fully contracted
Fractional Shortening (FS) [%]	= [(DD-SD)/DD] * 100	estimation of the contractility of the heart
Stroke Volume (SV) [µm³]	= π/4 * (DD^2 – SD^2)	estimated volume of hemolymph ejected during one contraction
Cardiac Output (CO) [µm³/s]	= SV * HR	estimated volume of hemolymph ejected per second

4.4 Genomic DNA extraction from adult flies

About 15 adult flies per sample were anesthetized with CO_2, transferred to a 1.5 ml reaction tube, and frozen at -80 °C. Alternatively, flies can be frozen on dry ice and processed immediately. Next, 200 µl of pre-chilled Cell Lysis Solution (*Qiagen* #1589056) was added to the frozen flies and the samples were homogenized thoroughly using a pellet pestle mixer. Additional 400 µl of Cell Lysis Solution was added, followed by a 15 min incubation at 65 °C. Then, 1.2 µL of RNAse A (10 mg/ml, *Qiagen*) was added to each sample and mixed by inverting the tube. After one hour at 37 °C, 200 µl of Protein

Precipitation Solution (*Qiagen* #158910) was added. Samples were vortexed vigorously for 20 s at high-speed following a centrifuge spin down for 10 min at 13000 rpm (rounds per minute). The precipitated proteins should form a tight pellet. The supernatant was transferred into a clean 1.5 ml reaction tube containing 600 µl of isopropanol (*Alfa Aesar*) to precipitate the DNA. Samples were mixed by inversion gently 50 times following centrifugation for 2 min at 13000 rpm. The supernatant was discarded, and the pellet was washed once with 600 µl of 70 % ethanol. Finally, the DNA pellet was air-dried for about 5 min and dissolved in 50 µl TE buffer or water by incubation overnight at room temperature or 1 h at 65 °C. Samples were stored at -20 °C.

4.5 Mapping UAS-*CG14964* RNAi P-element by inverse PCR

The UAS-*CG14964* RNAi fly line was created by randomly inserting the UAS-*CG14946* RNAi construct by P-element- mutagenesis into a w1118 background fly. For this, the RNAi construct was cloned into the pMF3 vector, which contains 10 UAS sites and a mini-white gene (among others), flanked by 3'P and 5'P (both ends of the P-Element). The pMF3 vector is derived from the pUAST vector, which is identical except that it only harbors 5 UAS sites. To locate the insertion site, where the UAS-*CG14946* RNAi was inserted into the fly genome of the recipient fly line, I adapted a protocol from E. Jay Rehm (Berkeley Drosophila Genome Project, https://www.fruitfly.org/ about/methods/inverse.pcr.html).

I. Restriction enzyme digestion:

First, genomic DNA was extracted from adult flies according to protocol (section 4.4), which was then digested using three different restriction enzymes (Sau3A I, HinP1 I, or HpaII (*New England BioLabs*)) in separate digestion reactions.

Reagent	**Volume**
Unpurified Genomic DNA (1 µg)	7.5 ul
10X buffer	2.5ul
100 ug/ml RNase	2.0ul
ddH_2O	x µl
Sau3A I, HinP1 I, or HpaII	10 units (Sau3AI) 20 U (HinP1I, HpaII) 2 µl
Total Volume	25

1. Incubate 22 h at 37 °C.
2. Heat for 20 min to 65 °C.
3. Check 5 µl (digested unpurified gDNA) of each digest on a 1 % agarose gel (*fisher bioreagents*).
4. Purification using the CHIP DNA Clean and Concentrator Kit (*Zymo Research*), elution in 230 µl EB-Buffer.

II. Ligation:

Under low concentrations of the digested DNA products, self-ligation was induced to achieve circular DNA products (each sample separately):

Reagent	Volume
digested genomic DNA	10 ng/µl
10 X ligation buffer	x
ddH2O	x
T4 DNA Ligase (800 U)	1 µl
Total Volume	x

1. Incubate 2h at 37 °C and overnight at 4 °C.
2. Heat inactivation for 10 min at 65 °C.
3. Purification using the CHIP DNA Clean and Concentrator Kit (*Zymo Research*) and elution in 20 µl EB-buffer.

III. Polymerase chain reaction

PCR reactions were set up with primers appropriate for the end of the P-element from which you want to recover the genomic sequence (3'P or 5'P). I used Plac4/Plac1 (5' end) and Pyr4/Pyr1 (3' end) primer pairs, complementary to the 3'P or 5'P of the P-element, which point outwards, so they amplify the circular DNA towards the unknown genomic DNA into which the P-element was inserted. PCR was performed using the Phusion® High-Fidelity PCR Master Mix with High-Fidelity Buffer from *New England BioLabs* (#M0531S). 5 µl of the PCR reactions was verified with gel electrophoresis on 1 % agarose gel (*fisher bioreagents*).

2-step PCR			**Cycling Protocol**	**time [mm:ss]**
	final concentration	**volume in µl**	98 °C	00:30
gDNA	100 ng (total)	X	98 °C	00:15
2x Master Mix (NEB)	1x	10,00	72 °C	03:00
Plac4 10µM	0.4 µM	0,80	go to step 2	**for 34 cycles**
Plac1 10µM	0.4 µM	0,80	72 °C	10:00
H2O	add up to 20 µl	X	4 °C	hold
		total: 20µL		

3-step PCR			**Cycling Protocol**	**time [mm:ss]**
	final concentration	**volume in µl**	98 °C	00:30
gDNA	100 ng (total)	X	98 °C	00:15
2x Master Mix (NEB)	1x	10,00	55 °C	00:30
Pyr4 10µM	0.4 µM	0,80	72 °C	03:00
Pyr1 10µM	0.4 µM	0,80	go to step 2	**for 34 cycles**
H2O	add up to 20 µl	X	72 °C	10:00
		total: 20µL	4 °C	hold

IV. Sequencing and Validation

PCR samples were purified using the CHIP DNA Clean and Concentrator Kit (*Zymo Research*) and eluted in 20 µl EB-Buffer. Samples amplified with Plac1/Plac4 primer pair were sequenced with the Sp1 primer (*Eurofins Genomics,* Ebersberg, Germany). Sequencing results were aligned to fly genome using *Flybase blast* and *Benchling* to identify the P-element insertion site. Finally, the results were validated by amplifying the genomic UAS-*CG14964* RNAi DNA using the Sp1 primer and a second primer (TN06), complementary to a sequence on the fly genome identified to be close to the P-element insertion site. The expected band size was verified by gel electrophoresis (1 % agarose gel, *fisher bioreagents*) and sequenced with the Sp1 primer (*Eurofins Genomics,* Ebersberg, Germany).

3-step PCR			**Cycling Protocol**	**time [mm:ss]**
	final concentration	**volume in µl**	98 °C	00:30
gDNA	20-30 ng (total)	X	98 °C	00:15
2x Master Mix (NEB)	1x	10,00	63 °C	00:45
Sp1	0.4 µM	0,80	72 °C	00:30
TN06	0.4 µM	0,80	go to step 2	**for 34 cycles**
H2O	add up to 20 µl	X	72 °C	10:00
		total: 20µL	4 °C	hold

4.6 Climbing assay

Climbing ability was quantified using the rapid iterative negative geotaxis (RING) assay according to Gargano et al.[190] with the following adaptions: Adult flies (n≈20) were anesthetized using FlyNap (*Carolina*®), transferred to an empty fly tube, and left to adapt for 10 min. The tubes were tapped three times to trigger the negative geotaxis response. Movies were recorded to document the distance the flies climb up within 30 s intervals. This experiment was performed in triplicates for each biological replicate and the mean was calculated to distinguish the climbing ability of each biological replicate.

4.7 RNA isolation and RT-qPCR

Total RNA was isolated from ~15-20 adult **fly hearts**, using TRIzol reagent (*Invitrogen*) combined with the Quick-RNA MicroPrep Kit (*Zymo Research*), including a step of DNAse-on-column treatment, following the manufacturer's instructions. RNA quality and quantity were respectively assessed using an Agilent RNA 6000 Pico kit on an Agilent 2100 Bioanalyzer (*Agilent Technologies*) and Qubit RNA HS

assay kit on a Qubit 3.0 Fluorometer (*Thermo Fisher Scientific*). Total RNA was reverse transcribed using the PrimeScript RT Master Mix (*Takara*).

RNA from **whole flies** was isolated using TRIzol reagent combined with chloroform/ethanol extraction. First, 100 µl TRIzol was added in a reaction tube containing three to five whole adult female flies followed by homogenization with a pellet pestle homogenizer (on ice). Volume was brought to 1 ml and after a 5 min incubation time, the samples were centrifuged for 10 min at 12 000 g (4 °C). The solution was transferred into a new tube and incubated for 5 min. 200 µl chloroform (*Fisher Scientific*) was added, samples were mixed and incubated for 3 min. After a 15 min centrifugation at 12 000 g (4 °C), the aqueous phase was transferred into a new reaction tube. 500 µl isopropanol (*Alfa Aesar*) was added, samples were mixed and let sit for 10 min. After a 10 min centrifugation at 12 000 g (4 °C), the supernatant was discarded and the pellet was washed with 500 µl 75 % ethanol. The samples were centrifuged for 5 min at 7500 g (4 °C), the ethanol removed and the RNA pellet air-dried. Lastly, the pellet was resuspended in RNAse free water and stored at -80 °C.

RNA quality and quantity were assessed using a Nanodrop spectrometer. cDNA was generated using Superscript IV Reverse Transcriptase (*Invitrogen*), with additional DNase I treatment or using a QuantiTect Reverse Transcription Kit (*Qiagen*). SYBR Green-based real-time qPCR (Sybr Green I Master Mix, *Roche*) was performed on a LightCycler 480 (set-up in Berlin, *Roche*) and a LightCycler 96 (set-up in San Diego, *Roche*). Gene expression quantification was determined using the $2^{-\Delta\Delta CT}$ method (Pfaffl, 2001)[191], with *Rp49* as a reference/housekeeping gene. Values were derived from technical duplicates and three to five biological replicates.

4.8 Immunohistochemistry

4.8.1 Adult fly hearts

Immunostaining of adult fly hearts was performed as described previously (Alayari et al., 2009).[192] Fly hearts were dissected as described for the SOHA method (see above), and myofibrils were relaxed using 10 mM EGTA (*bioPlus Chemicals*) followed by fixation in 4 % formaldehyde (*Polysciences*) for 15 min. After 3 x washes with 1X PBS (*MP Biomedicals*), fixed preparations can be stored at 4 °C. To stain fly hearts, fly thoraxes were removed, abdominal walls were trimmed and excess fat around the heart was removed. Cuticles with the hearts were transferred into 96-well plates containing 200 µl 1X PBS and washed three times with 0.3 % PBX (Triton-X 100 (*SIGMA*) in 1X PBS) for 10 min shaking. PBX was removed and replaced with 50 µl of primary antibody solution diluted in 0.3 % PBX. Samples were incubated overnight at 4 °C. The next day, the antibody solution was removed, and the samples were washed three times with 0.3 % PBX for 10 min. Next, 100 µl secondary antibody diluted in 0.3 % PBX was applied and incubated for 2 h at room temperature (covered from light, shaking). The sarcomeric

structure of the adult heart was visualized using Alexa Fluor 568 phalloidin (1:500, *Thermo Fisher Scientific*), which was added to the secondary antibody solution. After 3 washes in 0.3 % PBX for 10 min, samples can be stored in 1X PBS in the dark at 4 °C. The cuticle preparations were mounted with ProLong Gold antifade mounting medium with DAPI (*Invitrogen*) on 25 x 75 x 1 mm glass slides (18 x 18 mm No. 1 as bridges and No. 1.5 as coverslips). Slides were sealed with nail polish and stored 24 h at room temperature and then moved to 4 °C for long-term storage.

As an alternative, fly hearts can be stained in the petri dish they were dissected in. The immunostaining procedure is similar as described above, except that volumes are adjusted to sufficiently cover the flies. For primary and secondary antibody solutions 250 ul were applied and a small piece of parafilm was placed over the solution to seal the liquid over the hearts.

4.8.2 Larval *Drosophila* hearts

For larval heart preparations, 3rd instar larvae were dissected according to the *in situ* method previously described by Cooper et al.[193] with the following modifications: The preparation plate consists of a petri dish, which contains a silicon pad. Larvae were immobilized on ice for about 3 min prior to transferring them onto the dissection plate (ventral side up). Two pins (Austerlitz Insect Pins, *Minutiens*, 0.10 mm) were placed into the most anterior and posterior part of the larva to immobilize it to the plate. One drop of 1X PBS with EGTA (15 mM, *bioPlus Chemicals*) was added on top of the larva. To open up the larva, first, a small horizontal cut in the middle of the larva was made, and then incisions down the length of the longitudinal axis towards the anterior and posterior end were made. Four pins were used to pin the cuticle onto the dissection dish and open up the body cavity. Guts, fat bodies, and brains were carefully removed without damaging the heart or trachea. Larvae were washed one time with 1X PBS and fixed in 4 % formaldehyde (*Polysciences*) in 1X PBS for 25 min. After 3 washes in 1X PBS for 5 min, larvae are transferred into a 1.5 ml reaction tube containing 1X PBS and can be stored at 4 °C, or the staining process can be initiated. To reveal the sarcomere structure in the heart and muscles, the larvae were washed three times with 0.3 % PBX for 10 min (shaking), and incubated in phalloidin (Alexa Fluor 647 phalloidin, 1:500 in 0.3 % PBX) for 2 h in the dark. Next, the larvae were washed three times with 0.3 % PBX and one time in 1X PBS for 10 min (shaking). The stained larva preparations were mounted with ProLong Gold antifade mounting medium with DAPI (*Invitrogen*) on 25 x 75 x 1 mm glass slides (18 x 18 mm No. 1.5 as bridges and No. 1.5 as coverslips). Slides were sealed with nail polish and stored 24 h at room temperature and then moved to 4 °C for long-term storage.

4.8.3 Embryonic *Drosophila* hearts

For *Drosophila* embryo collection adult flies (ca. 40 female virgins and 20 males) were reared at 25 °C in cages, which were closed with petri dishes containing grape agar (400 ml grape juice + 16 g agar (*USBiological*) + 4.2 ml 95 % EtOH + 4 ml Glacial Acetic Acid (*Fisher Chemical*™) and yeast paste (active dry yeast (*Red Star*) + H_2O). Embryos were rinsed after 16.5 h into a mesh basket using a brush to collect 16-17 late-stage embryos. Embryos were rinsed with water and placed into bleach for 3 min for dechorination. Next, embryos were rinsed with water and transferred into a 1.5 ml reaction tube containing 4.5 % formaldehyde fixation solution (2:1:1, Heptane (*Fisher Scientific*), 2X PBS, 10 % formaldehyde). After 25 min incubation on a shaker, the bottom liquid phase in the vial was removed and 500 µl methanol (*Polysciences*) was added. Samples were vortexed for 1 min. Devitellinized embryos will sink to the bottom. All liquid was removed, and embryos were washed twice with 500 µl of methanol for 2 min (shaking) followed by a 1 h wash in 500 µl of methanol. Finally, the fixed embryos are stored in fresh methanol at -20 °C until staining.

For staining, the fixed embryos were washed three times in 0.3 % PBX for 40 min and the primary antibody (diluted in 0.3 % PBX) was added and then incubated at 4 °C overnight (shaking). The next day, the primary antibody was removed with three washed in 0.3 % PBX for 40 min. The secondary antibody (1:250 in 0.3 % PBX) was added and samples were incubated for 2 h at room temperature (shaking). After three washes in 0.3 % PBX for 40 min on the shaker, stained embryos are stored in 1X PBS. Prior to mounting the samples, the embryos were sorted according to their developmental stage under the microscope. Stage-17 embryos were placed on a 25 x 75 x 1 mm glass slides dorsal site facing up (18 x 18 mm No. 1.0 as bridges and No. 1.5 as coverslips). ProLong Gold antifade mounting medium with DAPI (*Invitrogen*) was added and slides were sealed with nail polish and stored for 24 h at room temperature and then moved to 4 °C for long-term storage.

4.8.4 Imaging

Samples were imaged at 10X or 40X magnification using the Leica TCS SP8 confocal microscopy setup of the Advanced Light Microscopy at Max Delbrück Center for Molecular Medicine (Berlin) or at 10X, 25X or 40 X magnification using the Zeiss Apotome.1 Imager Z1, a Hamamatsu C11440 ORCA-flash 4.0 OLT digital camera, and the Zeiss ZEN software (Bodmer lab, San Diego).

4.9 Ploidy assessment of cardiomyocyte nuclei in the adult fly

Ploidy in cardiomyocyte nuclei of adult fly hearts was assessed according to a modified protocol from Yu et al., 2013.[194] Flies were stained for DAPI in the same petri dish (as described above) to avoid batch effects between genotypes and imaged under identical emission intensities. z-stacks of stained cardiomyocyte nuclei were analyzed using FIJI (*ImageJ*) software. Here, the nuclei were manually

encircled in each z-stack slide, the integrated density was measured and the sum of the integrated density per nucleus was calculated representing the amount of DNA in each nucleus. Four to six nuclei per fly heart were measured and five fly hearts per genotype were analyzed.

4.10 Mhc protein level quantification

For Mhc protein level quantification in tissues, 1-week-old female mutant and control flies were stained in the same dish as described above using anti-Mhc (1:50, DSHB, 3E8-3D3) and anti-mouse-Alexa Fluor 488 (Jackson Labs, 1:500, 115-545-003). Fly hearts were imaged using a Zeiss Imager M.1 microscope equipped with a 25X dipping lens, with identical imaging settings for each fly (n=6-9 flies). Mean gray value (intensity) of 5 regions of interest (ROI) per tissue type (cardiomyocytes, body wall muscles, or ventral longitudinal muscle) were measured for each fly using FIJI (*ImageJ*), and the average of mean fluorescent intensity for each fly was calculated for each ROI.

4.11 Statistical analysis

Statistical analyses were conducted using *R* or GraphPad Prism. Statistical tests used are stated in the figure legends. For functional heart analysis mostly Kruskal-Wallis test, or Mann-Whitney U (Wilcoxon rank sum test) was performed assuming a non-normal distribution and to be more stringent. Fly heart data, which are presented as Cumming estimation plots, were calculated using the *R* package *dabestr*, which estimated the unpaired mean differences to the control mean.

4.12 Calculation of genetic interactions

As a basic principle of system genetics, it is assumed that there is no genetic interaction if the phenotype of the combined mutations is the product of the single phenotypes.[195] Expected value modeling was adapted from Saha et al. 2021.[196] Expected values were generated by random sampling from wild-type/gene1/gene2 and calculation of the *expected* phenotype as the product from each data triplet 20 times using an *R* script provided by Dr. Georg Vogler. This procedure was repeated 10 times and the average p-value was calculated. A significant difference between the observed and *expected* data was interpreted as a genetic interaction.

R script provided by Dr. Georg Vogler:

```
# Genetic interactions Drosophila
data <- openxlsx::read.xlsx("data.xlsx")

library(reshape2)
library(ggplot2)

genetic_interaction <- function(x)
{
  # Expecting 1st column control, 2nd and 3rd single genes and 4th column combined measurements
```

```
 # 1) Pick random control value
 ctrl_value <- x[sample(length(x[,1]),1, replace = TRUE),1]
 while(is.na(ctrl_value)){
  ctrl_value <- x[sample(length(x[,1]),1, replace = TRUE),1]
 }

 # 2) Pick random value from gene 1
 gene1_value <- x[sample(length(x[,2]),1, replace = TRUE),2]
 while(is.na(gene1_value)){
  gene1_value <- x[sample(length(x[,2]),1, replace = TRUE),2]
 }
 # 3) Pick random value from gene 2
 gene2_value <- x[sample(length(x[,3]),1, replace = TRUE),3]
 while(is.na(gene2_value)){
  gene2_value <- x[sample(length(x[,3]),1, replace = TRUE),3]
 }
 # 4) normalize to ctrl_value, computer PRODUCT of gene 1 x gene 2 as expected value

 expected_value <- (gene1_value / ctrl_value) * (gene2_value / ctrl_value)
 expected_value <- expected_value * ctrl_value
 # Return expected value
 expected_value

}

l <- list(a = data[,1], b = data[,2], c = data[1:3,3])
lengths(expand.grid(l))

# Number of runs
n <- 20
expected_data <- vector(length=n)

for (i in 1:n) {
  expected_data[[i]] <- genetic_interaction(data)
}

hist(data[,4])
hist(expected_data)

t.test(expected_data, data[,4])
wilcox.test(expected_data, data[,4])
wilcox.test(expected_data, data[,3])
expected_df <- data.frame(expected_data)

final_data <- melt(data)
final_data <- rbind(final_data, melt(expected_df))

ggplot(data = final_data, aes(x=variable, y=value)) + geom_boxplot(aes(fill=variable)) +
  geom_jitter(cex = 0.4) + theme_bw()+ theme(axis.text.x = element_text(angle = 45, hjust = 1))

write.csv(final_data, file = "expected vs observed.csv", row.names = F)
```

4.13 Construction of the cardiac-specific LifeAct reporter line

We used Gibson Assembly® to create a plasmid that harbors LifeAct-mScarlet downstream of the *R94C02* enhancer and can be integrated into the fly genome by microinjection coupled with targeted PhiC31 integrase-mediated site-specific transgenesis (*BestGene*). As templates we used the *pattB tinC-LifeActScarlet #1* plasmid and a *pMK3_R94C02* plasmid, kindly provided by Dr. Georg Vogler and the

Klassen lab, respectively. The aim was to replace the *tinC* enhancer (tin-C (Dm), 300 bp fragment identified by Yin et al., 1997)[197] of the *pattB tinC-LifeActScarlet #1* plasmid with the *R94C02* enhancer. Gibson Assembly® and bacterial transformation were performed according to protocol (*New England BioLabs*, Gibson Assembly® Master Mix – Assembly, #E2611S). Briefly, first, double-stranded DNA fragments containing 20-40 bp overlap with adjacent DNA fragments are generated by polymerase chain reaction (PCR) with specifically designed primers. Next, the Gibson assembly Master Mix is added and in a single reaction, an exonuclease first chews back DNA from the 5' ends, resulting in single-stranded DNA fragments that can anneal with adjacent DNA. Then, a DNA polymerase incorporates nucleotides to fill any gaps and lastly, a DNA ligase covalently joins the DNA fragments together. The ligation product is then introduced into competent bacteria by chemical transformation. For PCR we used Q5® High-Fidelity Polymerase (*New England BioLabs*, Q5® High-Fidelity 2X Master Mix, # M0492S). Primers to create the dsDNA fragments with overlapping ends are listed in **Table 2** (pattB tinC-LifeActScarlet FWD/ pattB tinC LifeActScarlet REV, pMK3_R94C02_F1/ pMK3_R94C02_ R2). Results were verified by Agarose gel electrophoresis and restriction enzyme digests (*New England BioLabs*). Before the Gibson Assembly reaction the PCR products were purified using the AxyPrep Magnetic Bead Purification Kit (*Axygen*®). For transformation XL1 -Blue competent cells (*Agilent*) were used. Successful ligation was verified by colony PCR (*New England BioLabs*, Q5® High-Fidelity 2X Master Mix, # M0492S) coupled with DNA sequencing (*EtonBio*, ABI 3730xl DNA sequencer) using colony PCR primers (see **Table 2**). Verified plasmids were amplified using QIAprep® Spin Miniprep Kit (*QIAGEN*). For additional verification, one plasmid was chosen to sequence its whole sequence and then sent for microinjection into *Drosophila* embryos to *BestGene*.

4.14 Semi-automated Optical Heartbeat analysis in Danio rerio (zebrafish)

All zebrafish experiments were performed in accordance with protocols approved by IACUC. Zebrafish were maintained under standard laboratory conditions at 28.5 °C. Gene expression was manipulated using microinjection of morpholinos (MO) antisense oligonucleotides[198] performed by Dr. Xin-Xin I Zeng. To create insertion/deletion mutations targeted mutagenesis was performed using CRISPR/Cas9 editing.[199–201]

For functional heart analysis zebrafish were treated with 10 µl of 1-phenyl 2-thiourea (PTU, in DMSO) at 24 hpf to inhibit melanogenesis and raised until 72 hours post-fertilization (hpf). Movie recording and analysis using SOHA software were performed according to standard protocol.[179,188] Briefly, larval zebrafish were immobilized in a small amount of low melt agarose (1.5 %, *fisher bioreagents*) and covered with conditioned water. Beating hearts were filmed for 30 s (up to 200 frames/s) using an Olympus BX61WI microscope with a Hamamatsu C9300 camera, and HCImage Live software.

5. Results – Chapter 1

5.1 Identification of myomesin-2 as a candidate gene in hypertrophic cardiomyopathy and Tetralogy of Fallot

5.1.1 Introduction

Under the auspices of the Einstein BIH Visiting Fellowship of the Stiftung Charité, the Rickert-Sperling lab (including my contribution) in collaboration with Rolf Bodmer's lab and Theresia Kraft's lab, studied a potential role of myomesin-2 *(MYOM2)* as a new, potentially causal CHD gene, which was published in *Disease Models and Mechanisms* in 2020.[3] In the following I outline the main findings of the study, followed by a detailed presentation of my contribution to the project.

With the aim to unravel the polygenic basis of congenital heart diseases, in particular, Tetralogy of Fallot (TOF) and Hypertrophic Cardiomyopathy (HCM) (see also Introduction section 1.3), the Rickert-Sperling lab identified mutations in *MYOM2* in two independent cohorts of unrelated patients with TOF and with HCM (**Figure 9**) which has not been associated with either of the diseases yet. In this study, four *MYOM2* mutations in a cohort of 13 clinically well-defined isolated TOF cases were identified, which carry, as described above (Introduction section 1.3), combinations of rare deleterious mutations in genes essential for cell growth, apoptosis, or sarcomere assembly, among others.[4] The cohort also comprises mutations in *MYH7* and *MYBPC3* and two of the patients harbored rare deleterious mutations in *TTN*, which were previously reported in CHD[202–205] which suggests that these variants might contribute to the TOF patients' phenotypes supporting an oligogenic origin. *MYOM2* mRNA levels in the TOF patients carrying variants in this gene were found to be upregulated compared to controls with normal hearts.[3] Furthermore, a cohort of 66 unrelated HCM patients was analyzed, who did not harbor any mutations in the known HCM disease genes, including *MYH7*, *MYBPC3*, *TNNT2*, *TNNI3*, *TPM1*, *MYL2*, *MYL3*, *ACTC1*, *TCAP*, *TNNC1*, *MYOZ2,* and *CSRP3*. Four HCM patients with potentially disease-causing *MYOM2* mutations were identified; three of which were missense mutations leading to amino acid changes and one was a truncating mutation leading to a premature stop codon. All eight mutations were rare or private (as for two HCM patients) with a minor allele frequency (MAF) less than 0.01 or zero, based on 71,702 genomes from unrelated individuals of the Genome Aggregation Database (gnomAD, https://gnomad.broadinstitute.org/).[206] The majority of the eight variants was predicted to be damaging based on PolyPhen2 (http://genetics.bwh.harvard.edu/pph2/)[207], SIFT (https://sift.bii.a-star.edu.sg/)[208] and MutationTaster (www.mutationtaster.org/).[209]

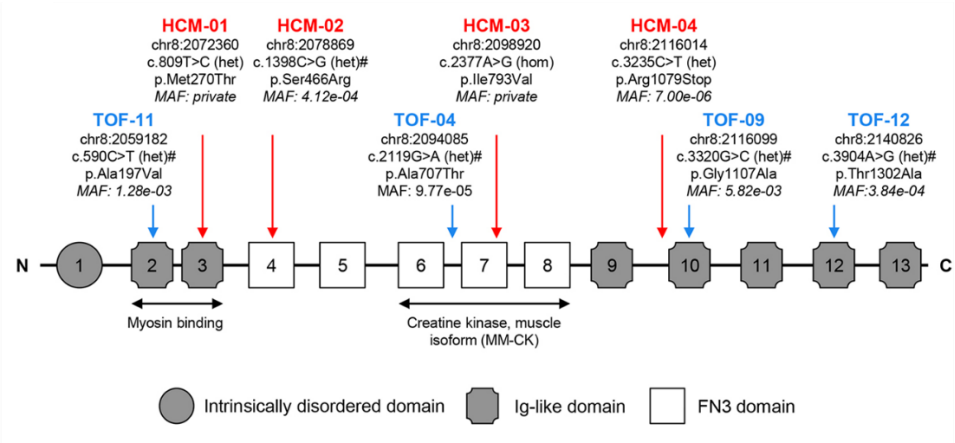

Figure 9: *MYOM2* mutations in TOF and HCM patients. Schematic of MYOM2, with its domain structure and mutations found in TOF (blue) and HCM (red) patients. Mutation positions are based on the human reference genome hg38. Nucleotide changes are based on transcript ENST00000262113. Amino acid changes are based on protein ENSP00000262113. Damage prediction by PolyPhen2, SIFT, or MutationTaster is indicated by '#'. The minor allele frequency is based on 71,702 genomes from unrelated individuals of the gnomAD (v3). The binding sites of two interaction partners, *MYH7* and creatine kinase (muscle isoform), are indicated below. Figure extracted from Auxerre-Plantié et al., 2020.[3]

The HCM patient carrying the S466R *MYOM2* variant (**Figure 9**) had to undergo septal myectomy. In collaboration with Theresia Kraft's lab morphological analysis of the tissue sections and force measurement on cardiomyocytes (CMs) isolated from the interventricular septum from the patient and five healthy age-matched controls were performed. Histological analysis revealed disarray of myofibrils and mild widening of the interstitial spaces in HCM-derived CMs indicative of HCM-dependent remodeling of the hypertrophic heart. One other major finding was a significantly lower passive force at increasing sarcomere lengths for the patient CMs compared to controls, suggesting that MYOM2 affects passive tension of CMs (*data not shown,* Figure 2 in Auxerre-Plantié et al., 2020).[3]

These findings suggested an important role for *MYOM2* in heart development and function. Thus, we investigated how alterations of this gene participate in a potentially interacting gene network involved in TOF and HCM pathogenesis by using *Drosophila melanogaster* as a heart model.

5.1.2 Acknowledgments

As part of the Einstein BIH Visiting Fellowship, Prof. Bodmer provided scientific consultation and Dr. Georg Vogler provided guidance on experimental design as well as fly stock resources and genetic interaction analysis, which was performed using an *R* script provided by Dr. Vogler. The Bodmer Lab performed RNAscope (ACDBio) experiments to localize *CG14964* (putative *MYOM2* homolog) expression and to confirm knockdown efficiencies of RNAi lines targeting *CG14964*. The fly experiments were performed together with Dr. Emilie Auxerre-Plantié and Olga Olejniczak. To generate a complete picture of the role of *CG14964* in *Drosophila*, data sets, which were not generated by myself were included and indicated as such in the text. Prof. Rickert-Sperling provided overall scientific input and project supervision, while Dr. Marcel Grunert performed bioinformatical analysis

and helped with *R* script-based SOHA data analysis and statistics. Note, that most of the figures derive from our publication (Auxerre-Plantié E.*, Nielsen T.*, Grunert M.* et al., 2020; *co-first authors) and are displayed in this work with a few modifications and adjustments.

5.1.3 Identification of *CG14964* as a putative *MYOM2 Drosophila* ortholog

Our first aim was to provide evidence for the hypothesis that *CG14964* is the *bona fide* fly ortholog to *MYOM2*, which is based on results of the *DSCR Integrative Ortholog Prediction Tool* (DIOPT) and comparison of protein domains of *CG14964* and *MYOM2*. According to DIOPT database, putative predicted orthologues of *MYOM2* are *bent* (*bt*), *CG14964, hibris* (*hbs*), and *sticks and stones* (*sns*) (date March 2018, www.flyrnai.org/cgi-bin/DRSC_orthologs.pl),[210] which all comprise FN3 and Ig-like domains, however only *CG14964* showed a protein domain arrangement close to *MYOM1, MYOM2*, and *MYOM3*. Sequence alignment of *MYOM2* and *CG14964* was performed by Dr. Auxerre-Plantié (**Figure 10** A). Since *CG14964* was predicted to be also similar to human myosin binding proteins H and H like (*MYBPH* and *MYBPHL*), as well as myosin binding proteins C (*MYBPC1*, *MYBPC2,* and *MYBPC3*) according to DIOPT, I performed sequence alignments using the online LAST tool, which is based on a modified standard seed-and-extend approach and allows plotting of an amino acid alignment in a dot plot manner (**Figure 10** B-D).[211] Like *MYOM2*, *MYBPH*, *MYBPHL,* and *MYBPC3* share a similar protein domain structure compared to *CG14964*. Therefore, we hypothesized that *CG14964* might exhibit the functional space of several sarcomere proteins in humans, including *MYOM2*, and we named the fly gene *myomesin and myosin binding protein* (*MnM*).

Similar to CG14964 and MYOM2, there are other sarcomere proteins that are conserved between fly and human, and which only share a common domain structure with orthology being less evident. For example, fly gene *sallimus* (*sls)* and *bent (bt)* both showed a conserved amino acid sequence with *TTN*, suggesting that both genes adopt the function of *TTN*. To confirm a potential role of *CG14964/MnM* in muscle and heart development, the Bodmer lab performed mRNA *in situ* hybridization (RNAscope*, ACDBio*) in the adult fly abdomen and found *CG14964* expressed in the heart (contractile CMs) and somatic muscles (data not shown).

In summary, the structural conservation of *CG14964* and the cardiac expression pattern suggests that *CG14964* is indeed the appropriate functional ortholog to study the cardiac role of *MYOM2*, as well as of other myosin binding proteins in the fly.

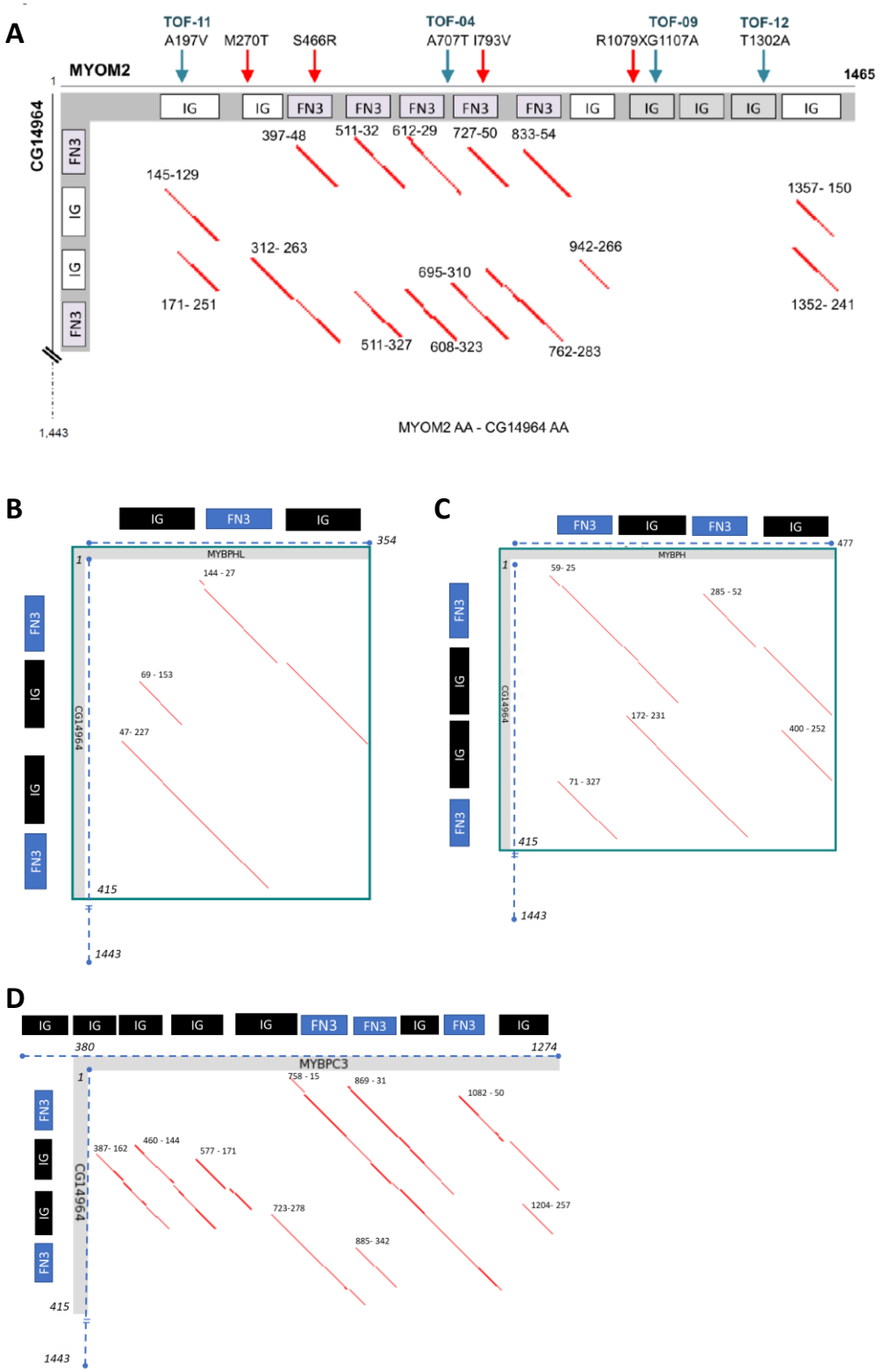

Figure 10: Amino acid alignments of *Drosophila* ortholog CG14964 with MYOM2, MYBPHL, MYBPH, and MYBPC3. (A) Alignment of CG14964 and MYOM2 show that both proteins are composed of fibronectin type III-like (FN3) and immunoglobulin-like (Ig) domains. Arrows indicate mutations in TOF (blue) and HCM patients (red), respectively. **(B-D)** Protein alignments of CG14964 with **(B)** MYPHL, **(C)** MYBPH, and **(D)** MYBPC3 show structural similarities between fly and human proteins. Figure extracted and modified from Auxerre-Plantié et al., 2020.[3]

5.1.4 Quantification of *CG14964* gene expression in transgenic fly lines

To characterize the role of *CG14964* in heart development and function in the *Drosophila* heart model, we used two different RNAi lines (GD line or also *CG14964*-GD (VDRC #43603) and TRiP line or also *CG14964*-T3 (BDSC #65245)) for targeted gene knockdown (KD) specifically in the heart and somatic muscles or the heart only (**Figure 11** A). For this, we utilized the inducible UAS-Gal4 system using the *Hand*$^{4.2}$-Gal4 driver (heart) or *Mef2*-Gal4 driver (heart and somatic muscles). In addition, we used a deficiency line, which contains a chromosomal deletion of 30 genes including *CG14964* (*CG14964*^{Df} = Df(3L)BSC672, BDSC #26524) and a *CG14964* CRISPR MiMIC (CRIMIC) mutant fly (*CG14964*^{CRIMIC} = CRIMIC line *CG14964*$^{CR01157\text{-}TG4.1}$, BDSC, #81199)[212] (**Figure 11** A, B).

I performed reverse transcription quantitative polymerase chain reaction (RT-qPCR) analysis to access *CG14964* mRNA levels in adult *CG14964*-GD knockdown flies with RNA extracted from fly heart tissue and in *CG14964*^{CRIMIC} mutant flies with RNA extracted from whole flies (**Figure 11** C, F, G). Quantification of *CG14964* expression in *CG14964*-T3 KD and heterozygous *CG14964*^{Df} flies were performed by Dr. Auxerre-Plantié (**Figure 11** D, E).

Both RNAi lines effectively reduced *CG14964* mRNA levels in the adult fly heart. Knockdown of *CG14964* in the heart (using *Hand*$^{4.2}$-Gal4 driver) is stronger in flies expressing TRiP RNAi (~70 % reduction), compared to GD RNAi (~50 % reduction), while there is no difference between both RNAi lines when expressed in the heart and muscles (using *Mef2*-Gal4 driver) (**Figure 11** C, D). The results for *Hand*$^{4.2}$-Gal4-driven knockdown efficiency were confirmed by *in situ* hybridization (RNAscope, *ACDBio*) by the Bodmer Lab.[3] For both systemic mutations, *CG14964*^{Df} and *CG14964*^{CRIMIC} we observed a ~50 % reduction in heterozygous flies (**Figure 11** E-G). In homozygous *CG14964*^{CRIMIC} flies or in a transheterozygous combination of the CRIMIC variant with the deficiency line, no *CG14964* mRNA was measured, suggesting that *CG14964*^{CRIMIC} mutation leads to a loss-of-function of the gene (**Figure 11** F, G). Note, that there were low levels of *CG14964* mRNA detected in homozygous CRIMIC mutants when using the TN35/36 primer pair. For both primer pairs, amplification efficiency and specificity were determined prior the experiment using a standard curve approach and by analyzing the melt curve of the obtained RT-qPCR products, respectively. Both primer pairs show good amplification efficiency (≈ 2) and specifically amplify *CG14964*. However, the low levels of *CG14964* mRNA detected in homozygous CRIMIC mutants using the TN35/36 primer pair are most likely products resulting from unspecific primer binding events, which can occur when no or low template cDNA is present. The RT-qPCR melt curve analysis of the respective reactions confirmed this hypothesis since it indicated multiple products with different melting temperatures.

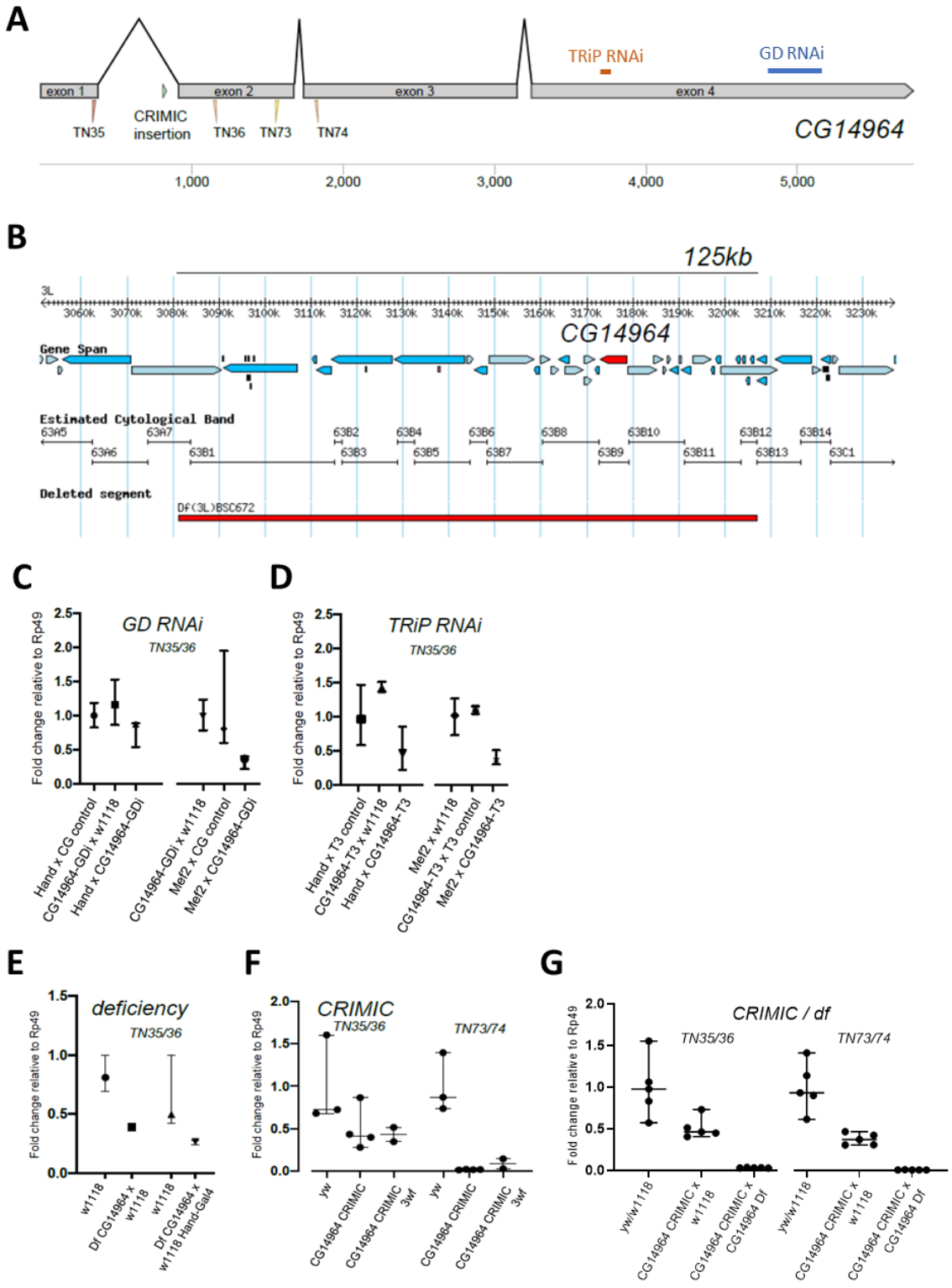

Figure 11: *CG14964* genomic locus and knockdown efficiency in different fly mutants. **(A)** Organization of the genomic locus of *CG14964* including CRIMIC insertion site, RNAi binding sites, and localization of RT-qPCR primers used. **(B)** Genomic region covered by Df(3L)BSC672 deficiency spanning multiple genes including *CG14964* (red). **(C-D)** RT-qPCR was performed in a heart-specific manner showing a knockdown of *CG14964* in **(C)** *CG14964*-GDi and **(D)** *CG14964*-T3 3 -weeks-old adult female hearts where the RNAi is expressed in heart only (*Hand*$^{4.2}$-Gal4) or muscle and heart (*Mef2*-Gal4). **(E-G)** RT-qPCR results performed from RNA isolated from whole **(E)** heterozygous *CG14964* deficiency female adult flies, **(F)** homozygous CRIMIC insertion flies, and **(G)** CRIMIC/Df transheterozygotes. Data depicted as median with range. TN35/36 and TN73/TN74 indicate the primer pair used. Hand = Hand$^{4.2}$-Gal4, Mef2 = Mef2-Gal4. Figure extracted and modified from Auxerre-Plantié et al., 2020.[3]

5.1.5 Heart- and muscle-specific knockdown of *CG14964* leads to cardiac and muscle defects

To assess changes in heart tube function I applied the semi-automated optical heartbeat analysis (SOHA) method to measure rhythmicity and contractility parameters in dissected semi-intact adult flies (see also 1.5.4 and 4.3.1) together with Dr. Auxerre-Plantié and Olga Olejniczak. While Dr. Auxerre-Plantié mainly focused on studying *CG14964*^{Df} and *CG14964*-T3, I assessed heart function in *CG14964*^{CRIMIC} mutants and *CG14964*-GD knockdown flies. Focusing on diastolic heart diameters (heart diameter in relaxed state), we found that flies with moderate (~50 %) reduction of *CG14964* mRNA levels (see **Figure 11**), *CG14964*-GD, and heterozygous deficient flies, show dilated heart tube diameters of the beating heart, as well as of fixed heart samples following immunostaining (**Figure 12** A-C). Strong reduction of *CG14964* as observed in flies with homozygous *CG14964*^{CRIMIC} mutation or a transheterozygous combination of *CG14964*^{CRIMIC} and *CG14964*^{Df}, exhibited cardiac constriction (**Figure 12** D). A similar but not significant trend was observed with a strong KD using the TRiP RNAi line *CG14964*-T3 (see also **Figure 15** D).[3] We did not observe any overt changes in other heart parameters, including fractional shortening or rhythmicity parameters, like heart period, upon diminished *CG14964* function. In the following gene interaction experiments, we therefore focused on heart diameters as a readout.

Since *CG14964* is also expressed in somatic muscles we evaluated its role for muscle function in general. We used the rapid negative geotaxis (RING) assay[190] to assess climbing ability in flies exhibiting *CG14964* knockdown in the heart and muscles using the *Mef2*-Gal4 driver. We found a significant locomotion defect in flies with *CG14964*-T3 mediated knockdown compared to controls (Dr. Auxerre-Plantié's work), while flies expressing *CG14964*-GD show no climbing defect (my work) (**Figure 13**). Furthermore muscle- and heart-specific KD of *CG14964* using *CG14964*-T3 significantly reduced life span with fewer than half of the flies surviving beyond 4 weeks of age (*data not shown*).[3] Life span experiments were performed by Dr. Emilie-Plantié with the support of Sandra Schochardt-Schuster. I also observed locomotion defects and reduced viability in *CG14964*^{CRIMIC} mutants, homozygous or transheterozygous with *CG14964*^{Df} (not quantified).

Overall, the cardiac defects together with diminished climbing ability and reduced survival imply impairment of overall muscle function, but also a specific role for *CG14964* in the heart.

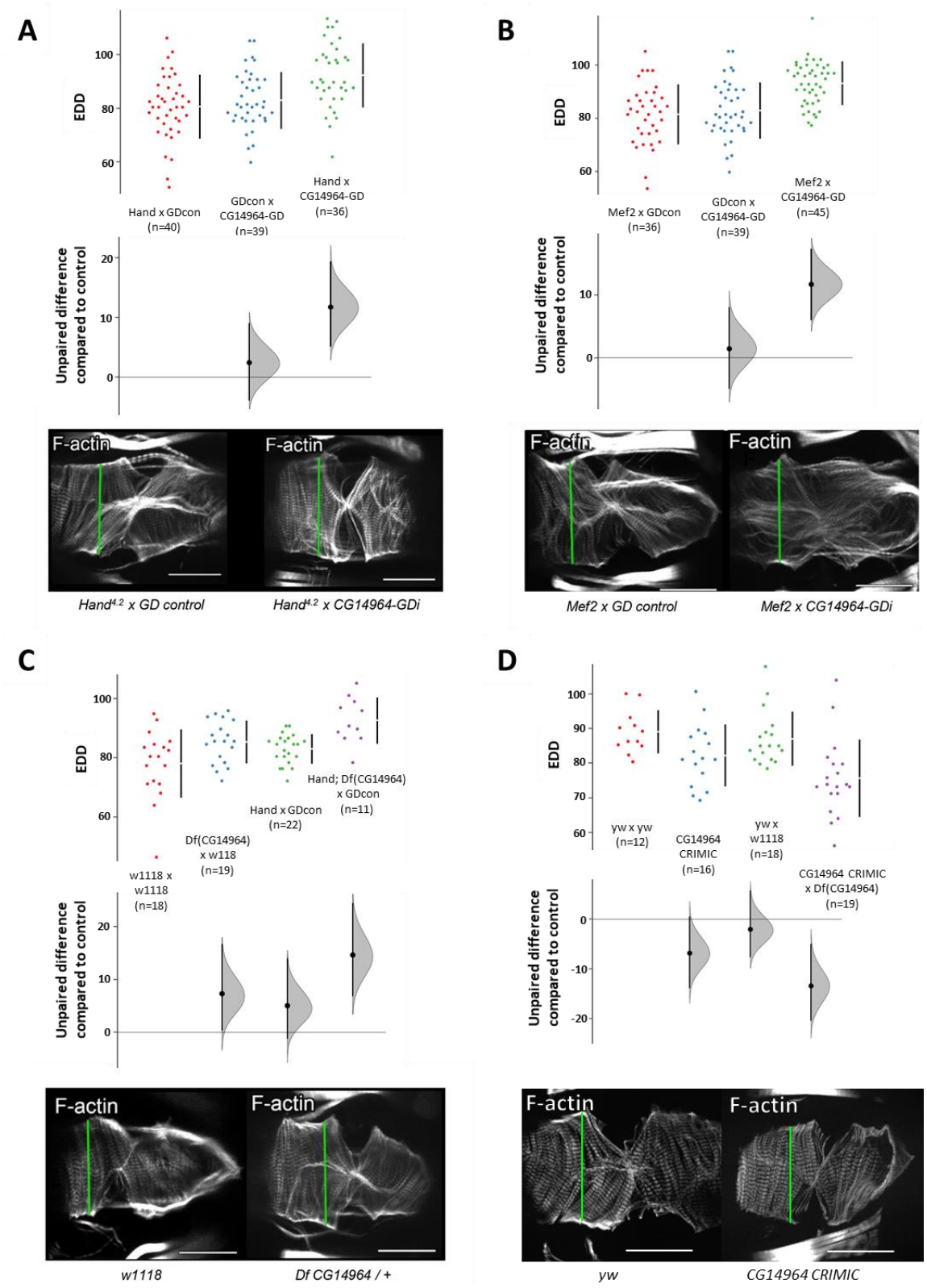

Figure 12: Cardiac-specific knockdown of *CG14964* leads to dosage-dependent heart defects in the adult fly. (A-D) End-diastolic diameter (EDD) of 3-week-old female flies with knockdown of *CG14964* by using **(A)** *CG14964*-GD crossed with *Hand*$^{4.2}$-Gal4, **(B)** *CG14964*-GD crossed with *Mef2*-Gal4, **(C)** heterozygous for *CG14964* deficiency, **(D)** homozygous for *CG14964*^{CRIMIC} or transheterozygous for *CG14964*^{CRIMIC}/deficiency. We observed heart dilation (A-C, mild knockdown) or constriction (D, strong knockdown). All raw data are shown (mean ± SD), as well as effect size and 95 % c.i. below the data. In addition, phalloidin-stained cardiac myofibrils show altered heart diameters in representative examples (measurements taken at the green lines). Scale bars: 50 µm. SOHA analysis of *CG14964*^{Df} and *CG14964*-T3 was performed by Dr. Auxerre-Plantié. Figure extracted and modified from Auxerre-Plantié et al., 2020.[3]

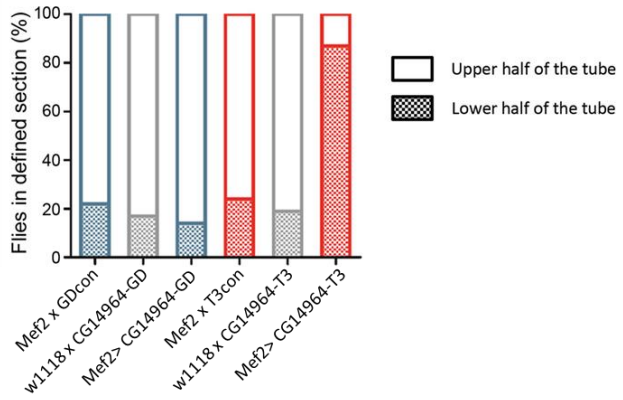

Figure 13: Muscle-specific knockdown of *CG14964* causes locomotion defects in adult flies. Locomotion test performed using the RING assay on adult flies expressing *CG14964*i-GD (left) and *CG14964*i-T3 (right) in muscles (*Mef2*-Gal4) showed reduced locomotion ability at 3 weeks in Mef2>*CG14964*i-T3 flies only. Graph shows percentage of fly population in a defined section of the vial after 20s (n=20 flies, mean of 3 repetitions, see also Methods section 4.6). Figure extracted from Auxerre-Plantié et al., 2020.[3]

5.1.6 Mapping of P-Element insertion site in *CG14964* RNAi GD fly genome

In contrast to TRiP fly lines, where the hairpin/RNAi-containing transgenes are inserted via site-specific recombination, the GD fly lines were constructed using P-elements to randomly insert hairpin RNAs (average 321 base pairs (bp)) into the genome and thus may disrupt other off-target genes. Since flies expressing *CG14964*-GD do not exhibit the same cardiac phenotypes compared to flies expressing *CG14964*-T3 or the *CG14964*^{CRIMIC} mutant flies, I performed an inverse PCR experiment to map the location, where the P-element was inserted into the *CG14964*-GD fly genome.

The inverse PCR (also inverted or inside-out PCR) is used to amplify DNA sequences that flank an unknown DNA sequence and for which no primers are available (for more details see Methods section 4.5). The P-element carrying the RNAi sequence of the GD line was inserted in an intron of the *death-associated inhibitor of apoptosis 1* (*diap1*) gene in the left arm of the 3rd chromosome (**Figure 14** A). It was already shown, that *diap1* can be involved in heart function,[213,214] so I assessed the expression level of *diap1* by RT-qPCR to exclude that *diap1* expression is altered in flies carrying the P-element construct. We saw a 50 % reduction in *diap1* gene expression in flies carrying the P-element construct (heterozygous) (**Figure 14** B, C). There was an even stronger (but not complete) knockdown in homozygous flies (**Figure 14** C), suggesting that not all splice forms of *diap1* are affected. This could be checked by RT-qPCR specifically designed to assess the levels of each transcript isoform individually (n=6 isoforms). However, observing that heterozygous *CG14964*-GD flies show downregulation of *diap1* of about 50 %, while we see no elevation in heart diameters with SOHA analysis (**Figure 12** A, B) suggests that *diap1* alteration does not cause the observed dilation phenotype in *CG14964*-GD KD flies. Of note, as a gene being involved in apoptosis, *diap1* could have an effect and could be involved in the differences we observed compared to the TRiP line and CRIMIC mutants.

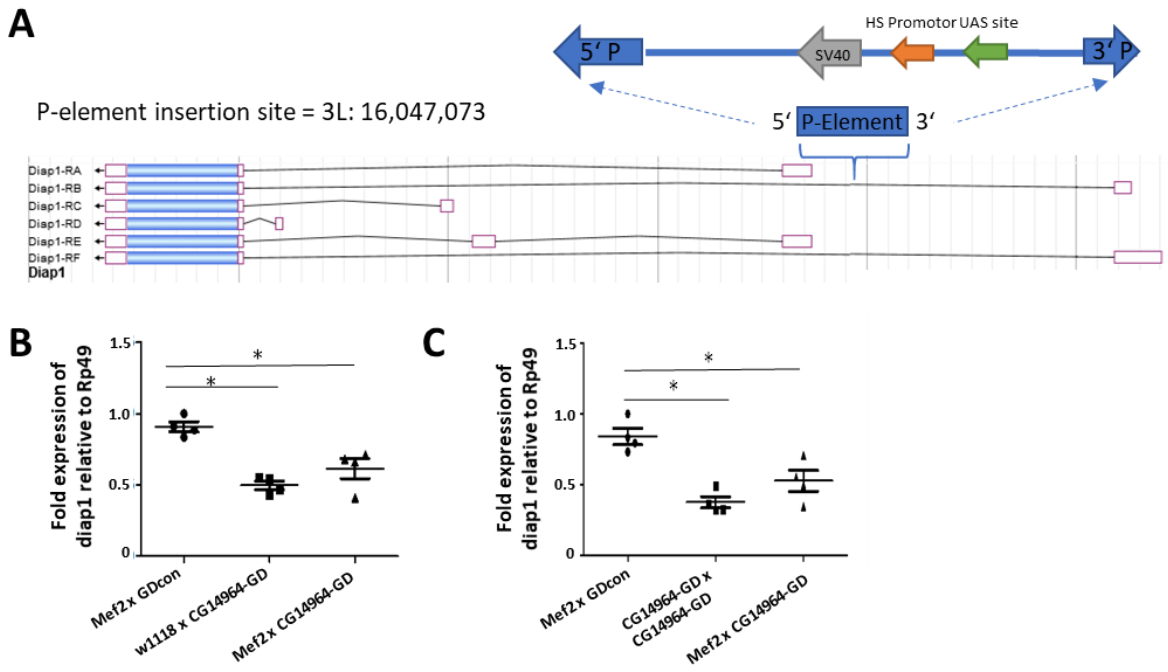

Figure 14: Mapping of inserted P-Element in the fly genome of *CG14964*-GD line flies and assessment of *diap1* expression in *CG14964*-GD line flies. (A) The P-Element containing the RNAi sequence targeting *CG14964* is inserted in an intron of the *diap1* gene as identified using inverse PCR. Modified screenshot from flybase.org. **(B)** RT-qPCR results showing fold expression of *diap1* normalized to *Rp49* (reference gene) and relative to Mef2 x GDcon. Depicted is the mean ± SEM of 4 biological replicates consisting of 3-6 dissected flies (dissection according to SOHA method) per replicate. Mef2 = Mef2-Gal4. Statistics: two-tailed Wilcoxon rank sum test, *p = 0.05.

5.1.7 Probing for genetic interactions between *CG14964* and other components of the sarcomere

In the sarcomere MYOM2 is believed to function as crosslinker between TTN and myosin as it was shown to bind both proteins in biochemical assays.[73–75] Both TTN and myosin variants were previously found to be associated with congenital heart disease.[4,48,203,215] In a system genetics approach, we tested for genetic interactions between *CG14964* and *TTN* fly orthologs *sallimus* and *bent* as well as *MYH6/7* fly ortholog *myosin heavy chain* (*Mhc)* to identify gene and gene networks perturbations following diminished *MYOM2* function, which could potentially be involved in the manifestation of complex cardiac traits**.**

5.1.7.1 Probing for genetic interactions between *CG14964* and *sallimus* or *bent*

To test for genetic interactions, I generated a fly line that carries the *Hand*$^{4.2}$-Gal4 driver together with a *sallimus* mutant allele (*sls*^{31}) (**Figure 15** A). In this mutant endogeneous exon 31 of the *sallimus* gene was removed and replaced by a sequence containing a dsRed marker and a termination sequence (gift from Dr. Frank Schnorrer, *unpublished*). I also attempted to combine the *Hand*$^{4.2}$-Gal4 driver with a *bent* mutant allele. However, *bent* lies on the very small 4th chromosome and combinations with mutant alleles on this chromosome are not trivial. During the combination process, some allele combinations were lethal, and I was not able to retrieve the required genotype

to generate the line. To test for a genetic interaction between *CG14964* and *bent,* I therefore used a deficiency line including *bent* and *CG14964*^{Df} (*CG14964*^{CRIMIC} was not available at this time point).
As a basic principle of system genetics, it is assumed that there is no genetic interaction if the phenotype of the combined mutations is the product of the single phenotypes (**Figure 15** B).[195] Using "animal fitness" as an example, it is called a negative interaction if the fitness (phenotype) of an organism with both mutations is worse than the product of the single phenotypes and it is called a positive interaction if it is better.[195]

Using the generated *Hand*$^{4.2}$-Gal4; *sls*^{31} sensitizer fly line, I tested for genetic interactions between *sls* and *CG14964* using the SOHA method. Consistent with former results we observe dilated diastolic heart diameters upon heart-specific knockdown of *CG14964* using *CG14964*-GD, while *CG14964*-T3 shows a tendency towards smaller parameters (**Figure 15** C, D). Heterozygous mutation of *sls* (*sls*^{31}) alone did not affect diastolic heart diameters. The combination of *CG14964* knockdown (GD or TRiP) in a *sls*^{31} heterozygous background resulted in intermediate heart diameters, indicating no synergistic interaction (**Figure 15** C, D). As an alternative approach, I tested *CG14964*^{Df} in combination with two further *sls* alleles (*sls*^{1} and *sls*^{j1D7}). *sls*^{1} is an ethyl methanesulfonate amorph (null) mutation and *sls*^{j1D7} is a *P{lacW}* insertion into an exon encoding part of the PEVK-2 domain (loss-of-function mutation). As described before, I observed dilated heart diameters in heterozygous *CG14964*^{Df} flies (**Figure 15** E-G), which in trans with *sls*^{1} heterozygosity showed further dilated heart diameters. (**Figure 15** E). Transheterozygous mutants for *CG14964*^{Df} and *sls*^{j1D7} show intermediate heart diameters equal to the product of the single mutant phenotypes (**Figure 15** F). Interestingly, *sls*^{31} and *sls*^{j1D7} both seem to reverse the dilation phenotype in *CG14964*-GD and *CG14964*^{Df} flies, while *sls*^{1} leads towards further dilation (not significant). At this point, our results can neither clearly confirm nor reject the possibility of a genetic interaction between *sls* and *CG14964*.

Flies carrying a heterozygous deletion of the 4th Chromosome that includes *bent*, show enlarged heart diameters compared to controls. This observation is consistent with previous results from Dr. Vogler, showing that heart-specific knockdown of *bent* causes a strong heart dilation and much reduced contractility (*unpublished*). In combination with *CG14964*^{Df}, transheterozygous mutants showed dilated heart diameters compared to controls (**Figure 15** G); however, no genetic interaction was observed. Further experiments with gene knockdown/knockouts specifically targeting *bent* and *CG14964* (in contrast to the deficiency lines used here) are needed to clearly reject a potential interaction between both genes.

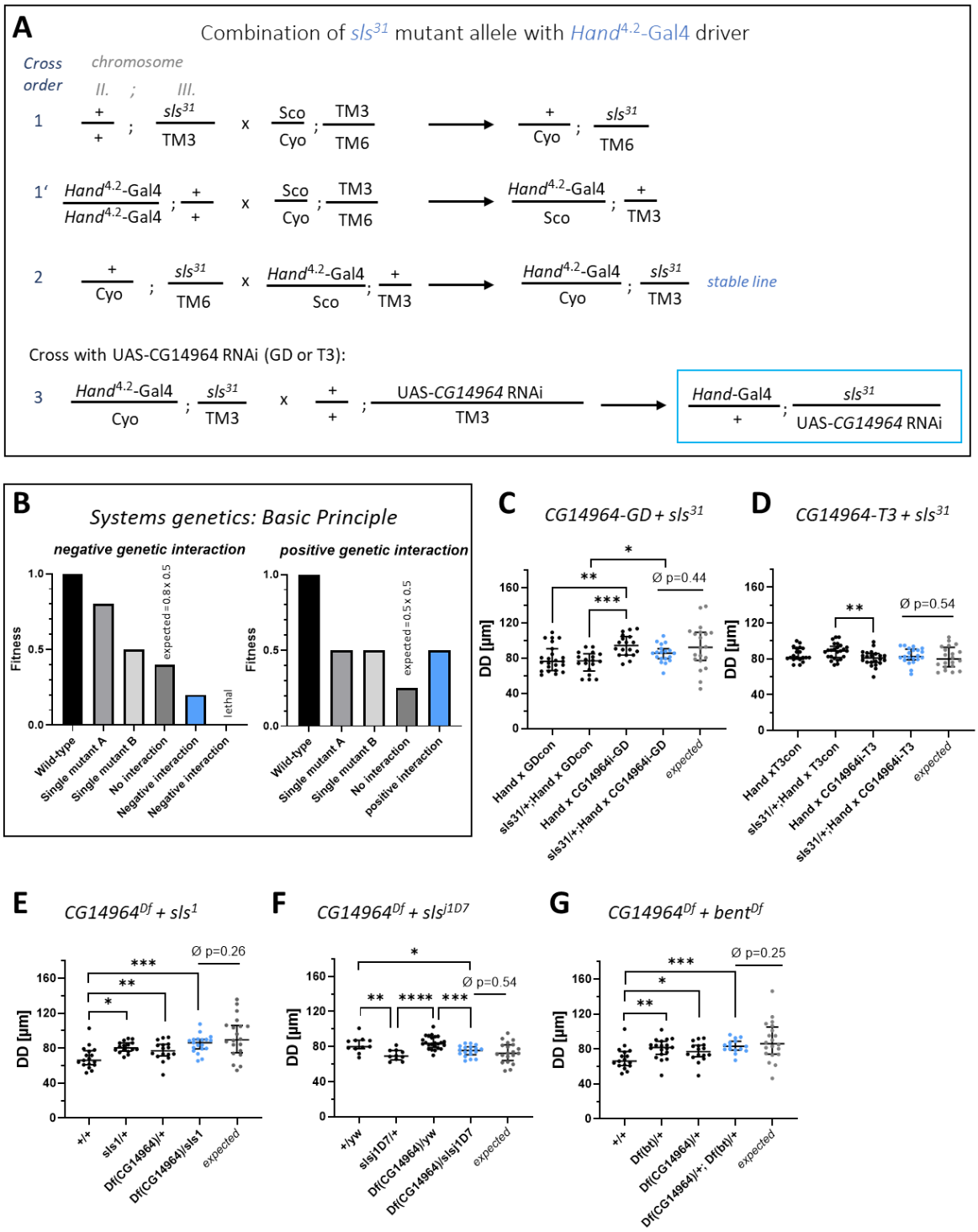

Figure 15: Probing for genetic interactions between *CG14964* and *sallimus* or *bent*. (A) Schematic crossing scheme to combine *sls*^{31} mutant allele with *Hand*$^{4.2}$-Gal4 driver. **(B)** Basic principle of system genetics displaying an example for negative or positive genetic interactions with animal fitness as readout. In a 'null model' of genetic interaction, it is assumed that the phenotype of the combined mutations is the product of the single phenotypes ('expected'). Graphs adapted from Costanzo et al. 2019).[195] **(C-G)** Expected values were generated by random sampling from wild-type/gene1/gene2 and computing the phenotype as the product from each data triplet 20 times (10 repetitions). The Ø p-value represents the average p-value of the 10 repetitions. A significant difference between the observed and *expected* data is interpreted as a genetic interaction (see also Methods section 4.12). **(C-D)** Diastolic Diameter (DD) of 3-week-old female flies with heart-specific *CG14964* knockdown using *CG14964*-GD **(C)** or *CG14964*-T3 **(D)** with or without additional *sallimus* mutation indicate no genetic interaction. **(E-F)** DD of 3-week-old female *CG14964*^{Df} heterozygotes with/without additional *sallimus* mutation. **(G)** DD of 3-week-old female *CG14964*^{Df} heterozygotes with/without additional deficiency for *bent*. Data depicted as median with interquartile range; each data point represents one fly. Statistics: Wilcoxon ranks sum test, *p<0.05, **p<0.01, ***p<0.001, ****p<0.0001. + = wild type allele; (E, G) w1118 genetic background, (F) w1118/yw genetic background.

5.1.7.2 Interaction between *CG14964* and *Mhc*

To test for genetic interactions between *Mhc (Drosophila MYH6/MYH7)* and *CG14964 in vivo* in the fly, we used a heterozygous null mutant for *Mhc* (*Mhc*^{1})[216,217] in combination with the *Hand*$^{4.2}$-Gal4 driver and crossed it with both RNAi lines (GD line and TRiP) (experiments performed by Dr. Auxerre-Plantié). *Mhc*^{1} heterozygosity causes constricted heart diameters, which were even further constricted in combination with a strong KD of *CG14964* (TRiP RNAi line) (**Figure 16** A). Although no significant synergistic interaction between both genes is observed, the data suggest a worsening of the *CG14964* TRiP KD phenotypes in a *Mhc* heterozygous background. Furthermore, I tested *CG14964*$^{\text{CRIMIC}}$ heterozygosity in a *Mhc*^{1} heterozygous background. Similarly, heterozygous *CG14964*$^{\text{CRIMIC}}$ mutants exhibit a trend towards further constrictions in a *Mhc*^{1} heterozygous background compared to the *expected* values (**Figure 16** B). In contrast, *Mhc*^{1} heterozygosity in combination with a mild KD of *CG14964* (GD RNAi) resulted in intermediate heart diameters suggesting that reduction of *Mhc* reverses the dilation phenotype towards wild type levels (**Figure 16** C). That is consistent with my finding that *CG14964*^{CRIMIC} mutants exhibit elevated Mhc protein levels compared to controls shown by protein level quantification in 1-week old homozygous *CG14964*^{CRIMIC} stained for Mhc (**Figure 16** D-G, see also Methods section 4.10). Mutant's Mhc levels were significantly higher in all tissues measured (cardiomyocytes, ventral longitudinal muscles, and body wall muscles) (**Figure 16** E-G) suggesting a systemic response of *CG14964* loss in all muscles. Note, that the integrity of the overall sarcomere structure in homozygous *CG14964*$^{\text{CRIMIC}}$ mutants was still preserved as demonstrated with an F-Actin – Mhc sarcomere pattern similar to controls (**Figure 16** H).

Our results point towards a genetic and functional interaction between *CG14964* and *Mhc* in the fly heart comparable to the postulated *MYOM2* and *MYH6/7* interaction in mammals.[73–75]

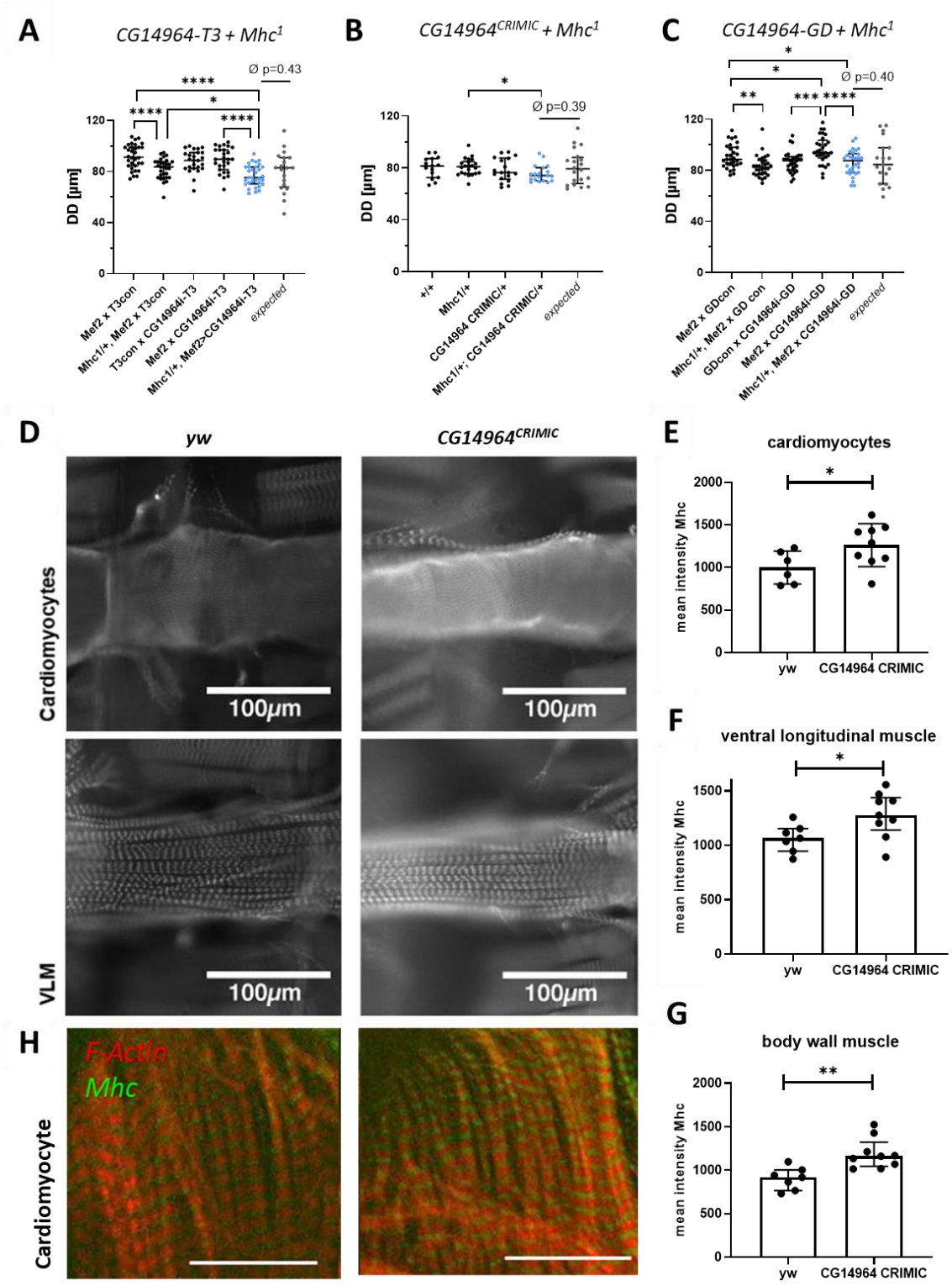

Figure 16: *CG14964* interacts with *Mhc* in the fly. (A) Diastolic Diameters (DD) are decreased in *Mhc*^{1} heterozygous flies and become further constricted upon strong *CG14964* knockdown. w1118 genetic background. **(B)** *Mhc*^{1} heterozygous flies show no constriction in a yw genetic background. Transheterozygous mutants carrying *Mhc*^{1} and *CG14964*^{CRIMIC} show smaller DD compared to *Mhc*^{1} heterozygosity alone. yw genetic background. **(C)** Mild *CG14964* knockdown causes enlarged hearts, which is restricted by *Mhc*^{1} heterozygosity. w1118 genetic background. Data depicted as median with interquartile range; each data point represents one fly (A-C). Statistics: Wilcoxon rank sum test, *p≤0.05, **p≤0.01, ***p≤0.001, ****p≤0.0001. **(D)** 1-week female *CG14964*^{CRIMIC} flies and controls were stained for Mhc and imaged using identical settings. **(E-G)** Mutant hearts have a stronger Mhc signal compared to controls in cardiomyocytes (E), but also ventral layer muscles (VLM) (F) and body wall muscles (G). Mean gray value (intensity) of five regions per cell type and fly were measured using ImageJ and the average was calculated (=mean Mhc intensity). Graphs display median with interquartile range and one data point represents

mean Mhc intensity per one fly. Statistics: unpaired two-sided Student's t-test, *p≤0.05, **p≤0.01. *CG14964* CRIMIC = homozygous *CG14964* CRIMIC mutants; all intensity values are artificial units. **(H)** Representative image showing intact sarcomere structure of 3-week-old homozygous *CG14964*^{CRIMIC} mutant and controls (yw) stained for F-Actin (red) and Mhc (green). Scale bar = 20 µm. + = wild type allele. Figure extracted and modified from Auxerre-Plantié et al., 2020.[3]

5.1.8 Assessment of hypertrophy markers in adult *CG14964*-deficient *Drosophila* hearts

Cardiac hypertrophy is a phenotype observed in TOF (RV hypertrophy) and HCM (LV hypertrophy) patients, which we aim to evaluate in our fly model. Based on the discovery, that the epidermal growth factor receptor (EGFR) pathway is involved in cardiac hypertrophy, Yu and colleagues established a hypertrophy fly model in 2013. They created a fly line expressing constitutively activated GTPase Ras under UAS control and expression specifically in the heart (Hand$^{4.2}$-Gal4>*Ras*85D^{V12}) led to elevated heart wall thickness and increased ploidy in cardiomyocytes.[194] We used this fly line as a positive control for assessing hypertrophy markers like heart wall thickness (HWT) or ploidy levels in *CG14964* KD flies.

To measure heart wall thickness of *CG14964* KD flies and controls we performed an antibody staining against α-spectrin, which specifically marks the heart walls (see **Figure 17** A-C). While Hand$^{4.2}$-Gal4>*Ras*85D^{V12} showed elevated wall thickness as expected (**Figure 17** C), knockdown of *CG14964* using *CG14964*-GD or *CG14964*-T3 showed no differences to control flies (**Figure 17** D, F) (data from Olga Olejniczak). I evaluated heart wall thickness in homozygous *CG14964*^{CRIMIC} mutant flies stained for α-spectrin, and also observed no increased wall thickness (**Figure 17** E).

Next, I examined cardiomyocyte ploidy levels in flies knocked down for *CG14964*, as a marker for hypertrophy (see Methods section 4.9). I was able to reproduce the results of Yu et al. by showing increased ploidy in Ras overexpressing flies (**Figure 17** J). Moreover, we observed elevated ploidy in cardiomyocytes of 3-weeks-old *Mef*2-Gal4>*CG14964*-GD flies (**Figure 17** K) compared to controls. Consistently, 1-week-old homozygous *CG14964* CRIMIC mutants also exhibited elevated polyploidy compared to controls (**Figure 17** L).

Overall, we found increased polyploidy in cardiomyocytes with diminished *CG14964* function, which is also a hallmark of hypertrophy, although heart wall thickness was not found elevated.

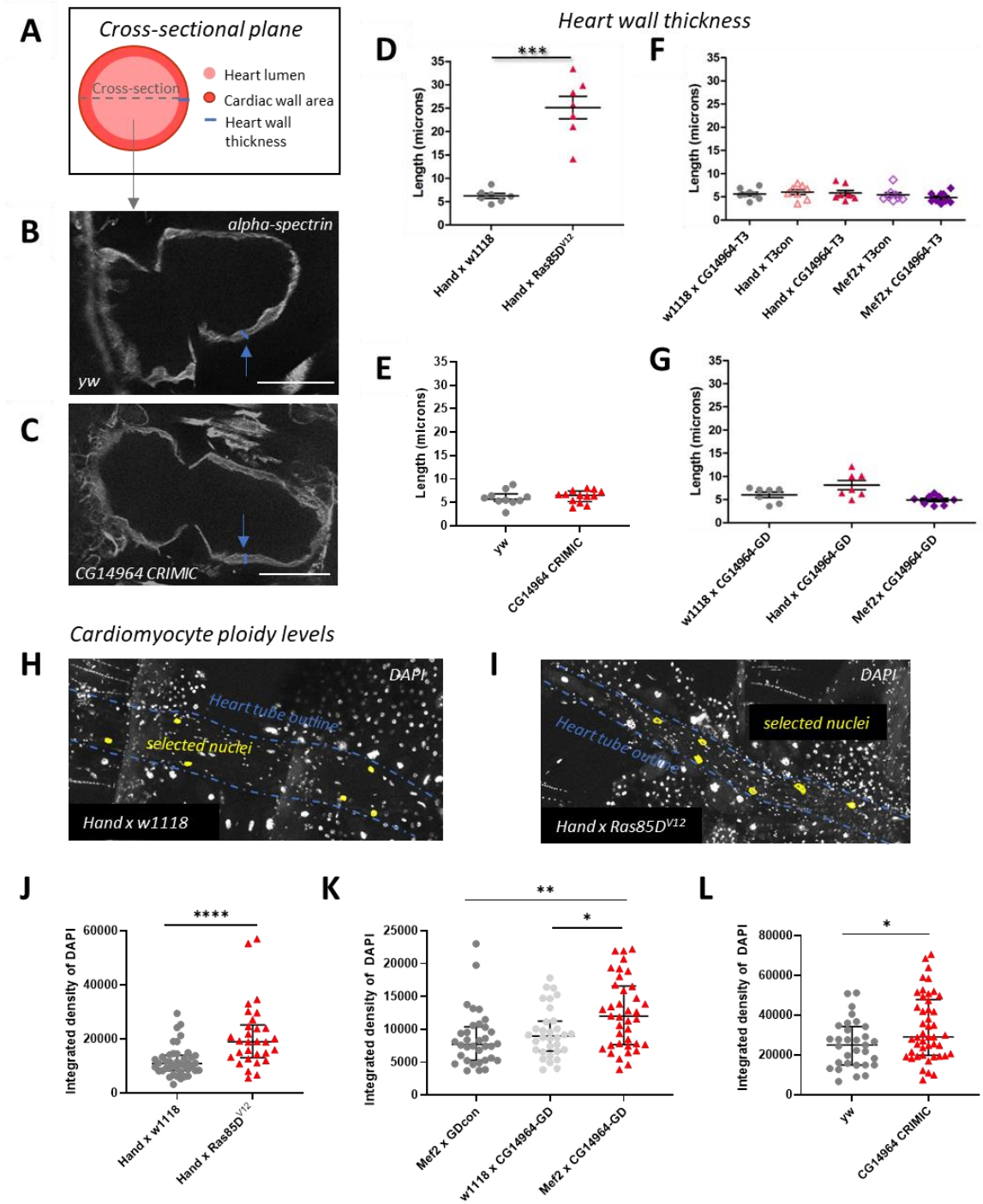

Figure 17: Assessment of hypertrophy markers in adult *CG14964* KD hearts and controls. (A) Scheme of a cross-section through the adult fly heart. **(B-C)** Longitudinal cross-section of 3-week-old female control flies (yw, B) or homozygous *CG14964* CRIMIC flies (C) stained for *α*-spectrin. Blue arrows indicated position of heart wall thickness measurements. Scale bar = 50 µm. **(D)** One-week-old female Hand>Ras85D^{V12} flies exhibit elevated heart wall thickness. **(E)** 3-week-old homozygous *CG14964*^{CRIMIC} mutants show no elevated heart walls thickness compared to control. **(F-G)** Flies with heart- or heart and muscle-specific *CG14964* KD using *CG14964*-GD (3-week-old females) or *CG14964*-T3 (1-week old females) show no change in heart wall thickness compared to controls. Each data point represents one fly heart. Mean ± SEM is depicted. Statistics: two-sided Wilcoxon rank sum test. ***p≤0.001. **(H-I)** Representative fly heart stained for DAPI from controls (H) and hypertrophic Hand x Ras85D^{V12} flies (I). Heart tube outline in blue and selected nuclei in yellow. **(J-L)** Depicted is the integrated density of DAPI of fly cardiomyocyte nuclei, measured in ImageJ and representing the amount of DNA in each nucleus. I observed elevated ploidy in cardiomyocytes of 1-week-old Hand>Ras85D^{V12} flies (J, n= 5 hearts per genotype), in 3-week-old Mef2>*CG14964*-GD flies compared to controls (K, n= 5 hearts per genotype) and in one-week-old homozygous CRIMIC mutants (L, n=10) compared to controls (n=6). Each data point represents one nucleus. Three - six nuclei per heart were measured. Data depicted as median with interquartile range. Statistics: two-sided Student's t-test, *p≤0.05, **p≤0.01, ****p≤0.0001; Hand = *Hand*$^{4.2}$-Gal4, Mef2 = *Mef2*-Gal4.

5.1.9 Discussion

Myofibrils in vertebrates and invertebrates mediate skeletal as well as cardiac muscle contractions and an alteration in the sarcomere protein composition influences their contractile performance.[218] The M-Band is an underestimated part of the sarcomere, not only due to its location but also due to its function as a mechanical stress absorber and its ability to respond in its composition to changes in demand.[69]

In this study, we identified rare and deleterious mutations in M-band protein myomesin-2 in HCM and TOF patients which share a common feature: hypertrophy (**Figure 9**). In humans, there are two other myomesin genes, *MYOM1* and *MYOM3*, besides *MYOM2*. However, the genetic redundancy of the myomesin proteins most likely cannot functionally compensate for the loss/malfunction of one of its homologs as demonstrated in the example of arthrogryposis.[219] Here, a loss-of-function variant of *MYOM2* was identified in an affected fetus, with cardiac and arthrogryposis phenotypes, which did not harbor any changes in *MYOM1* or *MYOM3*. Arthrogryposis is a term that describes a variety of conditions involving multiple joint contractures (or stiffness).

Only a few data exist concerning a potential pathogenic role of M-band protein variants in cardiomyopathies or TOF. We identified four TOF cases with *MYOM2* variants in a very homogenous cohort of 13 isolated TOF patients (31 %). In the so far biggest study of ca. 2800 CHD patients (Pediatrics Cardiac Genetics Consortium (PCGC)), only 14 cases with rare inherited or *de novo* mutations in *MYOM2* were found, two of those in TOF patients (14 %).[30] As in many CHD cohorts, the variety of CHDs with *MYOM2* variants was very wide, ranging from complex heterotaxias, such as double outlet RV, to isolated simple atrial or ventricular septal defects.[30] In our cohort of 66 HCM patients, we further identified four rare *MYOM2* variants, half of which were predicted to be damaging. Although a likely disease-associated mutation and seven variants of unknown significance (VUS) were identified in *MYOM1*, no rare variants in *MYOM2* had thus far been reported in cardiomyopathy patients.[82,220–224] In addition, there is currently no mammalian *MYOM2* model to elucidate the role of myomesin in sarcomere organization *in vivo.* In zebrafish four redundant myomesin paralogous are present and only *MYOM3* has been studied in slow muscles.[225] However, a recent report in BioRxiv claims that zebrafish mutants for RNA-binding protein *RBPMS2* exhibit differential alternative splicing of several genes potentially linked to cardiomyopathies in humans, including *myosin binding protein C3* (*mybpc3*), *phospholamban* (*pln*), as well as *myomesin 2a* (*myom2a*).[226] Both, *rbpms2*-null animals and *RBPMS2*-null hiPSC-CMs exhibit defects in sarcomere organization and calcium handling, potentially based on the misregulation of Rbpms2 targets.[226] This goes in line with the cellular and myofibrillar disarray we observed in CMs derived from an HCM patient with a *MYOM2* mutation. Additionally, the HCM-derived CMs showed reduced passive force

at increasing sarcomere lengths compared to controls, indicating that *MYOM2* might influence passive tension, which might result in altered diastolic function.

To study a potentially pathogenic role for *MYOM2* in the heart, we used *Drosophila melanogaster* due to its genetic conservation with humans and its less complex genome with decreased genetic redundancy. We identified the functional ortholog of *Drosophila*, *CG14964*, a gene that is similar to myomesins, but also other myosin binding proteins (we named it *MnM,* for *myomesin and myosin binding protein*) (**Figure 10**). Cardiac-specific KD or deletion of *MnM* led to dosage-depended cardiac defects, where a mild KD causes heart dilations (50 % in *CG14964*-GD or $CG14964^{Df}$) and strong KD heart constrictions (70 % in *CG14964*-T3) (**Figure 12**). The puzzling differences in the KD results may be explained by different RNAi efficiencies, given that the strongest KD phenotype was comparable to the combination of two strong alleles in trans ($CG14964^{CRIMIC}$/$CG14964^{Df}$). However, it is puzzling, that heterozygous $CG14964^{CRIMIC}$ mutants with a 50 % reduction of *CG14964* showed no cardiac dilation phenotype, unlike what we observed with *CG14964*-GD and $CG14964^{Df}$. Potentially, the genetic background of *CG14964*-GD, where the *diap1* gene is disrupted, and $CG14964^{Df}$, with the deletion of several genes, might also contribute to the dilation phenotype observed.

Since MYH7 and titin were shown to interact with MYOM2 in vitro[73–75], and in addition, *MYH7* is mutated in 30 to 50 % of HCM cases[215], we tested for genetic interactions between *CG14964* and *TTN* fly orthologs *sls* and *bent*, as well as *myosin* fly ortholog *Mhc.* We found that cardiac dilation caused by a mild reduction of *CG14964* was reversed by a reduction of *Mhc* or *sls* (**Figure 15**, **Figure 16**). However, we could not find a clear genetic interaction between *CG14964* and *sls* or *bent*, partly because the different *sls* mutant alleles tested caused different cardiac phenotypes. It was previously shown that *sls* has multiple isoforms which are expressed dependent on the muscle type and stage of *Drosophila* development.[227] Little is known about isoforms and their expression patterns in the heart, which could explain the differences in *sls* mutant phenotypes and consequently differences in their genetic interaction with *CG14964/MnM*, we observed in the fly heart (**Figure 15**).

Probing for genetic interactions with *Mhc*, we found that potential *CG14964* null mutants led to increased Mhc protein levels in various muscle tissues, including cardiomyocytes (**Figure 16**). Furthermore, a strong *CG14964/MnM* reduction in an *Mhc* heterozygous background led to further constriction of cardiac heart diameters, probably as a result of the excessive increase of Mhc. It was previously described that different mutations of *Mhc*, leading to inhibited or increased motor activity, cause cardiac dilation or constriction in the fly, respectively.[228,229] However, in contrast to *MnM* loss of function, in which we see preserved sarcomere integrity, strong KD of *Mhc* causes breakdown of the sarcomeres. Similarly, in humans, specific mutations in *MYH7* can give rise to dilations or

restriction.[204] Here, the cardiac phenotypes show great variety from late-onset dilated cardiomyopathy with mild to moderate dilation[230] to severe pediatric restrictive cardiomyopathy.[231]

Although we didn't observe an increase in heart wall thickness, we found increased ploidy levels in fly cardiomyocytes upon diminished *CG14964* function (**Figure 17**). In general, under both, physiological and pathological conditions, the human heart reacts to changes in mechanical workload with expansion in size, and physiological growth of the heart is linked to increased cardiomyocyte ploidy.[232,233] However, polyploidy is also associated with disease conditions, as abnormal high ploidy levels are often observed in connection with cardiac hypertrophy, for example.[234–237] A recent study demonstrated abnormal polyploidy in 50 % of CMs in HLHS tissue, indicating an intrinsic failure to complete cytokinesis and premature cell-cycle withdrawal.[238]

It was previously shown that cells can adjust total transcription to compensate for limited changes in cell size in fission yeast.[239] Therefore, we hypothesize that the increased ploidy, which we measured in fly cardiomyocytes with reduced *CG14964,* may be a cellular reaction to compensate for the disrupted sarcomere protein composition. As a result, cardiomyocytes may increase transcriptional output for protein synthesis, which again could lead to elevated Mhc levels as we observed them in homozygous *CG14964*^{CRIMIC} flies. We suggest that the levels of MnM are important to fine-tune sarcomere function, potentially by regulating Mhc levels, but not for the overall structure of the sarcomere as sarcomere integrity was preserved in the fly heart (**Figure 16**).

In summary, we identified novel rare, and probably disease-relevant, mutations in sarcomere gene *MYOM2* in patients suffering from HCM or TOF. Functional characterization of patient-derived HCM cardiomyocytes and fly gene *CG14964 (MnM),* both indicate an important role for *MYOM2* in heart development and function. Thus, *MYOM2* is a new potential disease gene for HCM and TOF, two diseases sharing the common feature: hypertrophy.

5. Results – Chapter 2

5.2 Generation of a *Drosophila* reporter line for studying F-Actin dynamics *in vivo*

5.2.1 Introduction

Life-imaging techniques, like the *in vivo* fluorescent heart assay, are important to study behavior and function on cellular and whole organism level *in vivo*. Our aim was to create a cardiac-specific reporter fly line for high-throughput screening analysis of F-Actin dynamics *in vivo*. To do so, we attempted to express LifeAct-mScarlet (monomeric Scarlet), a fluorescent marker to visualize F-Actin in the heart using the cardiac-specific *R94C02* enhancer (same enhancer was used for the tdtK reporter line).[181] LifeAct is a 17-amino-acid peptide derived from yeast, which specifically binds F-Actin in eukaryotic cells and tissues and it can be conjugated with different fluorescent proteins, like GFP or mScarlet.[240] LifeAct is supposed to not interfere with actin dynamics *in vitro* and *in vivo*[240], however, there are reports which raised concerns on LifeAct-associated artifacts at molecular and whole organism levels.[241–243] Therefore, after the generation of the transgenic lines, it was particularly important to perform functional and structural analyses of the *R94C02-LifeAct-Scarlet* fly strains generated. Note that in a former attempt Dr. Vogler created a fly line to express LifeAct-mScarlet from the cardiac-specific *tinC* enhancer (tin-C (Dm), 300 bp fragment identified by Yin et al., 1997)[244], which was not successful because no clear LifeAct signal was observed in the heart. In this work, the *tinC* enhancer in the *pattB tinC-LifeActmScarlet* plasmid (kindly provided by Dr. Vogler), was replaced with the *R94C02* enhancer using Gibson Assembly® (for more information see below and Methods section 4.13).

5.2.2 Acknowledgments

The LifeAct-mScarlet reporter line was generated (to equal parts) together with Dr. Katja Birker and under guidance of Dr. Vogler.

5.2.3 Generation of a *Drosophila* reporter line for studying F-Actin dynamics *in vivo*

Using Gibson Assembly® cloning methods, we generated a genetic construct carrying LifeAct-mScarlet, which was cloned downstream of the *R94C02* enhancer, as verified by genomic sequencing (**Figure 18** A, for more details, see Methods section 4.13). The plasmid was injected into *Drosophila* embryos using microinjection (*BestGene*) followed by integration into the genome utilizing the PhiC31 integrase-mediated site-specific transgenesis systems. For our purposes, the injected plasmid contained an *attB* site, which is integrated into an *attP2* site-containing fly strain with PhiC31 activity (**Figure 18** B).

We successfully generated a fly that showed *R94C02*-driven LifeAct-mScarlet expression specifically in the heart (**Figure 18**). We studied two different fly strains (M2 and M4) originating from different embryo injections. First, we validated that the LifeAct-mScarlet signal overlapped with F-Actin patterns visualized by phalloidin staining (**Figure 18** D). While some fly hearts heterozygous for *R94C02-LifeAct-mScarlet* showed F-Actin and myofibrillar organization comparable to controls (**Figure 18** C, D), about 50 % exhibited abnormal sarcomeric patterning of F-actin, indicating that LifeAct can induce morphological changes in the heart. Similar phenotypes are found in both fly strains M2 and M4 (representative pictures showing M4 fly line hearts are displayed in **Figure 18** D, E). Furthermore, *R94C02-LifeAct-mScarlet* M2 (heterozygous and homozygous) flies showed deformed heart tubes including dilations and constrictions (*data not shown*).

Note, that we also observe some staining of abdominal muscles when we acquired images of the LifeAct staining, while LifeAct is only supposed to be expressed in the heart tube. The staining of the abdominal muscles is most likely a bleed-trough fluorescence from the phalloidin staining. We did not observe any fluorescent signal in the abdominal muscles when we recorded the LifeAct signal *in vivo* in flies not stained with phalloidin (**Figure 18** F).

In parallel, we performed SOHA analysis on semi-intact fly preparations of heterozygous and homozygous *R94C02-LifeAct-mScarlet* flies and found systolic intervals significantly longer in LifeAct^{M4}-mScarlet flies (**Figure 18** I), while arrhythmicity parameters were not changed compared to controls (**Figure 18** M, N). Heart diameters of homozygous *R94C02-LifeAct-mScarlet* flies seem slightly constricted compared to controls (**Figure 18** J,K). Interestingly, despite the altered F-Actin patterns that we observed, we found fractional shortening not significantly changed (**Figure 18** L).

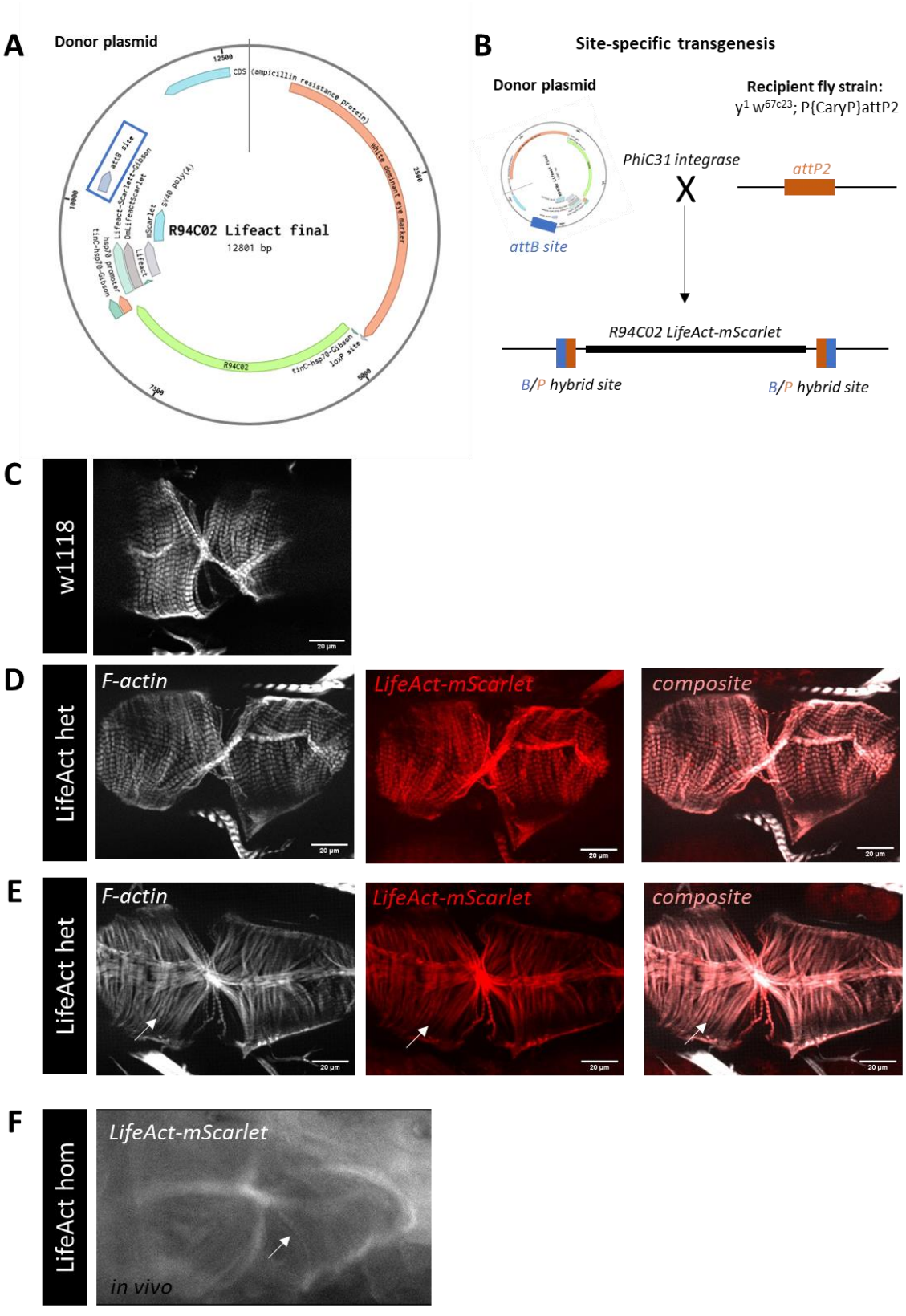

Figure legend on next page.

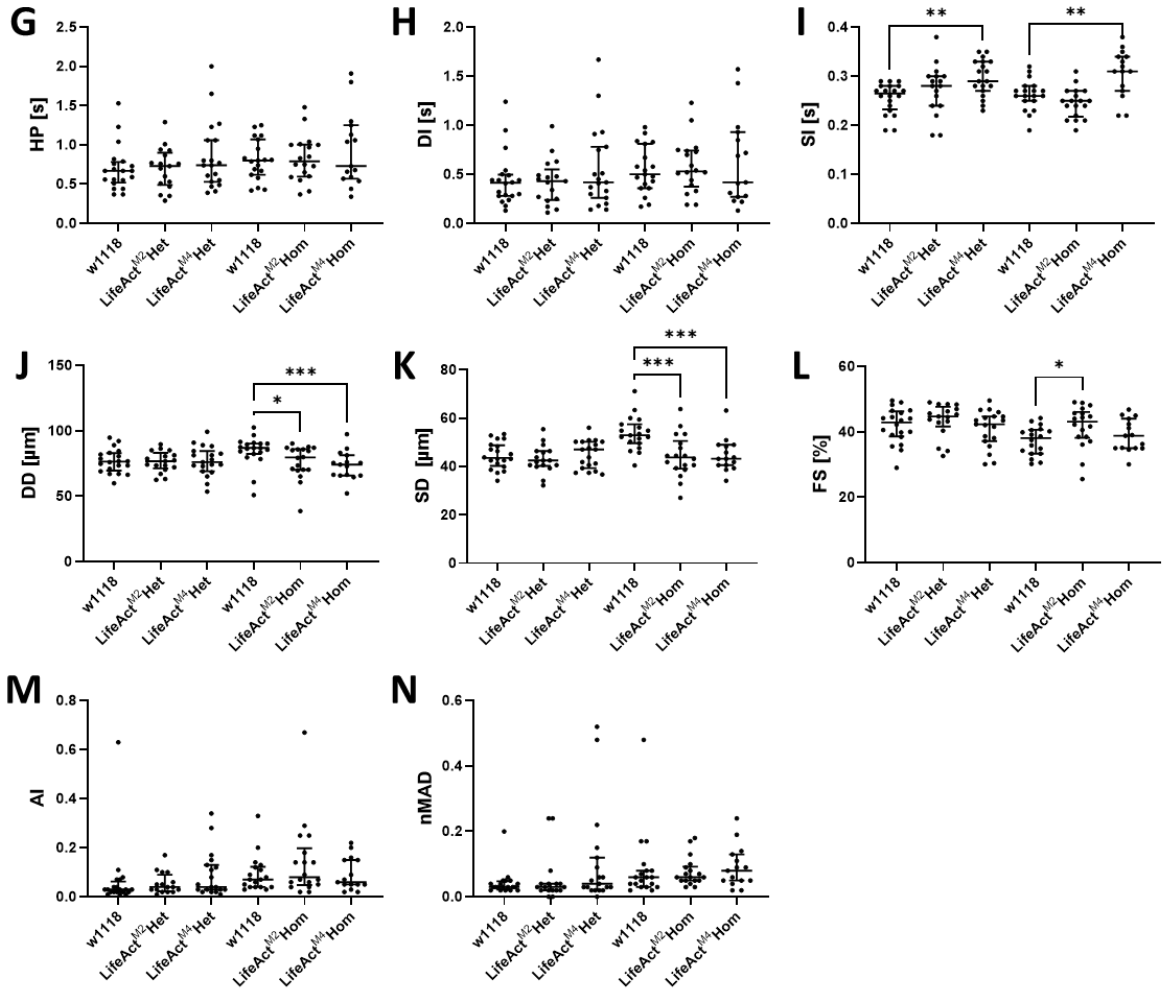

Figure 18: Generation of a cardiac *R94C02*-LifeAct-mScarlet reporter line. (A) Plasmid map showing construct carrying *R94C02* enhancer (green), LifeAct-mScarlet (light blue). *attB* site highlighted with blue frame. **(B)** Schematic showing PhiC31 integrase-mediated site-specific transgenesis systems. **(C-D)** One-week-old w1118 (control) flies (C) and heterozygous *LifeAct-mScarlet* flies (M4 insertion) (D) stained for F-Actin. Note, that *LifeAct-mScarlet* overlaps with F-Actin staining. **(E)** One-week-old heterozygous *LifeAct-mScarlet* flies (M4 insertion) stained for F-Actin, show abnormal sarcomeres with no distinct band patterning. **(F)** Single-frame of homozygous *LifeAct-mScarlet* fly heart (M4 insertion) extracted from movie recording. Arrow points towards sarcomere band pattern. **(G-N)** Heart period (G), diastolic interval (H) and systolic interval (I), diastolic diameter (J), systolic diameter (K), fractional shortening (L), arrhythmia index (M), and nMAD (N) in heterozygous (one-week-old females) or homozygous (3-week-old females) *R94C02-LifeAct-mScarlet* flies using the SOHA method. Heterozygous and homozygous LifeAct^{M4} flies show prolonged systolic intervals. Data depicted as median with interquartile range. One data point represents one fly. Statistics: Wilcoxon rank sum test, *p≤0.05, **p≤0.01, ***p≤0.001, ****p≤0.0001.

5.2.4 Discussion

We found that expression of LifeAct-mScarlet in the *Drosophila* heart led to LifeAct-associated artifacts in F-Actin organization and systolic intervals, while contractility is preserved. Shortly after generating our reporter line, a study was published which focused on possible side-effects induced by LifeAct-TagGFP2 in human bone marrow-derived stem cells and NIH/3T3 or COS-7 cells.[241] They found dose-dependent alterations in the actin cytoskeleton likely based on altered cofilin activity and reduced filament dynamics. Other cytoskeleton structures as well as the overall biophysical behavior

of the cells was also found affected.[240] The current hypothesis suggests that LifeAct induces an altered conformation of F-actin that affects the binding of cofilin, which impairs cell cytoskeletal dynamics.[242]

In *Drosophila,* it was shown that a strong LifeAct-mEGFP expression in the germline causes sterility and severe actin defects, while weak expression only causes mild to no effects.[243] The group used different Gal4-drivers and different temperatures to regulate expression levels of LifeAct-mEGFP under the control of pUAS. Note, that the choice of the promotor and fluorescent protein tag used in actin tracking probes can be linked to the strength of morphological aberrations.[245] We had chosen to express *LifeAct-mScarlet* using the *R94C02* enhancer to achieve constant expression of *LifeAct-mScarlet* in the heart, independent of a Gal4 driver. We only observe mild (not necessarily defective) LifeAct-associated artifacts (LifeAct^{M4}-mScarlet), and staining for other sarcomere proteins, like Mhc or sallimus, are needed to further characterize sarcomere integrity in *R94C02-LifeAct-mScarlet* flies*.* Further testing is also needed to see if *R94C02-LifeAct-mScarlet* is causing functional damages in our system. To do so, *R94C02-LifeAct-mScarlet* could be expressed in a partially compromised heart (i.e. *bent* or *sls* knockdown flies) to test if *bent* or *salimus* mutant phenotypes are different or worse in an *R94C02-LifeAct-mScarlet* background. This would indicate that LifeAct-associated artifacts translate into functional damage and sensitize the system towards failure. In this case, the use of another fluorescent protein tag could represent an alternative approach.

In conclusion, further testing will show whether the *R94C02-LifeAct-mScarlet* fly lines can be used to study F-Actin dynamics in the way we anticipated, or also just as an alternative fluorescent reporter line to tdtK for functional heart analysis. However, with further characterization underlying the observed phenotypes the fly lines could also be used as a potential sensitizer line.

5. Results – Chapter 3

5.3 Probing interactions between Hypoplastic Left Heart Syndrome candidate genes in model systems: focus on LRP2/WNT/SHH

5.3.1 Introduction

In collaboration with Dr. Nelson's and Dr. Olson's team at the Mayo Clinic, Dr. Colas' and Dr. Ocorr's lab at SBP, and the Bodmer Lab (including my contribution) generated a high-resolution genetic profile of HLHS index family ('5H') using whole genome sequencing and functionally evaluated the top 10 prioritized candidate genes, which was recently published in *eLife*.[5] Here, we showed that KD of *LDL Receptor Related Protein 2* (*LRP2*) in the fly heart causes arrhythmia and dilated hearts using the SOHA method and reduced proliferation in hiPSC-CMs. Notably, KD of *LRP2* in zebrafish resulted in ventricular cardiac, but not skeletal muscle defects, highlighting an important role for *LRP2* in cardiac proliferation and differentiation. Furthermore, burden analysis revealed enrichment of rare or moderately rare *LRP2* variants in a cohort of 130 HLHS patients compared to 861 controls, which had not previously been linked to HLHS within curated bioinformatic networks. Interestingly, six of the 10 prioritized genes together with their first neighbors were connected to growth-associated Sonic Hedgehog (SHH) and WNT signaling (as genetic and protein-protein interactions, BioGRID), which are key regulators of cardiac proliferation and differentiation[246,247] (**Figure 19**). Strikingly, these pathways were also attenuated in the proband's cells (*WNT1/3a/8a/10b* and *FZD10* was downregulated, *PTCH1* upregulated). In addition, KD of two candidate genes (*LRP2* and *APOB*) alter TP53 signaling, which regulates cell division, pointing towards proliferation-dependent HLHS disease-mechanism. However, these interactions and their role in cardiac development and function were in need of further investigation, which I address in this chapter, taking advantage of the fly for high-throughput genetic interaction studies (using the *in vivo* tdtK fluorescent heart method).

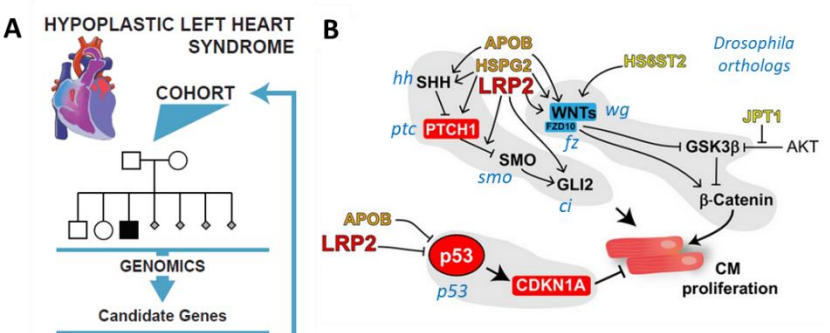

Figure 19: Genetic profile of HLHS index family. (A) Gene *prioritization* pipeline. **(B)** Gene network integrating HLHS (5H) family-specific candidate genes with heart development. Genes with cardiac phenotypes in iPSC/*Drosophila* assays (orange) or in *Drosophila* only (yellow). Genes up-regulated or downregulated in proband iPSC-CMs vs. parents (red or blue respectively). *Drosophila* orthologs (blue italic). Adapted from Theis et al., 2020.[5]

I hypothesize, that HLHS arises from an unfavorable combination of patient-specific alleles, which leads to an imbalance in core signaling pathways and eventually to HLHS. Such combinations

could also function as genetic sensitizers that affect the patient's outcome and/or the post-surgical cardiac performance. By testing for genetic interactions, I aim at reducing the knowledge gap between patient genomes and clinical phenotypes and identifying new markers for prenatal diagnostics and long-term risk for heart failure.

5.3.2 Acknowledgments

The bioinformatics analysis in this project related to the whole genome sequencing of the HLHS cohort at Mayo Clinic was performed by Dr. Jeanne Theis and Dr. Timothy Olson from Mayo Clinic, MN. The *Drosophila* BioGrid analysis was performed by Dr. Georg Vogler. I performed all genetic interaction studies in *Drosophila* using an *R* script provided by Dr. Vogler. *megalin* mutants mgl^{168}, mgl^{269}, mgl^{406}, mgl^{608} were a gift from Dr. Natalie Dye's lab at the Max Planck Institute of Molecular Cell Biology in Dresden, Germany.

5.3.3 Functional characterization of *megalin* in the *Drosophila* heart

I focused on characterizing the function of *LRP2* fly ortholog *megalin* (*mgl*) in the fly heart and probing for genetic interactions with genes of the WNT or SHH pathway. Single-cell RNA sequencing in late-stage *Drosophila* embryos by Dr. Vogler (Vogler et al., 2021, *bioRXiv*)[248] showed that *megalin* is expressed in the heart (personal communication). I tested the systemic and cardiac-specific effects of diminished *mgl* function on the adult fly heart. For this, I used a *mgl* MiMIC mutant (y^1 w^* Mi{MIC}$mgl^{MI14318}$/FM7h = $mgl^{MI14318}$), where a *Minos*-mediated integration cassette (MiMIC) transposon is inserted in exon 9 of the megalin gene. A MiMIC construct contains the mini-yellow marker ($y^{+mDint2}$) and Avic\GFP (a fluorescent marker) associated with a mutagenic gene-trap cassette.[249,250] MiMIC insertions in introns that are in the same reading orientation as the gene, thus should function as a gene trap. However, in the $mgl^{MI14318}$ mutant, it is inserted in the reverse orientation, presumably leading to gene disruption and loss of function. Homozygous $mgl^{MI14318}$ mutants are lethal. In addition to $mgl^{MI14318}$, we used four other mutant lines (mgl^{168}, mgl^{269}, mgl^{406}, mgl^{608}), which carry deletions in *mgl* and affect the open reading frame of the gene. No protein was detectable by immunohistochemistry[251], and homozygotes are lethal, as is the case for $mgl^{MI14318}$. To knockdown *megalin* specifically in the heart, I used a UAS-*megalin* RNAi and the $Hand^{4.2}$-Gal4 driver (see Materials for all fly stocks used, section 3.1).

Adult heterozygous $mgl^{MI14318}$ mutants showed dilated hearts compared to control flies and prolonged heart periods compared to controls (*yw/w1118*) (**Figure 20** A, **Figure 21** D) using the SOHA method. Immunohistochemistry staining for F-Actin showed normal sarcomere patterning in heterozygous $mgl^{MI14318}$ mutants similar to control hearts (**Figure 20** C). In contrast, heterozygous

mutants for *mgl*^{168}, *mgl*^{269,} and *mgl*^{608} exhibit significantly constricted hearts and *mgl*^{406} heterozygotes show a tendency towards smaller heart diameters (*in vivo* fluorescent heart method) (**Figure 20** B). Cardiac myofibrils of heterozygous mutants marked with phalloidin staining (F-Actin) showed normal sarcomere patterning similar to controls (**Figure 20** D). Heart-specific KD of *megalin* using RNAi caused no alterations in heart diameters (*in vivo* fluorescent heart method), in line with our previous findings using SOHA.[5] Of note, the difference between *mgl*^{MI14318} and the other *mgl* mutants tested may be in part because of the difference in genetic background: *mgl*^{MI14318} is in *yw* background that exhibits by itself a more constricted heart (diastolic diameter of *yw/w1118 (= yw/+)* is ~80 µm) compared to *w*^{1118} (= +/+) with a diastolic diameter of ~95 µm (**Figure 20** A, B). In general, a genetic background describes the genetic "*make-up*" of an organisms and refers to all the alleles at all loci (except the mutated/altered gene of interest).

In summary, I found that a systemic reduction of *megalin* affects heart diameters (dilation/constrictions) in heterozygous adult mutant flies, while heart-specific KD causes no change compared to controls, which could be due to non-autonomous effects of the systemic mutations on the heart or due to inefficiency of the *mgl* RNAi.

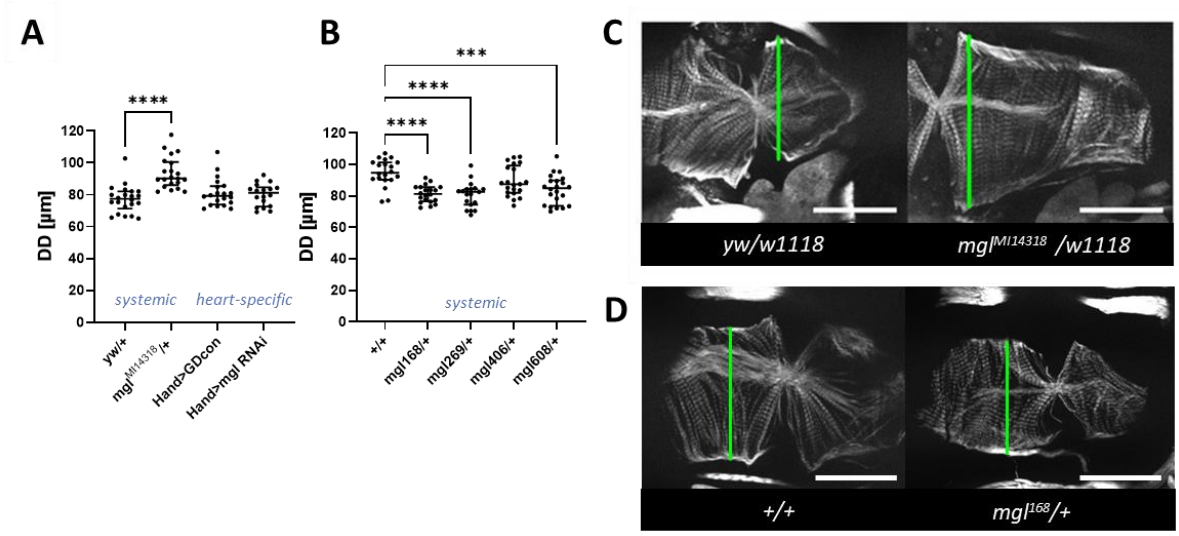

Figure 20: Functional heart analysis of *LRP2* fly ortholog *megalin* in *Drosophila.* (A-B) Quantification of Diastolic Diameters (DD) of heterozygous *megalin* mutants and heart-specific knockdown of *megalin* using RNAi combined with the *Hand*$^{4.2}$-Gal4 driver. + = *w1118* in (A); + = GDcon in (B, D). Note, that the GDcon fly strain from *VDRC* is of *w1118* background.[252] Data depicted as median with interquartile range; one data point represents one fly. Statistics: Mann-Whitney test, ***p<0.001, ****p<0.0001. **(C-D)** Representative images of heterozygous *mgl* mutants show increased (C) or decreased (D) heart diameters (measured at green line).

5.3.4 Probing for genetic interactions between *megalin* and *apolpp*

Besides *LRP2,* one other gene named *apolipoprotein B* (*APOB)* that was prioritized in the 5H HLHS proband caused phenotypes in both model systems, the *Drosophila* heart and hiPSC-CMs, upon gene KD.[5] *APOB* encodes for a short (B-48) and a long isoform (B-100), which are both components of

lipoproteins that carry fats and fat-like substances, such as cholesterol, through the blood stream. In *Drosophila*, it was shown that cardiomyocyte-derived apoB-lipoproteins (among them apolpp), like their fat body-derived counterparts, are involved in control and maintenance of systemic lipid homeostasis.[253] As mentioned before, the *LRP2* receptor binds a number of ligands that can be functionally and structurally different, like hormones and different lipoproteins.[254,255] Since apolipoprotein B100 is among those ligands[256,257], I wanted to investigate if *LRP2/mgl* and *APOB/apolpp* also act together specifically in the heart using the *Drosophila* model.

For this, I performed functional heart analysis using the SOHA method on transheterozygous mutants for *apolpp*^{MB07263} and *mgl*^{MI14318} (the only *mgl* allele available to me at the time point of the experiment). *apolpp*^{MB07263} (= y[1]; Mi{GFP[E.3xP3]=ET1}apolpp^{MB07263}) is a transposon insertion line, where the Mi{ET1}[258] construct was inserted in exon 3 of the *apolpp* gene, presumably leading to gene disruption.

mgl heterozygous mutants show a trend towards increased diastolic diameters (DD), while systolic diameters (SD) are not affected, leading to increased fractional shortening (**Figure 21** A-C). Note, that the increase in DD is not significant as seen before, potentially because of the different genetic background (*yw*/*yw*) compared to the previous experiment (*yw/w1118* in **Figure 20** A). Heart period is significantly increased in *mgl* heterozygotes compared to controls (**Figure 21** D). Heterozygous mutation for *apolpp* leads to smaller heart dimensions (DD and SD) (**Figure 21** A, B).

Assuming that apolpp (as a potential LRP2 ligand) acts upstream of LRP2 in the signaling cascade, I expected an epistatic relationship between both genes. Interestingly, transheterozyous mutants for *apolpp* and *mgl* show similar phenotypes compared to *apolpp* heterozygous mutation alone (no significant difference between both genotypes except for systolic intervals), indicating that *apolpp* mutation potentially masks the effect of *mgl* heterozygosity and that the manifestation of *mgl* mutant phenotypes could be dependent on *apolpp* expression levels. This becomes most overt looking at the diastolic intervals (DIs) of transheterozygotes, which are significantly different from the *expected* values. Here, *mgl* heterozygous mutation leads to increased DI, while *aplopp* heterozygous mutation also shows a tendency towards increased DDs. Thus, the product of both phenotypes would result in an even further increase in DIs. Here, transheterozygous mutants show a DI length comparable to *apolpp* heterozygotes, supporting that *apolpp* mutation potentially masks the effect of *mgl* heterozygosity and acts upstream of *mgl.* However, if apolpp acted through *mgl* receptors, KD of both genes should phenocopy each other. This might be the case for apolpp^{MB07263} and *mgl*^{168}, *mgl*^{269}, *mgl*^{406}, *mgl*^{608}, which all cause heart constrictions, but this has not been investigated yet. Although the variability of *mgl* phenotypes must be addressed before more conclusions can be made, these data encourage further studies of a potential interaction between *apolpp* and *mgl* regarding heart function.

Now, that the *mgl*^{168}, *mgl*^{269}, *mgl*^{406}, *mgl*^{608} mutants are available to us, the next step would be to study the interaction between those mutant alleles and *apolpp*^{MB07263} and/or a perform pull-down assay to determine physical protein-protein interaction between mgl and apolpp.

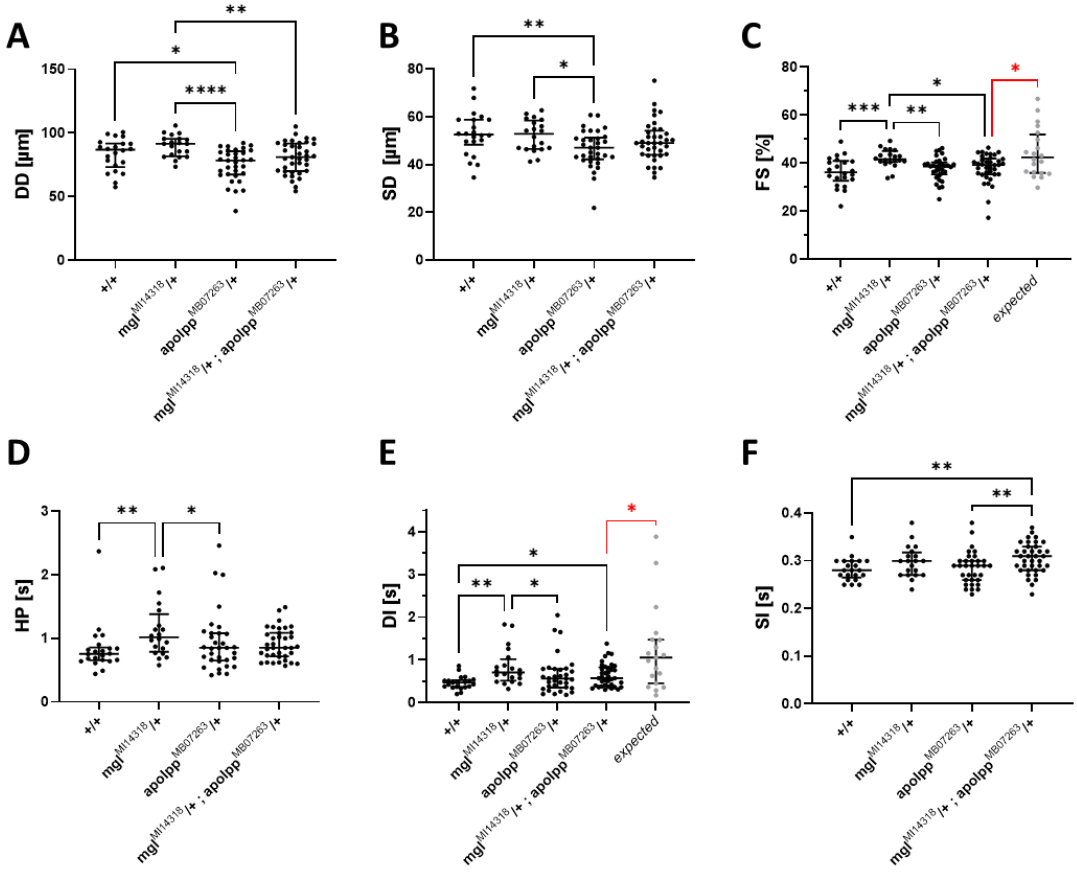

Figure 21: Functional heart analysis of *mgl* and *apolpp* transheterozygous mutants. (A-F) Heart parameters of 3-week-old female flies: (A) Diastolic Diameter, DD, (B) Systolic Diameter, SD, (C) Fractional Shortening, FS, (D) Heart Period, HP, (E) Diastolic Interval, DI, (F) Systolic Interval, SI. Data depicted as median with interquartile range; one data point represents one fly. Statistics: Kruskal-Wallis, *p=0.05, **p=0.01, ***p<0.001, ****p<0.0001. *Expected* value calculation as previously described (see also Methods section 4.12). + = *yw*.

5.3.5 Probing for genetic interactions between megalin and Hh or wg/Wnt signaling

As previously described, *LRP2* together with its first neighbors was connected with SHH and WNT signaling (Hh and Wnt/wg signaling in the fly) as genetic and protein-protein interactions have indicated, based on BioGRID analysis (Theis et al., 2020).[5] This was consistent with RNA sequencing analysis of the 5H family, where the negative regulator of SHH signaling, *PTCH1*, was upregulated in the proband cells, while agonists of WNT signaling, *WNT1/3a/8a/10b* and *FZD10* were downregulated, compared to parental cells. In a first attempt, the Colas lab tested whether LRP2 could regulate WNT and SHH signaling using hiPSC-CM. They found that KD of *LRP2* led to reduced *FZD10* and increased *PTCH1* RNA levels although *WNT1/3a/8/10a* were not affected.[5] Furthermore, in this publication, we reported induction of WNT and SHH signaling using the WNT agonist BIO[259] and siRNA against PTCH1[260] respectively, and we found that *LRP2* KD significantly reduced both BIO- and siPTCH1-induced

proliferation in hiPSC-CMs, suggesting that *LRP2* is required for both WNT- and SHH-regulated CM proliferation. To substantiate a link between *LRP2* and these two pathways ***in vivo***, I subsequently tested for genetic interactions in our *Drosophila* heart model.

To do so, I created a sensitizer line combining the *Hand*$^{4.2}$-Gal4 driver harboring the fluorescent heart reporter construct (tdtK) with the *mgl*^{MI14318} mutant allele (the only allele available to me at this time) (**Figure 22** A). First, I crossed the *mgl*^{MI14318} sensitizer line to transgenic fly lines to target genes of the Wnt/wg pathway: a deficiency line covering 24 genes, including wg*,* Wnt4*,* Wnt6 and Wnt10*,* and eight lncRNAs (Df(*wg*)); and RNAi lines targeting Wnt ligand receptor *frizzled* (*fz*) and *frizzled 2* (*fz2*). In the following experiments, the *in vivo* fluorescent reporter method was used for functional heart analysis in adult flies. For genetic interaction statistics, *expected values* were calculated only for parameters and gene combinations in question, where the data pointed towards potential synergistic genetic interactions (calculation as previously described with *R* script from Dr. Vogler, see also Methods section 4.12).

Since WNT signaling was downregulated in the HLHS patient cells compared to controls, we would expect that inhibition of Wnt/wg signaling would contribute to or worsen the *megalin* mutant heart phenotype. I found that Df(*wg*) heterozygosity alone had no effect on heart diameters (**Figure 22** B). If there was **no** genetic interaction, we would expect intermediate diameters in the transheterozygous mutants (*mgl*^{MI14318}/+; Df(*wg*)/+). Interestingly, the dilation of diastolic and systolic heart diameters observed in heterozygous *mgl*^{MI14318} mutants was completely reversed when combined with Df(*wg*) heterozygosity (DD: transheterozygotes vs. *expected* ****p= 0.000009), suggesting that *mgl* function is dependent on the presence of wg*,* Wnt4*,* Wnt6 and Wnt10 (**Figure 22** B). Furthermore, fractional shortening in transheterozygous mutants was significantly reduced compared to controls, while single mutants show no effect (*mgl*^{MI14318}) or had a (non-significant) tendency towards reduced fractional shortening (Df(*wg*)) (FS: transheterozygotes vs. *expected* *p= 0.019) (**Figure 22** D). Heart period of heterozygous Df(*wg*) flies was significantly prolonged, based on prolonged systolic intervals (SI) (**Figure 22** E). Heterozygous *mgl*^{MI14318} mutants also show prolonged SI (**Figure 22** G). Transheterozygous mutants in combination with Df(*wg*) exhibit prolonged SI, which are shorter than expected based on the single mutant phenotypes, again pointing towards a genetic interaction (SI: transheterozygotes vs. *expected* *p=0.011).

Heart-specific KD of *frizzled* and *frizzled 2* using RNAi led to dilated diastolic diameters (**Figure 22** B). In combination with heterozygous *mgl*^{MI14318} mutation, the product of both phenotypes, thus a further dilation would be expected (if there was **no** genetic interaction). I observed a tendency towards bigger diameters in heterozygous *mgl*^{MI14318} flies in conjunction with *fz* KD (**Figure 22** B). However, this dilation is not significantly bigger compared to heterozygous *mgl*^{MI14318} flies alone.

Heterozygous *mgl*^{MI14318} flies in conjunction with *fz2* KD show heart dimensions similar to the single mutants (thus no further dilation) suggesting a genetic interaction (DD: *mgl*$^{MI14318/+}$ + *fz* 2 RNAi vs. *expected* *p=0.027). Heart Period upon KD of *fz* and *fz2* was prolonged and in conjunction with *mgl* heterozygosity intermediate phenotypes were observed (**Figure 22** E). Interestingly, *fz* and *fz2* KD led to prolonged diastolic intervals (DI), which were normalized to control levels in combination with *mgl* mutation, indicating that *fz* and *fz2* phenotypes are dependent on *megalin* function (DI: *mgl*$^{MI14318/+}$ + *fz* RNAi vs. *expected* **p=0.003 and *mgl*$^{MI14318/+}$ + *fz* 2 RNAi vs. *expected* p=0.087) (**Figure 22** F).

To probe for interaction between *megalin* and the Hh pathway, I used the *mgl*^{MI14318} heterozygous background, two different loss-of-function *hh* mutants (*hh*^{2} and *hh*^{Ac}), two fly stocks overexpressing Hh antagonist UAS-*patched* (UAS-*ptc*), and RNAi lines targeting *smoothened* (*smo*) or *cubitus interruptus* (*ci*). Heterozygous mutants for *hh*^{2} and *hh*^{Ac} and flies overexpressing *ptc* in the heart have heart diameters similar to controls, while *mgl*^{MI14318} heterozygosity led to the expected dilation phenotype (**Figure 23** A). Combination of *mgl*^{MI14318} with *hh*^{2} and *hh*^{Ac} heterozygosity shows a non-significant tendency towards smaller (intermediate) diameters compared to *mgl* mutation alone, while *ptc* overexpression completely reversed the *mgl* dilation phenotype (DD: *mgl*$^{MI14318/+}$ + UAS-*ptc* I vs. *expected* **p = 0.006 and *mgl*$^{MI14318/+}$ + UAS-*ptc* II vs. *expected* ***p = 0.0006) (**Figure 23** A). A similar rescue effect was observed when knocking down *smo* in conjunction with *mgl* heterozygosity (*mgl*$^{MI14318/+}$ + *smo* RNAi vs. *expected* p = 0.136), however, *ci* KD does not rescue the *mgl* dilation phenotype (**Figure 23** G). Heart period was significantly prolonged when inhibiting Hh signaling in *hh*^{Ac} heterozygous mutants, upon *ptc* overexpression and *smo* or *ci* knockdown (**Figure 23** D, J). In conjunction with *mgl* heterozygous mutation, *ptc* overexpressing flies and *smo* KD flies show smaller heart period values than expected, indicating a genetic interaction (*mgl*$^{MI14318/+}$ + UAS-*ptc* I vs. *expected* p = 0.23 and *mgl*$^{MI14318/+}$ + UAS-*ptc* II vs. *expected* **p = 0.0017 and *mgl*$^{MI14318/+}$ + smo RNAi vs. *expected* ****p=0.00009) (**Figure 23** D, J).

Taken together, the overall data indicate an interplay between *mgl* and Hh or Wnt/wg pathways with a number of potential interactions. However, although all selected genetic transgenes were predicted to inhibit Hh or Wnt/wg pathways and similar effects on heart function were expected, there are some differences in how these different alleles affect heart function and morphology and how they act in combination with *mgl*. Differences in the strength of the alleles/RNAis could differently affect both signaling pathways and could account for some of the differences observed. Alternatively, non-canonical gene functions within the Hh or Wnt/wg pathways might play a role. However, further investigations are required on the exact molecular mechanism and the nature of the genetic interactions I identified to further characterize the link between LRP2 and SHH/WNT signaling in heart.

A Combination of *mgl* mutant allele with *Hand*$^{4.2}$-Gal4 driver

Cross order	chromosome I.	chromosome II.
I.	Cdc42/FM7 x sco/CyO → Y/FM7; +/sco and Y/FM7; +/CyO	
II.	mgl/FM7 x FM7/Y; +/CyO → mgl/FM7; +/CyO	
II.'	Y/FM7; +/sco x Hand,tdtK^{VK37}/Hand, tdtK VK37 → Y/FM7; Hand, tdtK^{VK37} /sco	
III.	mgl/FM7; +/CyO x Y/FM7; Hand, tdtK ^{VK37} /sco → *mgl*/FM7, Hand, tdtK^{VK37} /CyO	

Balancer: Cdc42[3]/FM7 or FM7/Y → Cdc42[3]/Y is lethal — males

mgl + wg/Wnt signaling *wg/Wnt* → *fz1/fz2* → *wg/Wnt target gene expression*

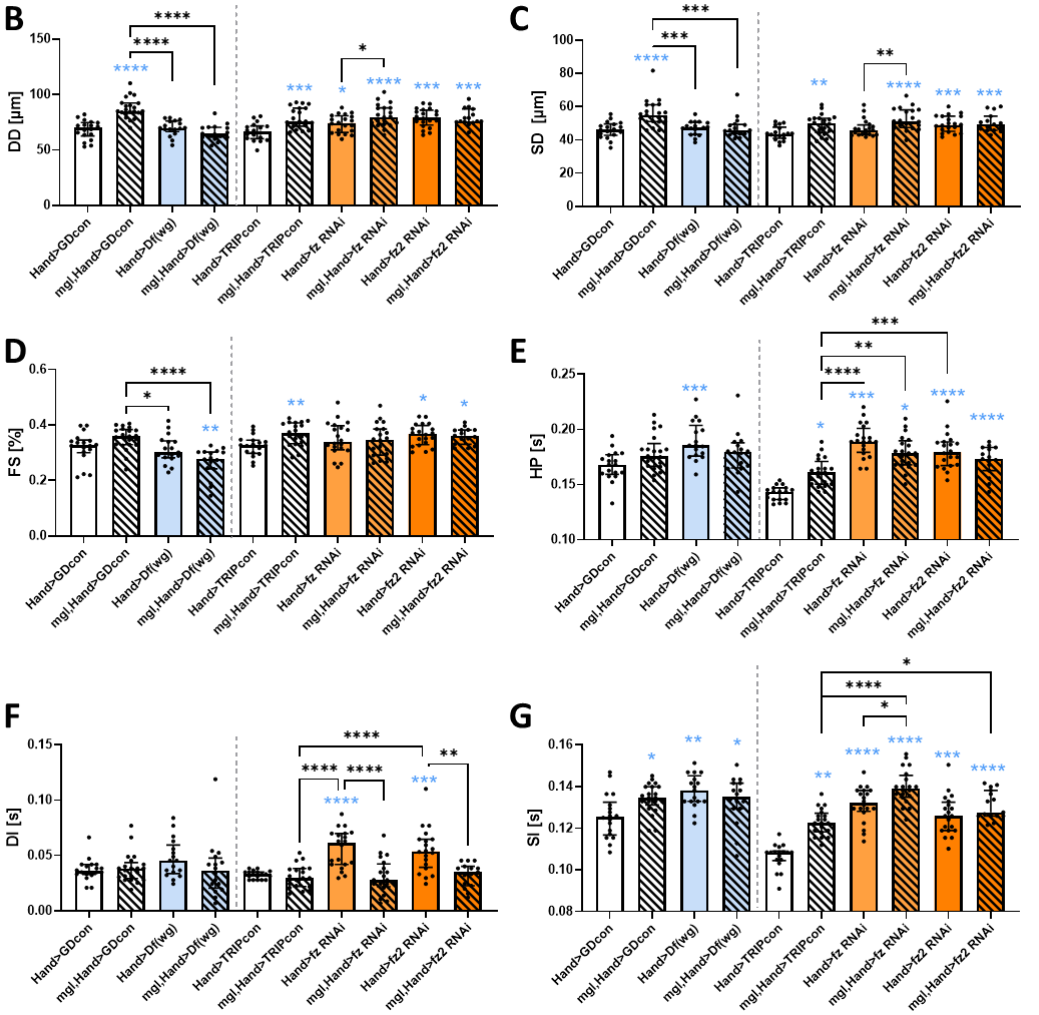

Figure 22: Interaction studies between *mgl* and *Wnt/wg signaling*. **(A)** Crossing scheme to generate sensitizer line *mgl*^{MI14318}*/FM7; Hand*$^{4.2}$,tdtK/CyO. **(B-G)** Heart parameters of 3-week-old female flies of Df(*wg*)/+ flies, *fz1* and *fz2* KD flies with and without additional *mgl*^{MI14318} heterozygous mutation: (B) Diastolic Diameter, DD, (C) Systolic Diameter, SD, (D) Fractional Shortening, FS, (E) Heart Period, HP, (F) Diastolic Interval, DI, (G) Systolic Interval, SI. mgl = *mgl*$^{MI14318/+}$, Hand = *Hand*$^{4.2}$-Gal4, tdtK. Note, that the *Hand*$^{4.2}$-Gal4 driver in the first four columns is irrelevant since *mgl*^{MI14318} and Df(*wg*) are systemic mutations and not Gal4 driven. Blue asterisks indicate significance to respective controls (Hand>GDcon or Hand>T3con). Data depicted as median with interquartile range; one data point represents one fly. Statistics: Kruskal-Wallis, *p= 0.05, **p=0.01, ***p<0.001, ****p<0.0001.

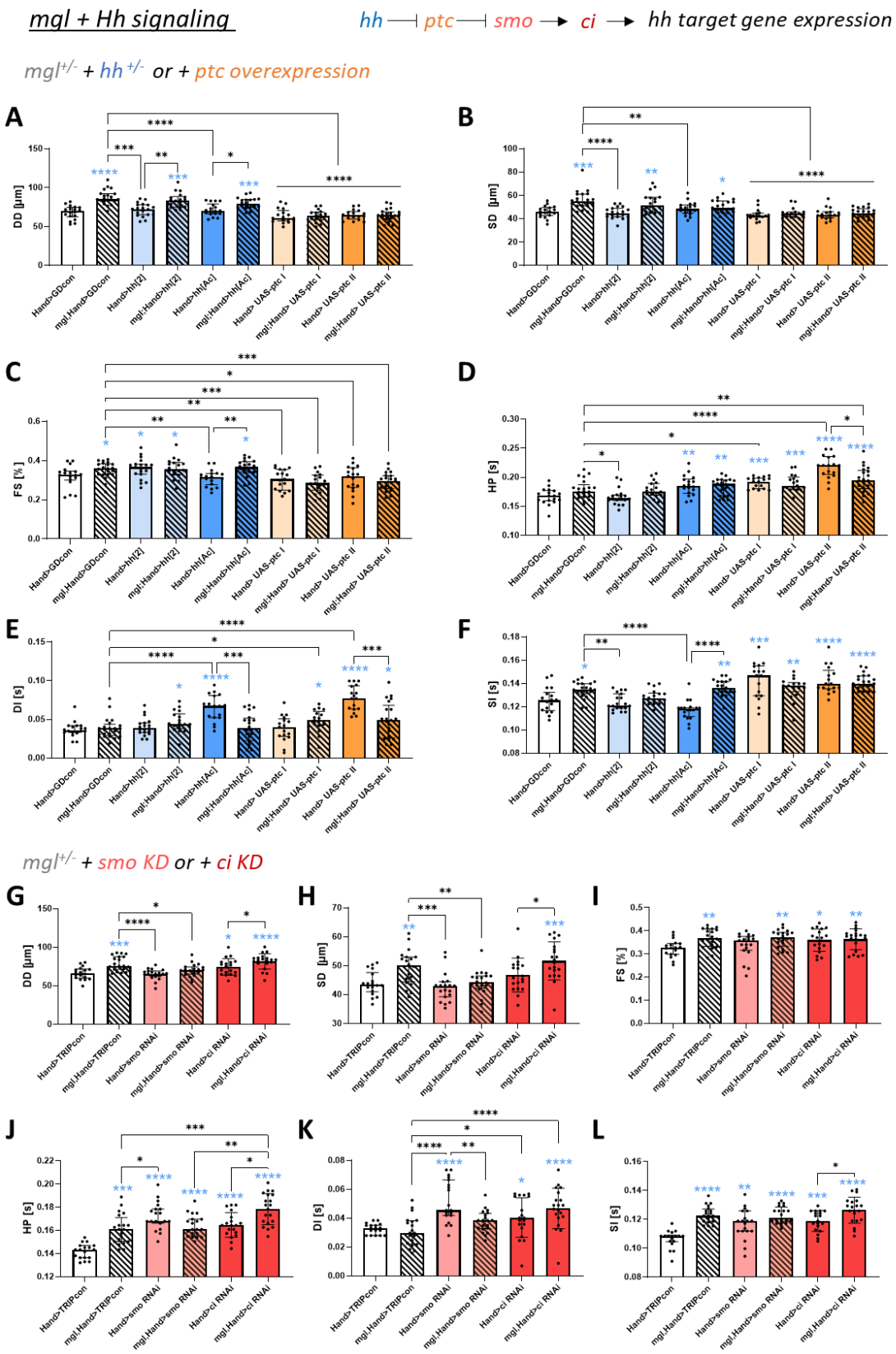

Figure 23: Interaction studies between *mgl* and Hh signaling. (A-F) Heart parameters of 3-week-old female flies of *hh* heterozygous flies, or *ptc* overexpressing flies with and without additional *mgl*^{MI14318} heterozygous mutation. Note, that *Hand*$^{4.2}$-Gal4 in column three to six is irrelevant, since *mgl*^{MI14318}, hh^{2} and *hh*^{Ac} are systemic mutations and not Gal4 driven. **(G-L)** Heart parameters of 3-week-old female *smo* or *ci* KD flies without additional *mgl*^{MI14318} heterozygous mutation. Blue asterisks indicate significances to respective controls. mgl = *mgl*$^{MI14318/+}$, Hand = *Hand*$^{4.2}$-Gal4, tdtK. Data depicted as median with interquartile range; one data point represents one fly. Statistics: Kruskal-Wallis, *p= 0.05, **p=0.01, ***p<0.001,

****p<0.0001. DD= Diastolic Diameter, SD= Systolic Diameter, FS= Fractional Shortening, HP= Heart Period, DI= Diastolic Interval, SI= Systolic Interval.

5.3.6 megalin (*mgl*^{MI14318}) mutation has no effect on early cardiogenesis in *Drosophila* embryos

To investigate a potential role for *megalin* during early cardiac development, I stained *mgl*^{MI14318} mutant embryos (heterozygous or hemizygous) for Myocyte Enhancer Factor-2 (Mef2), which marks somatic and visceral musculature, as well as the heart. Homozygous or hemizygous *mgl* mutation causes lethality during larval stages[251], thus equal ratios during embryonic stages are expected. At stage 17, overall morphology of mutant embryos is indistinguishable from controls (**Figure 24** A). In addition, no differences in heart structure, size, or cardiomyocyte number (marked by *Mef2*) were observed. Simultaneously, the embryos were stained for Hh pathway agonist smoothened (smo), which localizes at the parasegment borders and which is involved in anterior/posterior patterning of each segment in the embryo and shaping of their segmental polarity.[261] Since *smoothened* mutations have previously been shown to cause an enlargement of denticle bands[261], indicative of segmental polarity defects, I measured the width of denticle bands marked by smo protein expression in *mgl*^{MI14318} mutants to test if *mgl* loss affects *smo* localization. However, no difference in denticle band width between mutants and controls was found (**Figure 24** B).

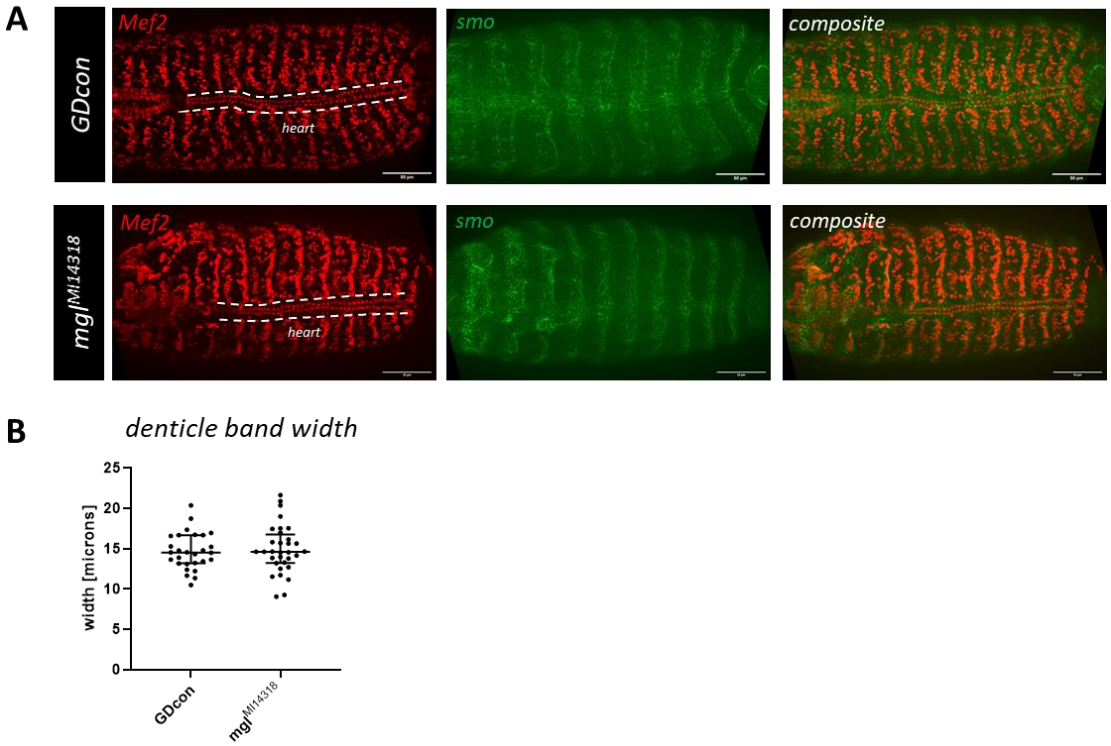

Figure 24: *mgl*^{MI14318} mutation does not affect early cardiogenesis in *Drosophila* embryos. (A) Representative stage-17 *mgl*^{MI14318} mutant embryos (hemi- or heterozygous) stained for *Mef2* and *smo* show no differences in heart morphology or *smo* localization compared to controls (GDcon). Scale bar= 50 µm. **(B)** Quantification of denticle band width measured on *smo* staining using ImageJ. Four denticle bands per embryo were measured, controls n=7, mutants n=8 (mix of hemizygous and heterozygous mutants).

5.3.7 Discussion

5.3.7.1 Implication of LRP2 in heart development and disease

Despite a clear genetic origin of the HLHS[99], our current understanding of how the genetic heterogeneity of HLHS converges in common perturbations in heart morphogenesis is still limited. Here, I first characterized how *mgl/LRP2* variants, which were found enriched in a cohort of HLHS patients, influences heart function and structure using *Drosophila* as a model, and second, I tested if *mgl* potentially interacts/acts through SHH/Hh and/or WNT/Wnt/wg pathways to identify novel mechanisms of action of *LRP2* during cardiogenesis. In general, LRP2 is appreciated as a multiligand clearance receptor, which regulates the concentration of extracellular essential metabolites and signaling molecules, and thus controls their availability to surrounding cells[109,112], however, the specific nature of the signaling molecules and their downstream effects controlled by LRP2 need further investigation.

I found that systemic loss of *LRP2* fly ortholog *mgl* in heterozygous mutants caused dilation (*mgl*^{MI14318}) or constriction (*mgl*^{168}, *mgl*^{269}, *mgl*^{608}, *mgl*^{406}) of the adult fly heart (**Figure 20**), while overall fly morphology was preserved. In line with my findings in *Drosophila*, we observed cardiac ventricle defects, but no skeletal muscle defects in zebrafish (Ocorr lab).[5] Why different *mgl* mutants cause opposite heart phenotypes is not clear to this point since all alleles are predicted Loss-of-function variants, that should result in 50 % *mgl* expression levels in heterozygous conditions. Note, that a reduction of *mgl* expression levels was not verified for *mgl*^{MI14318} mutants, while for *mgl*^{168}, *mgl*^{269}, *mgl*^{608}, *mgl*^{406} homozygous mutants it was previously described that no mgl protein was detectable.[251] One reason for phenotypic differences could be dissimilar genetic backgrounds. I found that flies with *yw/w1118* or *w1118/w1118* backgrounds have different heart diameters (**Figure 20**). Each strain has a unique set of background alleles that potentially can interact with and modify the expression of a mutation, transgene, or other genetic inserts, and even in well-defined background strains (as for *Drosophila*), undiscovered modifier genes can confound results, making them unexplainable. Influences of the genetic background have often been reported in mouse studies[262,263], and also in the mouse heart where genetic backgrounds can influence the susceptibility for ventricular arrhythmia[264] or adaption to cardiac hypertrophy.[265]

Heart-specific KD did not lead to alteration in heart diameters suggesting potential non-autonomous effects contributing to the heart phenotypes in systemic mutants. Furthermore, I did not observe arrhythmia in flies with heart-specific *mgl* KD or in any of the heterozygous *mgl* mutants as we observed it before upon heart-specific KD.[5] One explanation could be that it was because an alternative RNAi construct was used (VDRC v36389 instead of v27242) or that the hearts of *Hand*$^{4.2}$-

Gal4>*mgl* RNAi flies were tested using the SOHA method instead of the fluorescent reporter method, which is more sensitive for arrhythmia detection (as described in the Appendix section 8.1).

Furthermore, $mgl^{MI14318}$ mutants do not show any cardiac phenotypes in late-stage embryos (**Figure 24**) suggesting that cardiac phenotypes are acquired during later development or do not manifest themselves during embryonic stages. Alternatively, maternally deposited mRNAs could compensate for *mgl* loss in the early embryo so that no phenotypes are observed. mgl^{168}, mgl^{269}, mgl^{608}, mgl^{406} embryos must be tested to validate these results.

Formerly, mutations in *LRP2* have been associated with left ventricular non-compaction (LVNC) and other congenital heart defects in the mouse and Donnai-Barrow Syndrome in humans, a developmental disease that causes malformation of multiple parts of the body[114,115,266], but to this point not with HLHS. In combination with the results from hiPSCs (Colas lab) and zebrafish (Ocorr lab) (see Chapter introduction) the *Drosophila* data further support an implication for *LRP2* in cardiac proliferation and growth, although a definite link to HLHS must await further studies. Most likely, *LRP2,* like most other top CHD candidate genes (i.e. *NKX2.5, Notch, MYH6*)[15,95,97], is associated with the etiology of multiple CHDs, which often are oligogenic like HLHS and share many common risk factors.

5.3.7.2 A hypothetical pathogenic role for SHH, WNT, and LRP2 in HLHS

Heart development is a complex process where interaction of many pathways and tissues are involved; consequently, a large number of genes have been implicated in various types of CHDs.[29] In our collaborative study of *LRP2* we found evidence that SHH and WNT signaling might be involved in modulating cardiac proliferation and growth[246] upon *LRP2* loss since both pathways were found attenuated based on RNA sequencing in the index patient 5H carrying an *LRP2* variant and since *LRP2* was found connected with SHH/WNT signaling using BioGRID analysis (Theis et al, 2020).[5]

While other members of the LDLR receptor family like LRP1, which is known to interact with Fzd1 to downregulate Wnt signaling[267], or LRP5/LRP6, which function as Wnt co-receptors[268], have been linked to WNT signaling, no direct connection with LRP2 has been described so far. Consistent with our patient RNA sequencing data and results from *LRP2* KD in hiPSC-CMs, single-cell sequencing data from the subventricular zone tissues of the brain of *LRP2* deficient mice also show perturbation in WNT signaling (here β-catenin was downregulated).[269] In addition, proliferation activity of neuronal progenitors was reduced[269], consistent with reduced proliferation in 5H-patient derived hiPSCs.[5]

Testing for genetic interactions between *mgl* and Wnt/wg in an *in vivo* heart model, I inhibited Wnt/wg signaling in the fly heart using different RNAi lines and mutant alleles expecting to worsen *mgl* mutant phenotypes. Indeed, I observed reduced contractility in flies transheterozygous for $mgl^{MI14318}$ and Df(*wg)* which is not observed in single mutants (**Figure 22** D). However, I fail to see the

same effect in flies with *mgl*^{MI14318} and reducing Wnt/wg signaling via *fz* or *fz2* receptor knockdown (**Figure 22** D). In fact, *fz* and *fz2* were shown to be redundant and the presence of one receptor is sufficient for Wnt signal transduction in all cell types tested.[270] Therefore, simultaneous KD of both main wg/Wnt receptors *fz* and *fz2* receptors in a *mgl* mutant background would be required to completely block the pathway, which could explain some of the differences in phenotypes.[270] Note, that Df(*wg)* covers several Wnt genes, and some are unrelated to Wnt signaling, which could also potentially contribute to the differences in phenotype manifestation between *fz/fz2* KD and Df(*wg*) phenotypes.

Interestingly, KD of either of the receptors alone is sufficient to cause heart dilations (**Figure 22** B), which is consistent with previous studies on heterozygous mutants for Wnt/wg component *armadillo* (fly *β-catenin*) or its co-factor *pangolin* (fly HMG-box (TCF)), which also show increased diastolic diameters in adult flies.[271] Furthermore, *armadillo* mutants exhibit increase in diastolic intervals similar to *fz* and *fz2* KD flies (**Figure 22** F). Note, that in a *megalin* mutant background diastolic intervals (DIs) of *fz* and *fz2* KD flies are reversed to normal levels indicating synergism and suggesting that normal *LRP2* function might be required for *fz* and *fz2* KD-mediated phenotypes. Although this is not what was expected, i.e. a "worsening" of the *mgl* phenotype, there is a clear synergistic interplay between *mgl* and Wnt/wg signaling in the heart.

In contrast to *armadillo*, *pangolin* mutants did not show alteration in DIs.[271] A similar variability in phenotypes upon KD of different components of the signaling pathway was also observed in my data set (i.e compare SI of *fz* and *fz2* KD flies, **Figure 22** G). Overall, the variability of the phenotypes when blocking different elements of the Wnt pathway made it difficult to interpret the results and to determine the exact relationship and mechanism between Wnt/wg signaling and *mgl;* however, again, clear signs of synergism was observed between the two.

Blocking Hh signaling systemically or specifically in the fly heart using different mutant alleles and transgenes also leads to some variability in phenotype manifestation, as it was observed when blocking Wnt/wg signaling. While Hh signaling is well studied in early cardiogenesis, where it was shown to be important for cardiac progenitor specification and differentiation (reviewed in[165]), the functional consequence of Hh signaling loss for adult fly hearts is not known. Heart period was significantly prolonged when inhibiting Hh signaling (*hh*^{Ac} heterozygous mutant, *ptc* overexpression, *smo* or *ci* KD, **Figure 23** D, J). Overall, the data suggest that Hh pathway inhibition in conjunction with *mgl* heterozygous mutation somewhat reverses *mgl* mutant phenotypes, which indicates a synergistic interaction.

Two different models were proposed on how LRP2 controls signaling molecules and their downstream effectors (reviewed and discussed in[269]). First, the lack of LRP2 might result in impaired

clearance of morphogens from the cell surface, which leads to altered morphogen concentrations (i.e. WNTs), which again could perturb signal reception of other cell types in the same space. This model has been previously described for LRP2-mediated clearance of bone morphogenetic proteins (BMPs).[105,272] In the second model, altered Wnt signals could be the secondary consequence of alterations of other morphogen pathways affected by LRP2, as it was described in the developing retina, where loss of LRP2 leads to increased SHH activity, which in turn leads to Wnt downregulation.[111]

While we observed a downregulation of Wnt signaling in the hiPSC-CMs of index patent 5H, which carries a LRP2 mutation, SHH was not increased but potentially blocked by upregulation of *patched 1*. Interestingly, LRP2 has been shown to act as an auxiliary receptor for SHH that inhibits or activates its downstream signaling in a context and tissue dependent manner.[111,273]

A recent publication supports an interaction between LRP2 and SHH signaling in the heart, showing that LRP2 in the mouse heart was (among others) specifically expressed in SHH-responsive progenitor cells that contribute to outflow tract formation (OFT).[274] Here, the loss of LRP2 results in reduced SHH activity, leading to premature differentiation of cardiac progenitor cells and insufficient elongation of the OFT, resulting in a common arterial trunk. Interestingly, Wnt signaling was found unaffected upon LRP2 loss in this context, although canonical and non-canonical Wnt signaling is among those pathways that have been implicated in balancing proliferation versus differentiation fate decision in the second heart field.[275–279] Although those *LRP2* KO mice do not show HLHS phenotypes, altered blood flow as a consequence of valve or outflow tract defects has been hypothesized to be involved in HLHS etiology.[100,280] Since we found *LRP2* variants enriched in our HLHS cohort, this might be a potential mechanism of how *LRP2* could contribute to HLHS.

Furthermore, I hypothesis that LRP2 could play a similar role in controlling morphogenic pathway responses in other cell populations of the heart (i.e in the First heart field, which gives rise to the left ventricle), leading to intrinsic cardiomyocyte proliferation and maturation defects associated with left ventricle hypoplasia[5,101,103] and that mutation of *LRP2* variants together with other gene mutations could contribute to HLHS pathogenesis. The zebrafish *LRP2* mutant, in which we found CMs number predominantly reduced in the ventricle compared to controls, could be a suitable model to further evaluate the synergistic interaction I identified in the fly between *LRP2,* SHH, and WNT in the context of ventricular hypoplasia. The *Drosophila* heart model can be used to test for genetic interactions between LRP2 and other prioritized variants from the 5H patient and the other patients with *LRP2* variants, to build a gene network with high relevance to HLHS, and to get one step closer to characterize the oligogenic etiology underlying HLHS.

5. Results – Chapter 4

5.4 Functional analysis across model systems implicates ribosomal protein genes in growth defects associated with hypoplastic left heart syndrome

5.4.1 Introduction

As a consequence of the genetic heterogeneity and multigenic etiology of HLHS, the cellular and developmental mechanisms underlying HLHS are still poorly understood. Recently, multiple studies, including our own, suggest that defective cardiac differentiation and impaired cardiomyocyte (CM) proliferation are likely contributing to HLHS-associated heart defects[5,101,103,238] (see also Introduction section 1.4).

In collaboration with the Colas and Ocorr lab at SBP and the Mayo Clinic, we established an integrated analysis platform in multiple genetic model systems, which combines patients whole-genome sequencing (WGS) coupled with systematic functional screening in patient-derived iPSC-cardiomyocytes (hiPSC-CMs), *Drosophila,* and *Danio rerio* (zebrafish) to identify and functionally evaluate genes potentially associated with CHD/HLHS.[5] Based on our results, we suggest that ribosomal protein (RP) genes may play a critical role in cardiogenesis and are candidates for a novel class of genetic effectors in CHDs, such as HLHS. In the following, I will briefly outline our findings (*manuscript in progress, Nielsen T.*, Kervadec A.* et al.; *co-first authors*) and present my work in more detail in the result section below.

With proliferation defects being a likely hallmark of HLHS, we first sought to identify genes important for CM proliferation. The Colas lab performed a genome-wide siRNA screen of 21,888 genes on generic hiPSC-derived CMs and evaluated CM proliferation by EdU incorporation assay and total cell numbers at day 25. EdU (thymidine 5-ethynyl-20-deoxyuridine) is a nucleotide analog, which is incorporated into newly synthesized DNA. The top 152 hits which negatively influence proliferation (<0.5-fold EdU incorporation and 0.8 decrease in CM number) were subjected to gene ontology analysis, which revealed enrichment in genes associated primarily with “translation/ribosome” genes and p53 signaling. Interestingly, the most represented gene family was encoded by ribosomal protein (RP) genes, whose KD caused the strongest cell proliferation inhibition.

Furthermore, whole-genome sequencing and unbiased filtering for rare, predicted-damaging coding and non-coding variants were performed in a cohort of 25 HLHS proband-parent trios with poor clinical outcome (Mayo Clinic). Enrichment analysis revealed an overrepresentation of RPs when compared to a reference proteome using STRING[281] and PANTHER[282] (**Figure 25** A). Segregation analysis in a familial case (75H) identified a maternally inherited rare promoter variant affecting the ribosomal protein *RPS15A* that segregated with disease in a 5th degree relative, which also has CHD (**Figure 25** B). Supporting a biological impact, patient-derived hiPSC-CM proliferation was reduced

compared to the parents (see also Theis et al. 2020).[5] Furthermore, we found that knockdown of 60 (out of 80) RPs reduced proliferation in generic hiPSC-CMs, including *RPS15A* (Colas lab, **Figure 25** C, D).

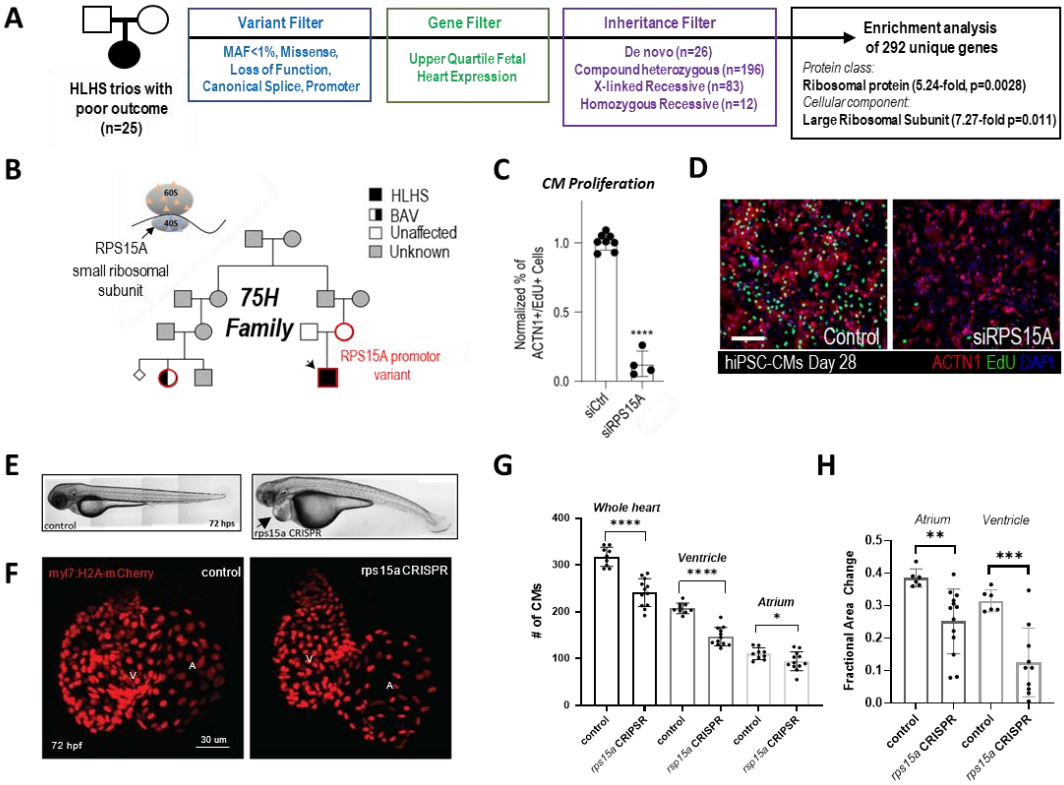

Figure 25: Implication of ribosomal protein gene variants in HLHS/CHD. (A) Gene prioritization scheme of 25 poor-outcome HLHS trios. **(B)** Pedigree of the 75H family. The black arrow indicates the proband. The HLHS-associated variant contains a G>A substitution in the *RPS15A* promoter (−95 upstream of the transcription start site), which is a region predicted (ENCODE) to be rich in TF binding sites. BAV = bicuspid aortic valve. **(C-D)** Representative immunofluorescence images of proliferation (EDU incorporation, green) of induced hiPSCs upon *RPS15A* knockdown (D) and quantification (C). Nuclei are in blue (DAPI). ACTN1 marks cardiomyocytes (CM) (red). Student's t-test, ****p<0.0001. **(E)** Lateral view (head to the left) of a wild-type control zebrafish larva and a *rps15a* mutant, which exhibits near normal body/tail but a notable pericardial edema (arrow). **(F)** Control and *rps15a CRISPR* mutant hearts marked by Tg(myl7:H2A-mCherry) (marks CM nuclei). **(G)** Total CM counts (mCherry+ cells) are reduced in *rps15a* mutants compared to controls shown in (F). **(H)** Fractional area change (FAC) is reduced in *rps15a* mutants compared to constrols. Student's t-test, *p<0.05, **p<0.01, ***p<0.001, ****p<0.0001.

Heart-specific knockdown of RPs in *Drosophila* led to a range of cardiac phenotypes, mostly a partial heart, 'no heart' or lethality was observed (more details in results part). For functional validation in a vertebrate model, we used zebrafish, *Danio rerio*, which has a two-chambered heart and can be easily genetically manipulated by morpholino (MO) injections or CRISPR-induced mutagenesis.[283–285] In addition, heart phenotypes can be directly observed and recorded in the developing zebrafish larva followed by SOHA analysis.[286]

Zebrafish *rps17* CRISPR mutants and *rpl39* morphants show mild cardiac phenotypes, while *rps15a* knockdown causes much reduced cardiomyocyte numbers, heart looping defects, and diminished contractility, without affecting overall embryonic development (**Figure 25** E-H).

Testing for cardiac-specific RP functions, we found synergistic interactions between *RPS15A* and cardiac transcription factors, including *tinman/NKX2.5,* in *Drosophila* and these genetic interactions

were similar in zebrafish, suggesting conserved mechanisms (see result part). Furthermore, *RPS15A* knockdown-induced defects were significantly reversed by *p53* knockdown in hiPSC-CMs and zebrafish and by Hippo pathway activation or *myc* knockdown in flies (the latter see result part).
As part of this collaborative project, I studied the role of RPs and *RPS15A* fly ortholog *RpS15Aa* in particular in the *Drosophila* heart, which I will describe and discuss in the following.

5.4.2 Acknowledgment

All bioinformatics analysis of the HLHS WGS data was done by Dr. Timothy M. Olson and Dr. Jeanne L. Theis at the Mayo Clinic. The genome-wide screen in generic hiPSC-CMs was performed by Dr. Maria A. Missinato (Colas lab) and all further work on generic and patient-derived hiPSC-CMs was performed by Dr. Anaïs Kervadec (Colas lab). Validation in zebrafish was performed by Dr. Xin-Xin I. Zeng (Ocorr lab) with exception of the interaction studies between *rps15a* and *tbx5a* in zebrafish, which I performed with the support of Dr. Zeng, who helped with morpholino injection into zebrafish embryos. I studied the role of ribosomal proteins in the fly under the guidance of Drs. Georg Vogler and Rolf Bodmer. I further want to acknowledge Dr. Analyne Schroeder from the Bodmer lab, who initially discovered the heart-loss phenotype upon heart-specific KD of *RpS15Aa* and *RpL13* in the fly.[124] I contributed to her publication (Schroeder et al. 2019)[124] by validation of these phenotypes using multiple RNAi lines (data shown in Appendix section 8.2). Fly stocks *corp*-EP and UAS-*corp*A were kindly gifted by the Golic lab and UAS-*yorkie* was received from Dr. D. Pan.

5.4.3 Knockdown of ribosomal proteins in the *Drosophila* heart causes severe cardiac defects

To study the role of ribosomal proteins in the fly heart *in vivo*, I performed knockdown of those ribosomal proteins, which were found mutated in the 25 HLHS poor outcome families and the familial HLHS case (75H). RNAi was specifically expressed in the fly heart using $Hand^{4.2}$-Gal4,tdtK driver followed by functional heart analysis using the fluorescent heart reporter line (see Methods section 4.3.2). We observed severe cardiac phenotypes upon knockdown (KD) of RPs ranging from constriction over complete/partial heart loss to lethality (**Figure 26** A, B). KD of *RPS15A* fly ortholog *RpS15Aa* led to a partial loss of the heart (**Figure 26** A, B), validating our results from a previous study (including my contribution) with KD of *RPS15A* and another RP gene (*RPL13A*).[124] Note, that in some flies with partial heart loss we observed a narrow larval-like aorta in the anterior segments (see **Figure 28** A). This suggested that RP loss might cause reduced protein synthesis, thus resulting in an atrophied anterior heart.

A

Human Gene	Proband (age, sex)	Mode of Inheritance	Variant	MAF%	CADD score	Fly gene	Phenotype with Hand4.2-Gal4 driver	Phenotype with tinD-Gal4 driver
RPL26L1	145H (3y, M)	Compound heterozygous	-1248A>G	0.029	-	*RpL26*	lethal, no heart	constricted, myofibrillar disarray
			V97M	0.032	21.3			
RPL36A		X-linked recessive	-1321C>T	0.055	-	*RpL36A*	lethal, no heart	ND
RPS15		Compound heterozygous	-1558C>T	0	-	*RpS15*	lethal	constricted, myofibrillar disarray
			T101S	0.102	23.5			
RPL39	151H (20y, M)	X-linked recessive	-1359T>C	0.653	-	*RpL39*	lethal, partial heart**	constricted, myofibrillar disarray
RPL3L	96H (22m, M)	Compound heterozygous	R200Q	0.966	21.2	*RpL3*	no heart	increased systolic diameters
			R242W	0.432	14.94			
RPL13A	201H	Compound heterozygous	-92-645C>T	0.72	-	*RpL13A*	no phenotype	ND
			-29-191C>T	0.046	-			
RPS17	325H	Homozygous Recessive	S136N	0	< 10	*RpS17*	lethal	most pupal lethal, constricted, myofibrillar disarray
RPL10	76H	X-linked Recessive	24-218G>A	0.583	-	*RpL10*	constricted	constricted, myofibrillar disarray
RPS28		Compound Heterozygous	-589G>A	0.061	-	*RpS28b*	ostia defect	ND
			-505A>T	0.08				
RPS15A	75H	segregates with CHD	c.-95G>A	0.662	-	*RpS15Aa*	no/partial heart	constricted, myofibrillar disarray*

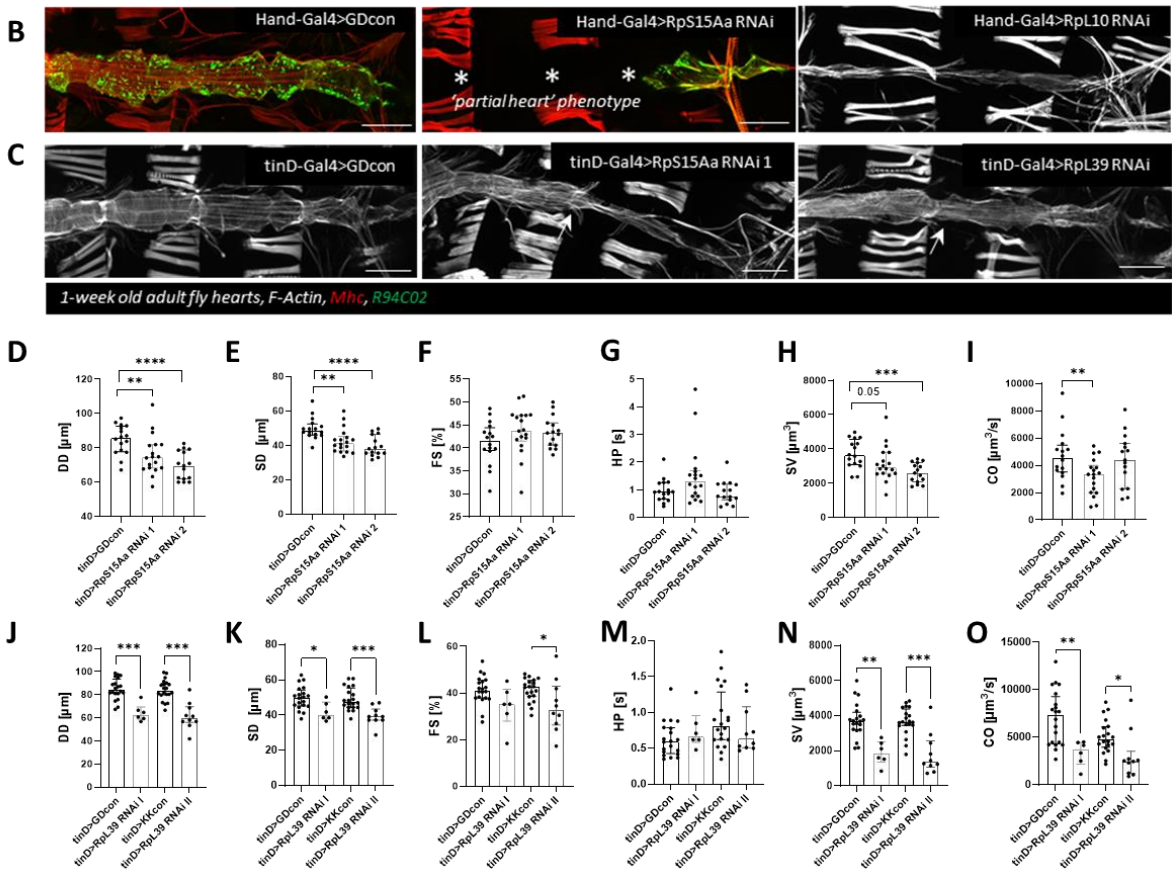

Figure 26: Functional evaluation of prioritized ribosomal protein genes during cardiogenesis. (A) Significant variants in ribosomal genes of HLHS patients. Summary of fly phenotypes with *Hand*$^{4.2}$-Gal4 or *tin*D-Gal4 driver. KD of the identified RP genes resulted mostly in a lethal or no heart phenotype. *Abbreviations*: *CADD*, combined annotation dependent depletion (missense variants); *MAF %,* minor allele frequency in gnomAD; *ND*, non-determined. Bioinformatic analysis performed by

Dr. Jeanne Theis and Dr. Timothy Olson. *experiment performed at 29 °C; **experiment performed at 18 °C. **(B)** Immunohistochemistry staining of 1-week-old adult fly hearts from controls and flies with heart specific *RpS15Aa* or *RpL10* KD (*Hand*$^{4.2}$-Gal4 driver) stained for Mhc (red) or F-Actin (white). In green, RFP expressed from heart specific enhancer *R94C02*. White asterisks indicate absence of heart structures in *RpS15Aa* KD animals. **(C)** Immunohistochemistry staining of 1-week-old adult fly hearts from controls and flies with heart specific *RpS15Aa* KD (at 29 °C) or *RpL39* KD during embryo stages only (*tin*D-Gal4 driver) stained for F-Actin (white). White arrows indicate constrictions of heart tube. **(D-O)** Functional heart analysis using SOHA method of 1-week-old *tin*D>*RpS15Aa* RNAi (D-I) and *tin*D>*RpL39* RNAi (J-O) flies, which show decreased cardiac diameters and reduced stroke volume (SV) as well as cardiac output (CO). DD= Diastolic Diameter, SD= Systolic Diameter, FS= Fractional Shortening, HP= Heart Period. Mann-Whitney test, *p<0.05, **p<0.01, ***p<0.001, ****p<0.0001. Hand-Gal4 = *Hand*$^{4.2}$-Gal4; tinD= *tin*D-Gal4, mid^{E19}GFP.

To determine, the temporal requirement for RP gene expression, I performed knockdown only in the precardiac mesoderm of the embryo (using *tin*D-Gal4 driver[197]), in contrast to life-long cardiac KD. 1-week adult flies were dissected and stained for F-Actin and KD of all RPs tested (except *RPL3*) led to constricted hearts with myofibrillar misarrangement (**Figure 26** A, C), suggesting an early requirement of RPs for cardiac differentiation. Functional heart analysis using the SOHA method was performed on *tin*D-Gal4>*RpS15Aa* RNAi and *tin*D-Gal4>*RpL39* RNAi flies (using two different RNAi lines per gene) and confirmed reduced heart diameters, which results in reduced stroke volume (SV) (**Figure 26** D-O). Furthermore, *tin*D-Gal4>*RpL39* RNAi flies exhibit reduced fractional shortening (FS) resulting in reduced cardiac output (CO) (**Figure 26** L, O).

Note, that *RpS15Aa* KD with *tin*D-Gal4 at 25 °C did not show any abnormalities in the adult heart. However, increasing RNAi KD efficiency at 29 °C (Gal4-mediated expression is temperature-sensitive) led to cardiac constrictions and myofibrillar disorganization suggesting that the phenotype's severity is dependent on knockdown efficiency. The same principle applied for *Hand*$^{4.2}$-Gal4,tdtK> RpL39 RNAi flies, which exhibit partial hearts at 18 °C but are lethal at 25 °C. To validate the dosage-dependency, I performed KD of *RpS15Aa* using *Hand*$^{4.2}$-Gal4 driver at different temperatures (18 °C, 21 °C, and 25 °C) and I observed less severe phenotypes at lower temperatures (**Figure 27**). Interestingly, in hiPSC-CM, the anti-proliferative effect of RP KD was also dose-dependent (Colas lab, *data not shown*).

Taken together, I found that KD of most ribosomal proteins in the heart leads to cardiac defects in a gene dosage-dependent manner, which can potentially explain the variety of phenotypes observed. Interesting, RPs are also required during early embryonic steps of cardiogenesis and RP loss during that critical timespan is sufficient to cause heart phenotypes in the adult fly.

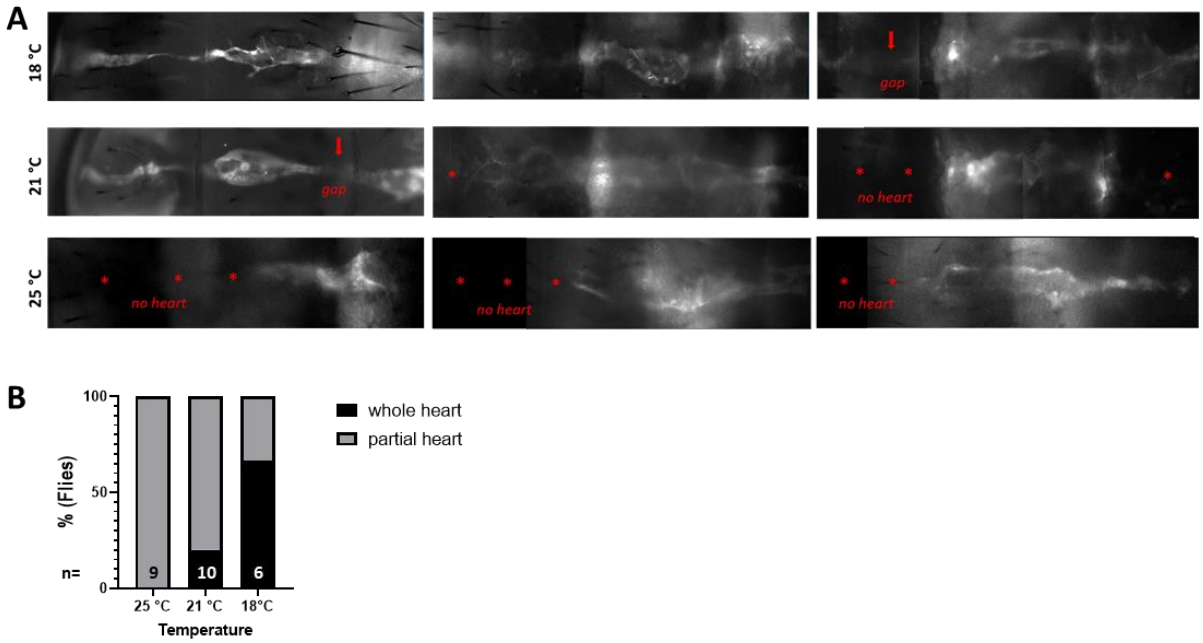

Figure 27: Severity of *RpS15Aa* knockdown phenotypes is dose-dependent. (A) Knockdown of *RpS15Aa* at different temperatures, which results in different Gal4 production and hence different KD efficiencies, reveals dose-dependency of *RpS15Aa* in causing cardiac defects in 1-week-old fly heart. Three examples per temperature are displayed. **(B)** Fly hearts were categorized into *whole heart* and *partial hearts*. Here, a *whole heart* was defined as a fly heart tube that spans from abdominal section A1-A7 without gaps (as seen in wildtypes), regardless of heart constrictions. Graph represents the percentage of flies with *whole* or *partial hearts*.

5.4.4 Knockdown of *RpS15Aa* in the embryo causes defects in early cardiogenesis

To investigate at which timepoint during development cardiac phenotypes occur, I characterized heart morphology in larvae and embryos with *RpS15Aa* KD. 3rd instar larvae with cardiac-specific *RpS15Aa* KD (using *Hand*$^{4.2}$-Gal4) were dissected to expose the heart structure and stained for F-Actin. Already at this stage, *RpS15Aa* KD hearts appear underdeveloped with constrictions and fewer myofibrils compared to controls, although overall structure (heart proper, aorta) is preserved (**Figure 28** B).

Given that KD of RPs during embryo stages **only** leads to cardiac phenotypes in the adult fly, which suggests an early requirement of RPs for cardiac differentiation, I next examined embryonic *Drosophila* hearts with *RpS15Aa* KD. Since the cardiac Gal4 driver lines, *Hand*$^{4.2}$-Gal4 driver and *tin*D-Gal4, only begin to be active from about stage 11-12 of embryonic development, I used a *RpS15Aa* deficiency mutant line, which is independent of Gal4 induction. This deficiency line carries a deletion in the first chromosome that covers *RpS15Aa* along with five other genes. I collected stage-17 hemizygous *RpS15Aa* mutants and stained them with a Neuromancer 1 (Nmr1) antibody, that specifically marks cardiomyocytes, but not pericardial cells. In wildtypes, at stage 17 the cardiac tube is formed by two opposing rows of cardioblasts (single-cell layer) at the dorsal midline. In hemizygous *RpS15Aa* mutants, I observed local increases in cardiomyocyte numbers, suggesting either

overproliferation, misalignment, or misspecification of cardiomyocytes (**Figure 28** C). To validate that this phenotype is specifically caused by loss of *RpS15Aa* (and not one of the other genes included in the chromosomal deletion) and to further characterize the abnormal cardiomyocytes, I performed *RpS15Aa*-specific knockdown using RNAi. Instead of the *Hand*$^{4.2}$-Gal4 driver, which is active from embryonic stage 12, I used the *tin*D-Gal4 and *twist*-Gal4 driver to achieve an earlier KD (embryonic stage 11-12 (*tin*D)[287] and 5 (*twist*)[288]. Both drivers carry the midE19::GFP (Jin et al., 2013)[287], a fluorescent reporter, which has high GFP expression in *tinman*-expressing cardioblasts. Normally, the cardiac tube has a 4+2 pattern of cardioblasts (2 *seven-up* and 4 *tinman* expression) (see also introduction section 1.5.1).

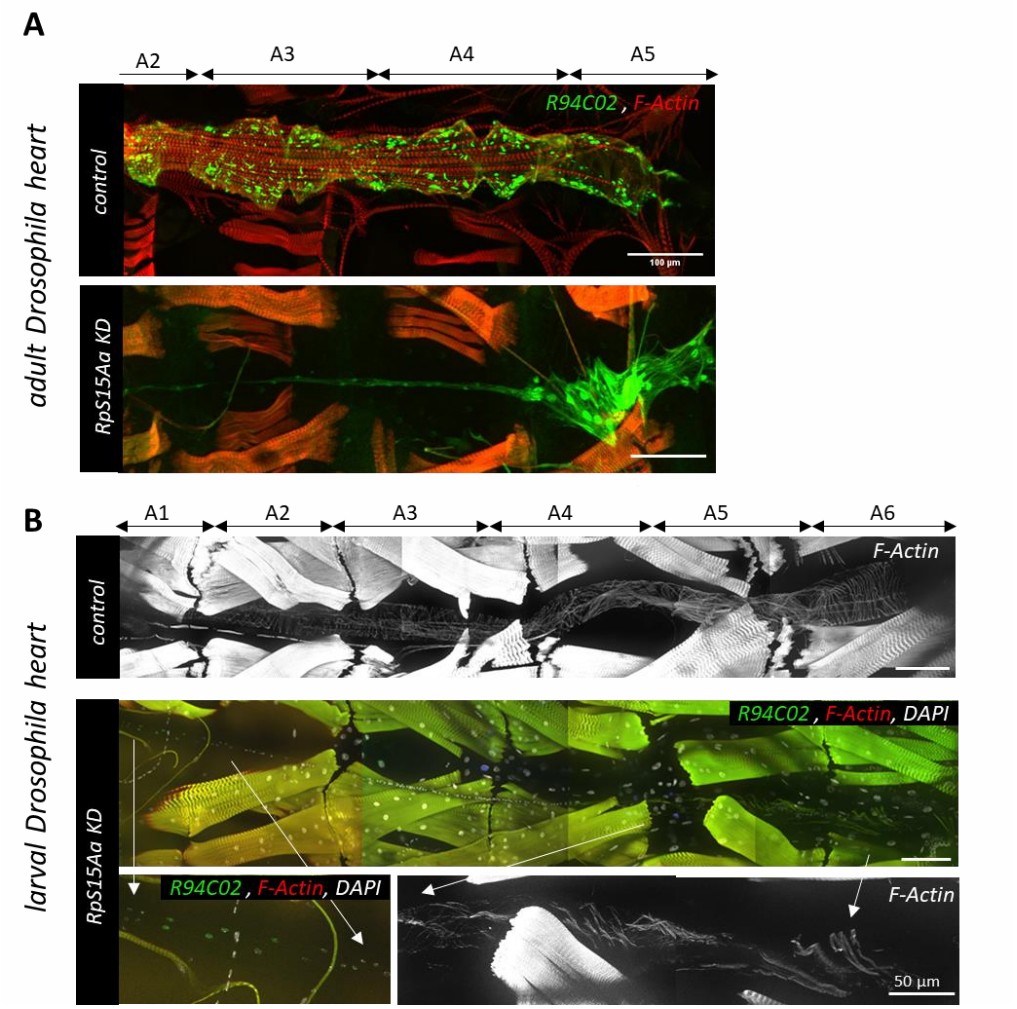

Figure legend on next page.

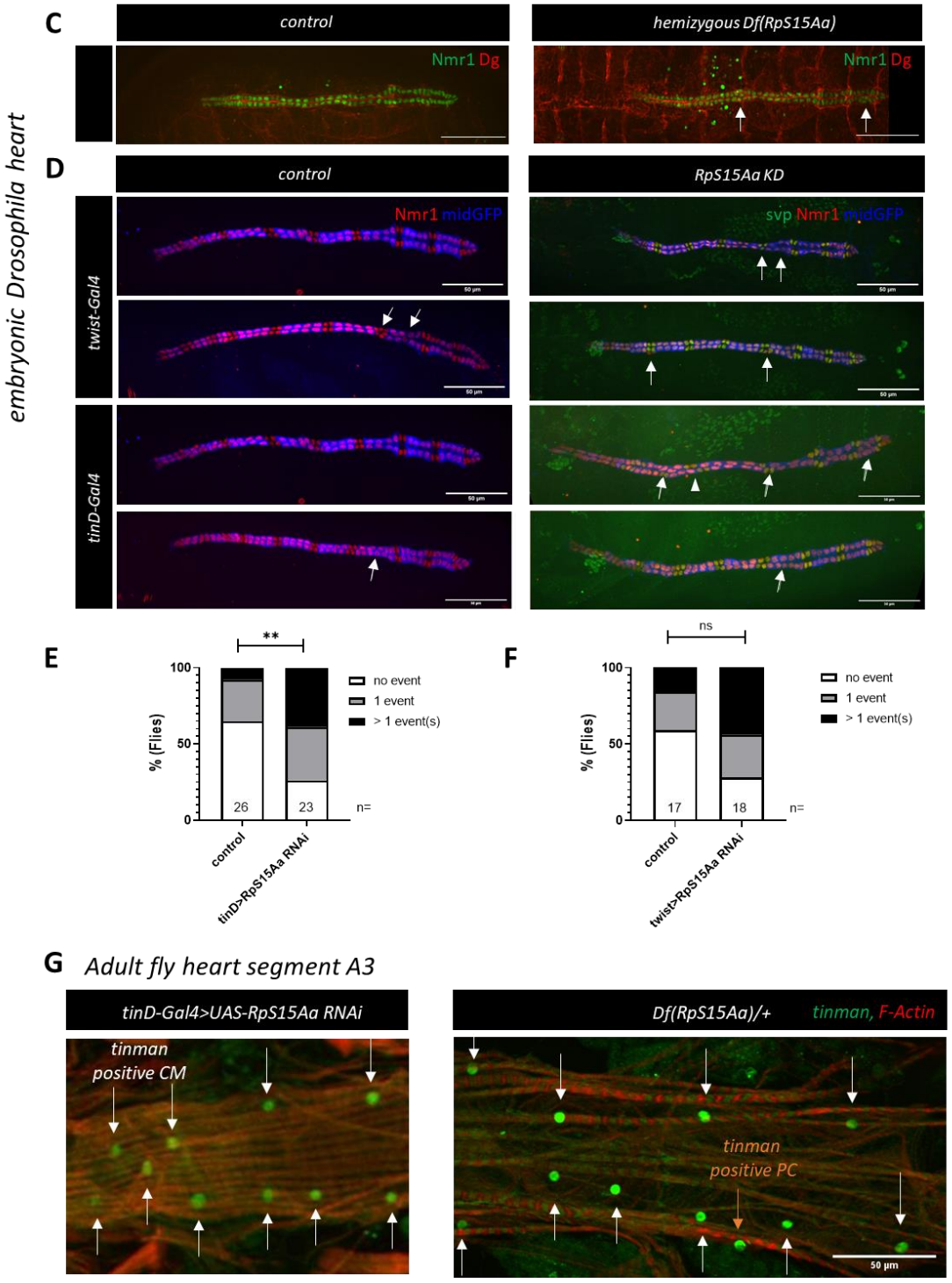

Figure 28: Requirement of *RpS15Aa* for cardioblast differentiation during early cardiac development. (A) tdTomato-labeled fly heart tube in intact fly (top) and fly heart structure of flies exhibiting knockdown of *RpS15Aa* using *Hand*$^{4.2}$-Gal4 driver at 18 °C (below). Note the narrow larval-like aorta in segment A1-A4. **(B)** 3rd instar larval hearts labeled with tdTomato and stained for F-Actin and DAPI. *Hand*$^{4.2}$-Gal4>*RpS15Aa* RNAi larval hearts appear atrophied with fewer myofibrils compared to controls. **(C)** Representative images of stage-17 embryonic fly hearts. Hemizygous Df(*RpS15Aa*) mutants stained for Neuromancer 1 (Nmr1) and Dystroglycan (Dg) show local increase in cardioblast (CB) numbers (white arrows). **(D)** *RpS15Aa* KD and control embryos were marked with *mid*^{E19}-GFP (marks Tinman-positive CBs) and stained for Seven-up (Svp) and Nmr1. Controls do not show Svp staining since the channel was blocked with UAS-Cd4 tdTomato, which served as a UAS control. Scalebar = 50 µm. **(E-F)** Quantification of abnormal CB numbers per segment (counted as "events"). Statistics: Fisher's exact test on absolute numbers. **p ≤ 0.01. (E): control = *tin*D-Gal4, *mid*^{E19}-GFP>UAS-CD4 tdTomato, *tin*D>*RpS15Aa* RNAi = *tin*D-Gal4, *mid*^{E19}-GFP>UAS-*RpS15Aa* RNAi. (F): control = *twist*-Gal4, *mid*^{E19}-GFP>UAS-CD4 tdTomato, *twist*>*RpS15Aa* RNAi = *twist*-Gal4, *mid*^{E19}-GFP>UAS-*RpS15Aa* RNAi. **(G)** Examples of 3-week old adult female fly hearts (*tin*D-Gal4>*RpS15Aa* RNAi and heterozygous Df(*RpS15Aa*)), which show 10 Tinman-positive CBs per abdominal segment instead of the normal 8.

As in hemizygous *RpS15Aa* deficiency embryos, I did not observe any severe morphological changes upon KD of *RpS15Aa* compared to controls but similarly observed locally altered numbers of cardiomyocytes. Furthermore, KD led to misspecification of cardiomyocytes with abnormal patterning (no 4+2 pattern), including missing or additional Seven-up or Tinman positive cardiomyocytes (**Figure 28** D). I observed 6, 10, or 12 Tinman-positive cardiomyocytes instead of the normal 8 per segment and 2, 3, or 5 Seven-up-positive cells per segment instead of 4, consistent with the type of cell division they underwent to originate from precursor cells (Tinman positive cells derive from symmetric and Seven-up-positive cells from asymmetric cell division). This mispatterning in *RpS15Aa* KD embryos further caused misalignment of cardiomyocytes within the cardiac tube, where normally cardiomyocytes of the same kind (Seven-up or Tinman positive) are facing each other.

In *tin*D-Gal4>*RpS15Aa* RNAi embryos these misspecifications appear significantly more often compared to controls (**Figure 28** E). *twist*-Gal4>*RpS15Aa* RNAi embryos show a trend towards more mispatterning; however not significantly (**Figure 28** F). The mispatterning and misalignment of cardiomyocytes were also observed in adult *tin*D>*RpS15Aa* KD flies and heterozygous Df(*RpS15Aa)*/+ flies indicating that once specified, the fly cannot correct for misspecified cardiomyocytes (for example during cardiac remodeling during metamorphosis) (**Figure 28** G).

Taken together, these results highlight the importance of *RpS15Aa* during embryo stages, first for cardiac precursor cell differentiation during early cardiac development, but also for heart growth in later stages, given that KD of *RpS15Aa* during embryo stages causes constricted hearts in adult flies.

5.4.5 Heart loss in *Drosophila* inflicted by *RpS15Aa* KD can be partially rescued by Hippo pathway activation and *myc KD*

To study the consequence of siRNA-mediated loss of ribosomal protein genes on the transcriptional levels, we characterized gene expression in hiPSCs and hiPSC-CMs following siRNA treatment targeting *RPS15A* and *RPL39* using whole transcriptome sequencing. Knockdown of both genes showed a common response with strong activation of TP53 target genes, inhibition of cell cycle genes, and DNA damage response (Colas lab and Dr. Vogler's work). These results were confirmed by RT-qPCR and by showing elevated phospho-TP53 staining in hiPSC-CMs following KD of most RP genes (Colas lab, *data not shown*). Consistent with these findings, we found that KD of *TP53* can rescue the reduced proliferation phenotype observed in hiPSC-CMs with RP KD. In zebrafish, co-KD of *p53* and *rps15a* using MO could partly reverse the *RPS15A* MO phenotypes, including reduction in heart size and cardiomyocyte numbers (Ocorr lab). Strikingly, we found that bradycardia, heart looping, and reduced contractility phenotypes of *rps15a* morphants were also rescued by co-KD of *p53*. These observations robustly support our hypothesis that RP-dependent control of proliferation is a critical mechanism in HLHS since re-establishment of normal CM proliferation rates and numbers by KD of

p53 not only restores heart size but also complex functional aspects of the heart, like contractility, heart looping and heart period (Ocorr lab, *data not shown*).

The fly heart develops similarly to the vertebrate heart at early stages[143] and a link between RPs and cell cycle-regulating pathways, such as p53 and Hippo pathways[289], has been proposed to be conserved between mammals and flies.[290] To test whether *p53* has a similar function in fly heart development as in hiPSC-CMs (at the time of the experiments we didn't have zebrafish data), I performed cardiac co-KD of *RpS15Aa* and *p53* and we examined heart function in flies using the fluorescent heart reporter methods. For this, I created a fly line that harbors the *Hand*$^{4.2}$-Gal4 driver, the cardiac tdtK reporter and the *RpS15A* RNAi construct. Given the severe cardiac phenotypes in *Hand*$^{4.2}$-Gal4>*RpS15Aa* RNAi KD flies, the fly stock was stabilized with a balancer containing a Gal80 construct (CyO, *tub* P-Gal80), which is ubiquitous expressed from the *tubulin* enhancer and antagonizes Gal4 activity by occupying the activation domain of Gal4 and preventing interaction between Gal4 and the transcriptional machinery[291] (**Figure 29**). This fly line can then be crossed to UAS-*p53* RNAi or other transgenic fly lines. Similarly, I created a *Hand*$^{4.2}$-Gal4/CyO; UAS-Stinger fly line (Stinger is an EGFP tagged with a nuclear localization signal), with the purpose to control for multiple UAS-sites.

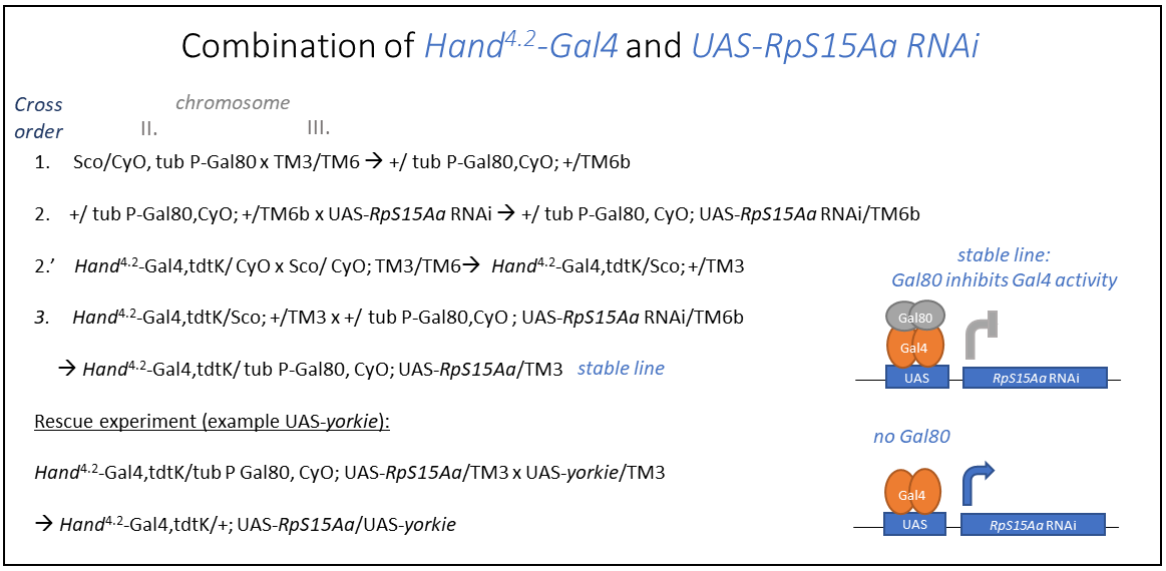

Figure 29: Crossing scheme to combine *Hand*$^{4.2}$-Gal4 and UAS-*RpS15Aa* RNAi. In the stabilized fly line that I created, Gal80 antagonizes Gal4 activity, preventing interaction between Gal4 and the transcriptional machinery.

The co-KD of *RpS15Aa* and *p53* did not rescue the cardiac defects in *RpS15Aa* KD flies (**Table 5**). I suspected that this might be due to the fact that *p53* has different, context-dependent roles in fly compared to human.[290,292] As a positive control, I overexpressed UAS-*RpS15Aa* specifically in the fly heart of *RpS15Aa* KD flies, to restore normal *RpS15Aa* expression levels. However, this did not restore normal heart morphology (**Table 5**), which was likely because the *RpS15Aa* RNAi was degrading most of the overexpressed *RpS15Aa* mRNA as well. I hypothesize that a way to address this problem would

be to overexpress *RpS15Aa* transcript with different coding sequence (i.e. from another *Drosophila* species or even mammalian forms), which would not be targeted by the *RpS15Aa* RNAi.

To probe for other genes that are involved in mediating the cardiac pathologies inflicted by *RpS15Aa* KD and can potentially alleviate them, I screened additional candidate genes involved in the p53 pathway (*corp/MDM2*), genes associated with apoptosis (*XIAP/diap-1, CASP7/Drice, CDK5R1/p35*) or growth (*YAP/yorkie, B-MYB/myb, MYC/myc*) (**Table 5**).

Table 5: List of genes tested for potential rescue of RpS15Aa KD phenotypes. KD = knockdown, OE = overexpression, DN = dominant-negative.

human	***fly orthologue***	***genetic modification***	***genetic construct***	***fly line/source***	***result***
RpS15A	*RpS15Aa*	OE	UAS-RpS15Aa	F000765	no rescue
TP53	*p53*	KD	UAS-p53 DN	#8421	no rescue
			UAS-p53 DN	#8420	no rescue
			p53 RNAi	#41720	no rescue
			p53 RNAi	#v103001	no rescue
			p53 RNAi	#v38235	no rescue
TP53	*Xrp1*	KD	Xrp1 RNAi	#34521	no rescue
MDM2	*corp*	OE	corp-EP	Golic lab	no rescue
			UAS-corpA	Golic lab	no rescue
XIAP	*diap-1*	OE	UAS-Diap	#6657	no rescue
CASP7	*Drice*	KD	Drice RNAi	#7788	no rescue
CDK5R1	*p35*	KD	UAS-p35	#5072	no rescue
	grim, hid, reaper, sickle	Deficiency	Df(3L)H99	#1576	no rescue
YAP	*yorkie*	OE	UAS-yorkie	D. Pan	partial rescue
		OE	UAS-YAP$^{2\text{-}5}$ (M4)	this work	lethal with *Hand*$^{4.2}$- and *tin*C-Gal4 driver; viable with *tin*HE-Gal4
		OE	UAS-yki$^{S168A.V5}$	#28818	no rescue
		OE	UAS-yki^{S111A,S168A,S250A}	#28817	lethal with *Hand*$^{4.2}$-Gal4 driver; viable with *tin*HE-Gal4
YAP + TEAD1/2/3/4	*yorkie + sd*	yorkie OE + sd KD			rescue by yorkie OE is mediated by scalloped
MYC	*myc*	KD	myc RNAi	#25784	partial rescue
			myc RNAi	#v106066	partial rescue
		OE	UAS-myc	#9674	no rescue
B-MYB (TF, binds to YAP)	*myb*	OE	UAS-myb	#32044	no rescue
				#35053	no rescue
		KD	myb RNAi	#58482	no rescue

Remarkably, I found that overexpressing the Hippo pathway gene *yorkie* (y*ki*), the fly ortholog of *YAP*, in the developing heart along with *RpS15Aa* KD, can partly restore the *RpS15Aa* KD-induced heart loss in *Drosophila* (**Figure 30**). The restored heart tube shape and myofibrillar structure are still atrophied; however, I observed formation of adult ostial structures (**Figure 30** C, RpS15Aa + yorkie OE, heart 2), which was not observed in the *RpS15Aa* KD flies. Further, I found that *yki*-mediated rescue is dependent on *yorkie*'s co-factor encoded by *scalloped* (*sd*, *Drosophila TEAD1/2/3/4*) since with simultaneous *sd* KD, *yki* OE can no longer rescue the *RpS15Aa* KD-induced heart loss (**Figure 30** C, D). For this experiment I created a fly line combining UAS-*yorkie* and *sd* RNAi to cross it to the *Hand*$^{4.2}$-

Gal4/CyO, Gal80; UAS-*RpS15Aa* RNAi/TM3 line (**Figure 30** A). In parallel, I generated a fly stock combining UAS-*yorkie* and UAS-GFP with the purpose to control for multiple UAS-sides (**Figure 30** A). Moreover, KD of *sd* in a *RpS15Aa* KD background (without *yki* OE) worsens the *RpS15Aa* KD phenotype, in the way that in some flies no remnant posterior heart structures remain (**Figure 30** C, D).

I further tested whether apoptosis plays a role in the *RpS15Aa* KD mediated heart loss by co-KD of cell death-related genes, including *Drice* (*dCASP7*) or overexpression of anti-apoptotic genes like *p35* or *diap1* (*dXIAP*) in a *RpS15Aa* KD background. The inhibition of apoptosis was unable to reverse or partially rescue the heart phenotype, consistent with the interpretation that the partial heart phenotype is not based on apoptosis induction in the heart.

A well-known master regulator of ribosome biogenesis is oncogenic transcription factor *myc*, which regulates the expression of several components of the protein synthesis machinery including RP gene expression.[293] First, I tested whether overexpression of *myc* could compensate for reduced *RpS15Aa* levels in the fly, but overexpression of *myc* in conjunction with *RpS15Aa* KD did not rescue the heart loss (**Table 5**). In contrast, it was the co-KD of *myc* and *RpS15Aa* that restored heart structures (predominantly in the anterior segments of the abdomen (A1-A3)), while *myc* KD by itself had little effect (**Figure 30** C, E). The restored hearts showed adult-like heart structures; however, myofibrils were poorly developed, probably due to a lack of sufficient protein synthesis.

Overall, these results highlight the sensitivity to gene expression changes in the highly controlled and fine-tuned processes that regulates cardiac development. Although *yorkie* overexpression and *myc* KD could not completely rescue the *RpS15Aa* KD, both rescuing gene functions point towards growth as a critical component involved in cardiac phenotypes upon ribosomal protein loss.

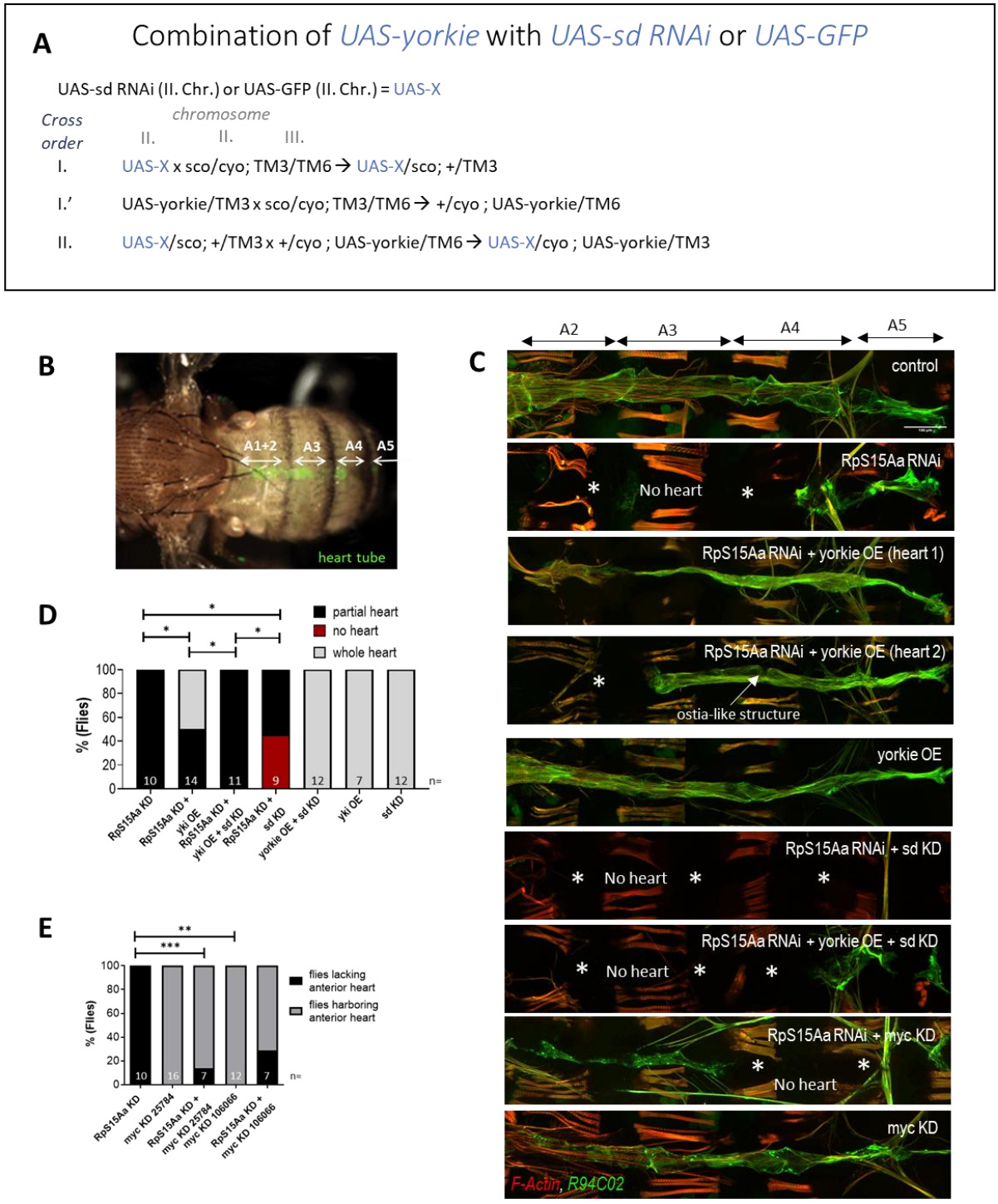

Figure 30: Rescue of *RpS15Aa* KD-mediated heart tube loss in *Drosophila* by *myc* KD or *YAP/yki* overexpression depending on its co-factor *TEAD/sd*. (A) Crossing scheme combining UAS-*yorkie* and UAS-*sd* or UAS-GFP. **(B)** Adult fly with heart tube labeled with green fluorescence. A1-A5 represent abdominal segments 1-5. **(C)** Representative images of RFP expressing fly hearts (green) co-stained for F-Actin (red). *RpS15Aa* KD-mediated heart tube loss can be partially rescued by overexpression of *yorkie* (RpS15Aa RNAi + yorkie OE) and KD of *myc* (RpS15Aa RNAi + myc KD). The rescue by *yki* OE depends on its co-factor *sd* (compare 3rd/4th and 7th panel). Representative images of fly hearts from control (*Hand*$^{4.2}$-Gal4,tdtK/+;UAS-Stinger), RpS15Aa RNAi (*Hand*$^{4.2}$-Gal4,tdtK/+;UAS-RpS15Aa-RNAi/+;UAS-Stinger/+), RpS15Aa RNAi + yorkie OE (*Hand*$^{4.2}$-Gal4,tdtK/UAS-GFP;UAS-*RpS15Aa*-RNAi/UAS-*yorkie*/+), yorkie OE (*Hand*$^{4.2}$-Gal4,tdtK/UAS-GFP;UAS-*yorkie*/+), RpS15Aa RNAi + yorkie OE + sd RNAi (*Hand*$^{4.2}$-Gal4,tdtK/UAS-*sd* RNAi;UAS-*RpS15Aa*-RNAi/UAS-*yorkie*), RpS15Aa KD + sd KD (*Hand*$^{4.2}$-Gal4,tdtK/UAS-*sd* RNAi; UAS-*RpS15Aa*-RNAi/+), RpS15Aa KD + myc KD (*Hand*$^{4.2}$-Gal4,tdtK/UAS-*myc* RNAi;UAS-*RpS15Aa*/+) or myc KD (*Hand*$^{4.2}$-Gal4,tdtK/UAS-*myc* RNAi; UAS-Stinger/+) flies. Flies were raised at 25 °C. **(D)** Quantification of percentage

of flies exhibiting *whole heart tube* versus *partial heart loss* (defined as 25-75 % heart tube length compared with wild type) or *no heart tube*. Statistics: Fisher's exact test on absolute numbers, *p<0.05. **(D)** Quantification of percentage of flies exhibiting anterior part of the heart (heart in segment A1-A3) compared to flies lacking anterior part. Statistics: Chi-square test on absolute numbers, *p<0.05, **p<0.005, ***p<0.001**.** One-week-old flies were quantified.

5.4.6 *RpS15Aa* knockdown in the heart leads to induction of pro-apoptotic *hid* in the epidermis

In the previous section I mentioned that knockdown of anti-apoptotic genes could not rescue the *RpS15Aa*-induced heart phenotype. In parallel, I checked if apoptosis is induced in the fly heart with *RpS15Aa* KD by using a *hid-EGFP* reporter line that harbors the 5' regulatory sequence of *hid* driving expression of GFP. *hid* is a pro-apoptotic gene and is induced along with *reaper* and *grim* in response to many apoptotic stimuli (reviewed in[294]). I crossed the *hid* reporter line to *Hand*$^{4.2}$-Gal4/*CyO,* Gal80, tdtK; *RpS15Aa* RNAi/TM6b (**Figure 31** A), dissected the (non-balancer containing) *RpS15Aa* KD progeny flies to expose the heart tube and screened for *hid* expression. I did not observe any *hid-EGFP* in the adult cardiomyocytes, however, I observed strong *hid* expression in the fly epidermis, which was not present in the controls (**Figure 31** B). Assuming that *hid* expression could be initiated in earlier stages of development, I screened 3rd instar larvae with *RpS15Aa* KD using the *hid* reporter line. Like adults, I did not observe *hid-EGFP* in the larval cardiomyocytes, just in the epidermis (**Figure 31** C). For further validation, I combined *hid-EGFP* with another cardiac driver *tin*C-Gal4 and crossed this line with UAS-*RpS15Aa* RNAi. Here, *hid* expression was also observed in the epidermis (*data not shown*). These results point towards a non-autonomous induction of *hid* in the epidermis originating from KD of *RpS15Aa* in the heart, while the cardiomyocytes were not affected.

Furthermore, my preliminary data suggest that the epidermal *hid* expression is rescued by *myc* knockdown. For this experiment, I combined *hid-EGFP* with UAS-*myc* RNAi to cross this line with *Hand*$^{4.2}$-Gal4/*CyO,*Gal80, tdtK; *RpS15Aa* RNAi/TM6b (**Figure 31** D). The progeny of this cross was collected as larvae and sorted according to the presence of *hid* expression. Once the respective larvae hedged as adults, I genotyped them by sorting for CyO and TM6b balancers and I examined the adult hearts using the tdtK fluorescent heart method. All *hid* negative larvae turned out to express UAS-*myc* RNAi together with UAS-*RpS15Aa* RNAi and showed a partial rescue of the heart as described in the previous sections, while *hid* positive larvae express UAS-*RpS15Aa* RNAi alone and show the expected *partial heart loss* phenotype (**Figure 31** E, F).

One hypothesis is that when *myc* KD is ameliorating the cardiac phenotypes upon *RpS15Aa* KD, it could lead to blockage of the signaling from the heart to the epidermis that is triggering non-autonomous *hid* expression in the epidermis. Further investigations are needed to characterize the cell type in which *hid* expression is initiated and how the loss of a ribosomal protein gene can trigger expression of pro-apoptotic *hid* in the epidermis in a non-autonomous way.

A

Experiment setup:

control:
hid-EGFP/ *hid*-EGFP x *Hand*$^{4.2}$-Gal4,tdtk/ *Hand*$^{4.2}$-Gal4,tdtK → *hid*-EGFP/+; *Hand*$^{4.2}$-Gal4,tdtK/+

***RpS15Aa* knockdown:**
hid-EGFP/ *hid*-EGFP x *Hand*$^{4.2}$-Gal4,tdtK/cyo,Gal80; *RpS15Aa* RNAi/TM6b → *hid*-EGFP/+; *Hand*$^{4.2}$-Gal4,tdtK/+; UAS-*RpS15Aa* RNAi/+

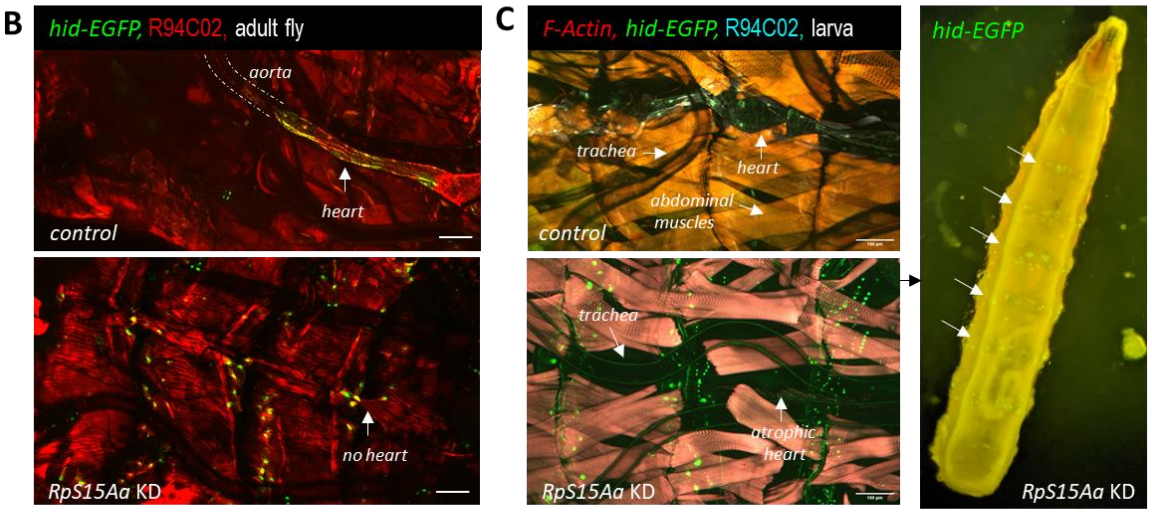

D

Rescue experiment setup:

Combination of *hid-EGFP* and *UAS-myc RNAi*:

Cross order	chromosome I.	III.

I. Cdc42/FM7 x TM3/TM6→ Y/FM7; +/TM3 and Y/FM7; +/TM6

II. *hid*-EGFP/*hid*-EGFP x FM7/Y; +/TM3 → *hid*-EGFP/FM7; +/TM3

II.' UAS-*myc* RNAi/TM3 x Y/FM7; +/TM6 → Y/FM7; UAS-*myc* RNAi/TM6

III. *hid*-EGFP/FM7; +/TM3 x Y/FM7; UAS-*myc* RNAi /TM6b→ *hid*-EGFP/FM7; UAS-*myc* RNAi /TM3

Rescue:

IV. *hid*-EGFP; UAS-*myc* RNAi/TM3 x *Hand*,tdtK;*RpS15Aa* RNAi/TM6b

→ *hid*-EGFP/+; *Hand*,tdtK/+; *RpS15Aa* RNAi/TM3 **or** *hid*-EGFP/+; *Hand*,tdtK/+; *RpS15Aa* RNAi/*myc* RNAi

E

	***hid* positive**	***hid* negative**
number of collected larvae	9 (5 died within 1st week)	6
genotype	*hid*-EGFP/+; *Hand*,tdtK/+; *RpS15Aa* RNAi/TM3	*hid*-EGFP/+; *Hand*,tdtK/+; *RpS15Aa* RNAi/*myc* RNAi
heart phenotype	partial heart	partial rescue
wing phenotype	wing blisters	wing blisters

F

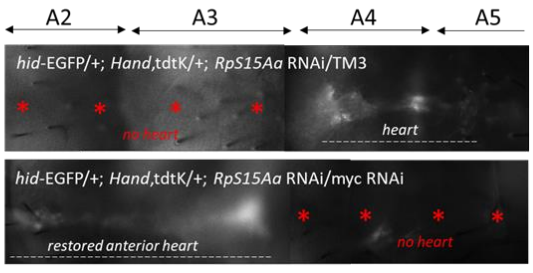

Figure 31: *RpS15Aa* knockdown in the heart leads to non-autonomous induction of *hid* in the epidermis. (A) Experimental setup and crossing scheme to investigate *hid-EGFP* in *RpS15Aa* RNAi KD flies. **(B)** 1-week old adult flies with *RpS15Aa* KD (*hid*-EGFP/+; Hand$^{4.2}$-Gal4,tdtK/+; UAS-*RpS15Aa* RNAi/+) show *hid-EGFP* expression in the epidermis, which is not present in the controls (*hid*-EGFP/+; Hand$^{4.2}$-Gal4,tdtK/+; UAS-GFP). Note that the heart tube of the controls shows some GFP staining due to a floating UAS-GFP in the genetic background. In *RpS15Aa* KD flies no heart structures are observed. **(C)** 3rd instar larvae

knocked-down for *RpS15Aa* show an atrophied heart tube and *hid-EGFP* expression in the epidermis, which is not observed in controls (genotypes as in B). **(D)** Experimental setup and crossing scheme to investigate rescue of *hid-EGFP* in *RpS15Aa* RNAi KD flies by simultaneous KD of *myc.* **(E)** Summary of genotype and phenotypes observed in adult flies, which were separated in larval stages according to presence of *hid* expression. **(F)** Representative tdtK expressing heart tube of *hid*-EGFP/+; Hand,tdtK/+; *RpS15Aa* RNAi/TM3 and *hid*-EGFP/+; *Hand*,tdtK/+; *RpS15Aa* RNAi/*myc* RNAi flies filmed with the fluorescent heart reporter method. Note, the rescue of the anterior heart in *hid*-EGFP/+; *Hand*,tdtK/+; *RpS15Aa* RNAi/*myc* RNAi flies. Hand = $Hand^{4.2}$- Gal4.

5.4.7 *Drosophila RpS15Aa* genetically interacts with cardiac transcription factors *tinman, pannier and Dorsocross*

To investigate how *RPS15A* KD causes cardiac-specific phenotypes in *Drosophila* and zebrafish, we tested for genetic interactions between *RpS15Aa/rps15a* and core cardiogenic genes (CCGs), such as *tinman/NKX2-7, pannier/GATA5,* and *Dorsocross/TBX5a*.

In a first attempt, two different *tinman* null mutants (tin^{346} and tin^{EC40}) were crossed with $Hand^{4.2}$-Gal4/*CyO,*Gal80; *RpS15Aa* RNAi/TM3 followed by functional analysis of the heart using the fluorescent reporter method. Control and experimental flies were reared at 18 °C or 21 °C to achieve weaker *RpS15Aa* knockdown and thus less severe phenotypes compared to 25 °C (**Figure 32**). tin^{346} and tin^{EC40} heterozygous mutants show a tendency towards reduced diastolic heart diameters. *RpS15Aa* knockdown at 18 °C leads to structurally impaired, constricted fly hearts (as previously described, **Figure 27**), which are even further constricted in combination with a heterozygous mutation of *tinman* for both alleles (**Figure 32** A, B). $tin^{346/+}$ in combination with *RpS15Aa* knockdown indicates a synergistic genetic interaction since heart diameters were even further constricted as expected, but hearts from $tin^{EC40/+}$ mutants in combination with *RpS15Aa* knockdown were not significantly different from the expected value, pointing towards an additive effect of both phenotypes (**Figure 32** B). At 21 °C *RpS15Aa* knockdown causes structurally impaired fly heart (as previously described, **Figure 27**), which show a similar trend as at 18 °C towards further constriction in combination with $tin^{346/+}$. However, *RpS15Aa* KD + $tin^{346/+}$ was not significantly different from the expected outcome, probably since *RpS15Aa* KD alone already shows strong constriction at 21 °C. Note, that tin^{346} and tin^{EC40} fly lines are in two different genetic backgrounds (*w1118* and *yw*, respectively), while the controls are in a *yw* background. The wild type control and single mutants ($tin^{346/+}$ and $tin^{EC40/+}$) furthermore carry UAS-Stinger, which controls for the presence of UAS sites in UAS-RpS15Aa RNAi KD flies. I saw before that the genetic background can influence the heart size, however I selected those controls which I found most suitable for this experimental genetic set-up. Despite differences in genetic background, both *tinman* alleles lead to heart constrictions. With both alleles, I observed a similar effect towards more severe constriction in *RpS15Aa* KD + $tin^{-/+}$ compared to *RpS15Aa* KD alone and I expect the influence of genetic background to be minimal given the severe phenotypes upon *RpS15Aa* knockdown.

Experiments to reproduce and validate these data at a later timepoint failed. I was not able to see the same interactions (more severe constriction in *RpS15Aa* KD + *tin*$^{-/+}$ compared to *RpS15Aa* KD alone), since *RpS15Aa* KD by itself already showed severe constriction. Note, that I used another *Hand*$^{4.2}$-Gal4/*CyO,*Gal80; *RpS15Aa* RNAi/TM3 line for the second set of experiments (*Hand*$^{4.2}$-Gal4/*CyO,*Gal80; *RpS15Aa* RNAi/TM6b). The initial stock had to be re-created, since the *RpS15Aa* RNAi construct got lost with time, probably due to genetic selection pressure. Taken together, these results highlight again the sensitivity of cardiac development for ribosomal protein gene dosage and the importance of a good experimental design to investigate and uncover genetic interactions. Conclusively, a less severe *RpS15Aa* phenotype is needed to be able to observe genetic interactions with better clarity.

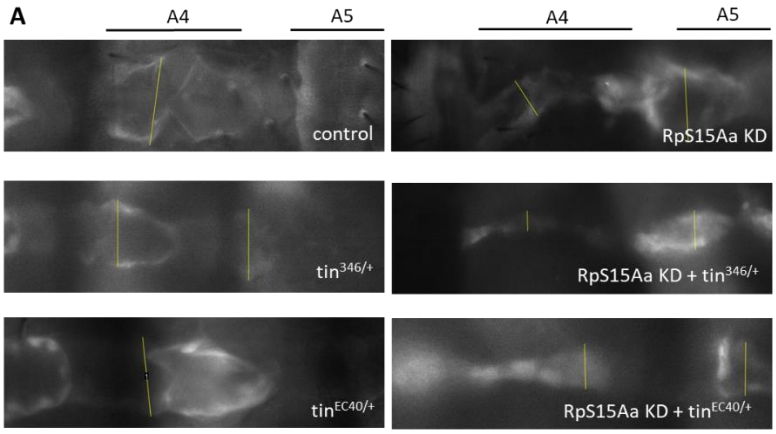

abbreviation	genotypes
control	yw/+; Hand,tdtk/+; UAS-Stinger/+
tin$^{346/+}$	+/+; Hand,tdtk/+; *tin*346/UAS-Stinger
tin$^{EC40/+}$	yw/+; Hand,tdtk/+; *tin*EC40/UAS-Stinger
RpS15Aa KD	yw/+; Hand,tdtk/+; UAS-*RpS15Aa* RNAi/+
RpS15Aa KD + tin$^{346/+}$	+/+; Hand,tdtk/+; UAS-*RpS15Aa* RNAi/*tin*346
RpS15Aa KD + tin$^{EC40/+}$	yw/+; Hand,tdtk/+; UAS-*RpS15Aa* RNAi/*tin*EC40

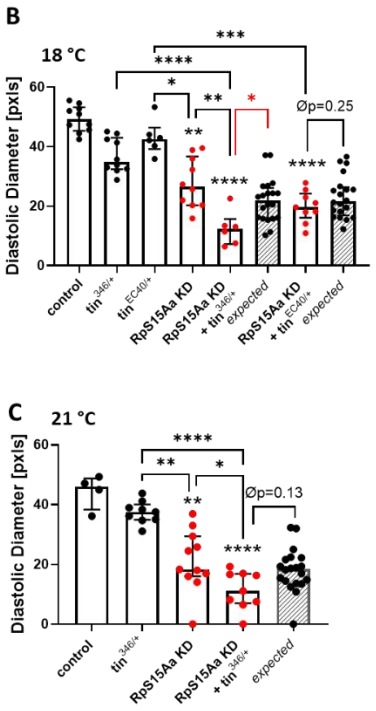

Figure 32: *RpS15Aa* knockdown leads to a structurally impaired fly heart, which is further constricted in combination with a heterozygous *tinman* mutation. (A) Representative control heart, *tinman* mutant heart, *RpS15Aa* KD heart, or *RpS15Aa* KD in combination with additional *tinman* mutations at 18 °C. Yellow lines indicate the position of diameter measurements in segment A4 and/or A5 on fluorescent heart recordings using ImageJ (20X magnification). **(B-C)** Quantification of maximum diastolic heart diameters (pxls= pixels) of *RpS15Aa* knockdown flies with or without additional *tinman* mutation, *tinman* heterozygous mutants and control hearts in segment A4 at 18 °C (B) and at 21 °C (C). Graph shows median with interquartile range and each data point represents one fly. Expected value calculation as previously described (p-value between *combination* and *expected* represents the average p-value from 10 iterations, see also Methods section 4.12). Statistics: Kruskal-Wallis test, *p ≤ 0.05, **p ≤ 0.01, ***p ≤ 0.001, ****p ≤ 0.0001. Genotypes in A-C as indicated in the table.

Thus, I next tested a fly line with a deficiency in the first chromosome covering *RpS15Aa* (along with five other genes) to probe for genetic interactions. For this, I combined the deficiency with the *Hand*$^{4.2}$-Gal4,tdtK driver (**Figure 33** A). Note, that *Hand*$^{4.2}$-Gal4 driver is not of relevance for this interaction experiment since I used systemic mutants (independent from a Gal4 driver). However, the

Df(*RpS15Aa*)/FM7; *Hand*$^{4.2}$-Gal4,tdtK fly line was used so that I can assess heart function with the tdtK fluorescent heart reporter method.

RpS15Aa heterozygosity causes only mild phenotypes in adult flies (mild dilation) (**Figure 33**, **Figure 35**). In contrast, when *RpS15Aa* deficiency was placed in trans to heterozygous loss of function alleles for *tinman, pannier,* or *Dorsocross1/2/3* the corresponding hearts were markedly deformed with significant myofibrillar disarray, which is not observed in either single heterozygotes, thus indicating a genetic interaction (**Figure 33**, **Figure 34**). Of note, *RpS15Aa* deficiency in combination with *Mef2*$^{+/-}$ did not show deformed hearts or myofibrillar misarrangements.

In addition, I performed functional heart analysis on the double and single mutants using the tdtK method. Using our in-house *R* script software, diastolic and systolic diameters are automatically extracted from fluorescent heart recordings at up to six positions along the heart tube and the average was calculated. Since the hearts of transheterozygous mutants show dilations and constrictions, as seen in the immunohistochemistry stainings (**Figure 34**), the average heart diameters displayed in the graphs do not reflect the actual heart dimensions that vary along the heart tube (=deformation). Thus, the parameters for diastolic and systolic diameter (DD and SD) as well as fractional shortening, do not reflect the deformation phenotype and must be interpreted with caution.

Using this fluorescent *in vivo* method *tin*$^{346/+}$ and *Df(*pnr)/+ heterozygous mutants show prolonged heart periods (HPs), while *Dorsocross* heterozygous mutants exhibit shorter HPs. The heart period of Df(*RpS15Aa)* heterozygotes is significantly prolonged in two out of four experiments. Interestingly, *tin*$^{346/+}$, *tin*$^{EC40/+}$, *pnr*$^{VX6/+}$ and *Df(*pnr)/+ in combination with Df(*RpS15Aa)*/+ show prolonged heart periods, which are even longer compared to single mutants and controls (**Figure 35**), which is not observed in mutants transheterozygous for Df(*RpS15Aa)* and *Dorsocross* or *Mef2.* This suggests that there may be differences in how CCGs interact with RP (*RpS15Aa*) deficiency.

Taken together, I identified genetic interactions between cardiac transcription factors *tinman, pannier,* and *Dorsocross* and ribosomal protein gene *RpS15Aa.* Taking into account that Df(*RpS15Aa*) heterozygous mutants show overall normal body morphology while having cardiac defects, the genetic interactions of RPs with cardiac transcription factors could potentially explain how those cardiac-specific defects develop.

A Combination of *Hand*$^{4.2}$*-Gal4,tdtK*^{VK37} with *Df(RpS15Aa)/FM7c*

Cross order	chromosome I.	chromosome I.	chromosome II.
I.	Df(*RpS15Aa*)/FM7c x	FM7/Y; *Hand*$^{4.2}$-Gal4,tdtK^{VK37}/CyO (lab stock)	→ Df(*RpS15Aa*)/FM7; +/CyO
II.	Df(*RpS15Aa*)/FM7; +/CyO x	Y/FM7; *Hand*$^{4.2}$-Gal4,tdtK^{VK37}/CyO	→ Df(RpS15Aa)/FM7, *Hand*$^{4.2}$-Gal4, tdtK ^{VK37}/CyO

males

B

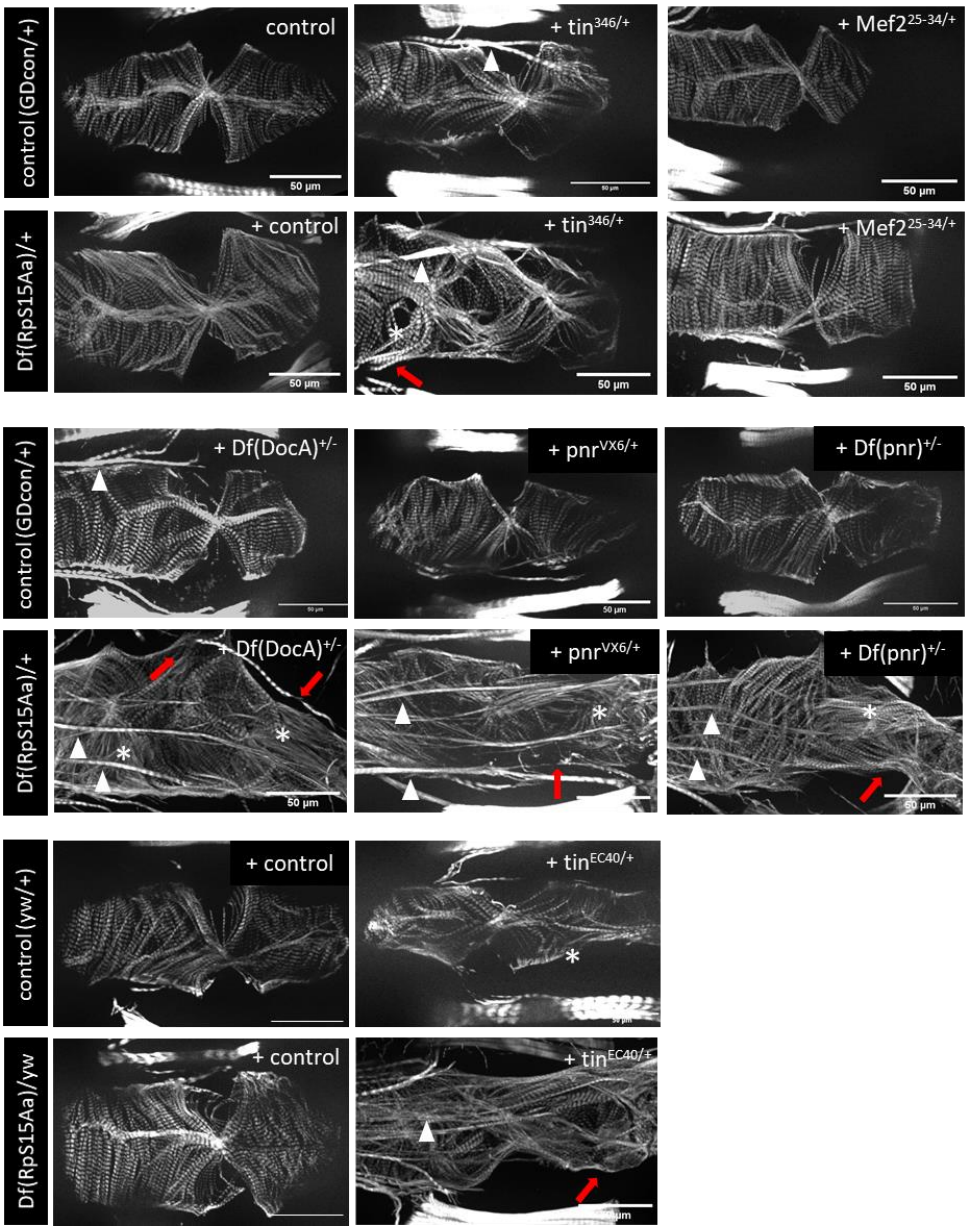

Figure 33: *Drosophila RPS15A* genetically interacts with cardiac transcription factors. (A) Crossing scheme for combination of *Hand*$^{4.2}$-Gal4,tdtK with Df(*RpS15Aa*). **(B)** Representative fly heart segment (A4) from control flies, heterozygous mutants (*tin*$^{346/+}$, *tin*$^{EC40/+}$, *pnr*$^{VX6/+}$ and Df(*pnr*)/+, Df(*Doc*A)/+, *Mef2*$^{25-34/+}$, Df(*RpS15Aa*)/+) and transheterozygous mutants. Note the deformation and myofibrillar disorganization in the transheterozygous mutants (except for Df(*RpS15Aa*)/+ in combination with *Mef2*$^{25-34/+}$). Red arrows point towards locale constriction/dilation. White asterix indicate myofibrillar misarrangement. White arrowheads point to ventral longitudinal muscle (VLM) fibers. Note that not every single VLM fiber is marked by arrowheads. All genotypes (listed in Table 6) have *Hand*$^{4.2}$-Gal4,tdtK in the background since the Df(RpS15Aa)/FM7; *Hand*$^{4.2}$-Gal4,tdtK/CyO fly stock was used. However, *Hand*$^{4.2}$-Gal4 is not of relevance here, since I used systemic mutants (independent from a Gal4 driver). *tin*^{EC40} is of *yw* background, while other alleles are in a *w1118* background. GDcon flies were used as w1118 background controls (*GDcon* = *w1118*). Scale bar = 50 µm.

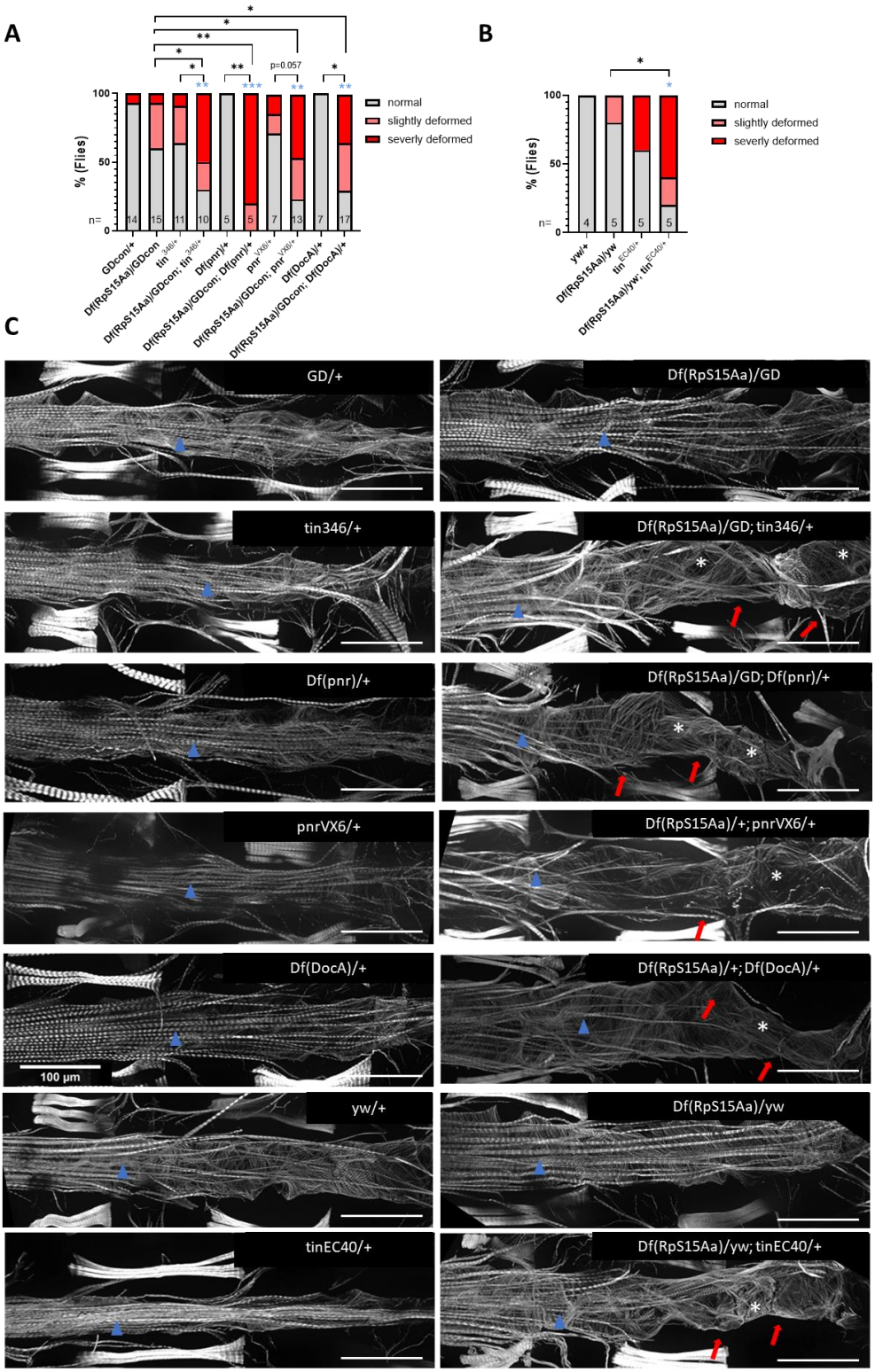

Figure 34: *Drosophila RPS15A* genetically interacts with cardiac transcription factors. (A) Fly hearts from 3-week-old female control flies, heterozygous mutants (*tin*$^{346/+}$, *tin*$^{EC40/+}$, *pnr*$^{VX6/+}$ and Df(*pnr*)/+, Df(*Doc*A)/+, Df(*RpS15Aa*)/+) and transheterozygous mutants were categorized according to their structure into *normal, slightly deformed, severely deformed* (genotypes as in Figure 33 and Table 6). Graphs display the percentage of flies in each category. Statistics: Fisher's exact test on absolute numbers testing *normal* vs. *severely deformed* hearts. *p<0.05, **p<0.005, ***p<0.001, ****p<0.0001. **(B)** Representative whole length fly hearts from 3-week-old female control flies, heterozygous mutants (*tin*$^{346/+}$, *tin*$^{EC40/+}$, *pnr*$^{VX6/+}$ and Df(*pnr*)/+, Df(*Doc*A)/+, Df(*RpS15Aa*)/+) and transheterozygous mutants stained for F-Actin. Note the deformation and myofibrillar disorganization in the transheterozygous mutants. Red arrows point towards locale constriction/dilation. White

asterix indicate myofibrillar misarrangement. Blue arrowheads point to ventral longitudinal muscle (VLM) layer. Note, that in transheterozygotes very few VLM fibers are present in posterior part of the heart compared to single mutants and controls. All genotypes as in Table 6. + = wild type. Scale bar = 100 µm.

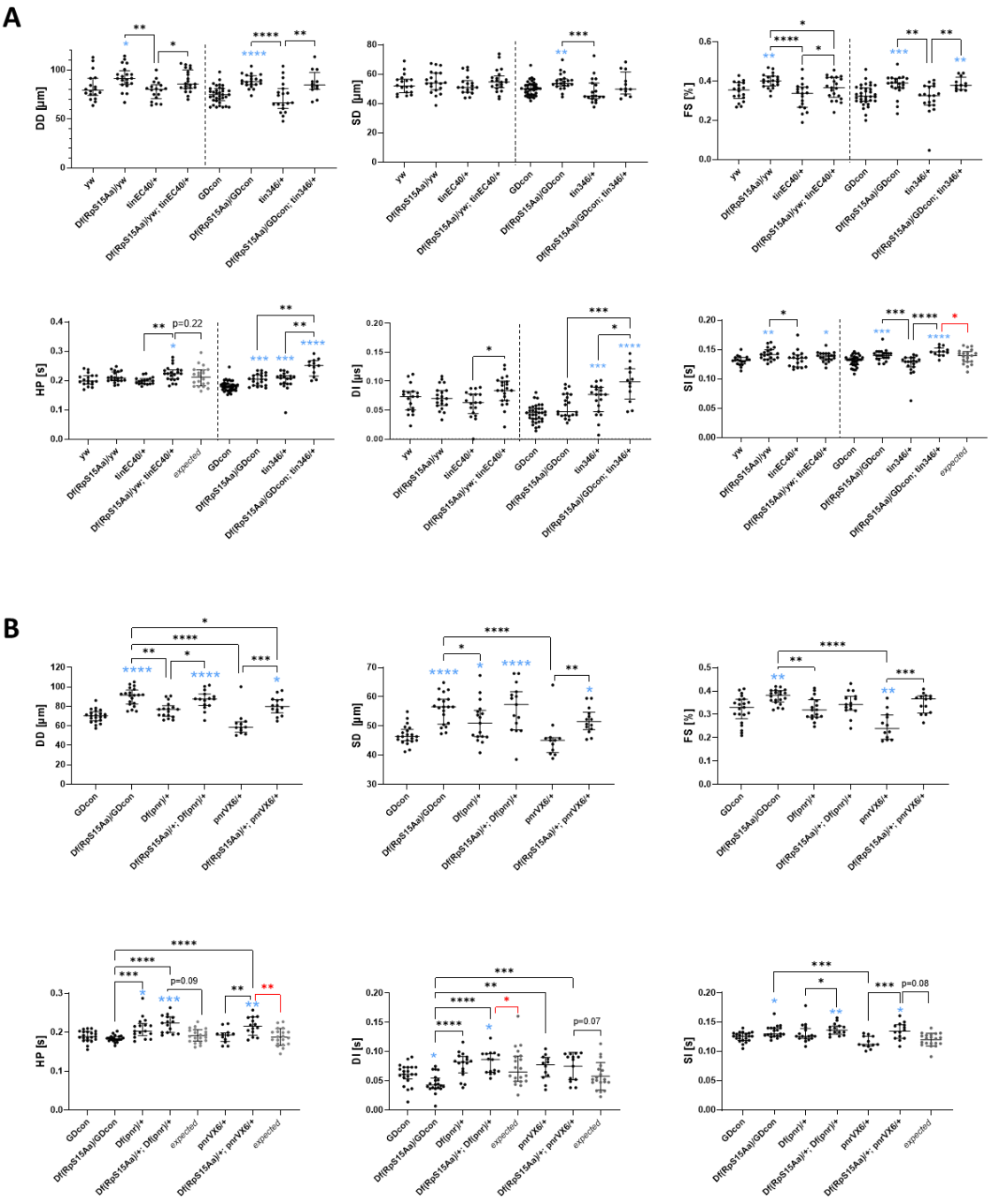

Figure legend on next page.

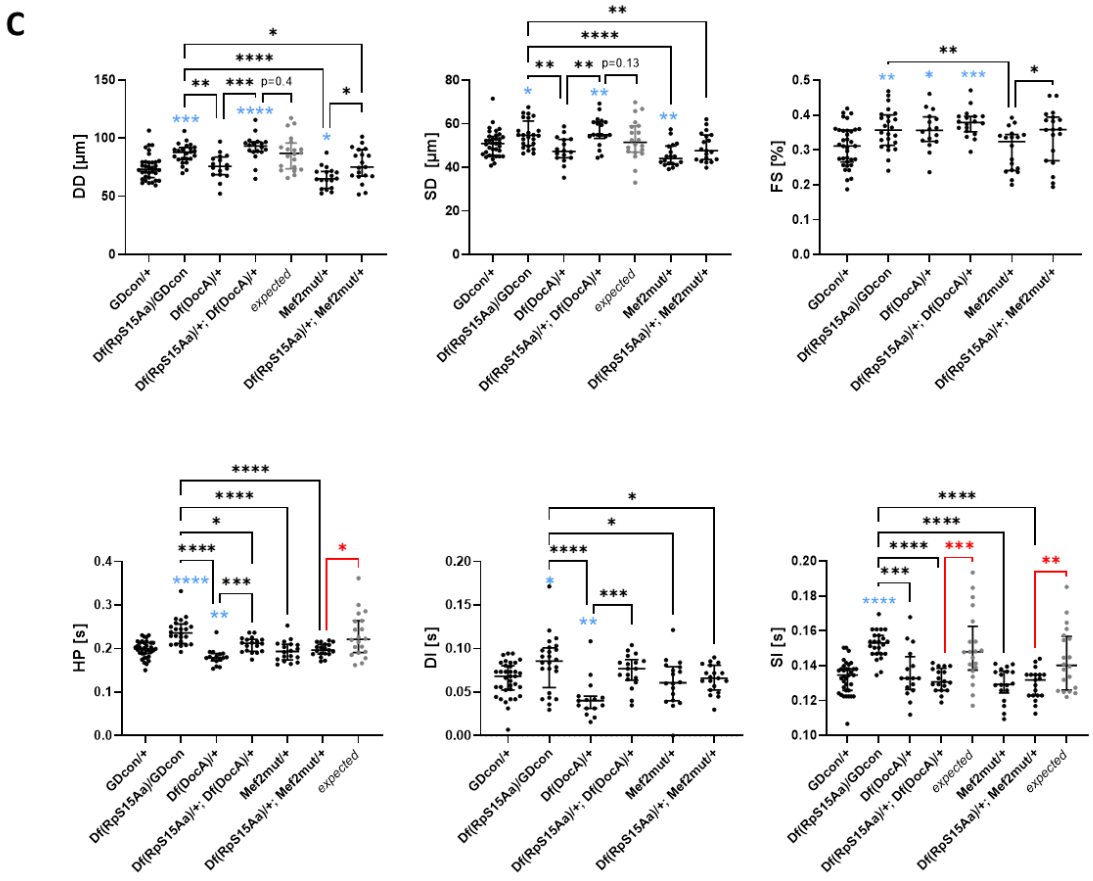

Figure 35: *RpS15Aa* and *tinman* or *pannier* transheterozygous mutants show prolonged heart periods compared to single mutants. (A-C) Structural and rhythmicity parameters of 3-week-old female flies displayed in Figure 33 and 34 using the *in vivo* fluorescent heart assay (genotypes as in Table 6). Diastolic Diameter (DD), Systolic Diameter (SD), Fractional Shortening (FS), Heart Period (HP), Diastolic Interval (DI) and Systolic Interval (SI) of control and heterozygous *RpS15Aa* deficient flies with or without additional heterozygous mutation in *tinman* (A), *pannier* (B), *Dorsocross* or *Mef2* (C). Statistics: Kruskal-Wallis, *p<0.05, **p<0.005, ***p<0.001, ****p<0.0001. Calculation of *expected* values and statistics as described before (Methods section 4.12). Mef2mut= $Mef2^{25\text{-}34/+}$.

Table 6: Genotypes corresponding to interaction experiments (Figure 33-36).

gene combinations	*genotypes*
control (GDcon/+)	GDcon/+; GDcon/Hand,tdtk; GDcon/+
$tin^{346/+}$	+/+; Hand,tdtk/+; tin346/+
$Mef2^{25\text{-}34/+}$	+/+; Hand,tdtk/Mef2[25-34]; +/+
Df(RpS15Aa)/GDcon	Df(RpS15Aa)/GDcon; Hand,tdtk/GDcon; +/GDcon
Df(RpS15Aa)/+; $tin^{346/+}$	+/Df(RpS15Aa); Hand,tdtk/+; tin346/+
Df(RpS15Aa)/+; $Mef2^{25\text{-}34/+}$	+/Df(RpS15Aa); Hand,tdtk/+; $Mef2^{25\text{-}34/+}$
$pnr^{VX6/+}$	+/+; Hand,tdtk/+; pnrVX6/+
Df(RpS15Aa)/+; $pnr^{VX6/+}$	+/Df(RpS15Aa); Hand,tdtk/+; pnrVX6/+
Df(pnr)/+	+/+; Hand,tdtk/+; Df(pnr)/+
Df(RpS15Aa)/+; Df(pnr)/+	+/Df(RpS15Aa); Hand,tdtk/+; Df(pnr)/+
Df(DocA)/+	+/+; Hand,tdtk/+; Df(DocA)/+
Df(RpS15Aa)/+; Df(DocA)/+	+/Df(RpS15Aa); Hand,tdtk/+; Df(DocA)/+
control (yw/+)	yw/+; yw/Hand,tdtk/yw; yw/+
Df(RpS15Aa)/yw	yw/Df(RpS15Aa); yw/Hand,tdtk; yw/+
$tin^{EC40/+}$	yw/Df(RpS15Aa); yw/Hand,tdtk; tinEC40/+
Df(RpS15Aa)/yw; $tin^{EC40/+}$	yw/Df(RpS15Aa); yw/Hand,tdtk; tinEC40/+

5.4.8 Higher frequency of outflow tract defects in *tinman* heterozygotes in a Df*(RpS15Aa)* sensitized background

While recording the beating fluorescent hearts *in vivo*, I noticed that many fly hearts carrying heterozygous mutations in *tinman, pannier* or Df(*RpS15Aa*), as well as transheterozygotes mutants, exhibit outflow tract defects (ostia defects). Using *in vivo* fluorescent heart reporter recordings, I categorized defects according to dysfunction and/or appearance, which is easy to assess in the moving heart in slow motion movies (i.e shifted ostia, floppy ostia, deformed ostia, missing ostia opening, hypertrophic ostia) (**Figure 36** D). "Floppy ostia" are ostia which are ballooning outwards in systole (see **Figure 36** D). One category was assigned per ostia and I quantified the percentage of flies that harbor ostia defects as well as the relative distribution of ostia defects per genotype. Control flies (GDcon and yw) show no or mainly mild ostia defects (floppy ostia), while Df(*RpS15A*)/+ heterozygotes (Df(*RpS15A*)/GDcon or Df(*RpS15A*)/yw) show ostia defects including deformed ostia and floppy ostia (**Figure 36** A-C). Note, that in some cases the whole heart tube was deformed and not only the outflow tract structure. Heterozygous Df(*pnr)* mutants show milder phenotypes (floppy ostia, some hypertrophic ostia), while in combination with Df(*RpS15A*)/+ I observed more severe effects including missing and additional ostia openings (**Figure 36** A-B). In addition, transheterozygous mutants exhibit overall deformed heart tubes (as previously described in **Figure 34**), which probably translates into the deformed ostia. pnr^{VX6} heterozygotes by itself already show missing and additional ostia openings as well as ostia shifts or deformed ostia. There is no significant difference between single mutants (pnr^{VX6}) and transheterozygotes (pnr^{VX6}/+; Df(*RpS15A*)/+) in the percentage of flies with ostia defects, however the transheterozygotes tend to exhibit a higher percentage of flies with severe defects, like missing ostia openings, compared to heterozygous pnr^{VX6} (single) mutants (**Figure 36** A-B). About 40 % of $tin^{346/+}$ heterozygotes show affected outflow tracts (ostia shifts, hypertrophic ostia and floppy ostia), while in transheterozygous mutants with Df(*RpS15A*)/+ the amount of flies with defects significantly increased to about 90 % (missing ostia openings, deformed ostia (+ deformed hearts), ostia shifts, hypertrophic ostia and floppy ostia) (**Figure 36** A, C). For the second *tinman* allele, tin^{EC40}, there is no significant different between single mutant and transheterozygotes with Df(*RpS15A*)/+. Interestingly $tin^{EC40/+}$ heterozygotes on their own exhibit already a high proportion of ostia with ostia shifts, which is higher than $tin^{346/+}$ heterozygotes. In transheterozygotes, I predominantly observed deformed ostia and floppy ostia (**Figure 36** A-C). The different phenotypes between both null alleles tin^{EC40} and tin^{346} might be based to some extent on the difference in genetic background (*yw* and *w1118*, respectively). Interestingly, also in humans *NKX2-5* mutations are associated with a range of congenital heart diseases with different phenotypical manifestation; and *NKX2-5* mutations can be even found in healthy individuals with no heart conditions.[15–17] This phenomenon might also reflect the differences

in genetic background between individuals harboring different complements of potential modifier variants in other genes, again consistent with the postulated oligogenic nature of CHDs.

In order to have a closer look at ostia structures of transheterozygous mutants I stained adult fly hearts for Tinman and F-Actin. As described before control hearts show four pairs of Tinman-positive nuclei per segment between two outflow tracts, which are clearly visible with their *V*-like shapes (**Figure 36** E). Flies transheterozygous for Df(*RpS15Aa*) and *tinman, pannier* as well as Df(*Doc*) show additional Tinman-positive nuclei (marked by white dashed squares) (**Figure 36** E). Those additional cardiomyocytes are most likely the cause of defective ostia structures, like hypertrophic ostia, ostia shifts or deformed ostia as well as overall deformed heart tubes. Missing or additional ostia openings would also point towards misspecification of Svp- (marking ostia) and Tinman-positive cardioblasts (marking the working myocardium) during cardiac development leading to missing or abnormal valve or outflow tract formation. At this point it would be interesting to performed Svp staining in adult flies to mark the ostial cells. Unfortunately, the Svp antibody results in high background staining in adults. As described before, additional Tinman-positive cardiomyocytes were also observed in adults lacking *RpS15Aa* alone (Df(*RpS15Aa*)/+ and tinD>*RpS15Aa* RNAi) (***Figure 28*** G). Importantly and in line with the observations above, additional as well as missing *tinman* or *seven-up* expressing cardioblasts were observed in Df(*RpS15Aa*) and *tin*D-Gal4>*RpS15Aa* RNAi embryos (**Figure 28** C-F), suggesting that we would find similar embryonic phenotypes in embryos transheterozygous for Df(*RpS15Aa*) and *tinman, pannier* or *Dorsocross.*

Taken together, the *tinman* and *pannier* heterozygotes exhibit mild ostia defects (except of pnr^{VX6}), which become more severe in a *RpS15Aa* deficient background. Those defects can be likely traced back to misspecification of cardioblasts during embryo stages. Given the highly controlled interplay between cardiac transcription factors during heart formation (reviewed in Bodmer and Frasch, 2010)[132], where levels and timing is highly critical for correct cardioblast specification, I hypothesize that intact ribosomal protein function and/or composition is critical during early embryogenesis to regulate and fine-tune the translation of cardiac transcription factors and their targets.

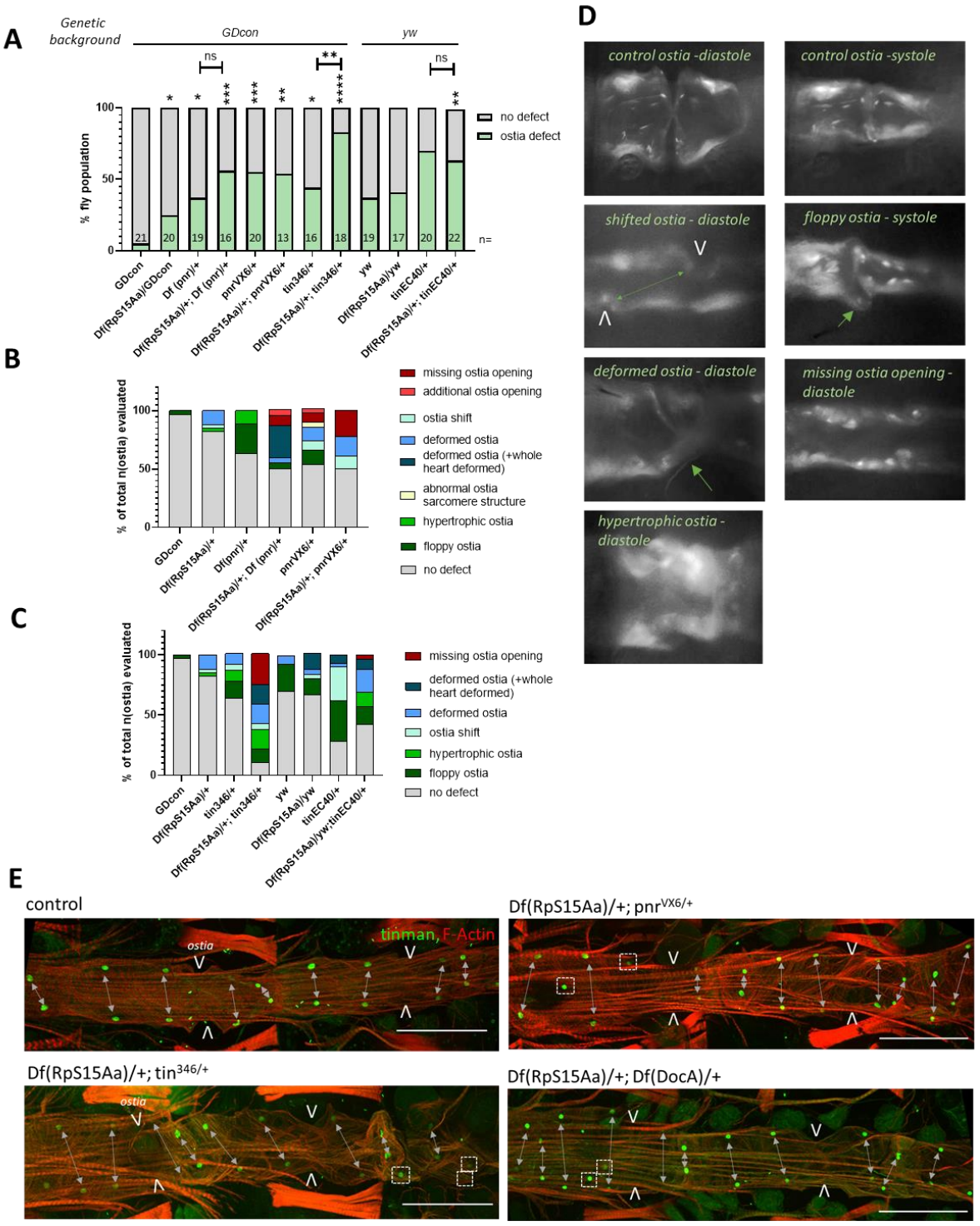

Figure 36: Transheterozygous mutants for *tinman* and Df(*RpS15Aa*) show outflow tract defects. (A) Quantification of percentage of fly population with or without outflow tract defects in single heterozygous (Df(*RpS15Aa), tin*^{EC40}*, tin*^{346}*, pnr*^{VX6}*,* Df(*pnr*)) and transheterozygous mutants. All genotypes have *Hand*$^{4.2}$-Gal4,tdtK in the background since the Df(RpS15Aa)/FM7; *Hand*$^{4.2}$-Gal4,tdtK/CyO fly stock was used (gentypes as in Table 6). Fisher's exact test on absolute numbers. Significances compared to respective genetic background controls (*GDcon* or *yw*) or as indicated. *p = 0.05, **p = 0.01, ***p = 0.001, ****p = 0.0001. **(B-C)** Distribution of the different ostia defect categories per genotype in flies transheterozygous for *pannier* and Df(*RpS15Aa)* mutation compared to single mutants (B) and in flies transheterozygous for *tinman* and Df(*RpS15Aa)* mutation compared to single mutants (C). **(D)** Examples of outflow tract defects observed in hearts carrying the cardiac tdtK reporter. **(E)** Representative images of adult fly heart stained for Tinman and F-Actin. Control hearts show four pairs of Tinman positive nuclei per segment (between two outflow tracts marked with white "v"). Flies transheterozygous for Df(*RpS15Aa)* and *tinman, pannier,* and *Df(Doc)* show additional Tinman positive nuclei (marked by white dashed square).

5.4.9 Zebrafish *RPS15A* genetically interacts with cardiac transcription factors *nkx2.7/tinman and tbx5a/Dorsocross*

For validation in a vertebrate model system, we tested for genetic interactions between *nkx2.7/tinman* and *tbx5a/Dorsocross* in zebrafish. Zebrafish express the *NKX2-5* ortholog *nkx2.7* in the heart and functional studies have shown that both *nkx2.5* and *nkx2.7* play critical roles in cardiac development.[295] To determine whether *rps15a* and *nkx2.7* or *tbx5a* genetically interact in zebrafish, we injected low doses of *rps15a*[296] MO, in combination with *nkx2.7*[297] (experiment performed by Dr. Zeng, analysis my work) or *tbx5a* MO (MO injection by Dr. Zeng, heart recordings and SOHA analysis my work). Briefly, embryos were injected with morpholinos in single-cell status, and hearts were recorded with high-speed imaging at 72 hours post fertilization (hpf) *in vivo* followed by SOHA analysis (see also Methods section 4.14).[286]

First, I performed a dosage-response analysis for *tbx5a* injected with 0.5 nm, 1 ng, or 1.5 ng of morpholino into zebrafish fertilized eggs to define the optimal dose for genetic interaction studies aiming for no or minimal cardiac phenotypes. Validating phenotypes previously described by Fink et al.[286], I observed tendencies towards reduced fractional area change (FAC), which reflects reduced contractility of the zebrafish heart, and prolonged heart periods (**Figure 37** A-D). Since the heart period is significantly prolonged upon injection of the lowest dosage of *tbx5a* MO, I selected 0.5 ng for the genetic interaction studies.

Each MO alone (*tbx5a, nkx2.7, rps15a*) had little effect on heart size, cross-sectional area, or contractility, whereas double morphants exhibited dramatic cardiac dysfunction, with contraction virtually abolished in some animals (**Figure 37** G, J). Furthermore, we saw a synergistic prolongation of the heart period in double morphants in comparison to each MO alone (**Figure 37** M, N). These findings are consistent with the results obtained in *Drosophila* described above, where I observed prolonged heart periods in transheterozygous mutants for Df(*RpS15Aa*)$^{+/-}$ with *tinman*$^{+/-}$ and *pannier*$^{+/-}$. Together, these results are indicative of similar, synergistic interactions between RPs and cardiogenic genes in both zebrafish and fly hearts. Collectively, these data reveal the likely existence of an evolutionarily conserved genetic interaction between RPs and CCGs in heart development.

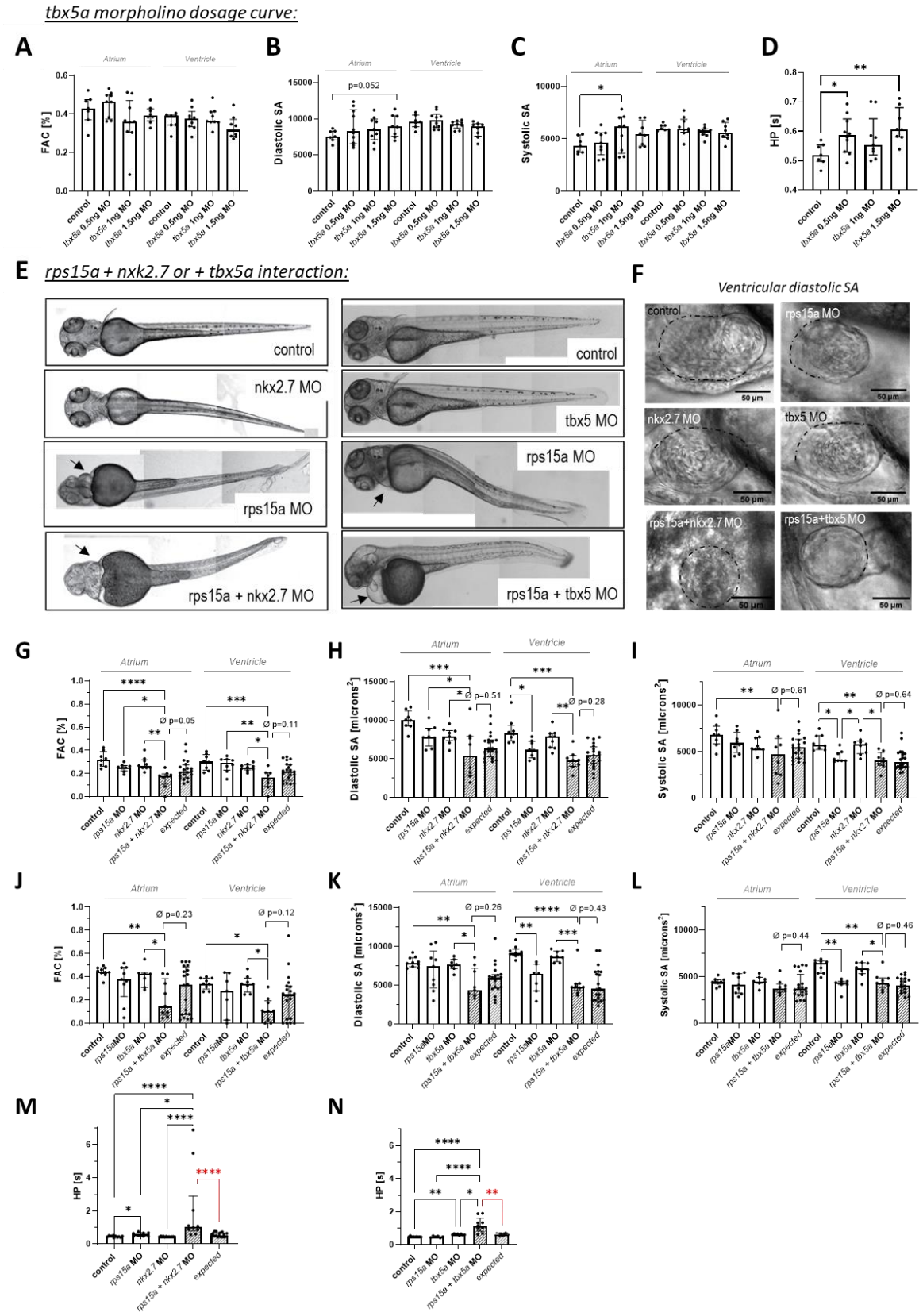

Figure 37: Zebrafish *RPS15A* genetically interacts with *nkx2.7* and *tbx5a* to regulate heart contractility and heart period. **(A-D)** Fractional Area Change (FAC), Diastolic Surface Area (SA) and Systolic SA, and Heart Period (HP) of the atria and ventricles at 72 hpf in zebrafish embryos injected with 0.5 ng, 1 ng and 1.5 ng of *tbx5a* morpholino. **(E)** Representative images of zebrafish with *rps15a* KD, *tbx5a* KD, *nkx2.7* KD or combinations (72 hpf). Note the mild edema in *rps15a* morphants, which is more severe in zebrafish injected with both *rps15a* and *tbx5s* (arrow, only visible in lateral view but also observed in *rps15a*

+ nkx2.7 morphants). **(F)** Representative images of heart ventricles in diastole from zebrafish hearts described in (G-N). **(G-N)** FAC, Diastolic SA, Systolic SA and HP of the atria and ventricles at 72 hpf in zebrafish embryos injected with 0.5 ng *rps15a* and/or 1 ng *nkx2.7* MOs (G, H, I, M) or 0.5 ng *rps15a* and/or 0.5 ng *tbx5* MOs (J, K, L, N). Note, that FAC and heart periods show synergistic genetic interaction between *rps15a* and *nkx2.7* and *tbx5a.* Statistics: Kruskal-Wallis. Statistics for genetic interactions as previously described (Methods section 4.12). *p<0.05, **p<0.005, ***p<0.001, ****p<0.0001.

5.4.10 Identification of potential paternal inherited modifier genes required for cardiac differentiation and proliferation in *Drosophila*

Since HLHS is likely of oligogenic etiology, the Mayo Clinic provided a list of bioinformatical prioritized genes of the 75H proband (harboring the *RPS15A* variant – inherited from the mother), which carry rare predicted-damaging variants inherited from the father, to identify parental modifier genes, which could come together in the proband to contribute to disease manifestation. First, the paternal candidate genes (*CDK4, ENPP1, CCD8, KSR1, EWSR2, STK11, MRC1, TJP1, SF1, ATP1A3*) were evaluated for proliferation and differentiation capacity in generic Day 25 hiPSC-CMs (**Figure 38** A, Colas lab). Furthermore, mRNA expression levels of these candidate genes in proband- and parent-derived hiPSCs were measured (**Figure 38** B, Colas lab). Four genes (*MRC1, TJP1, SF1, ATP1A3)* reduced CM proliferation, CM differentiation or iPSC number and additionally exhibited reduced mRNA expression in the father's and probands hiPSCs compared to the mother's hiPSCs and were selected for genetic interaction testing with *RPS15A* (maternally inherited) using *Drosophila* (**Figure 38** A-C).

According to the DIOPT prediction tool, *Tight junction protein ZO-1 (TJP1), Splicing factor 1 (SF1), ATPase Na+/K+ Transporting Subunit Alpha 3 (ATP1A3)* have orthologs in the fly with DIOPT scores above 10 (human/fly = *TJP1/pyd; SF1/SF1; ATP1A3/Atpalpha*), while *MRC1* has no predicted fly ortholog (**Figure 38** E). *SF1* is a nuclear pre-mRNA splicing factor and is required for the ATP-dependent first step of spliceosome assembly.[298,299] *TJP1* is a scaffolding protein that links tight junction (TJ) transmembrane proteins to actin cytoskeleton. In humans, it was further found to be important for maintaining appropriate atrioventricular node conduction through maintaining gap junction protein localization.[300] Lastly, *ATP1A3* is the catalytic unit of the enzyme, which catalyzes the hydrolysis of ATP coupled with the exchange of sodium and potassium ions across the plasma membrane. In *ATP1A3*-related syndromes, an increased prevalence of ECG dynamic abnormalities is observed with a risk of life-threatening cardiac rhythm abnormalities.[301]

To probe for genetic interactions I used the Df(*RpS15Aa*)/FM7; *Hand*$^{4.2}$-Gal4,tdtK sensitizer line. As previously described, Df(*RpS15Aa*) heterozygosity causes modest increased heart dimensions and a tendency towards longer heart periods (**Figure 38** F-K). Hence, for the following analysis, I focus on these two parameters.

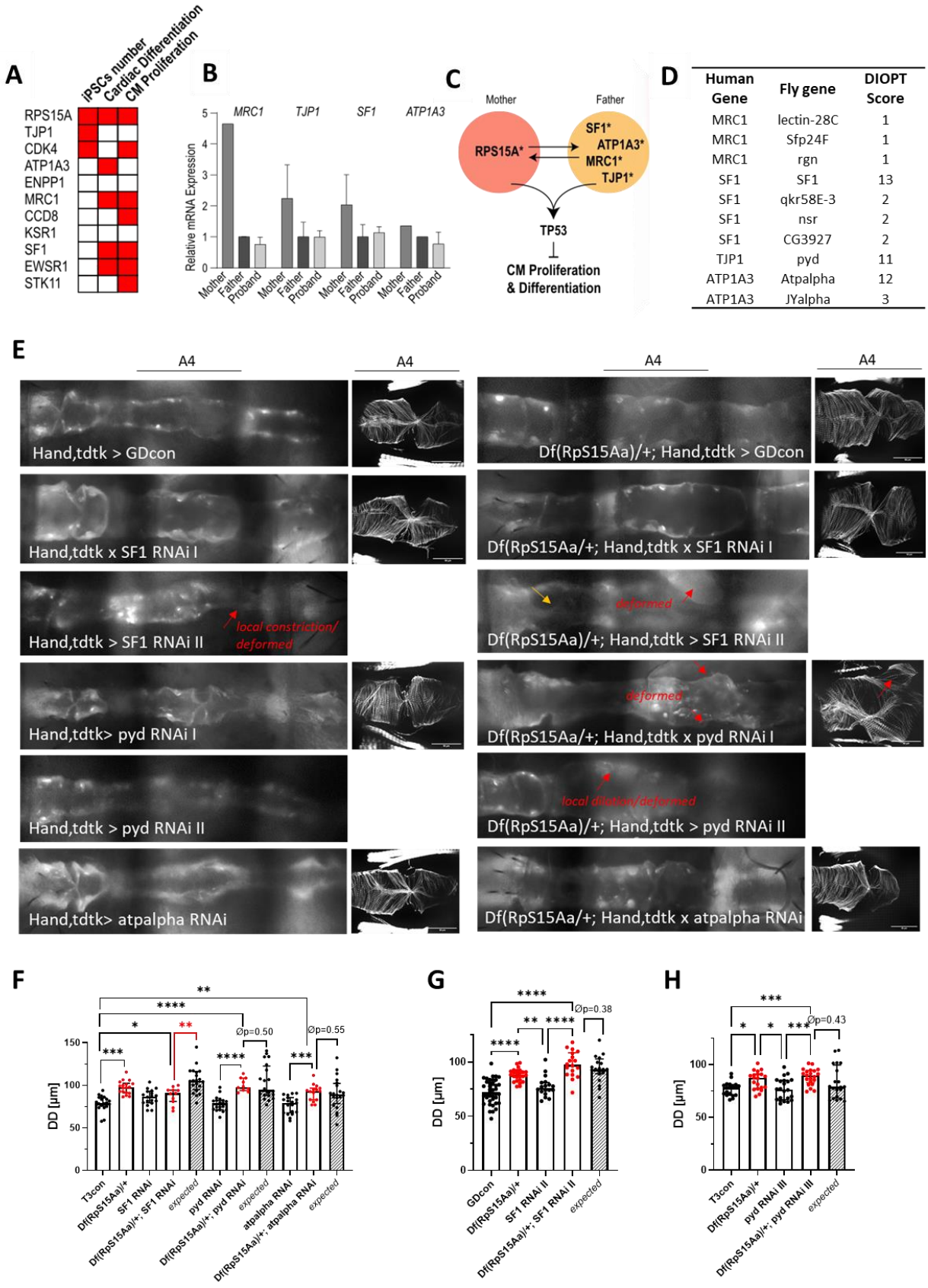

Human Gene	Fly gene	DIOPT Score
MRC1	lectin-28C	1
MRC1	Sfp24F	1
MRC1	rgn	1
SF1	SF1	13
SF1	qkr58E-3	2
SF1	nsr	2
SF1	CG3927	2
TJP1	pyd	11
ATP1A3	Atpalpha	12
ATP1A3	JYalpha	3

Figure legend on next page.

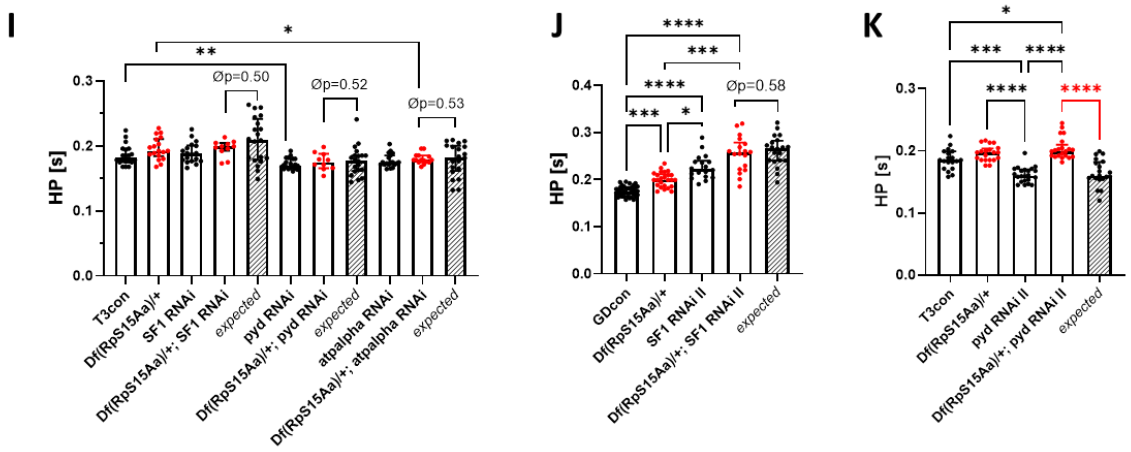

Figure 38: Identification of *pyd* as potential paternal modifier gene in 75H HLHS patient. (A) Heatmap summarizing the influence of candidate paternal modifier genes on hiPSC proliferation, cardiac differentiation, and proliferation (significant hits in red). **(B)** *MRC1, TJP1, SF1* and *ATP1A3* mRNA levels are reduced in proband and father hiPSCs as compared to mother hiPSCs. **(C)** Proposed model of paternal and maternal variant interaction leading to left ventricular hypoplasia phenotype. (A-C) work and analysis performed by Dr. Anaïs Kervadec from Colas lab. **(D)** Fly orthologs of *MRC1, TJP1, SF1* and *ATP1A3* predicted by DIOPT database (Hu et al., 2011)[302]. **(E)** Representative images of tdtK expressing fly hearts (3-week-old females) expressing RNAi against *SF1, pyd* or *atpalpha* with or without additional Df(*RpS15Aa)* heterozygosity. For *SF1* and *pyd* two different RNAis (I and II) were tested. Yellow arrow points towards abnormal heart structure in Df(*RpS15Aa)*/+; Hand, tdtK> SF1 RNAi II flies. Red arrows point to local constriction/dilation and deformed heart sections. Hand = *Hand*$^{4.2}$-Gal4. **(F-K)** Diastolic Diameters (DD) and Heart period (HP) of flies displayed in (E). Statistics: Kruskal-Wallis. Statistics for genetic interactions as previously described (Methods section 4.12). *p<0.05, **p<0.005, ***p<0.001, ****p<0.0001. (E-J) All genotypes carry *Hand*$^{4.2}$-Gal4, tdtK in the background, i.e T3con = *Hand*$^{4.2}$-Gal4>T3con or Df(*RpS15Aa*)/+ = Df(*RpS15Aa*)/+; *Hand*$^{4.2}$-Gal4,tdtK >T3con.

One out of two RNAi lines against *SF1* KD (by itself) causes a deformed heart (*SF1* RNAi II), which is also observed in a Df(*RpS15Aa*) background (**Figure 38** E). *SF1* KD using *SF1* RNAi I shows a tendency towards bigger diastolic diameters (**Figure 38** F). Interestingly, these diameters are not further exaggerated when combined with Df(*RpS15Aa)/+* (as it would be expected), suggesting a epistatic interaction between both genes (**Figure 38** F). However, since the two RNAi lines show different phenotypes (**Figure 38** E-G), the results must be confirmed with additional *SF1* RNAi lines or mutants. A clear synergistic interaction is observed between Df(*RpS15Aa)* and *pyd/TPJ1 (polychaetoid).* While *pyd* KD alone causes no effects on heart diameters and little effects on heart period (**Figure 38** F, H, I, K), it leads to severe malformations in the heart tube in conjunction with Df(*RpS15Aa)* (with two independent RNAi lines) (**Figure 38** E). Knockdown of *atpalpha* has no effect on heart function and shows no interaction with *RpS15Aa* (**Figure 38** E, F, I). However, a second RNAi line or an *atpalpha* mutant allele should be tested to confirm these results.

Taken together, I found a synergistic interaction between *RpS15Aa* and *pyd,* while further testing is needed to confirm interaction/no interaction with *SF1* and *atpalpha*, respectively. In conclusion, this is consistent with the hypothesis that the *RpS15Aa* variant inherited from the mother and the *pyd* variant from the father both contribute to disease manifestation in the HLHS proband in a synergistic manner. The next step would be to investigate how exactly *RpS15Aa* and *pyd* genetically interact and at which time point this interaction is critical for proper heart development.

5.4.11 Discussion

5.4.11.1 Implication of ribosomal protein variants as potential genetic modulators in HLHS/CHD pathogenesis

Recent work, including our own, has suggested that defective cardiac differentiation and impaired CM proliferation likely contribute to HLHS-associated heart defects.[5,101,103] Importantly, an increasing number of variants in RP genes have been linked to CHD in humans; most notably in ~30% of patients with Diamond-Blackfan anemia[123], a ribosomopathy characterized by hypo-proliferative, proapoptotic erythropoiesis. Moreover, *RpL13* was recently identified as a potential candidate gene involved in CHD from a screen for *de novo* copy number variations (CNVs) in 167 patients with CHD (including my contribution).[124] Furthermore, the Pediatric Cardiac Genomics Consortium (PCGC) exome dataset of 2871 patients with CHD identified several rare, predicted-damaging *de novo* variants in RP genes, 2 of which were associated with HLHS.[30] Our present study highlights a potential role for ribosomal protein function in cardiac development and HLHS/CHD pathogenesis, since we found that **(1)** ribosomal proteins (RP) are central regulators of cardiomyocyte proliferation (genome-wide siRNA screen in hiPSC-CMs – Colas lab *unpublished*), **(2)** RP variants are enriched in a cohort of poor-outcome HLHS patients and a rare predicted-damaging promoter variant in *RPS15A* segregates with disease within an HLHS family (75H) (Olson lab - Mayo Clinic), and **(3)** knockdown of RPs *in vivo* cause cardiac defects in hiPSC-CMs, *Drosophila* and zebrafish.

Knockdown of *RPS15A* in generic hiPSC-CMs drastically reduced CMs proliferation. In *Drosophila*, heart specific KD of *RpS15Aa* throughout development caused a partial/or total heart loss in the adult fly (**Figure 26**). A temporal restricted KD of *RpS15Aa* to embryo stages only, also caused cardiac phenotypes in the adult flies, indicating a requirement of *RpS15Aa* during early heart development (**Figure 26**). These results are in line with former studies, where we have shown the same temporal role in the embryonic fly heart for *RPL13.*[124] In zebrafish, *rps15a* CRISPR mutants exhibited smaller hearts and reduced number of cardiomyocytes, as well as reduced contractility and bradycardia (**Figure 25**).

We found enrichment of RP variants in a cohort of poor-outcome HLHS families, where we identified 9 variants in different RP genes, most of them fitting a recessive inheritance disease model (**Figure 25**, **Figure 26**). Knockdown of 5 of those RP candidate genes (*RPL39, RPL26L1, RPS15, RPS17, RSPS28*) reduced hiPSC-CMs proliferation. Heart-specific KD in the flies caused various phenotypes, ranging from outflow tract defect and constrictions to partial/complete heart loss (*RpL26, RpL39, RpL36A, RpL3)* or even lethality (*RpS17, RpL39, RpS15, RpL26, RpL36A*) (**Figure 26**). We validated two other RP candidate genes in our zebrafish model and found that *rpl39* CRISPR mutants exhibited reduced ventricle size, whereas *rps17* CRISPR mutants showed systolic dysfunction in the atrium and shortened heart period (*data not shown*). The variability in phenotypes might point towards

specialization in ribosomal protein function and the concept of ribosomal heterogeneity.[116,303,304] However, we did show that phenotypes severity is dosage-dependent in hiPSC-CMs and *Drosophila* (**Figure 27**), suggesting that the phenotype variability could also result from different gene KD efficiencies. Supporting this hypothesis, I showed that KD of RPs during embryo stages only (using *tinD*-Gal4 driver) leads to similar phenotypes for all RPs tested, except *RpL3*. Note, that *RpL3* is the only ribosomal protein of the gene list, which is not a *Minute* gene, meaning it is not causing a *Minute* phenotype (delayed growth, short bristles)[118] in heterozygous flies (see also Introduction 1.4.2). Furthermore, it was shown that one member of a duplicate gene pair (in the case of *RpS15Aa, RpS15Ab*) is usually expressed only in few tissues and/or at relatively low levels and is not associated with *Minute* phenotypes.[118] Consistently, we found that knockdown of *RpS15Ab* in the fly heart using *Hand*$^{4.2}$-Gal4 had no effect on the heart (*data not shown)*.

As many top CHD gene candidates, such as *Nkx2-5* and *Notch*, *RPs are* most likely also involved in the etiology of other CHDs, for example, bicuspid aortic valve (BAV), which we found in the 5th degree relative of the 75H proband (**Figure 25**). It is still an open question, why ribosomopathies, where one would expect to have global and in fact lethal effects on a developing organism, exhibit tissue-specific defects, like in Diamond-Blackfan anemia.[123] In zebrafish with globally reduced *rps15a* function, we see cardiac-specific phenotypes, while overall body morphology was largely unchanged (**Figure 25**).

To further address the question if RP genes could have a cardiac-specific function, we tested for genetic interactions between RP gene *RPS15A* and cardiogenic genes (*Nkx2.7/tinman, Tbx5a/Dorsocross*) in zebrafish and *Drosophila*. We found similar synergistic interaction in both model organisms leading to worsening of cardiac phenotypes, indicative of the existence of an evolutionarily conserved genetic interaction between RPs and cardiogenic genes in heart development. Furthermore, I found that KD of *RpS15Aa* leads to cardioblast misspecification leading to abnormal numbers of *tinman* and *seven-up* positive cardiomyocytes in the embryonic *Drosophila* heart. *tinman* and *seven-up* are part of the highly controlled interplay between cardiac transcription factors during cardiogenesis, where expression patterns and timing are highly critical for correct cardioblast specification.[134,148,305] Given the genetic interaction between CCGs and *RpS15Aa*, I hypothesize that intact RP function and/or composition is critical during early embryogenesis to regulate and fine-tune the translation of cardiac transcription factors and/or their targets (**Figure *39***). RP gene variants in patients might play a role as negative genetic sensitizers in the oligogenic pathogenesis of HLHS and other CHDs.

5.4.11.2 Heart remodeling and differentiation dependent on Hippo pathway and *myc* in *Drosophila*

Heart-specific knockdown of *RPS15A* fly ortholog, *RpS15Aa*, throughout development using the *Hand*$^{4.2}$-Gal4 driver caused atrophied larval hearts and underdeveloped/truncated/larval-like hearts in the adult fly (called "no heart" or "partial heart" phenotypes). We observed variability in the phenotype's severity, since *RpS15Aa* KD can led to an almost complete heart loss in some cases. Interestingly, co-KD with *p53* did not rescue the cardiac defects of *RpS15Aa* KD in *Drosophila*, unlike the observed rescue of proliferation in hiPSC-CMs and zebrafish. We hypothesize that this might be due to different, context-dependent roles of *p53* between fly and human.[290,292]

We characterized expression levels in hiPSCs and hiPSC-CMs following siRNA treatment targeting *RPS15A* and *RPL39* using RNAseq (whole transcriptome sequencing), which showed a common response with strong activation of TP53 target genes, inhibition of cell cycle genes and DNA damage response (Colas lab and Dr. Vogler's work). Those signaling pathways were previously associated with nucleolar stress response, which can be initiated upon RP loss.[292,306,307] In flies, induction of nucleolar stress induces *Minute*-like phenotypes mediated by RP loss.[308] However, in contrast to humans, where the main stress response is mediated via p53, a study in *Drosophila* where nucleolar stress was induced via KD of nucleolar gene *Nopp140* proposed JNK signaling as the central stress response effector (independently of *p53*).[309] Importantly, nucleolar stress inducted apoptosis in wing discs could not be rescued by p53 KD.[309] We hypothesize that the loss of RPs, in conjunction with reduced protein synthesis, might cause nucleolar stress, that triggers a cell-intrinsic signaling cascade, leading to a partial heart loss.

In this study we found that co-knockdown of *myc* can partly rescue the anterior segments A1-A3 of the heart, which were lost upon cardiac *RpS15Aa* KD knockdown (**Figure 30**). Although still seemingly underdeveloped, the restored heart shows more similarity to an adult heart. There has been evidence that MYC as the master regulator of ribosome biogenesis is conserved between humans and flies.[293] In humans, many mutations in ribosomal proteins have been shown to cause a predisposition to cancer including some linked to MYC activation (reviewed in Destefanis et al., 2020)[293] and I hypothesize an upregulation of *myc* upon RP loss in the fly heart (**Figure 39**). Furthermore, MYC was shown to induce the impaired ribosome biogenesis checkpoint (IRBC) complex, RPL5, RPL11, and 5SrRNA, which binds and inhibits MDM2, stabilizing p53, while MYC depletion decreases the availability of the IRBC complex in human cell lines.[310] RPL5 and RPL11 function as negative regulators of MYC expression during ribosomal biogenesis in a feedback mechanism.[311] Consistently, when ribosome-free RPs (including RPL5 and RPL11) are released from the nucleolus in response to nucleolar stress, MYC was shown to be downregulated.[306] Going in line with this, I hypothesize that a reduction of *myc* in the fly heart might ameliorate nucleolar stress as well as reduce its downstream stress response (like potentially upregulated *myc*) upon RP loss leading to a partial

rescue of the *RpS15Aa* KD phenotype (**Figure 39**). However, this hypothesis needs further investigations.

The role of the Hippo pathway to regulate cell growth/organ size, proliferation, and survival, and its importance in cardiac biology is conserved between humans and fly.[312–315] The Hippo-YAP pathway is a cell-intrinsic pathway that regulates cardiomyocyte proliferation and thus heart size during development.[316] While Hippo activation was shown to prevent cardiac overgrowth, YAP was shown to drive postnatal cardiomyocytes to re-enter the cell cycle; making Hippo signaling a promising therapeutic target for cardiac regenerative medicine.[317] Here, we showed that overexpression of *yorkie*, *Drosophila* ortholog of *YAP/TAZ*, could partly rescue the *RpS15Aa* KD phenotype (**Figure 30**, **Figure 39**). The restored heart exhibited similarities to a larval heart, with a thicker posterior heart proper and a thinner anterior aorta with no adult outflow tract structures; however, some adult ostia-like structures could be observed in the more posterior region, which indicates that the heart underwent partly heart remodeling. Using *Drosophila* flight muscles as a model, there has been recent evidence that the Hippo pathway and Yorkie, under the regulation of Dlg5 and STRIPAK, can control timing and levels of sarcomere genes, thus regulating the key components that mediate muscle growth.[318] The authors further propose that this mechanism could be conserved in human muscle or cardiomyocyte growth, since (1) Dlg5, STRIPAK and Hippo pathway are conserved between human and fly and since (2) in mammalian cardiomyocytes, like in *Drosophila* flight and heart muscles, growth after birth is achieved post-mitotically by cellular hypertrophy.[318] It has been further shown that YAP1 is not only an important regulator of cardiomyocyte proliferation in the embryo but also promotes

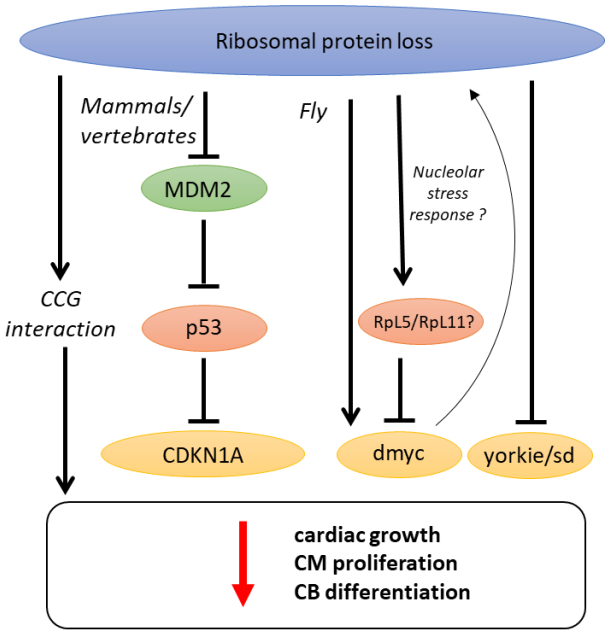

Figure 39: Proposed signaling cascade upon ribosomal protein loss. In mammals/vertebrates, diminished RP function leads to reduced proliferation (hiPSC-CM) and reduced CM numbers accompanied by functional as well as structural cardiac defects (zebrafish) via upregulation of MDM2/p53 signaling. In flies, RP loss/knockdown leads to cardiac defects (impaired cardiac growth and CB misspecification), that can be partly rescued by knockdown of *myc* or overexpression of Hippo effector gene *yorkie.* RP loss potentially leads to an upregulation of *myc*, which in turn controls the expression of RP genes. Upon nucleolar stress ribosome-free RPs (including RPL5 and RPL11) are released from the nucleolus and inhibit *myc* mRNA transcription.[306] Similar to the nucleolar stress response, *myc* KD might attenuate RP KD-mediated phenotypes in the fly heart. Furthermore, in vertebrates and flies, RPs synergistically interact with core cardiogenic genes (CCG), representing a potential mechanism how systemic RP loss could lead to cardiac specific defects that can potentially contribute to HLHS/CHD disease manifestation. CB= cardioblast.

cardiomyocyte survival and growth in the postnatal heart, which is in line with findings in *Drosophila* flight muscles.[319,320]

The rescue of the *RpS15Aa* KD phenotype we observed was dependent on *yorkie*'s downstream factor *scalloped* (*Drosophila* ortholog of *TEAD1/2/3/4)* since upon co-KD of *scalloped,* overexpression of *yorkie* could not rescue the *RpS15Aa* KD phenotype anymore. Interestingly, a proband among the PCGC HLHS patients was transheterozygous for *RPL15* and *TEAD4.*[30] The incomplete rescue by *yorkie* overexpression and *myc* KD highlights the complexity of the RP loss phenotype and points towards involvement of further critical genetic components contributing to gene network disturbance mediated by RP loss and needs further investigation.

Overall, our results point towards a critical role of ribosomal proteins for heart development and function in *Drosophila* with growth as an essential factor depending on ribosome biogenesis master regulator *myc* and Hippo pathway effector gene *yorkie*. Further investigations are needed to identify the other genes and pathways involved in cardiac phenotype manifestation based on RP loss. For example, I am currently investigating the induction of nucleolar stress in the fly heart upon RP KD utilizing different marker genes, like Fibrillarin, and by testing for JNK pathway activation.

5.4.11.3 Identification of *TJP-1/pyd* as a potential paternal modifier gene in HLHS patient 75H

HLHS is most likely oligogenic in origin and to test for potential modifier genes that could contribute to disease manifestation in the 75H HLHS patient, I tested three bioinformatically prioritized genes with paternally inherited rare, predicted-damaging variants for effects on *Drosophila* heart function and morphology. In addition, I probed for genetic interactions between those candidates and *RpS15Aa,* which harbors a promotor variant inherited from the mother. While I could not show a clear interaction between *RpS15Aa* and splicing factor *SF1* or catalytic subunit *ATP1A3,* I found a synergistic genetic interaction with *tight junction protein 1* (*TJP1),* which is *polychaetoid* (*pyd*) in the fly. ZO-1 (Zona occludens 1), an important scaffold protein in the tight junctions, which is encoded by *TJP1,* interacts with the actin cytoskeleton, gap junctions, and adheres junctions and localizes to the intercalate disc in cardiomyocytes.[300] Furthermore, it was shown to be important for maintaining appropriate atrioventricular node conduction through maintaining gap junction protein localization in mouse hearts.[300] In flies, *pyd* mutations cause disruptions during embryo morphogenesis through altered cell adhesion or cytoskeletal interactions leading to defects in tracheal structures or during dorsal closure[321,322]; however, the role of *pyd* in the fly heart has not been studied to this point. Here, I show that knockdown specifically in the heart causes a shortening of the heart periods, while heart dimensions are preserved (**Figure 38**). How *pyd* KD can cause shorter heart periods remains to be explored starting with the localization of *pyd* in the fly heart.

Furthermore, I show a synergistic genetic interaction between *RpS15Aa* and *pyd* in the fly, since KD of both genes in combination causes severe deformation, with some fly hearts showing overgrowth in the posterior end of the heart, which is not observed in single gene KD/mutants. In tracheal cells for example, *pyd* localizes to the adherens junctions and seems to be important for cell specification and regulation of the dynamic state of adherens junctions during tracheal morphogenesis.[321] I hypothesize that *pyd* potentially could have a similar role for heart morphogenesis and that the functional defects upon *pyd* KD might only become crucial and visible in a Df(*RpS15Aa*) background, where hearts show structural phenotypes (dilation) and abnormal number of *tinman* and *seven-up* expressing cardiomyocytes due to cardioblast misspecification during embryo stages. Next, it would be important to test how exactly *pyd* and Df(*RpS15Aa*) interact and at which step of heart development the defects occur.

In the future, plan to test further bioinformatically prioritized HLHS candidate genes, which are inherited from the mother or father, in order to identify novel HLHS-associated genes and to probe for potential interaction with ribosomal protein *RpS15Aa* and among those genes (including *pyd, alpalpha* and *SF1*). Newly identified genes and genetic interactions will be integrated into the currently rudimentary gene regulatory network underlying cardiac development and can help build a family-specific gene network of high relevance for HLHS. Furthermore, positive hits will be confirmed in zebrafish model and hiPSC-CM. Eventually, additional HLHS families with RP variants will be included for HLHS-gene identification and interaction studies to generate a RP-centric network of potential HLHS-relevant genes. The top candidate genes will be subjected to cohort-wide enrichment analysis in the HLHS cohort from Mayo Clinic. I hope that the expected insights gained will help improve patient-specific treatments and genetic familial counseling.

6. Conclusions and Outlook

Over the years decreasing sequencing costs have led to the identification of thousands of putative human disease variants, however, although *in silico* methods have been developed to predict variant pathogenicity, establishing which variants within a patient participate in causing disease remains challenging. *In vivo* functional analysis of genes and gene combinations, based on rare, likely-damaging patient-specific variants in a high-throughput manner using the fly heart model together with other models like patient-derived cardiomyocytes, generic hiPSC-CMs or zebrafish, provides a framework for evaluating these genes and gene networks for a potential contribution to heart disease and for further prioritizing the patients' genetic variants. In this thesis, I present my work on the successful identification of *MYOM2, LRP2,* and ribosomal protein genes as novel potential CHD-associated genes by characterizing their role in cardiac development and by probing for potential interaction partners and interlinked pathways involved and potentially contributing to disease.

A similar multi-model system approach, which combines studies in *C. elegans, Drosophila,* and zebrafish, has led to significant progress in the discovery of novel gene-disease relationships associated with rare diseases by the *Model Organism Screening Center* (*MOSC*) of the *Undiagnosed Disease Network*, highlighting a central role for model organisms for continued discovery of disease genes.[323] Under the auspices of this project, the fly in particular, has emerged as a critical tool to interpret variants of unknown significance identified in patients[324], due to state-of-the-art techniques to easily manipulate the *Drosophila* genome in many different ways. Here, a protocol for the generation of fly lines expressing human cDNA (*UAS-human cDNA*) with and without patient-specific variants was generated, that allows rapid, *in vivo* assessments of putative human disease-causing gene mutations,[325] which could be a valuable addition to our screening pipeline and a logical next step in further studying our newly identified CHD-associated candidate genes.

To study the mechanisms underlying *MYOM2, LRP2,* and RPs, *deep dives* into the individual gene functions and their associated pathways in the heart are now needed. For example, an interesting question is how disruption of *MnM* (*MYOM2*) in the fly heart leads to an upregulation of *Mhc* (*MYH6/7*) protein levels, a gene that was previously associated with cardiomyopathies in both flies and humans.[67,167,204,326] Those mechanistic studies could be addressed by leveraging the disease models that are available to me (*Drosophila,* hiPSC-CMs, zebrafish), however, given the individual limitations of each model system for heart research (i.e. the simpler heart structure), further extension into higher vertebrates (i.e. mouse models) could be necessary.

As previously discussed in the individual chapters, a direct link between *LRP2* and ribosomal protein variants with HLHS and between *MYOM2* variants and HCM/TOF awaits further confirmation. Addressing the mechanisms underlying disease manifestations, there is growing evidence of an

oligogenic etiology of complex CHDs. For example, in a recent investigation three missense single-nucleotide variants in sarcomeric gene *MYH7* and transcription factors *MKL-2* and *NKX2–5* were identified in three offspring with early-onset cardiomyopathy using whole-genome sequencing, suggesting that human heart diseases can be caused by a combination of rare inherited heterozygous mutations.[11] Further analysis in murine hearts and hiPSC-CMs suggests that the identified *NKX2–5* variant functions as a genetic modifier. Supporting the importance of key cardiac transcriptions factors in CHD pathogenesis, recent data revealed enrichment of *de novo* variants in proteins that interact with GATA4 and TBX5 within the PCGC cohort that includes 2,645 CHD parent-offspring trios.[327] Consistently, my data indicated genetic interactions between HLHS-associated candidate gene *RPS15A* and *GATA4, NKX2-5,* and *TBX5* in the fly.

Further highlighting the oligogenic aspect and the importance of differences in the genetic background in complex CHD manifestations, the only HLHS mouse model to date, a bigenic mutant for *pcdha9* and *Sap130,* only has a penetrance of ca. 30 %.[103] This model provides evidence that *pcdha9* affects aortic growth, whereas *Sap130* can cause a more severe HLHS-like phenotype. Such a multi-hit model and modular etiology for HLHS caused by sub-threshold hypomorphic alleles represent an attractive explanation not only for HLHS but also for many other complex CHDs. Within this multi-hit model, several genetic variants could potentially disrupt common pathways, like SHH, WNT, or Hippo, that modulate critical biological systems during heart development, thus ultimately leading to disease. In our studies, we found that both index families 5H (*LRP2*) and 75H (*RPS15A*) show upregulation of the TP53 pathway, pointing towards reduced CM proliferation as a hallmark in HLHS pathogenesis. Interestingly, RNA sequencing of the 5H family followed by gene ontology analysis also showed strong enrichment in genes associated with “Protein synthesis” comparable to the mRNA profile in the 75H patient.[5]

The next step is to test clustered, patient-specific gene mutation patterns prioritized in index patient 75H or additional families with RP variants as well as in patient-parent trios with *LRP2* variants (including high-risk factors *GATA4, NKX2-5,* and *TBX5*). Our *Drosophila* heart model provides the perfect framework to identify novel multiplex gene interactions and associated pathways to build a gene network with high relevance for cardiac development and disease.

Our expected results could provide valuable insights for genetic familial counseling but also for the identification of risk factors involved in long-term patient outcomes (i.e high susceptibility for heart failure) which could be crucial for the patients’ prioritization for organ transplantation and overall clinical management. Especially for the latter, ribosomal protein genes represent an interesting class of potential genetic effectors for further investigations, since variants were found enriched in a sub-set of HLHS patients with poor clinical outcome. Eventually, our results could be implicated in the

design of new therapeutic approaches, like for example *in utero* gene therapy and genome editing approaches (among others), which is a developing field with great potential to treat congenital diseases.[328] In classical gene therapy approaches, the particular gene of interest is packaged into a viral vector encapsulated by a lipid layer for delivery to the patient. As an alternative, *Moderna* recently presented the development of an mRNA-based therapeutic (AZD8601) to promote cardiac health in patients that undergo coronary artery bypass grafting that recently was tested in Phase II clinical trial (called EPICCURE).[329] Here, the "naked" mRNA that encodes for the vascular endothelial growth factor (VEGF-A) is directly injected into patients' hearts to promote regeneration and growth of blood vessels.[329] Currently, gene therapy approaches are tested only for monogenic diseases[328,330,331]; however, with more technical and biological advances there is much promise for gene therapies for more complex oligogenic diseases, like many CHDs.

Taken together, integration of genomic data with developmental biology as we do it here, combined with *deep-dive* mechanistic analysis in multiple model systems promises to increase our understanding of cardiac development in general and the pathogenesis of CHD.

7. References

1. Hoffman, J. I. E. & Kaplan, S. The incidence of congenital heart disease. *J. Am. Coll. Cardiol.* **39**, 1890–1900 (2002).

2. Rickert-Sperling, S., Kelly, R. & Driscoll, D. *Congenital Heart Diseases: The Broken Heart. Clinical Features, Human Genetics and Molecular Pathways.* (Springer, 2016).

3. Auxerre-Plantié, E. *et al.* Identification of MYOM2 as a candidate gene in hypertrophic cardiomyopathy and Tetralogy of Fallot, and its functional evaluation in the Drosophila heart. *Disease Models & Mechanisms* **13**, (2020).

4. Grunert, M. *et al.* Rare and private variations in neural crest, apoptosis and sarcomere genes define the polygenic background of isolated Tetralogy of Fallot. *Hum. Mol. Genet.* **23**, 3115–3128 (2014).

5. Theis, J. L. *et al.* Patient-specific genomics and cross-species functional analysis implicate LRP2 in hypoplastic left heart syndrome. *eLife* **9**, e59554 (2020).

6. Witman, N., Zhou, C., Grote Beverborg, N., Sahara, M. & Chien, K. R. Cardiac progenitors and paracrine mediators in cardiogenesis and heart regeneration. *Seminars in Cell & Developmental Biology* **100**, 29–51 (2020).

7. Eichler, E. E. *et al.* Missing heritability and strategies for finding the underlying causes of complex disease. *Nat. Rev. Genet.* **11**, 446–450 (2010).

8. Zaidi, S. *et al.* De novo mutations in histone-modifying genes in congenital heart disease. *Nature* **498**, 220–223 (2013).

9. Blue, G. M., Kirk, E. P., Sholler, G. F., Harvey, R. P. & Winlaw, D. S. Congenital heart disease: current knowledge about causes and inheritance. *Medical Journal of Australia* **197**, 155–159 (2012).

10. Kodo, K., Uchida, K. & Yamagishi, H. Genetic and Cellular Interaction During Cardiovascular Development Implicated in Congenital Heart Diseases. *Frontiers in Cardiovascular Medicine* **8**, 170 (2021).

11. Gifford, C. A. *et al.* Oligogenic inheritance of a human heart disease involving a genetic modifier. *Science* **364**, 865–870 (2019).

12. Fahed, A. C., Gelb, B. D., Seidman, J. G. & Seidman, C. E. Genetics of Congenital Heart Disease: The Glass Half Empty. *Circ Res* **112**, (2013).

13. Gelb, B. D. & Chung, W. K. Complex Genetics and the Etiology of Human Congenital Heart Disease. *Cold Spring Harb Perspect Med* **4**, a013953 (2014).

14. Zaidi, S. & Brueckner, M. Genetics and Genomics of Congenital Heart Disease. *Circulation Research* **120**, 923–940 (2017).

15. Elliott, D. A. *et al.* Cardiac homeobox gene NKX2-5 mutations and congenital heart disease: associations with atrial septal defect and hypoplastic left heart syndrome. *J. Am. Coll. Cardiol.* **41**, 2072–2076 (2003).

16. McElhinney, D. B., Geiger, E., Blinder, J., Woodrow Benson, D. & Goldmuntz, E. NKX2.5mutations in patients with congenital heart disease. *Journal of the American College of Cardiology* **42**, 1650–1655 (2003).

17. Stallmeyer, B., Fenge, H., Nowak-Göttl, U. & Schulze-Bahr, E. Mutational spectrum in the cardiac transcription factor gene NKX2.5 (CSX) associated with congenital heart disease. *Clinical Genetics* **78**, 533–540 (2010).

18. Akhirome, E., Walton, N. A., Nogee, J. M. & Jay, P. Y. The Complex Genetic Basis of Congenital Heart Defects. *Circ J* **81**, 629–634 (2017).

19. Lage, K. *et al.* Genetic and environmental risk factors in congenital heart disease functionally converge in protein networks driving heart development. *Proc. Natl. Acad. Sci. U.S.A.* **109**, 14035–14040 (2012).

20. Campbell, M. Genetic and environmental factors in congenital heart disease. *Q J Med* **18**, 379–391 (1949).

21. Schott, J. J. *et al.* Congenital heart disease caused by mutations in the transcription factor NKX2-5. *Science* **281**, 108–111 (1998).

22. Garg, V. *et al.* GATA4 mutations cause human congenital heart defects and reveal an interaction with TBX5. *Nature* **424**, 443–447 (2003).

23. Basson, C. T. *et al.* Mutations in human TBX5 [corrected] cause limb and cardiac malformation in Holt-Oram syndrome. *Nat. Genet.* **15**, 30–35 (1997).

24. Kirk, E. P. *et al.* Mutations in Cardiac T-Box Factor Gene TBX20 Are Associated with Diverse Cardiac Pathologies, Including Defects of Septation and Valvulogenesis and Cardiomyopathy. *The American Journal of Human Genetics* **81**, 280–291 (2007).

25. Garg, V. *et al.* Mutations in NOTCH1 cause aortic valve disease. *Nature* **437**, 270–274 (2005).

26. Marian, A. J. Molecular genetic studies of complex phenotypes. *Translational Research* **159**, 64–79 (2012).

27. Cordell, H. J. *et al.* Genome-wide association study identifies loci on 12q24 and 13q32 associated with Tetralogy of Fallot. *Hum Mol Genet* **22**, 1473–1481 (2013).

28. Cordell, H. J. *et al.* Genome-wide association study of multiple congenital heart disease phenotypes identifies a susceptibility locus for atrial septal defect at chromosome 4p16. *Nature Genetics* **45**, 822–824 (2013).

29. Pierpont, M. E. *et al.* Genetic Basis for Congenital Heart Disease: Revisited. *Circulation* **138**, e653–e711 (2018).

30. Jin, S. C. *et al.* Contribution of rare inherited and *de novo* variants in 2,871 congenital heart disease probands. *Nature Genetics* **49**, 1593–1601 (2017).

31. Egbe, A., Lee, S., Ho, D., Uppu, S. & Srivastava, S. Prevalence of congenital anomalies in newborns with congenital heart disease diagnosis. *Ann Pediatr Cardiol* **7**, 86–91 (2014).

32. Homsy, J. *et al.* De novo mutations in congenital heart disease with neurodevelopmental and other congenital anomalies. *Science* **350**, 1262–1266 (2015).

33. Burton, G. J. & Jauniaux, E. Development of the Human Placenta and Fetal Heart: Synergic or Independent? *Front Physiol* **9**, 373 (2018).

34. Sylva, M., Hoff, M. J. B. van den & Moorman, A. F. M. Development of the human heart. *American Journal of Medical Genetics Part A* **164**, 1347–1371 (2014).

35. Buckingham, M., Meilhac, S. & Zaffran, S. Building the mammalian heart from two sources of myocardial cells. *Nat Rev Genet* **6**, 826–835 (2005).

36. Tanaka, M., Chen, Z., Bartunkova, S., Yamasaki, N. & Izumo, S. The cardiac homeobox gene Csx/Nkx2.5 lies genetically upstream of multiple genes essential for heart development. *Development* **126**, 1269–1280 (1999).

37. Lyons, I. *et al.* Myogenic and morphogenetic defects in the heart tubes of murine embryos lacking the homeo box gene Nkx2-5. *Genes Dev* **9**, 1654–1666 (1995).

38. Gittenberger-de Groot, A. C., Bartelings, M. M., Deruiter, M. C. & Poelmann, R. E. Basics of Cardiac Development for the Understanding of Congenital Heart Malformations. *Pediatric Research* **57**, 169–176 (2005).

39. Christoffels, V. M. *et al.* Chamber formation and morphogenesis in the developing mammalian heart. *Dev Biol* **223**, 266–278 (2000).

40. Cuypers, J. A. A. E. *et al.* Unnatural history of tetralogy of Fallot: prospective follow-up of 40 years after surgical correction. *Circulation* **130**, 1944–1953 (2014).

41. Villafañe, J. *et al.* Hot topics in tetralogy of Fallot. *J Am Coll Cardiol* **62**, 2155–2166 (2013).

42. Kola, S. *et al.* Mutational analysis of JAG1 gene in non-syndromic tetralogy of Fallot children. *Clin Chim Acta* **412**, 2232–2236 (2011).

43. Baban, A. *et al.* Identification of TBX5 mutations in a series of 94 patients with Tetralogy of Fallot. *Am J Med Genet A* **164A**, 3100–3107 (2014).

44. Goldmuntz, E., Geiger, E. & Benson, D. W. NKX2.5 mutations in patients with tetralogy of fallot. *Circulation* **104**, 2565–2568 (2001).

45. Greenway, S. C. *et al.* De novo copy number variants identify new genes and loci in isolated sporadic tetralogy of Fallot. *Nat Genet* **41**, 931–935 (2009).

46. Silversides, C. K. *et al.* Rare copy number variations in adults with tetralogy of Fallot implicate novel risk gene pathways. *PLoS Genet* **8**, e1002843 (2012).

47. Bansal, V. *et al.* Outlier-based identification of copy number variations using targeted resequencing in a small cohort of patients with Tetralogy of Fallot. *PLoS One* **9**, e85375 (2014).

48. Andersen, T. A., Troelsen, K. de L. L. & Larsen, L. A. Of mice and men: molecular genetics of congenital heart disease. *Cell. Mol. Life Sci.* **71**, 1327–1352 (2014).

49. Nemer, G. *et al.* A novel mutation in the GATA4 gene in patients with Tetralogy of Fallot. *Hum Mutat* **27**, 293–294 (2006).

50. Tomita-Mitchell, A., Maslen, C. L., Morris, C. D., Garg, V. & Goldmuntz, E. GATA4 sequence variants in patients with congenital heart disease. *J Med Genet* **44**, 779–783 (2007).

51. Rauch, R. *et al.* Comprehensive genotype-phenotype analysis in 230 patients with tetralogy of Fallot. *J Med Genet* **47**, 321–331 (2010).

52. McDermott, D. A. *et al.* TBX5 genetic testing validates strict clinical criteria for Holt-Oram syndrome. *Pediatr Res* **58**, 981–986 (2005).

53. Yagi, H. *et al.* Role of TBX1 in human del22q11.2 syndrome. *Lancet* **362**, 1366–1373 (2003).

54. Töpf, A. *et al.* Functionally significant, rare transcription factor variants in tetralogy of Fallot. *PLoS One* **9**, e95453 (2014).

55. Eldadah, Z. A. *et al.* Familial Tetralogy of Fallot caused by mutation in the jagged1 gene. *Hum Mol Genet* **10**, 163–169 (2001).

56. Sheng, W. *et al.* DNA methylation status of NKX2-5, GATA4 and HAND1in patients with tetralogy of fallot. *BMC Medical Genomics* **6**, 46 (2013).

57. Bittel, D. C. *et al.* Gene expression in cardiac tissues from infants with idiopathic conotruncal defects. *BMC Med Genomics* **4**, 1 (2011).

58. Maron, M. S. *et al.* Hypertrophic cardiomyopathy is predominantly a disease of left ventricular outflow tract obstruction. *Circulation* **114**, 2232–2239 (2006).

59. Jones, B. M. *et al.* How Symptomatic Should a Hypertrophic Obstructive Cardiomyopathy Patient Be to Consider Alcohol Septal Ablation? *J Am Heart Assoc* **6**, e006292 (2017).

60. Ho, C. Y. *et al.* Homozygous mutation in cardiac troponin T: implications for hypertrophic cardiomyopathy. *Circulation* **102**, 1950–1955 (2000).

61. Lekanne Deprez, R. H. *et al.* Two cases of severe neonatal hypertrophic cardiomyopathy caused by compound heterozygous mutations in the MYBPC3 gene. *J Med Genet* **43**, 829–832 (2006).

62. Richard, P. *et al.* Hypertrophic cardiomyopathy: distribution of disease genes, spectrum of mutations, and implications for a molecular diagnosis strategy. *Circulation* **107**, 2227–2232 (2003).

63. Richard, P. *et al.* Homozygotes for a R869G mutation in the beta -myosin heavy chain gene have a severe form of familial hypertrophic cardiomyopathy. *J Mol Cell Cardiol* **32**, 1575–1583 (2000).

64. Van Driest, S. L., Ommen, S. R., Tajik, A. J., Gersh, B. J. & Ackerman, M. J. Sarcomeric genotyping in hypertrophic cardiomyopathy. *Mayo Clin Proc* **80**, 463–469 (2005).

65. Erdmann, J. *et al.* Mutation spectrum in a large cohort of unrelated consecutive patients with hypertrophic cardiomyopathy. *Clin Genet* **64**, 339–349 (2003).

66. Girolami, F. *et al.* A molecular screening strategy based on beta-myosin heavy chain, cardiac myosin binding protein C and troponin T genes in Italian patients with hypertrophic cardiomyopathy. *J Cardiovasc Med (Hagerstown)* **7**, 601–607 (2006).

67. Kong, S. W. *et al.* Heart Failure–Associated Changes in RNA Splicing of Sarcomere Genes. *Circulation: Cardiovascular Genetics* **3**, 138–146 (2010).

68. Grunert, M. *et al.* Comparative DNA methylation and gene expression analysis identifies novel genes for structural congenital heart diseases. *Cardiovasc. Res.* **112**, 464–477 (2016).

69. Lange, S., Pinotsis, N., Agarkova, I. & Ehler, E. The M-band: The underestimated part of the sarcomere. *Biochimica et Biophysica Acta (BBA) - Molecular Cell Research* **1867**, 118440 (2020).

70. Grove, B. K. *et al.* A new 185,000-dalton skeletal muscle protein detected by monoclonal antibodies. *J Cell Biol* **98**, 518–524 (1984).

71. Masaki, T. & Takaiti, O. M-Protein*. *The Journal of Biochemistry* **75**, 367–380 (1974).

72. Schoenauer, R. *et al.* Myomesin 3, a Novel Structural Component of the M-band in Striated Muscle. *Journal of Molecular Biology* **376**, 338–351 (2008).

73. Obermann, W. M. *et al.* The structure of the sarcomeric M band: localization of defined domains of myomesin, M-protein, and the 250-kD carboxy-terminal region of titin by immunoelectron microscopy. *J Cell Biol* **134**, 1441–1453 (1996).

74. Obermann, W. M., Plessmann, U., Weber, K. & Fürst, D. O. Purification and biochemical characterization of myomesin, a myosin-binding and titin-binding protein, from bovine skeletal muscle. *Eur J Biochem* **233**, 110–115 (1995).

75. Obermann, W. M. J., van der Ven, P. F. M., Steiner, F., Weber, K. & Fürst, D. O. Mapping of a Myosin-binding Domain and a Regulatory Phosphorylation Site in M-Protein, a Structural Protein of the Sarcomeric M Band. *MBoC* **9**, 829–840 (1998).

76. Lange, S. *et al.* Dimerisation of Myomesin: Implications for the Structure of the Sarcomeric M-band. *Journal of Molecular Biology* **345**, 289–298 (2005).

77. Auerbach, D. *et al.* Different Domains of the M-Band Protein Myomesin Are Involved in Myosin Binding and M-Band Targeting. *Mol Biol Cell* **10**, 1297–1308 (1999).

78. Agarkova, I., Auerbach, D., Ehler, E. & Perriard, J.-C. A Novel Marker for Vertebrate Embryonic Heart, the EH-myomesin Isoform*. *Journal of Biological Chemistry* **275**, 10256–10264 (2000).

79. Grove, B. K., Cerny, L., Perriard, J. C. & Eppenberger, H. M. Myomesin and M-protein: expression of two M-band proteins in pectoral muscle and heart during development. *J Cell Biol* **101**, 1413–1421 (1985).

80. Schoenauer, R. *et al.* EH-myomesin splice isoform is a novel marker for dilated cardiomyopathy. *Basic Res Cardiol* **106**, 233–247 (2011).

81. Bollen, I. A. E. *et al.* Myofilament Remodeling and Function Is More Impaired in Peripartum Cardiomyopathy Compared with Dilated Cardiomyopathy and Ischemic Heart Disease. *Am J Pathol* **187**, 2645–2658 (2017).

82. Siegert, R. *et al.* A myomesin mutation associated with hypertrophic cardiomyopathy deteriorates dimerisation properties. *Biochemical and Biophysical Research Communications* **405**, 473–479 (2011).

83. Wang, X., Liu, X., Wang, S. & Luan, K. Myofibrillogenesis regulator 1 induces hypertrophy by promoting sarcomere organization in neonatal rat cardiomyocytes. *Hypertens Res* **35**, 597–603 (2012).

84. Koebis, M. *et al.* Alternative splicing of myomesin 1 gene is aberrantly regulated in myotonic dystrophy type 1. *Genes to Cells* **16**, 961–972.

85. Beqqali, A., Alternative splicing in cardiomyopathy. *Biophys Rev.* 10 (4) :1061-1071 (2018).

86. Fukuzawa, A. *et al.* Interactions with titin and myomesin target obscurin and obscurin-like 1 to the M-band – implications for hereditary myopathies. *Journal of Cell Science* **121**, 1841–1851 (2008).

87. Hang, C. *et al.* Knockout of MYOM1 in human cardiomyocytes leads to myocardial atrophy via impairing calcium homeostasis. *Journal of Cellular and Molecular Medicine* **25**, 1661–1676 (2021).

88. Radke, M. H. *et al.* Deleting Full Length Titin Versus the Titin M-Band Region Leads to Differential Mechanosignaling and Cardiac Phenotypes. *Circulation* **139**, 1813–1827 (2019).

89. Gordon, B. M., Rodriguez, S., Lee, M. & Chang, R.-K. Decreasing number of deaths of infants with hypoplastic left heart syndrome. *J Pediatr* **153**, 354–358 (2008).

90. Reller, M. D., Strickland, M. J., Riehle-Colarusso, T., Mahle, W. T. & Correa, A. Prevalence of congenital heart defects in metropolitan Atlanta, 1998-2005. *J Pediatr* **153**, 807–813 (2008).

91. Crucean, A. *et al.* Re-evaluation of hypoplastic left heart syndrome from a developmental and morphological perspective. *Orphanet J Rare Dis* **12**, 138 (2017).

92. Urencio, M., Greenleaf, C., Salazar, J. D. & Dodge-Khatami, A. Resource and cost considerations in treating hypoplastic left heart syndrome. *Pediatric Health Med Ther* **7**, 149–153 (2016).

93. Agopian, A. J. *et al.* Genome-Wide Association Studies and Meta-Analyses for Congenital Heart Defects. *Circ Cardiovasc Genet* **10**, e001449 (2017).

94. Martin, L. J., Pilipenko, V. & Benson, D. W. Role of Segregation for Variant Discovery in Multiplex Families Ascertained by Probands With Left Sided Cardiovascular Malformations. *Front Genet* **9**, 729 (2018).

95. Theis, J. L. *et al.* Compound heterozygous NOTCH1 mutations underlie impaired cardiogenesis in a patient with hypoplastic left heart syndrome. *Hum Genet* **134**, 1003–1011 (2015).

96. Glessner, J. T. *et al.* Increased frequency of de novo copy number variants in congenital heart disease by integrative analysis of single nucleotide polymorphism array and exome sequence data. *Circ Res* **115**, 884–896 (2014).

97. Theis, J. L. *et al.* Recessive MYH6 Mutations in Hypoplastic Left Heart With Reduced Ejection Fraction. *Circ Cardiovasc Genet* **8**, 564–571 (2015).

98. Esposito, G. *et al.* Somatic mutations in NKX2–5, GATA4, and HAND1 are not a common cause of tetralogy of Fallot or hypoplastic left heart. *Am J Med Genet A* **155A**, 2416–2421 (2011).

99. Yagi, H. *et al.* The Genetic Landscape of Hypoplastic Left Heart Syndrome. *Pediatr Cardiol* **39**, 1069–1081 (2018).

100. Grossfeld, P., Nie, S., Lin, L., Wang, L. & Anderson, R. H. Hypoplastic Left Heart Syndrome: A New Paradigm for an Old Disease? *J Cardiovasc Dev Dis* **6**, (2019).

101. Gaber, N. *et al.* Fetal reprogramming and senescence in hypoplastic left heart syndrome and in human pluripotent stem cells during cardiac differentiation. *Am. J. Pathol.* **183**, 720–734 (2013).

102. Paige, S. L. *et al.* Patient-Specific Induced Pluripotent Stem Cells Implicate Intrinsic Impaired Contractility in Hypoplastic Left Heart Syndrome. *Circulation* **142**, 1605–1608 (2020).

103. Liu, X. *et al.* The complex genetics of hypoplastic left heart syndrome. *Nat Genet* **49**, 1152–1159 (2017).

104. Cases, O. *et al.* Cubilin, a high affinity receptor for fibroblast growth factor 8, is required for cell survival in the developing vertebrate head. *J Biol Chem* **288**, 16655–16670 (2013).

105. Spoelgen, R. *et al.* LRP2/megalin is required for patterning of the ventral telencephalon. *Development* **132**, 405–414 (2005).

106. Cases, O. *et al.* Foxg1-Cre Mediated Lrp2 Inactivation in the Developing Mouse Neural Retina, Ciliary and Retinal Pigment Epithelia Models Congenital High Myopia. *PLoS One* **10**, e0129518 (2015).

107. Storm, T., Heegaard, S., Christensen, E. I. & Nielsen, R. Megalin-deficiency causes high myopia, retinal pigment epithelium-macromelanosomes and abnormal development of the ciliary body in mice. *Cell Tissue Res* **358**, 99–107 (2014).

108. Willnow, T. E. *et al.* Defective forebrain development in mice lacking gp330/megalin. *Proc Natl Acad Sci U S A* **93**, 8460–8464 (1996).

109. Willnow, T. E. & Christ, A. Endocytic receptor LRP2/megalin-of holoprosencephaly and renal Fanconi syndrome. *Pflugers Arch* **469**, 907–916 (2017).

110. Christ, A., Herzog, K. & Willnow, T. E. LRP2, an auxiliary receptor that controls sonic hedgehog signaling in development and disease. *Dev. Dyn.* **245**, 569–579 (2016).

111. Christ, A. *et al.* LRP2 Acts as SHH Clearance Receptor to Protect the Retinal Margin from Mitogenic Stimuli. *Developmental Cell* **35**, 36–48 (2015).

112. Fisher, C. E. & Howie, S. E. M. The role of megalin (LRP-2/Gp330) during development. *Developmental Biology* **296**, 279–297 (2006).

113. Assémat, E. *et al.* Overlapping expression patterns of the multiligand endocytic receptors cubilin and megalin in the CNS, sensory organs and developing epithelia of the rodent embryo. *Gene Expression Patterns* **6**, 69–78 (2005).

114. Li, Y. *et al.* Global genetic analysis in mice unveils central role for cilia in congenital heart disease. *Nature* **521**, 520–524 (2015).

115. Baardman, M. E. *et al.* Common arterial trunk and ventricular non-compaction in Lrp2 knockout mice indicate a crucial role of LRP2 in cardiac development. *Disease Models & Mechanisms* **9**, 413–425 (2016).

116. Shi, Z. & Barna, M. Translating the genome in time and space: specialized ribosomes, RNA regulons, and RNA-binding proteins. *Annu. Rev. Cell Dev. Biol.* **31**, 31–54 (2015).

117. Wang, W. *et al.* Ribosomal Proteins and Human Diseases: Pathogenesis, Molecular Mechanisms, and Therapeutic Implications. *Med Res Rev* **35**, 225–285 (2015).

118. Marygold, S. J. *et al.* The ribosomal protein genes and Minute loci of Drosophila melanogaster. *Genome Biology* **8**, R216 (2007).

119. Lambertsson, A. The minute genes in Drosophila and their molecular functions. *Adv Genet* **38**, 69–134 (1998).

120. Farley-Barnes, K. I., Ogawa, L. M. & Baserga, S. J. Ribosomopathies: Old Concepts, New Controversies. *Trends Genet.* **35**, 754–767 (2019).

121. Kondrashov, N. *et al.* Ribosome-mediated specificity in Hox mRNA translation and vertebrate tissue patterning. *Cell* **145**, 383–397 (2011).

122. Terzian, T. *et al.* Rpl27a mutation in the sooty foot ataxia mouse phenocopies high p53 mouse models. *J Pathol* **224**, 540–552 (2011).

123. Vlachos, A. *et al.* The Increased Prevalence of Congenital Heart Disease (CHD) in Children with Diamond Blackfan Anemia (DBA) Suggests Unrecognized DBA as a Cause of CHD in the General Population: A Report of the Diamond Blackfan Anemia Registry. *Circ Genom Precis Med* **11**, e002044 (2018).

124. Schroeder, A. M. *et al.* Model system identification of novel congenital heart disease gene candidates: focus on RPL13. *Hum. Mol. Genet.* **28**, 3954–3969 (2019).

125. Casad, M. E. *et al.* Cardiomyopathy Is Associated with Ribosomal Protein Gene Haplo-Insufficiency in Drosophila melanogaster. *Genetics* **189**, 861–870 (2011).

126. Tiu, G. C. *et al.* A p53-dependent translational program directs tissue-selective phenotypes in a model of ribosomopathies. *Developmental Cell* **0**, (2021).

127. Zaffran, S. & Frasch, M. Early Signals in Cardiac Development. *Circulation Research* **91**, 457–469 (2002).

128. Bier, E. & Bodmer, R. Drosophila, an emerging model for cardiac disease. *Gene* **342**, 1–11 (2004).

129. Olson, E. N. Gene regulatory networks in the evolution and development of the heart. *Science* **313**, 1922–1927 (2006).

130. Bodmer, R. The gene tinman is required for specification of the heart and visceral muscles in Drosophila. *Development* **118**, 719–729 (1993).

131. Bodmer, R., Jan, L. Y. & Jan, Y. N. A new homeobox-containing gene, msh-2, is transiently expressed early during mesoderm formation of Drosophila. *Development* **110**, 661–669 (1990).

132. Bodmer, R. & Frasch, M. Chapter 1.2 - Development and Aging of the Drosophila Heart. in *Heart Development and Regeneration* (eds. Rosenthal, N. & Harvey, R. P.) 47–86 (Academic Press, 2010). doi:10.1016/B978-0-12-381332-9.00002-5.

133. Vogler, G. & Bodmer, R. Cellular Mechanisms of Drosophila Heart Morphogenesis. *J Cardiovasc Dev Dis* **2**, 2–16 (2015).

134. Bodmer, R. & Frasch, M. 5 - Genetic Determination of Drosophila Heart Development. in *Heart Development* (eds. Harvey, R. P. & Rosenthal, N.) 65–90 (Academic Press, 1999). doi:10.1016/B978-012329860-7/50007-6.

135. Roth, S., Stein, D. & Nüsslein-Volhard, C. A gradient of nuclear localization of the dorsal protein determines dorsoventral pattern in the Drosophila embryo. *Cell* **59**, 1189–1202 (1989).

136. Leptin, M. twist and snail as positive and negative regulators during Drosophila mesoderm development. *Genes Dev.* **5**, 1568–1576 (1991).

137. Stathopoulos, A., Tam, B., Ronshaugen, M., Frasch, M. & Levine, M. pyramus and thisbe: FGF genes that pattern the mesoderm of Drosophila embryos. *Genes Dev* **18**, 687–699 (2004).

138. Lin, X., Buff, E. M., Perrimon, N. & Michelson, A. M. Heparan sulfate proteoglycans are essential for FGF receptor signaling during Drosophila embryonic development. *Development* **126**, 3715–3723 (1999).

139. Bryantsev, A. L. & Cripps, R. M. Cardiac gene regulatory networks in Drosophila. *Biochim Biophys Acta* **1789**, 343–353 (2009).

140. Ward, E. J. & Skeath, J. B. Characterization of a novel subset of cardiac cells and their progenitors in the Drosophila embryo. *Development* **127**, 4959–4969 (2000).

141. Han, Z. & Bodmer, R. Myogenic cells fates are antagonized by Notch only in asymmetric lineages of the Drosophila heart, with or without cell division. *Development* **130**, 3039–3051 (2003).

142. Park, M., Yaich, L. E. & Bodmer, R. Mesodermal cell fate decisions in Drosophila are under the control of the lineage genes numb, Notch, and sanpodo. *Mech Dev* **75**, 117–126 (1998).

143. Bodmer, R. Heart development in Drosophila and its relationship to vertebrates. *Trends in Cardiovascular Medicine* **5**, 21–28 (1995).

144. Srivastava, D. & Olson, E. N. A genetic blueprint for cardiac development. *Nature* **407**, 221–226 (2000).

145. Zaffran, S. *et al.* Cardioblast-intrinsic Tinman activity controls proper diversification and differentiation of myocardial cells in Drosophila. *Development* **133**, 4073–4083 (2006).

146. Reim, I. & Frasch, M. The Dorsocross T-box genes are key components of the regulatory network controlling early cardiogenesis in Drosophila. *Development* **132**, 4911–4925 (2005).

147. Klinedinst, S. L. & Bodmer, R. Gata factor Pannier is required to establish competence for heart progenitor formation. *Development* **130**, 3027–3038 (2003).

148. Han, Z. & Olson, E. N. Hand is a direct target of Tinman and GATA factors during Drosophila cardiogenesis and hematopoiesis. *Development* **132**, 3525–3536 (2005).

149. Sellin, J., Albrecht, S., Kölsch, V. & Paululat, A. Dynamics of heart differentiation, visualized utilizing heart enhancer elements of the Drosophila melanogaster bHLH transcription factor Hand. *Gene Expr Patterns* **6**, 360–375 (2006).

150. Rotstein, B. & Paululat, A. On the Morphology of the Drosophila Heart. *Journal of Cardiovascular Development and Disease* **3**, 15 (2016).

151. Monier, B., Astier, M., Sémériva, M. & Perrin, L. Steroid-dependent modification of Hox function drives myocyte reprogramming in the Drosophila heart. *Development* **132**, 5283–5293 (2005).

152. Lehmacher, C., Abeln, B. & Paululat, A. The ultrastructure of Drosophila heart cells. *Arthropod Struct Dev* **41**, 459–474 (2012).

153. Schaub, C., März, J., Reim, I. & Frasch, M. Org-1-dependent lineage reprogramming generates the ventral longitudinal musculature of the Drosophila heart. *Curr Biol* **25**, 488–494 (2015).

154. Molina, M. R. & Cripps, R. M. Ostia, the inflow tracts of the Drosophila heart, develop from a genetically distinct subset of cardial cells. *Mech Dev* **109**, 51–59 (2001).

155. Dulcis, D. & Levine, R. B. Innervation of the heart of the adult fruit fly, Drosophila melanogaster. *J Comp Neurol* **465**, 560–578 (2003).

156. Dowse, H. *et al.* A congenital heart defect in Drosophila caused by an action-potential mutation. *J Neurogenet* **10**, 153–168 (1995).

157. Piazza, N. & Wessells, R. J. Drosophila Models of Cardiac Disease. *Prog Mol Biol Transl Sci* **100**, 155–210 (2011).

158. Taghli-Lamallem, O., Plantié, E. & Jagla, K. Drosophila in the Heart of Understanding Cardiac Diseases: Modeling Channelopathies and Cardiomyopathies in the Fruitfly. *J Cardiovasc Dev Dis* **3**, (2016).

159. Wolf, M. J. Modeling dilated cardiomyopathies in Drosophila. *Trends Cardiovasc. Med.* **22**, 55–61 (2012).

160. Wolf, M. J. *et al.* Drosophila as a model for the identification of genes causing adult human heart disease. *PNAS* **103**, 1394–1399 (2006).

161. Bodmer, R. & Venkatesh, T. V. Heart Development in Drosophila and Vertebrates: Conservation of Molecular Mechanisms. *Dev Genet*. **22** (3): 181-6 (1998).

162. Cripps, R. M. & Olson, E. N. Control of cardiac development by an evolutionarily conserved transcriptional network. *Dev Biol* **246**, 14–28 (2002).

163. Meganathan, K., Sotiriadou, I., Natarajan, K., Hescheler, J. & Sachinidis, A. Signaling molecules, transcription growth factors and other regulators revealed from in-vivo and in-vitro models for the regulation of cardiac development. *Int J Cardiol* **183**, 117–128 (2015).

164. Tao, Y. & Schulz, R. A. Heart development in Drosophila. *Semin Cell Dev Biol* **18**, 3–15 (2007).

165. Ahmad, S. M. Conserved signaling mechanisms in Drosophila heart development. *Developmental Dynamics* **246**, 641–656 (2017).

166. Cammarato, A. *et al.* A mighty small heart: the cardiac proteome of adult Drosophila melanogaster. *PLoS One* **6**, e18497 (2011).

167. Cammarato, A. *et al.* Myosin transducer mutations differentially affect motor function, myofibril structure, and the performance of skeletal and cardiac muscles. *Mol Biol Cell* **19**, 553–562 (2008).

168. Taghli-Lamallem, O. *et al.* Dystrophin deficiency in Drosophila reduces lifespan and causes a dilated cardiomyopathy phenotype. *Aging Cell* **7**, 237–249 (2008).

169. Abraham, D. M. & Wolf, M. J. Disruption of Sarcoendoplasmic Reticulum Calcium ATPase Function in Drosophila Leads to Cardiac Dysfunction. *PLOS ONE* **8**, e77785 (2013).

170. Ocorr, K. *et al.* KCNQ potassium channel mutations cause cardiac arrhythmias in Drosophila that mimic the effects of aging. *PNAS* **104**, 3943–3948 (2007).

171. Johnson, E., Ringo, J., Bray, N. & Dowse, H. Genetic and pharmacological identification of ion channels central to the Drosophila cardiac pacemaker. *J Neurogenet* **12**, 1–24 (1998).

172. Gu, G. G. & Singh, S. Pharmacological analysis of heartbeat in Drosophila. *J Neurobiol* **28**, 269–280 (1995).

173. Lin, N. *et al.* A method to measure myocardial calcium handling in adult Drosophila. *Circ Res* **108**, 1306–1315 (2011).

174. Warmke, J. W. & Ganetzky, B. A family of potassium channel genes related to eag in Drosophila and mammals. *PNAS* **91**, 3438–3442 (1994).

175. Curran, M. E. *et al.* A molecular basis for cardiac arrhythmia: HERG mutations cause long QT syndrome. *Cell* **80**, 795–803 (1995).

176. Ocorr, K. *et al.* Age-dependent electrical and morphological remodeling of the Drosophila heart caused by hERG/seizure mutations. *PLoS Genet* **13**, e1006786 (2017).

177. Nerbonne, J. M. Studying cardiac arrhythmias in the mouse--a reasonable model for probing mechanisms? *Trends Cardiovasc Med* **14**, 83–93 (2004).

178. Brand, A. H. & Perrimon, N. Targeted gene expression as a means of altering cell fates and generating dominant phenotypes. *Development* **118**, 401–415 (1993).

179. Ocorr, K., Fink, M., Cammarato, A., Bernstein, S. I. & Bodmer, R. Semi-automated Optical Heartbeat Analysis of Small Hearts. *J Vis Exp* (2009) doi:10.3791/1435.

180. Vogler, G., Bodmer, R. & Akasaka, T. A Drosophila model for congenital heart disease. *Drug Discovery Today: Disease Models* **6**, 47–54 (2009).

181. Klassen, M. P. *et al.* Age-dependent diastolic heart failure in an in vivo Drosophila model. *eLife* **6**, e20851 (2017).

182. Geier, C. *et al.* Mutations in the Human Muscle LIM Protein Gene in Families With Hypertrophic Cardiomyopathy. *Circulation* **107**, 1390–1395 (2003).

183. Kabaeva, Z. T. *et al.* Systematic analysis of the regulatory and essential myosin light chain genes: genetic variants and mutations in hypertrophic cardiomyopathy. *Eur J Hum Genet* **10**, 741–748 (2002).

184. Mogensen, J. *et al.* Clinical and genetic characteristics of α cardiac actin gene mutations in hypertrophic cardiomyopathy. *Journal of Medical Genetics* **41**, e10–e10 (2004).

185. Perrot, A., Posch, M. G. & Osterziel, K. J. Deletion of Glu at codon 13 in the TCAP gene encoding the Z-disc protein titin-cap/telethonin is a rare non-synonymous polymorphism. *Molecular Genetics and Metabolism* **88**, 199–200 (2006).

186. Posch, M. G. *et al.* Sequence analysis of myozenin 2 in 438 European patients with familial hypertrophic cardiomyopathy. *Med Sci Monit* **14**, CR372-374 (2008).

187. Perrot, A. *et al.* Prevalence of cardiac beta-myosin heavy chain gene mutations in patients with hypertrophic cardiomyopathy. *J Mol Med* **83**, 468–477 (2005).

188. Fink, M. *et al.* A new method for detection and quantification of heartbeat parameters in Drosophila, zebrafish, and embryonic mouse hearts. *Biotechniques* **46**, 101–113 (2009).

189. Cammarato, A., Ocorr, S. & Ocorr, K. Enhanced assessment of contractile dynamics in Drosophila hearts. *BioTechniques* **58**, 77–80 (2015).

190. Gargano, J. W., Martin, I., Bhandari, P. & Grotewiel, M. S. Rapid iterative negative geotaxis (RING): a new method for assessing age-related locomotor decline in Drosophila. *Exp Gerontol* **40**, 386–395 (2005).

191. Pfaffl, M. W. A new mathematical model for relative quantification in real-time RT–PCR. *Nucleic Acids Research* **29**, e45–e45 (2001).

192. Alayari, N. N. *et al.* Fluorescent labeling of Drosophila heart structures. *J Vis Exp* (2009) doi:10.3791/1423.

193. Cooper, A. S., Rymond, K. E., Ward, M. A., Bocook, E. L. & Cooper, R. L. Monitoring Heart Function in Larval Drosophila melanogaster for Physiological Studies. *J Vis Exp* 1596 (2009) doi:10.3791/1596.

194. Yu, L., Daniels, J., Glaser, A. E. & Wolf, M. J. Raf-mediated cardiac hypertrophy in adult Drosophila. *Dis Model Mech* **6**, 964–976 (2013).

195. Costanzo, M. *et al.* Global Genetic Networks and the Genotype-to-Phenotype Relationship. *Cell* **177**, 85–100 (2019).

196. Saha, S. *et al. Genetic architecture of natural variations of cardiac performance in flies*. 2021.06.08.447524 https://www.biorxiv.org/content/10.1101/2021.06.08.447524v1 (2021) doi:10.1101/2021.06.08.447524.

197. Yin, Z., Xu, X. L. & Frasch, M. Regulation of the twist target gene tinman by modular cis-regulatory elements during early mesoderm development. *Development* **124**, 4971–4982 (1997).

198. Westerfield M. *The zebrafish book : a guide for the laboratory use of zebrafish (Brachydanio rerio).* (M. W, editor: University of Oregon Press).

199. Talbot, J. C. & Amacher, S. L. A streamlined CRISPR pipeline to reliably generate zebrafish frameshifting alleles. *Zebrafish* **11**, 583–585 (2014).

200. Gagnon, J. A. *et al.* Efficient mutagenesis by Cas9 protein-mediated oligonucleotide insertion and large-scale assessment of single-guide RNAs. *PLoS One* **9**, e98186 (2014).

201. Irion, U., Krauss, J. & Nüsslein-Volhard, C. Precise and efficient genome editing in zebrafish using the CRISPR/Cas9 system. *Development* **141**, 4827–4830 (2014).

202. Postma, A. V. *et al.* Mutations in the Sarcomere Gene MYH7 in Ebstein AnomalyClinical Perspective. *Circulation: Genomic and Precision Medicine* **4**, 43–50 (2011).

203. Schafer, S. *et al.* Titin-truncating variants affect heart function in disease cohorts and the general population. *Nat Genet* **49**, 46–53 (2017).

204. Hershberger, R. E., Hedges, D. J. & Morales, A. Dilated cardiomyopathy: the complexity of a diverse genetic architecture. *Nat Rev Cardiol* **10**, 531–547 (2013).

205. Hu, J., Theis, J., O, 'Leary Patrick, Qureshi, M. & Olson, T. Genetic association between hypoplastic left heart syndrome and cardiomyopathies via the mybpc3 gene. *Journal of the American College of Cardiology* **73**, 636–636 (2019).

206. Karczewski, K. J. *et al.* The mutational constraint spectrum quantified from variation in 141,456 humans. *Nature* **581**, 434–443 (2020).

207. Adzhubei, I., Jordan, D. M. & Sunyaev, S. R. Predicting functional effect of human missense mutations using PolyPhen-2. *Curr Protoc Hum Genet* **Chapter 7**, Unit7.20 (2013).

208. Vaser, R., Adusumalli, S., Leng, S. N., Sikic, M. & Ng, P. C. SIFT missense predictions for genomes. *Nat Protoc* **11**, 1–9 (2016).

209. Schwarz, J. M., Rödelsperger, C., Schuelke, M. & Seelow, D. MutationTaster evaluates disease-causing potential of sequence alterations. *Nat Methods* **7**, 575–576 (2010).

210. Hu, Y. *et al.* An integrative approach to ortholog prediction for disease-focused and other functional studies. *BMC Bioinformatics* **12**, 357 (2011).

211. Kiełbasa, S. M., Wan, R., Sato, K., Horton, P. & Frith, M. C. Adaptive seeds tame genomic sequence comparison. *Genome Res* **21**, 487–493 (2011).

212. Lee, P.-T. *et al.* A gene-specific T2A-GAL4 library for Drosophila. *Elife* **7**, (2018).

213. Walls, S. M. *et al.* Ceramide-Protein Interactions Modulate Ceramide-Associated Lipotoxic Cardiomyopathy. *Cell Reports* **22**, 2702–2715 (2018).

214. Martínez-Morentin, L. *et al.* Cardiac deficiency of single cytochrome oxidase assembly factor scox induces p53-dependent apoptosis in a Drosophila cardiomyopathy model. *Human Molecular Genetics* **24**, 3608–3622 (2015).

215. Vermeer, A. M. C., Wilde, A. A. M. & Christiaans, I. Human Genetics of Cardiomyopathies. in *Congenital Heart Diseases: The Broken Heart: Clinical Features, Human Genetics and Molecular Pathways* (eds. Rickert-Sperling, S., Kelly, R. G. & Driscoll, D. J.) 675–686 (Springer, 2016). doi:10.1007/978-3-7091-1883-2_59.

216. O'Donnell, P. T. & Bernstein, S. I. Molecular and ultrastructural defects in a Drosophila myosin heavy chain mutant: differential effects on muscle function produced by similar thick filament abnormalities. *Journal of Cell Biology* **107**, 2601–2612 (1988).

217. Wells, L., Edwards, K. A. & Bernstein, S. I. Myosin heavy chain isoforms regulate muscle function but not myofibril assembly. *EMBO J* **15**, 4454–4459 (1996).

218. Hamdani, N. *et al.* Sarcomeric dysfunction in heart failure. *Cardiovasc Res* **77**, 649–658 (2008).

219. Pehlivan, D. *et al.* The Genomics of Arthrogryposis, a Complex Trait: Candidate Genes and Further Evidence for Oligogenic Inheritance. *Am J Hum Genet* **105**, 132–150 (2019).

220. Bottillo, I. *et al.* Molecular analysis of sarcomeric and non-sarcomeric genes in patients with hypertrophic cardiomyopathy. *Gene* **577**, 227–235 (2016).

221. Kostareva, A. *et al.* Genetic Spectrum of Idiopathic Restrictive Cardiomyopathy Uncovered by Next-Generation Sequencing. *PLOS ONE* **11**, e0163362 (2016).

222. Shanks, G. W., Tester, D. J., Nishtala, S., Evans, J. M. & Ackerman, M. J. Genomic Triangulation and Coverage Analysis in Whole-Exome Sequencing–Based Molecular Autopsies. *Circulation: Cardiovascular Genetics* **10**, e001828 (2017).

223. Akinrinade, O. *et al.* Genetics and genotype-phenotype correlations in Finnish patients with dilated cardiomyopathy. *Eur Heart J* **36**, 2327–2337 (2015).

224. Marston, S. *et al.* OBSCN Mutations Associated with Dilated Cardiomyopathy and Haploinsufficiency. *PLOS ONE* **10**, e0138568 (2015).

225. Xu, J. *et al.* Functional analysis of slow myosin heavy chain 1 and myomesin-3 in sarcomere organization in zebrafish embryonic slow muscles. *J Genet Genomics* **39**, 69–80 (2012).

226. Akerberg, A. A. *et al. RBPMS2 is a conserved regulator of alternative splicing that promotes myofibrillar organization and optimal calcium handling in cardiomyocytes*. 2021.03.08.434502 https://www.biorxiv.org/content/10.1101/2021.03.08.434502v2 (2021) doi:10.1101/2021.03.08.434502.

227. Burkart, C. *et al.* Modular Proteins from the Drosophila sallimus (sls) Gene and their Expression in Muscles with Different Extensibility. *Journal of Molecular Biology* **367**, 953–969 (2007).

228. Cammarato, A. *et al.* Myosin Transducer Mutations Differentially Affect Motor Function, Myofibril Structure, and the Performance of Skeletal and Cardiac Muscles. *MBoC* **19**, 553–562 (2007).

229. Kronert, W. A. *et al.* Prolonged cross-bridge binding triggers muscle dysfunction in a Drosophila model of myosin-based hypertrophic cardiomyopathy. *Elife* **7**, e38064 (2018).

230. Villard, E. *et al.* Mutation screening in dilated cardiomyopathy: prominent role of the beta myosin heavy chain gene. *European Heart Journal* **26**, 794–803 (2005).

231. Ware, S. M. *et al.* Pediatric restrictive cardiomyopathy associated with a mutation in β-myosin heavy chain. *Clinical Genetics* **73**, 165–170 (2008).

232. Bergmann, O. *et al.* Dynamics of Cell Generation and Turnover in the Human Heart. *Cell* **161**, 1566–1575 (2015).

233. Adler, C.-P. DNS in Kinderherzen. Biochemische und zytophotometrische Untersuchungen. *Beiträge zur Pathologie* **158**, 173–202 (1976).

234. Vliegen, H. W., Eulderink, F., Bruschke, A. V., van, der L. A. & Cornelisse, C. J. Polyploidy of myocyte nuclei in pressure overloaded human hearts: a flow cytometric study in left and right ventricular myocardium. *Am J Cardiovasc Pathol* **5**, 27–31 (1995).

235. Brodsky, V. Y., Arefyeva, A. M., Gvasava, I. G., Sarkisov, D. S. & Panova, N. W. Polyploidy in cardiac myocytes of normal and hypertrophic human hearts; range of values. *Vichows Archiv A Pathol Anat* **424**, 429–435 (1994).

236. Adler, C. P. & Friedburg, H. Myocardial DNA content, ploidy level and cell number in geriatric hearts: Post-mortem examinations of human myocardium in old age. *Journal of Molecular and Cellular Cardiology* **18**, 39–53 (1986).

237. Gilsbach, R. *et al.* Distinct epigenetic programs regulate cardiac myocyte development and disease in the human heart in vivo. *Nat Commun* **9**, 391 (2018).

238. Krane, M. *et al. Sequential defects in cardiac lineage commitment and maturation cause hypoplastic left heart syndrome*. 2021.04.24.441110 https://www.biorxiv.org/content/10.1101/2021.04.24.441110v1 (2021) doi:10.1101/2021.04.24.441110.

239. Zhurinsky, J. *et al.* A Coordinated Global Control over Cellular Transcription. *Current Biology* **20**, 2010–2015 (2010).

240. Riedl, J. *et al.* Lifeact: a versatile marker to visualize F-actin. *Nat Methods* **5**, 605–607 (2008).

241. Flores, L. R., Keeling, M. C., Zhang, X., Sliogeryte, K. & Gavara, N. Lifeact-TagGFP2 alters F-actin organization, cellular morphology and biophysical behaviour. *Sci Rep* **9**, 3241 (2019).

242. Courtemanche, N., Pollard, T. D. & Chen, Q. Avoiding artefacts when counting polymerized actin in live cells with LifeAct fused to fluorescent proteins. *Nat Cell Biol* **18**, 676–683 (2016).

243. Spracklen, A. J., Fagan, T. N., Lovander, K. E. & Tootle, T. L. The pros and cons of common actin labeling tools for visualizing actin dynamics during Drosophila oogenesis. *Developmental Biology* **393**, 209–226 (2014).

244. Yin, Z., Xu, X. L. & Frasch, M. Regulation of the twist target gene tinman by modular cis-regulatory elements during early mesoderm development. *Development* **124**, 4971–4982 (1997).

245. Patel, S. *et al.* Functional characterisation of filamentous actin probe expression in neuronal cells. *PLOS ONE* **12**, e0187979 (2017).

246. Briggs, L. E. *et al.* Wnt/β-catenin and sonic hedgehog pathways interact in the regulation of the development of the dorsal mesenchymal protrusion. *Dev. Dyn.* **245**, 103–113 (2016).

247. Gessert, S. & Kühl, M. The multiple phases and faces of wnt signaling during cardiac differentiation and development. *Circ. Res.* **107**, 186–199 (2010).

248. Vogler, G., Hum, B., Tamayo, M., Altman, Y. & Bodmer, R. *Single-cell sequencing of the Drosophila embryonic heart and muscle cells during differentiation and maturation*. 2021.01.15.426556 https://www.biorxiv.org/content/10.1101/2021.01.15.426556v1 (2021) doi:10.1101/2021.01.15.426556.

249. Venken, K. J. T. *et al.* MiMIC: a highly versatile transposon insertion resource for engineering Drosophila melanogaster genes. *Nature Methods* **8**, 737–743 (2011).

250. Nagarkar-Jaiswal, S. *et al.* A library of MiMICs allows tagging of genes and reversible, spatial and temporal knockdown of proteins in Drosophila. *eLife* **4**, e05338 (2015).

251. Riedel, F., Vorkel, D. & Eaton, S. Megalin-dependent Yellow endocytosis restricts melanization in the Drosophila cuticle. *Development* **138**, 149–158 (2011).

252. Dietzl, G. *et al.* A genome-wide transgenic RNAi library for conditional gene inactivation in Drosophila. *Nature* **448**, 151–156 (2007).

253. Lee, S., Bao, H., Ishikawa, Z., Wang, W. & Lim, H.-Y. Cardiomyocyte Regulation of Systemic Lipid Metabolism by the Apolipoprotein B-Containing Lipoproteins in Drosophila. *PLoS Genet* **13**, e1006555 (2017).

254. Herz, J. & Strickland, D. K. LRP: a multifunctional scavenger and signaling receptor. *J Clin Invest* **108**, 779–784 (2001).

255. Kozyraki, R. & Gofflot, F. Multiligand endocytosis and congenital defects: roles of cubilin, megalin and amnionless. *Curr Pharm Des* **13**, 3038–3046 (2007).

256. Stefansson, S., Chappell, D. A., Argraves, K. M., Strickland, D. K. & Argraves, W. S. Glycoprotein 330/low density lipoprotein receptor-related protein-2 mediates endocytosis of low density lipoproteins via interaction with apolipoprotein B100. *J Biol Chem* **270**, 19417–19421 (1995).

257. May, P. & Herz, J. LDL Receptor-Related Proteins in Neurodevelopment. *Traffic* **4**, 291–301 (2003).

258. Bellen, H. J. *et al.* The Drosophila gene disruption project: progress using transposons with distinctive site specificities. *Genetics* **188**, 731–743 (2011).

259. Tseng, A.-S., Engel, F. B. & Keating, M. T. The GSK-3 Inhibitor BIO Promotes Proliferation in Mammalian Cardiomyocytes. *Chemistry & Biology* **13**, 957–963 (2006).

260. Kawagishi, H. *et al.* Sonic hedgehog signaling regulates the mammalian cardiac regenerative response. *Journal of Molecular and Cellular Cardiology* **123**, 180–184 (2018).

261. Wieschaus, E. & Nüsslein-Volhard, C. The Heidelberg Screen for Pattern Mutants of Drosophila: A Personal Account. *Annu. Rev. Cell Dev. Biol.* **32**, 1–46 (2016).

262. Vignier, N., Mougenot, N., Bonne, G. & Muchir, A. Effect of genetic background on the cardiac phenotype in a mouse model of Emery-Dreifuss muscular dystrophy. *Biochem Biophys Rep* **19**, 100664 (2019).

263. Medert, R. *et al.* Genetic background influences expression and function of the cation channel TRPM4 in the mouse heart. *Basic Res Cardiol* **115**, 70 (2020).

264. Jelinek, M., Wallach, C., Ehmke, H. & Schwoerer, A. P. Genetic background dominates the susceptibility to ventricular arrhythmias in a murine model of β-adrenergic stimulation. *Sci Rep* **8**, 2312 (2018).

265. Waters, S. *et al.* Genetic background influences adaptation to cardiac hypertrophy and Ca2+ handling gene expression. *Frontiers in Physiology* **4**, 11 (2013).

266. Kantarci, S. *et al.* Mutations in LRP2, which encodes the multiligand receptor megalin, cause Donnai-Barrow and facio-oculo-acoustico-renal syndromes. *Nat Genet* **39**, 957–959 (2007).

267. Zilberberg, A., Yaniv, A. & Gazit, A. The low density lipoprotein receptor-1, LRP1, interacts with the human frizzled-1 (HFz1) and down-regulates the canonical Wnt signaling pathway. *J Biol Chem* **279**, 17535–17542 (2004).

268. MacDonald, B. T. & He, X. Frizzled and LRP5/6 receptors for Wnt/β-catenin signaling. *Cold Spring Harb Perspect Biol* **4**, a007880 (2012).

269. Zywitza, V., Misios, A., Bunatyan, L., Willnow, T. E. & Rajewsky, N. Single-Cell Transcriptomics Characterizes Cell Types in the Subventricular Zone and Uncovers Molecular Defects Impairing Adult Neurogenesis. *Cell Reports* **25**, 2457-2469.e8 (2018).

270. Chen, C. M. & Struhl, G. Wingless transduction by the Frizzled and Frizzled2 proteins of Drosophila. *Development* **126**, 5441–5452 (1999).

271. Tang, M. *et al.* Pygopus maintains heart function in aging Drosophila independently of canonical Wnt signaling. *Circ Cardiovasc Genet* **6**, 472–480 (2013).

272. Gajera, C. R. *et al.* LRP2 in ependymal cells regulates BMP signaling in the adult neurogenic niche. *Journal of Cell Science* **123**, 1922–1930 (2010).

273. Christ, A. *et al.* LRP2 Is an Auxiliary SHH Receptor Required to Condition the Forebrain Ventral Midline for Inductive Signals. *Developmental Cell* **22**, 268–278 (2012).

274. Christ, A., Marczenke, M. & Willnow, T. E. LRP2 controls sonic hedgehog-dependent differentiation of cardiac progenitor cells during outflow tract formation. *Hum Mol Genet* **29**, 3183–3196 (2020).

275. Rochais, F., Mesbah, K. & Kelly, R. G. Signaling Pathways Controlling Second Heart Field Development. *Circulation Research* **104**, 933–942 (2009).

276. Francou, A. *et al.* Second heart field cardiac progenitor cells in the early mouse embryo. *Biochimica et Biophysica Acta (BBA) - Molecular Cell Research* **1833**, 795–798 (2013).

277. Dyer, L. A. & Kirby, M. L. The role of secondary heart field in cardiac development. *Developmental Biology* **336**, 137–144 (2009).

278. Kwon, C. *et al.* Canonical Wnt signaling is a positive regulator of mammalian cardiac progenitors. *PNAS* **104**, 10894–10899 (2007).

279. Cohen, E. D. *et al.* Wnt/β-catenin signaling promotes expansion of Isl-1–positive cardiac progenitor cells through regulation of FGF signaling. *J Clin Invest* **117**, 1794–1804 (2007).

280. Saraf, A., Book, W. M., Nelson, T. J. & Xu, C. Hypoplastic left heart syndrome: From bedside to bench and back. *Journal of Molecular and Cellular Cardiology* **135**, 109–118 (2019).

281. Szklarczyk, D. *et al.* STRING v11: protein-protein association networks with increased coverage, supporting functional discovery in genome-wide experimental datasets. *Nucleic Acids Res* **47**, D607–D613 (2019).

282. Mi, H., Muruganujan, A., Ebert, D., Huang, X. & Thomas, P. D. PANTHER version 14: more genomes, a new PANTHER GO-slim and improvements in enrichment analysis tools. *Nucleic Acids Res* **47**, D419–D426 (2019).

283. Evans, S. M., Yelon, D., Conlon, F. L. & Kirby, M. L. Myocardial lineage development. *Circ Res* **107**, 1428–1444 (2010).

284. Liu, J. & Stainier, D. Y. R. Zebrafish in the study of early cardiac development. *Circ Res* **110**, 870–874 (2012).

285. Bakkers, J. Zebrafish as a model to study cardiac development and human cardiac disease. *Cardiovasc Res* **91**, 279–288 (2011).

286. Fink, M. *et al.* A new method for detection and quantification of heartbeat parameters in Drosophila, zebrafish, and embryonic mouse hearts. *Biotechniques* **46**, 101–113 (2009).

287. Jin, H. *et al.* Genome-Wide Screens for In Vivo Tinman Binding Sites Identify Cardiac Enhancers with Diverse Functional Architectures. *PLOS Genetics* **9**, e1003195 (2013).

288. Akiyama-Oda, Y. & Oda, H. Early patterning of the spider embryo: a cluster of mesenchymal cells at the cumulus produces Dpp signals received by germ disc epithelial cells. *Development* **130**, 1735–1747 (2003).

289. Furth, N., Aylon, Y. & Oren, M. p53 shades of Hippo. *Cell Death Differ* **25**, 81–92 (2018).

290. Baker, N. E., Kiparaki, M. & Khan, C. A potential link between p53, cell competition and ribosomopathy in mammals and in Drosophila. *Dev. Biol.* **446**, 17–19 (2019).

291. Ma, J. & Ptashne, M. The carboxy-terminal 30 amino acids of GAL4 are recognized by GAL80. *Cell* **50**, 137–142 (1987).

292. James, A., Wang, Y., Raje, H., Rosby, R. & DiMario, P. Nucleolar stress with and without p53. *Nucleus* **5**, 402–426 (2014).

293. Destefanis, F., Manara, V. & Bellosta, P. Myc as a Regulator of Ribosome Biogenesis and Cell Competition: A Link to Cancer. *Int J Mol Sci* **21**, 4037 (2020).

294. Steller, H. Regulation of apoptosis in Drosophila. *Cell Death Differ* **15**, 1132–1138 (2008).

295. Lee, K. H., Xu, Q. & Breitbart, R. E. A new tinman-related gene, nkx2.7, anticipates the expression of nkx2.5 and nkx2.3 in zebrafish heart and pharyngeal endoderm. *Dev Biol* **180**, 722–731 (1996).

296. Uechi, T. *et al.* Ribosomal Protein Gene Knockdown Causes Developmental Defects in Zebrafish. *PLOS ONE* **1**, e37 (2006).

297. Targoff, K. L., Schell, T. & Yelon, D. Nkx Genes Regulate Heart Tube Extension and Exert Differential Effects on Ventricular and Atrial Cell Number. *Dev Biol* **322**, 314–321 (2008).

298. Corioni, M., Antih, N., Tanackovic, G., Zavolan, M. & Krämer, A. Analysis of in situ pre-mRNA targets of human splicing factor SF1 reveals a function in alternative splicing. *Nucleic Acids Research* **39**, 1868–1879 (2011).

299. Rino, J., Desterro, J. M. P., Pacheco, T. R., Gadella, T. W. J. & Carmo-Fonseca, M. Splicing Factors SF1 and U2AF Associate in Extraspliceosomal Complexes. *Mol Cell Biol* **28**, 3045–3057 (2008).

300. Dai, W. *et al.* ZO-1 Regulates Intercalated Disc Composition and Atrioventricular Node Conduction. *Circ Res* **127**, e28–e43 (2020).

301. Balestrini, S. *et al.* Cardiac phenotype in ATP1A3-related syndromes: A multicenter cohort study. *Neurology* **95**, e2866–e2879 (2020).

302. Hu, Y. *et al.* An integrative approach to ortholog prediction for disease-focused and other functional studies. *BMC Bioinformatics* **12**, 357 (2011).

303. Genuth, N. R. & Barna, M. Heterogeneity and specialized functions of translation machinery: from genes to organisms. *Nat. Rev. Genet.* **19**, 431–452 (2018).

304. Shi, Z. *et al.* Heterogeneous Ribosomes Preferentially Translate Distinct Subpools of mRNAs Genome-wide. *Molecular Cell* **67**, 71-83.e7 (2017).

305. Azpiazu, N. & Frasch, M. tinman and bagpipe: two homeo box genes that determine cell fates in the dorsal mesoderm of Drosophila. *Genes Dev.* **7**, 1325–1340 (1993).

306. Yang, K., Yang, J. & Yi, J. Nucleolar Stress: hallmarks, sensing mechanism and diseases. *Cell Stress* **2**, 125–140 (2018).

307. Boulon, S., Westman, B. J., Hutten, S., Boisvert, F.-M. & Lamond, A. I. The nucleolus under stress. *Mol Cell* **40**, 216–227 (2010).

308. Cui, Z. & DiMario, P. J. RNAi knockdown of Nopp140 induces Minute-like phenotypes in Drosophila. *Mol Biol Cell* **18**, 2179–2191 (2007).

309. James, A. *et al.* Nucleolar stress in Drosophila melanogaster. *Nucleus* **4**, 123–133 (2013).

310. Morcelle, C. *et al.* Oncogenic MYC Induces the Impaired Ribosome Biogenesis Checkpoint and Stabilizes p53 Independent of Increased Ribosome Content. *Cancer Res* **79**, 4348–4359 (2019).

311. Dai, M.-S., Sears, R. & Lu, H. Feedback regulation of c-Myc by ribosomal protein L11. *Cell Cycle* **6**, 2735–2741 (2007).

312. Barron, D. A. & Kagey, J. D. The role of the Hippo pathway in human disease and tumorigenesis. *Clin Transl Med* **3**, 25 (2014).

313. Del Re, D. P. The hippo signaling pathway: implications for heart regeneration and disease. *Clin Trans Med* **3**, 27 (2014).

314. Wang, J., Liu, S., Heallen, T. & Martin, J. F. The Hippo pathway in the heart: pivotal roles in development, disease, and regeneration. *Nat Rev Cardiol* **15**, 672–684 (2018).

315. Yu, L., Daniels, J. P., Wu, H. & Wolf, M. J. Cardiac hypertrophy induced by active Raf depends on Yorkie-mediated transcription. *Sci. Signal.* **8**, ra13–ra13 (2015).

316. Monroe, T. O. *et al.* YAP Partially Reprograms Chromatin Accessibility to Directly Induce Adult Cardiogenesis In Vivo. *Developmental Cell* **48**, 765-779.e7 (2019).

317. Xiao, Y., Leach, J., Wang, J. & Martin, J. F. Hippo/Yap Signaling in Cardiac Development and Regeneration. *Curr Treat Options Cardiovasc Med* **18**, 38 (2016).

318. Kaya-Çopur, A. *et al.* The Hippo pathway controls myofibril assembly and muscle fiber growth by regulating sarcomeric gene expression. *Elife* **10**, e63726 (2021).

319. Del Re, D. P. *et al.* Yes-associated protein isoform 1 (Yap1) promotes cardiomyocyte survival and growth to protect against myocardial ischemic injury. *J Biol Chem* **288**, 3977–3988 (2013).

320. von Gise, A. *et al.* YAP1, the nuclear target of Hippo signaling, stimulates heart growth through cardiomyocyte proliferation but not hypertrophy. *Proc Natl Acad Sci U S A* **109**, 2394–2399 (2012).

321. Jung, A. C., Ribeiro, C., Michaut, L., Certa, U. & Affolter, M. Polychaetoid/ZO-1 Is Required for Cell Specification and Rearrangement during Drosophila Tracheal Morphogenesis. *Current Biology* **16**, 1224–1231 (2006).

322. Choi, W. *et al.* The single Drosophila ZO-1 protein Polychaetoid regulates embryonic morphogenesis in coordination with Canoe/afadin and Enabled. *MBoC* **22**, 2010–2030 (2011).

323. Baldridge, D. *et al.* Model organisms contribute to diagnosis and discovery in the undiagnosed diseases network: current state and a future vision. *Orphanet J Rare Dis* **16**, 206 (2021).

324. Bellen, H. J., Wangler, M. F. & Yamamoto, S. The fruit fly at the interface of diagnosis and pathogenic mechanisms of rare and common human diseases. *Hum Mol Genet* **28**, R207–R214 (2019).

325. Harnish, J. M., Deal, S. L., Chao, H.-T., Wangler, M. F. & Yamamoto, S. In Vivo Functional Study of Disease-associated Rare Human Variants Using Drosophila. *J Vis Exp* (2019) doi:10.3791/59658.

326. Carniel, E. *et al.* Alpha-myosin heavy chain: a sarcomeric gene associated with dilated and hypertrophic phenotypes of cardiomyopathy. *Circulation* **112**, 54–59 (2005).

327. Gonzalez-Teran, B. *et al. Integration of Protein Interactome Networks with Congenital Heart Disease Variants Reveals Candidate Disease Genes*. 2021.01.05.423837 https://www.biorxiv.org/content/10.1101/2021.01.05.423837v1 (2021) doi:10.1101/2021.01.05.423837.

328. Hartman, H. A., Rossidis, A. C. & Peranteau, W. H. In Utero Gene Therapy and Genome Editing. *Curr Stem Cell Rep* **4**, 52–60 (2018).

329. Anttila, V. *et al.* Synthetic mRNA Encoding VEGF-A in Patients Undergoing Coronary Artery Bypass Grafting: Design of a Phase 2a Clinical Trial. *Molecular Therapy - Methods & Clinical Development* **18**, 464–472 (2020).

330. Gonçalves, G. A. R. & Paiva, R. de M. A. Gene therapy: advances, challenges and perspectives. *Einstein (Sao Paulo)* **15**, 369–375 (2017).

331. Bose, S. K., Menon, P. & Peranteau, W. H. In Utero Gene Therapy: Progress and Challenges. *Trends in Molecular Medicine* **27**, 728–730 (2021).

332. Grunert, M., Appelt, S., Dunkel, I., Berger, F. & Sperling, S. R. Altered microRNA and target gene expression related to Tetralogy of Fallot. *Sci Rep* **9**, 19063 (2019).

333. Wilson, K. D. *et al.* A Rapid, High-Quality, Cost-Effective, Comprehensive and Expandable Targeted Next-Generation Sequencing Assay for Inherited Heart Diseases. *Circ Res* **117**, 603–611 (2015).

334. Bergstralh, D. T., Lovegrove, H. E. & St Johnston, D. Discs Large Links Spindle Orientation to Apical-Basal Polarity in Drosophila Epithelia. *Curr Biol* **23**, 1707–1712 (2013).

335. Yoo, T. *et al.* A DLG2 deficiency in mice leads to reduced sociability and increased repetitive behavior accompanied by aberrant synaptic transmission in the dorsal striatum. *Mol Autism* **11**, 19 (2020).

336. Craven, S. E. & Bredt, D. S. PDZ Proteins Organize Synaptic Signaling Pathways. *Cell* **93**, 495–498 (1998).

337. Roberts, S., Delury, C. & Marsh, E. The PDZ protein discs-large (DLG): the 'Jekyll and Hyde' of the epithelial polarity proteins. *The FEBS Journal* **279**, 3549–3558 (2012).

338. Hellbach, A. Dlg1 is required for myofibrillar arrangement in the Drosophila heart. (Ludwig-Maximilians-Universität München, 2013).

339. Gomez-Cavazos, J. S. & Hetzer, M. W. The nucleoporin gp210/Nup210 controls muscle differentiation by regulating nuclear envelope/ER homeostasis. *J. Cell Biol.* **208**, 671–681 (2015).

340. Liu, X. *et al.* Genome Wide Association Study Identifies L3MBTL4 as a Novel Susceptibility Gene for Hypertension. *Scientific Reports* **6**, 30811 (2016).

341. Zaidi, S. *et al.* De novo mutations in histone modifying genes in congenital heart disease. *Nature* **498**, 220–223 (2013).

342. Bruneau, B. G. The developmental genetics of congenital heart disease. *Nature* **451**, 943–948 (2008).

8. Appendix

8.1 CHD candidate gene screen (Rickert-Sperling lab)

8.1.1 Introduction

As side project in the Rickert-Sperling lab, I screened a subset of potential novel CHD candidate genes to functionally characterize and prioritize them for further in-depth studies. The Rickert-Sperling lab developed a new bioinformatical approach to identify novel genes involved in CHD. For candidate gene identification, sequencing data sets of patients suffering from CHD and healthy individuals were combined, which were collected over 15 years of cardiovascular genetic research of the lab. This comprises data generated by whole genome sequencing, exome sequencing, and targeted re-sequencing. Furthermore, genome-wide methylation sequencing data, mRNA, and microRNAs sequencing were included.[4,68,332] At least publicly available gene lists and lists available for the Rickert-Sperling lab were added, with genes identified as cardiac relevant based on patient-derived sequencing data. In the next step, the genes were ranked by assigning them to six different categories, which are described as follows:

1. **Annotation** (gene overlaps with list of cardiovascular-associated genes from Cardiovascular Gene Annotation Initiative in collaboration with EMBL-EBI or is heart- or muscle relevant based on NimbleGen sequence capture array[4])
2. **Expression** (gene is differentially expressed in CHD patients)
3. **Methylation** (gene is differentially methylated in CHD patients)
4. **CNV** (gene is located in a copy number variation, which is associated with CHD)
5. **CHD gene** (gene overlaps with list of known CHD genes[2,48,333])
6. **miRtarget** (gene is differentially expressed and targeted by differentially expressed miRNA in CHD patients)

Five top candidate genes were selected, which were assigned to four different categories, but which were not annotated as cardiac-related (category 1) or CHD gene (category 5) at the time point of the analysis: Discs Large MAGUK Scaffold Protein 2 (*DLG2*), Lethal(3)Malignant Brain Tumor-Like Protein 4 (*L3MBTL4*), Nucleoporin 210 (*NUP210*), Zinc Finger FYVE-Type Containing 28 (*ZFYVE28*) and the Lysine Demethylase 5B (*KDM5B*).

DLG2 encodes a membrane-associated scaffold protein and is known to be involved in cell polarization and signal transduction.[334–337] Its fly ortholog *dlg1* is known to be essential for the myofibrillar arrangement in cardiomyocytes and *dlg1* knockdown leads to cardiac myofibrillar misarrangement (doctoral thesis Annette Hellbach, 2013, *unpublished*).[338] ***NUP210*** is a protein of the nuclear pore complex, which regulates the flow of macromolecules between the nucleus and the cytoplasm, and *NUP210* was shown to be a critical regulator of neuronal and muscle differentiation.[339]

L3MBTL4 is a histone methylase binding protein and a putative polycomb group protein, which acts as a transcriptional repressor and is already known as tumor repressor. It has been published that, overexpression of L3MBTL4 triggers hypertrophy and aorta thickening in rats.[340] **ZFYVE28** acts as a negative regulator of epidermal growth factor receptor (EGFR) signaling but has no direct link to CHD development yet. For the last candidate gene **KDM5B**, a Lysine Demethylase, Zaidi et al. found *de novo* mutations of *KDM5B* in patients with coarctation of the aorta. However, at this time point, it is not functionally analyzed, whether *KDM5B* is involved in causing the cardiac phenotype.[341]

8.1.2 Acknowledgments

All bioinformatical analysis was performed by Dr. Marcel Grunert. Functional heart analysis using the SOHA method was done to equal parts together with Dr. Emilie Auxerre-Plantié, while I mainly performed functional heart analysis using the Klassen method. Dr. Georg Vogler provided guidance regarding fly genetics and experiments and Prof. Rickert-Sperling overall scientific input and supervision.

8.1.3 Results and Discussion

In order to dissect the cardiac role of our highly promising candidate genes, we first took advantage of commercially available fly lines (Bloomington Drosophila Stock Center, Vienna Drosophila Resource Center) or fly lines kindly provided by other labs (overview in **Table 7**). Functional characterization of the fly lines was carried out using the SOHA method and the fluorescence-based Klassen method. Comparing the results generated with both methods (see **Table 7**) we observe the same heart phenotypes (except for the *l(3)mbt* overexpression lines). However, it becomes obvious, that the tdtK method is more sensitive in detecting altered heart parameters (i.e. SOHA method indicates a trend towards bigger heart diameters for UAS-*CG6051* RNAi 25500 or UAS-RFP::*l(3)mbt* III driven by the *Hand*$^{4.2}$-Gal4 driver, while the Klassen method indicates a significant increase in diameters). Furthermore, the SOHA method just partly detected altered heart parameters for flies overexpressing *l(3)mbt*, which we found severely affected with the Klassen method. On the other hand, the SOHA method detected increased arrhythmia for UAS-RFP::*l(3)mbt* II (*Hand*$^{4.2}$ -Gal4 driver), which was not seen with the tdtK method. Either this is a result of the dissection procedure, which is part of the SOHA method, or this phenotype becomes only visible independent from the nervous system inputs suggesting a kind of compensatory effect. We could test this hypothesis using an arrhythmia fly model.

In the following, I want to focus on the results obtained with the Klassen method, since it is more sensitive and reflects the gene function *in vivo* in the intact fly.

When the *Drosophila* ortholog *l(3)mbt* was overexpressed specifically in heart tissue of the fly using the *Hand*$^{4.2}$-Gal4,tdtK driver, I could already observe severe structural abnormalities and reduced fractional shortening of the fluorescence fly heart under the microscope. Analyses of the high frame rate movies revealed an increase of systolic heart diameters, which explains the reduced fractional shortening (**Figure 40** A). I performed immunohistochemistry staining on *Hand*$^{4.2}$-Gal4, tdtK>GFP::*l(3)mbt* (exemplarily shown in **Figure 40** C), *Hand*$^{4.2}$-Gal4, tdtK>RFP::*l(3)mbt* II and III to highlight the sarcomere structure of the fly hearts. I observed, that the myofibrils, which are normally circularly oriented around the heart tube, show a disordered structure in the *l(3)mbt* overexpressing flies. Furthermore, I observed a ballooning of some heart tube segments, most often around the ostia. Overexpression of *l(3)mbt* in heart and muscle tissue (using the *Mef2*-Gal4 driver) causes lethality.

For further examination of the role of *l(3)mbt* in the heart, an RNAi targeting *l(3)mbt* was expressed in the heart. Furthermore, two different mutations, which express a truncated version of the protein and a deficiency line, which exhibit a partial deletion of the third chromosome including *l(3)mbt*, were analyzed. I did not observe any alterations in fly heart parameters in heterozygous mutants (**Figure 40** B). Gene KD by RNAi didn't lead to morphological abnormalities revealed by phalloidin staining (F-Actin), while the mutants haven't been tested yet. With SOHA analysis we furthermore saw that the transheterozygous mutant combining both *l(3)mbt* mutations develops contractility and rhythmicity defects suggesting that a loss of *l(3)mbt* can also lead to heart defects, similar to the overexpression of the gene.

Another gene that I found to cause severe functional and structural disorders in the fly heart when knocked down is *discs large 1* (*Dlg1*), the fly ortholog of human Discs Large MAGUK Scaffold Protein 2 (***DLG2***). The effect of two different RNAi lines targeting *Dlg1* in the heart was examined. Flies expressing *Dlg1*i #41134 RNAi show elevated heart diameters and a reduced fractional shortening, while *Dlg1*i #41136 RNAi show no differences in heart diameters, but also reduced fractional shortening (**Figure 41**). A third RNAi line caused lethality when expressed in the heart. Both fly lines, which exhibit a *Dlg1* knockdown show a chaotic myofibrillar arrangement (Dlg1i #41134 is exemplarily shown in **Figure 41 B**). Note, that the UAS-line by itself without a Gal4 driver (middle panel **Figure 41 B**) already shows a slightly disorganized myofibril organization. The UAS-line is probably "leaky" so that a low amount of RNAi is expressed in absence of a driver. The structural defects confirm the observations from Dr. Annette Hellbach in 2013.[338]

Table 7: Overview of fly lines and results of functional gene analysis. Antibody staining was used to assess knockdown (KD) or overexpression (OE) of a gene of interest (last column). IHC = Immunohistochemistry. SD = systolic diameter, DD = diastolic diameter, FS = fractional shortening, SI = systolic interval, DI = diastolic interval, SV = stroke volume, CO = cardiac output. tbd = to be done, " -" = no data

human Gene	fly gene	transgenic type	fly line	driver line	heart phenotype (SOHA method)	heart phenotype (Klassen method)	structural phenotype (IHC)	protein expression (antibody staining)
L3MBTL4	l(3)mbt	RNAi (knockdown)	UAS-l(3)mbt RNAi	Hand4.2-Gal4	no effect	no effect	no phenotype	reduced l(3)mbt expression
				Mef2-Gal4	no effect	-	tbd	-
		mutant	l(3)mbt GM76 (heterozygous)		no effect	no effect	tbd	-
			l(3)mbt E2 (heterozygous)		no effect	no effect	tbd	-
			l(3)mbt GM76/ l(3)mbt E2 (transheterozygous)		increased arrhythmia and increased SD	-	tbd	-
		Deficiency	Df (l(3)mbt) (heterozygous)		-	no effect	tbd	-
		overexpression	UAS-GFP::l(3)mbt	Hand4.2-Gal4	no effect	increased SD, decreased FS	myofibrilar misarrangement, variable diamters within the heart	increased l(3)mbt expression
				Mef2-Gal4	lethal	-	-	-
			UAS-RFP::l(3)mbt II	Hand4.2-Gal4	increased arrhythmia	increased SD, decreased FS	myofibrilar misarrangement, variable diamters within the heart	increased l(3)mbt expression
				Mef2-Gal4	increased lethality at 25 °C	-	-	-
				Mef2-Gal4	no significant phenotype at 18 °C	-	-	-
			UAS-RFP::l(3)mbt III	Hand4.2-Gal4	trend towards increased diameters	increased SD and DD, trend towards decreased FS	myofibrilar misarrangement, variable diamters within the heart	-
				Mef2-Gal4	lethal	-	-	-
ZFYVE28	CG6051	RNAi (knockdown)	UAS-CG6051 RNAi 25500	Hand4.2-Gal4	trend to bigger DD and SD	increased SD and DD	tbd	no antibody
				Mef2-Gal4	prolonged HP (prolonged DI and SI), increased arrhythmia; decreased CO	-	-	
			UAS-CG6051 RNAi 25503	Hand4.2-Gal4	trend to bigger SD and DD	increased DD	tbd	
				Mef2-Gal4	bigger DD and SD; increased FS and SV; trend to increased CO	-	-	
DLG2	Dlg1	RNAi (knockdown)	UAS-Dlg1 RNAi 41134	Hand4.2-Gal4	increased DD and SD	increased SD and DD, decreased FS	dilated heart, myofibrilar misarrangement	reduced Dlg1 expression
				Mef2-Gal4	lethal	-	-	-
			UAS-Dlg1 RNAi 33620	Hand4.2-Gal4	lethal	lethal	in progress	-
				Mef2-Gal4	lethal	-	-	-
			UAS-Dlg1 RNAi 41136	Hand4.2-Gal4	-	decreased FS	dilated heart, myofibrilar misarrangement	reduced Dlg1 expression
				Mef2-Gal4	-	-	-	-
NUP210	Gp210	mutant	Gp210 mut (heterozygous)		-	decreased DD	tbd	antibody available, assessment of protein expression of Gp210 tbd
		mutant	Gp210 MIMICin (heterozygous)		-	no effect	tbd	
		mutant	Gp210 MIMICex (heterozygous)		-	no effect	tbd	
		Deficiency	Df (Gp210) (heterozygous)		-	no effect	tbd	
KDM5B	lid	mutant	lid 10424 (heterozygous)		-	constricted, shorter HR	mild myofibrilar misarrangement	no antibody
			lid C386 (heterozygous)		-	decreased DD	-	

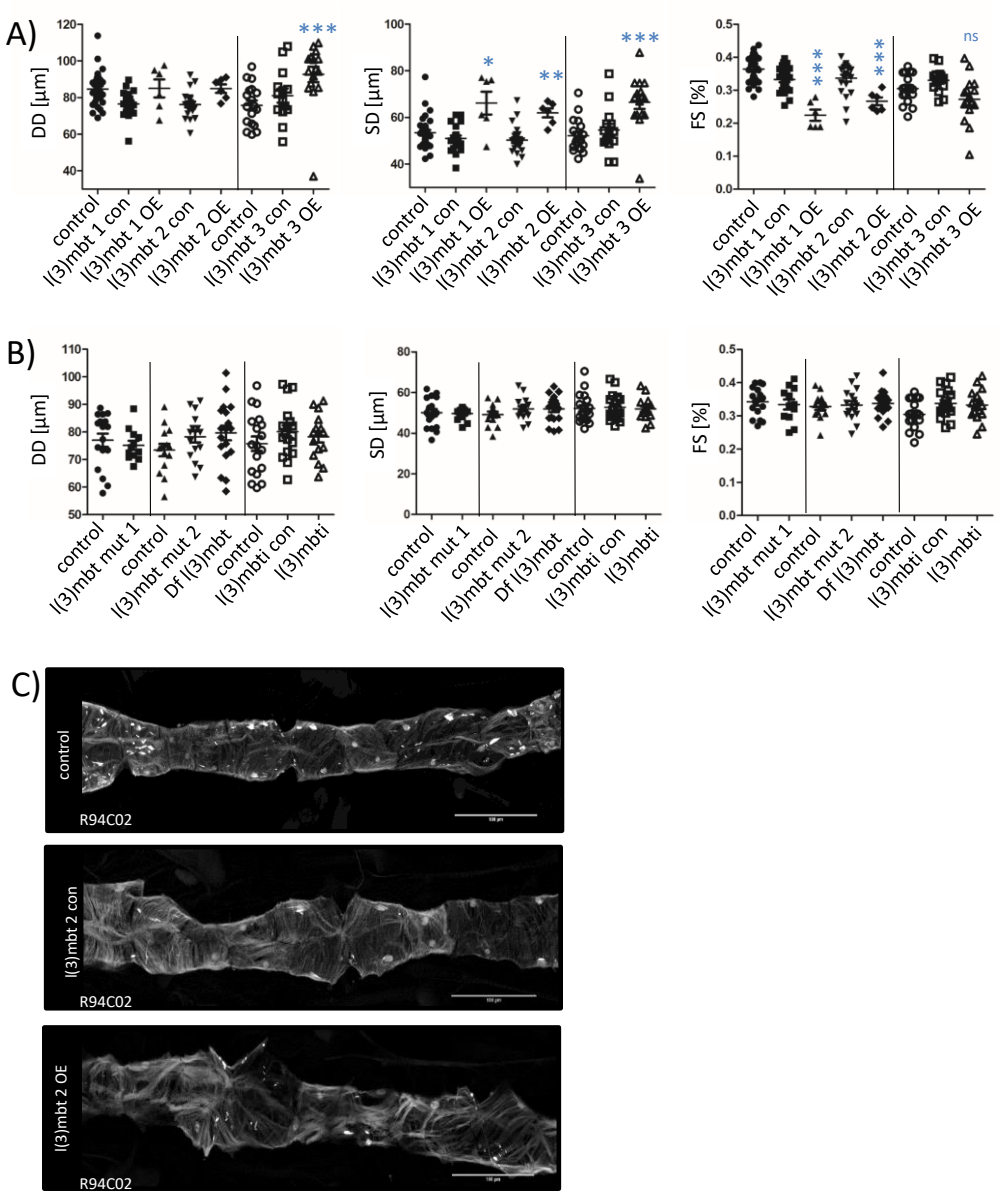

Figure 40: Overexpression of *l(3)mbt* specifically in the fly heart leads to decreased fractional shortening and structural abnormalities. Functional heart analysis of 3-week-old flies using the Klassen method (n(flies) =7 – 21, each dot represents one fly**.** Displayed is the mean ± SEM of the diastolic and systolic diameters and fractional shortening (FS=DD/SD). (**A)** Three fly lines, which overexpress *l(3)mbt* specifically in the heart using the *Hand*$^{4.2}$-Gal4,tdtK driver. l(3mbt 1 = *l(3)mbt*::RFP II, l(3mbt 2 = *l(3)mbt*::GFP, l(3)mbt 3 = *l(3)mbt*::RFP III. l(3)mbt 1/2/3 con (= UAS-*l(3)mbt* x GDcon) check for effects by the UAS line by itself without driver. (**B)** Flies harboring a heterozygous mutation of *l(3)mbt* (l(3)mbt mut 1 = *l(3)mbt*$^{E2/+}$, l(3)mbt mut 2 = *l(3)mbt*$^{GM76/+)}$ or a heterozygous deficiency for *l(3)mbt (*Df l(3)mbt = *l(3)mbt*$^{Deficiency/+}$). Last three genotypes display flies expressing RNAi against *l(3)mbt* (*l(3)mbt*i) in the heart using the *Hand*$^{4.2}$-Gal4,tdtK driver. *l(3)mbt*i con checks for effects by the UAS line itself. Statistics: Mann-Whitney-U test. Significances indicated are compared to control (Hand,tdtK x GDcon or tdtK x GDon). The vertical line separates two data sets generated at different time points. (**C)** Representative images of 3-week-old female fly hearts overexpressing *l(3)mbt* and controls, which express RFP from the *R94C02* heart enhancer.

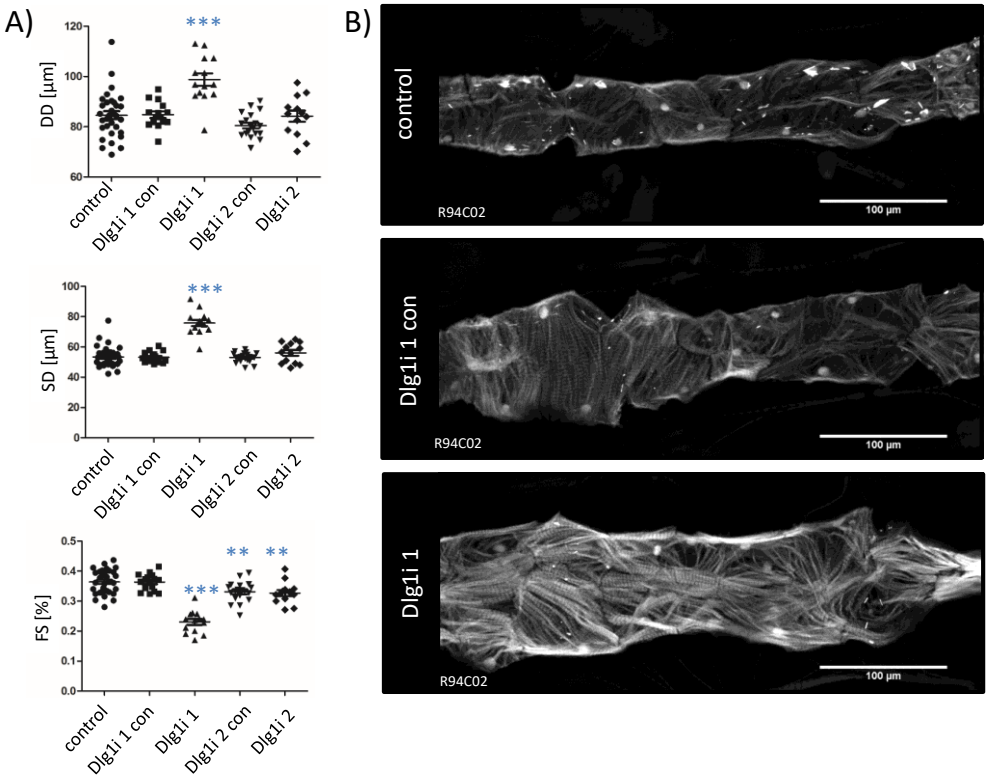

Figure 41: Flies knocked down for *Dlg1* in the heart show decreased fractional shortening and a chaotic myofibrillar arrangement. Fluorescence –based heart analysis of 3-week-old flies (n = 14 – 25, each dot represents one fly). **(A)** Displayed are diastolic and systolic diameters and fractional shortening (FS=DD/SD) of flies, which express RNAi targeting *Dlg1* specifically in the heart using the Hand$^{4.2}$-Gal4,tdtK driver (Dlg1i 1 = *Dlg1* RNAi #41134, Dlg1i 2 = *Dlg1* RNAi #41136). Hand,tdtK;GDcon flies serve as wild type control. Dlg1i 1 con and Dlg1i 2 con check for effects by the UAS lines themselves without Gal4 driver. Depicted is the mean ± SEM. Statistics: Mann-Whitney-U test. Significances indicated are compared to control. (**B)** Representative image of 3-week-old female fly hearts knocked down for *Dlg1*, which express RFP from the *R94C02* heart enhancer.

We further investigated the nucleopore protein ***NUP210*** fly ortholog, *Glycoprotein 210* (*Gp210*). I tested several different fly lines, which are predicted to lead to a decrease in *Gp210* expression (3 different mutant lines, named Gp210mut, Gp210MIMICin, and Gp210MIMICex, and one deficiency line including *Gp210* gene deletion). Heterozygous Gp210mut mutant flies show a significant decrease in diastolic diameters, while Gp210MIMICin and Gp210MIMICex heterozygotes show no alteration in heart parameters (**Figure 42** A). The basis of the conflicting results could be different levels of gene knockdown in the different Gp210 mutants and therefore, Gp210 gene and/or protein expression should be determined.

When knocking down the *zinc finger FYVE-type containing 28* (***ZFYVE28***) fly ortholog *CG6051* in heart tissue using two different RNAi (**Figure 42** B), I observed dilation of the heart. While the diastolic diameters are increased for both RNAi lines, the systolic diameter is only significantly increased in *Hand*$^{4.2}$-Gal4,tdtK>CG6051 RNAi #25500 flies.

The last candidate gene obtained from the bioinformatic ranking is *lid*, which is the fly ortholog of Lysine-specific demethylase 5B (***KDM5B***). Two independent heterozygous *lid* mutants show

constriction of the heart tube (see **Table 7**). Furthermore, *lid*^{10424} heterozygotes exhibit a decrease in heart rate along with arrhythmia of the heart, indicated by an increase of MAD_DI (trend towards higher values) and significantly increase of MAD_SI. (**Figure 42** C). MAD is the abbreviation for Median Absolute Deviation (for example: MAD_DI indicates the Median Absolute Deviation of the ΔDIs (ΔDI = difference between one diastolic interval compared to the following diastolic interval).

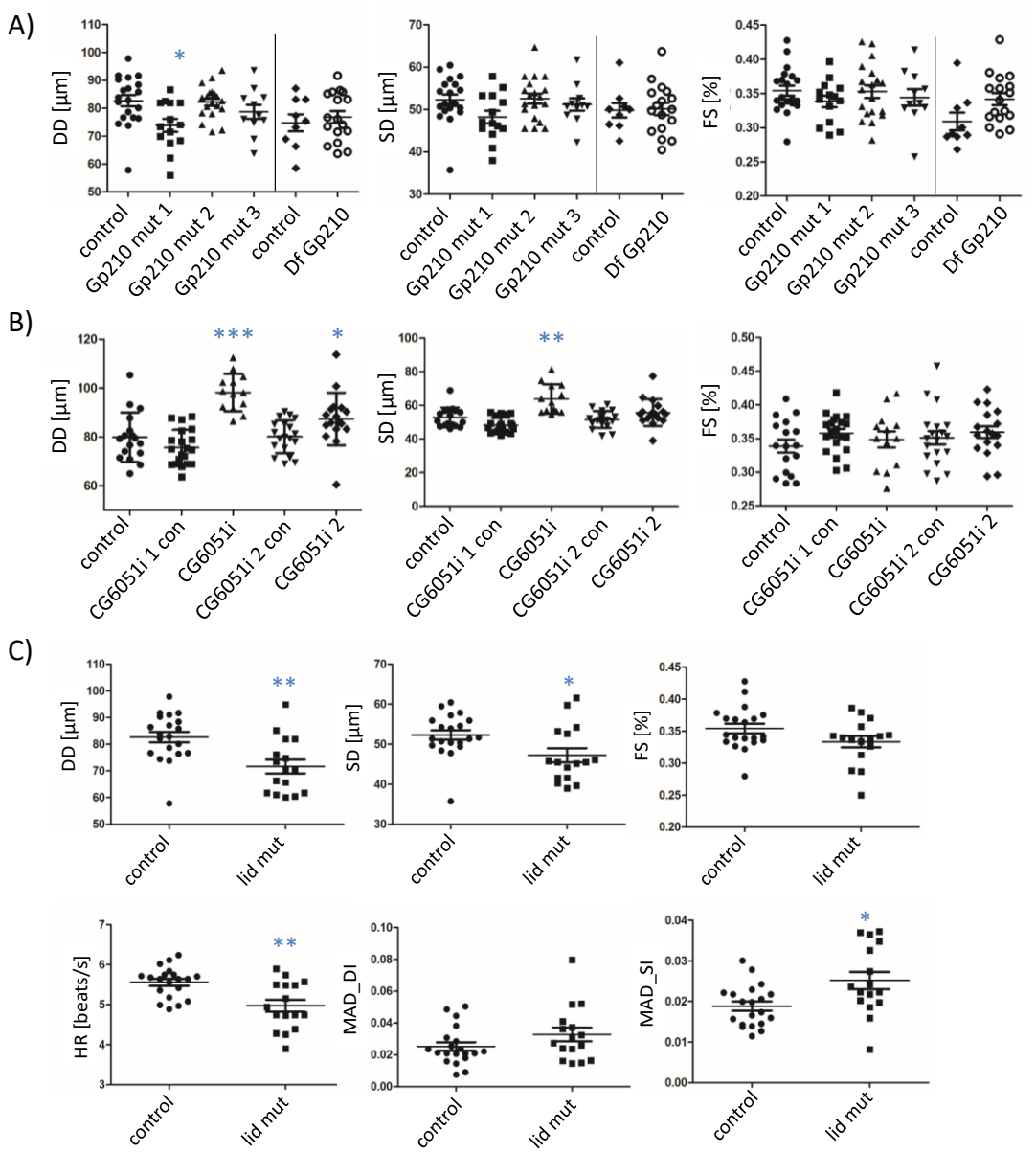

Figure 42: Effect of fly ortholog *CG6051, Gp210,* and *lid* on heart function of adult flies. Fluorescence –based heart analysis of 3-week-old flies (n = 11 – 25, each dot represents one fly). **(A)** Displayed are the mean ± SEM of diastolic and systolic diameter and fractional shortening (FS=DD/SD) of three heterozygous Gp210 mutant fly lines and one heterozygous *Gp210* deficiency fly line. Gp210 mut 1 = *Gp210* mut/+, Gp210 mut 2 = *Gp210* MIMICex/+, Gp210 mut 2 = *Gp210* MIMICin/+. tdtK;yw and tdtK;GDcon serve as controls. **(B)** Displayed are the mean ± SEM of diastolic and systolic diameter and fractional shortening (FS=DD/SD) of flies knocked down for *CG6051* (CG6051i 1 = *CG6051* RNAi 25550, CG6051i 2 = *CG6051* RNAi 25503). Hand$^{4.2}$-Gal4,tdtK;GDcon flies serve as controls. CG6051i 1/2 con check for effects by the UAS-line itself in absence of a Gal4 driver line. **(C)** Mean ± SEM of the diastolic diameters, systolic diameters, and fractional shortening (FS=DD/SD) of heterozygous *lid* mutant flies (lid mut = *lid*$^{10424/+}$) as well as heart rate (HR) and MAD_DI and MAD_SI (explanation in the text). Statistics: Whitney-Mann-U test or Kruskal-Wallis test. Significances indicated are compared to the respective control (Hand,tdtK;GDcon, tdtK;GDcon or tdtK;yw). MAD= Median Absolute Deviation.

In summary, while a potential role of *Gp210* in the heart requires further investigation, I found that manipulation of *l(3)mbt, CG6051, lid* and *Dlg1* gene levels in the fly leads to cardiac defects, which prioritizes those genes as highly promising novel CHD candidate genes for in-depth investigations. As a next step, it would be interesting to dissect the genetic pathways underlying the fly heart phenotypes by probing for the genetic interaction partners and downstream effectors of these genes. Given the polygenic etiology underlying many CHDs, I further propose to test for genetic interactions between the candidates and known CHD genes with a focus on cardiac transcription factors *NKX2-5/tinman*, *GATA4/pannier,* and *TBX5*/*Dorsocross*, which when muted lead to discrete CHDs in humans.[342] Identifying genetic interactors (i.e by observing a worsening of heart phenotypes upon gene combinations) could help unravel the mechanisms of action of our candidate genes and how they could potentially contribute to the development of CHDs.

8.2 Validation of *RpS15Aa* and *RpL13* knockdown phenotype

Table 8: Validation of RpS15Aa and RpL13 knockdown phenotypes for work of Dr. Analyne Schroeder.[124] Functional heart analysis with fluorescent reporter in 1-week old female flies. DD= diastolic diameter, SD= systolic diameter, FS= fractional shortening, HP= heart period, DI= diastolic interval, SI= systolic interval, MAD_SI= median absolute deviation (SI), Hand= Hand$^{4.2}$-Gal4. Arrows indicate significant increase or decrease of parameters compared to controls.

Cross	heart phenotype	DD	SD	FS	HP	DI	SI	MAD_SI
Hand, tdtk x RpS15Aa RNAi GD19198	partial heart	-	-	-	-	-	-	-
Hand, tdtk x RpS15Aa RNAi GD50635	constriction	↓	↓					
Hand, tdtk x RpS15Aa RNAi TRIP	constriction	↓	↓		↓			
Hand, tdtk x RpS15Aa RNAi 2033R-2 III	short heart period				↓		↓	
Hand, tdtk x RpS15Aa RNAi 2033R-3 III/TM3	partial /no heart	-	-	-	-	-	-	-
Hand, tdtk x RpS15Aa RNAi # 50344	partial heart	-	-	-	-	-	-	-
tdtk x Df(RpS15Aa)	dilation			↑	↓	↓		-

Cross	heart phenotype	DD	SD	FS	HP	DI	SI	MAD_SI
Hand, tdtk x RpL13 KK109503	pupal lethal	-	-	-	-	-	-	-
Hand, tdtk x RpL13 4651 R-2	partial heart, severe constrictions	-	-	-	-	-	-	-
Hand, tdtk x RpL13 RNAi 4651 R-1	some constrictions		-		↑	↑		
tdtk x RpL13 mutant	dilation	↑	↑		↓	↓	↓	↓

Publication list

Publications

Auxerre-Plantié*, E., **Nielsen*, T.**, Grunert*, M., Olejniczak, O., Perrot, A., Oezcelik, C., Harries, D., Matinmehr, F., Del Remedios, C., Muehlfeld, C., Kraft, T., Bodmer, R., Vogler, G.# and Rickert-Sperling, S.# (2020) Identification of MYOM2 as a candidate gene in hypertrophic cardiomyopathy and Tetralogy of Fallot and its functional evaluation in the Drosophila heart. *Disease Models and Mechanisms*. dmm.045377, doi: 10.1242/dmm.045377. *co-first authors

Schroeder A. M.*, Allahyari M.*, Vogler G., Theis J. L., Missinato M. A., **Nielsen T.,** Yu M. S., Larsen L. A., Goyal P., Rosenfeld J., Nelson T. J., Olson T. M., Colas A. R., Bodmer R., Grossfeld P. (2019). Model System Identification of Novel Congenital Heart Disease Gene Candidates: focus on RPL13. *Human Molecular Genetics* 28, 23:3954-3969.

Theis*, J. L., Vogler*, G., Missinato*, M. A., Li*, X., **Nielsen, T.,** Zeng, X-X I., Martinez-Fernandez*, A., Walls, S., Kervadec, A., Kezos, J. N., Birker, K., Evans, J. M., O'Byrne, M. M., Fogarty, Z. C., Ocorr, K., Terzic, A., Grossfeld, P., Ocorr, K., Nelson, T. J. #, Olson, T. M. #, Colas, A. R. #, Bodmer, R. # and the Wanek Family Foundation for Hypoplastic Left Heart Syndrome. (2020). Patient-specific genomics and cross-species functional analysis implicate LRP2 in hypoplastic left heart syndrome. *eLife* 2020;9:e59554, doi: 10.7554/eLife.59554.

Nielsen*, T., Kervadec*, A., Zeng, Xin-Xin I., Theis, J. L., Walls, S., Missinato M. A., Schroeder, A., Birker, K., Olson, T. M., Nelson, T. J., Ocorr, K., Grossfeld, P., Colas, A. R., Bodmer, R., Vogler, G. Functional analysis across model systems implicates ribosomal protein genes in growth defects associated with hypoplastic left heart syndrome. *In submission.* *co-first authors

Oral presentations

Nielsen, T., Kervadec A, Zeng X-X I., Schroeder A, Theis J, Olson T, Ocorr K, Grossfeld P, Colas, AR, Vogler G, Bodmer R (2020). "Rescue of a missing heart: The role of ribosomal proteins in congenital heart disease"**.** Talk (The Allied Genetics Conference (TAGC) 2020, Online format).

Nielsen, T. (2018). Unraveling Genetic Heterogeneity of Congenital Heart Disease by FLASHING into gene function. Talk (MDC-FMP PhD retreat, Berlin, Germany).

Nielsen, T. (2018). Flashing into gene function: A new method for Facing Genetic Heterogeneity of Congenital Heart Disease. Talk (DZHK symposium partner side Berlin, Germany).

Poster presentations

Nielsen, T., Kervadec, A., Zeng, Xin-Xin I., Schroeder, A., Theis, J. L., Olson, T. M., Ocorr, K., Grossfeld, P., Colas, A. R., Vogler, G., Bodmer, R. (2020) Rescue of a missing heart: The role of ribosomal proteins in congenital heart disease. (19th Annual Trainee Research Symposium, Sanford Burnham Prebys, La Jolla, USA).

Nielsen, T., Vogler, G., Missinato, M. A., Theis, J. L., Kervadec, A., Olson, T. M., Nelson, T. J., Colas, A., Bodmer, R. (2019) Identification of new disease-related interactions in HLHS applying systems genetics in hiPSCs and the Drosophila heart. (18th Annual Trainee Research Symposium, Sanford Burnham Prebys, La. Jolla, USA).

Plantié, E.*, Olejniczak, O.*, **Nielsen, T.*,** Grunert, M., Vogler, G., Bodmer, R. and Rickert-Sperling, S. (2018). A potential role for *MYOM2* in Tetralogy of Fallot and Hypertrophic Cardiomyopathy Using the *Drosophila* Heart as a Model. Poster (Muscle Development, Regeneration and Disease Conference, Berlin, Germany). *co-first authors

Nielsen T., Plantié E., Olejniczak O., Grunert M., Vogler G., Bodmer R. and Rickert-Sperling S. (2018). Unravel Genetic Heterogeneity in Congenital heart diseases by flashing into gene function. Poster (6th DZHK Retreat and 5th Young DZHK Retreat, Königstein im Taunus, Germany).

Nielsen T., Plantié E., Olejniczak O., Grunert M., Vogler G., Bodmer R. and Rickert-Sperling S. (2017). Large-scale in vivo functional analyses of the genetic network involved in Congenital Heart Diseases using the Drosophila heart as a model. Poster (5th DZHK Retreat and 4th Young DZHK Retreat, Warnemünde, Germany).

Acknowledgements

At this point, I would like to take the opportunity and thank all the people who made this doctoral thesis possible! Unfortunately, I won't be able to mention every single one!

First of all, I would like to thank Prof. Silke Rickert-Sperling, who gave me the opportunity to start my doctoral thesis in her lab on a very exciting topic. I would like to thank you for the excellent scientific support; I have particularly benefited from your way of critical questioning scientific experiments and causalities, which has accompanied me positively and helpful in my everyday laboratory work since.

My deep thanks go to Prof. Rolf Bodmer, without whose help I could not have completed this doctoral thesis! In particular, I would like to thank you for your trust by inviting me to be part of your lab in San Diego, as well as, of course, for your scientific supervision/support, inspiration and all the encouraging words, especially in the second part of my doctoral thesis!
Someone who has supervised me from beginning to the end, first through numerous zoom calls "Berlin-San Diego" and then here in the Bodmer lab, is "*Drosophila* expert" Dr. Geo Vogler! It feels like I owe you ca. 80 % of my *Drosophila* knowledge! "*Geo, can I ask you something*?" - "*You just did*!" But I always got an answer, support, and new inspirations for my projects! Thanks very much!

My thanks to our collaboration partners, the Colas Lab, and the Mayo Clinic for effective and great collaboration in the fight against HLHS! I would also like to thank *Disease Models and Mechanism* for the permission to use the contents from our publication in this thesis!

Warmest thanks also to the other members of the Rickert-Sperling lab! I would particularly like to thank Dr. Emilie Auxerre-Plantié, who did a great job teaching me how to dissect fly hearts and got me started in *Drosophila* research! We had lots of small detail and big picture discussions, and you always had an open ear! Warmest thanks to Olga Olejniczak - my Ph.D. student lab partner and very good friend through thick and thin! Exploring the *Drosophila* world and Berlin together was a lot of fun! Thanks also to Kerstin, Marcel, and Sandra, and all the rest of the Rickert-Sperling Group, which supported me in my projects and with who I shared lots of fun lunches and Christmas market/beer garden visits!
I also want to thank the "fly ladies" Annelie, Eva, and Sarah for our monthly *Drosophila* heart meetings with lots of good discussions, troubleshooting, and one or two after-work drinks!

A big "thank you" goes to the Bodmer-Ocorr lab who immediately welcomed me to San Diego! Many thanks to Prof. Karen Ocorr for her scientific input and the well-thought feedback during our lab meetings. Many thanks to my SPB gang: Katja, Cristiana, Marco, and Jimmy! The time in the lab, but also outside the lab (!), would not have been nearly the same without you, guys! Katja, thanks for your

Canadian-style helpfulness from the very beginning (even before I got to San Diego) till the end; such an impressively organized person with such crazy laugh attacks is a rare find!
Thanks also to all additional and former members of the Bodmer lab (Analyne, Stan, Clara, Natalie, Helia, Bill, Soda, Kara, Bosco, Sean, Arthur, Kat, Katya, Sreehari, Kathy, hope I got everyone…) for all kinds of support in my project, for all the scientific and non-scientific discussions that kept me motivated, for the brewery outings, taco truck visits, and beach parties!

Finally, my deepest thanks go to all my beloved ones, and especially to my parents, who supported me unconditionally in every step I took, who endured my ups and downs during my Ph.D., always had a motivating word for me and on whom I can always rely on! Without all of you, I would not have been able to master this intense time! Thank you all! - *Schließlich gilt mein tiefster Dank all meinen Liebsten, und besonders meinen Eltern, die mich in jedem meiner Schritte bedingungslos unterstützt haben, die meine Aufs und Abs im Ph.D. ertragen haben, stets ein motivierendes Wort für mich hatten und auf die ich mich immer verlassen kann! Ohne euch alle hätte ich diese intensive Zeit nicht meistern können! Dankeschön!* -